EPA-460/3-73-007

CONDENSER AND FAN DEVELOPMENT FOR RANKINE CYCLE ENGINES

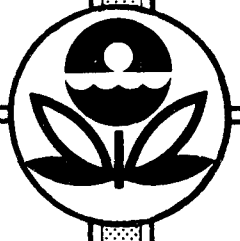

U.S. ENVIRONMENTAL PROTECTION AGENCY
Office of Air and Water Programs
Office of Mobile Source Air Pollution Control
Alternative Automotive Power Systems Division
Ann Arbor, Michigan 48105

EPA-460/3-73-007

CONDENSER AND FAN DEVELOPMENT FOR RANKINE CYCLE ENGINES

Prepared by

J. Killackey, R. Morgan, C. Morse,
B. Foster, and C. Lee

AiResearch Manufacturing Company
2525 West 190th Street
Torrance, California 90509

Contract No. 68-01-0407

EPA Project Officers:

W. Zeber, P. Sutton, and E. Beyma

Prepared for

U.S. ENVIRONMENTAL PROTECTION AGENCY
Office of Air and Water Programs
Office of Mobile Source Air Pollution Control
Alternative Automotive Power Systems Division
Ann Arbor, Michigan 48105

November 1973

This report is issued by the Office of Mobile Source Air Pollution Control, Office of Air and Water Programs, Environmental Protection Agency, to report technical data of interest to a limited number of readers. Copies of this report are available free of charge to Federal employees, current contractors and grantees, and non-profit organizations - as supplies permit - from the Air Pollution Technical Information Center, Environmental Protection Agency, Research Triangle Park, North Carolina 27711, or may be obtained, for a nominal cost, from the National Technical Information Service, 5285 Port Royal Road, Springfield, Virginia 22151.

This report was furnished to the U.S. Environmental Protection Agency by AiResearch Manufacturing Company, Torrance, California, in fulfillment of Contract No. 68-01-0407 and has been reviewed and approved for publication by the Environmental Protection Agency. Approval does not signify that the contents necessarily reflect the views and policies of the agency. The material presented in this report may be based on an extrapolation of the "State-of-the art." Each assumption must be carefully analyzed by the reader to assure that it is acceptable for his purpose. Results and conclusions should be viewed correspondingly. Mention of trade names or commercial products does not constitute endorsement or recommendation for use.

Publication No. EPA-460/3-73-007

PREFACE

This report (AiResearch Report 73-9034) describes development conducted by the AiResearch Manufacturing Company of California, a division of The Garrett Corporation, for the Environmental Protection Agency, Advanced Automotive Power Systems Development Division, under Contract No. 68-01-0407. The work was performed under the direction of Mr. K.O. Parker of AiResearch and Messrs. W. Zeber, P. Sutton, and E. Beyma of EPA.

CONTENTS

CONTENTS (Continued)

ILLUSTRATIONS

ILLUSTRATIONS (Continued)

ILLUSTRATIONS (Continued)

ILLUSTRATIONS (Continued)

ILLUSTRATIONS (Continued)

TABLES

NOMENCLATURE

A	Heat transfer area, sq ft
A_C	Cross-sectional flow area, sq ft
D	Tube or duct diameter, ft
f	Fanning friction factor, dimensionless
F_o	Wall shear stress multiplied by g_c, $lb_m/ft\ hr^2$
F_{ty}	Tensile stress at material yield point, psi
g_c	Conversion factor, $4.175 \times 10^8\ lb_m\ ft/lb_f\ hr^2$
G	Mass velocity = W/A_c, $lb_m/hr\ ft^2$
h	Heat transfer coefficient, $Btu/hr\ ft^2\ ^oF$
k	Thermal conductivity, $Btu/ft\ hr\ ^oF$
L_o	Total condensing length between qualities $x = 1$ and $x = 0$, ft
M_t	Torque, in.-lb
N	Rotational speed, rpm
N_o	Design Point operating speed, rpm
P_{amb}	Ambient pressure, in. H_2O
Pr	Prandtl number, dimensionless
P_s	Static pressure, in. H_2O
P_T	Total pressure, in. H_2O
P_v	Dynamic pressure, in. H_2O
Q	Heat transfer rate, But/hr; Volumetric flow, cfm
Re_T	Reynolds number based on total flow rate and local vapor density = $\frac{4W_T}{\pi D \mu_v}$, dimensionless
S	Circumference, ft

NOMENCLATURE (Continued)

T	Absolute temperature, ^{o}R
u	Fluid velocity, ft/hr
U	Overall coefficient of heat transfer, Btu/hr ft^2 ^{o}F
UA	Thermal conductance, product of U x A, Btu/hr ^{o}F
W	Fluid flow rate, lb_m/hr
x	Fluid quality, dimensionless
y	Total liquid layer plus oil film thickness, ft
z	Location along condensing length, ft
α	Void fraction, dimensionless
δ	Liquid layer thickness, ft
ΔPs	Static pressure rise, in. H_2O
ΔP_T	Total pressure rise, in. H_2O
η_f	Fan total efficiency, percent
μ	Viscosity, lb_m/ft hr
ρ	Fluid density, lb_m/cu ft
σ	Ratio of air density to standard air density
θ	Angle that vapor flow vector makes with the horizontal, deg

Subscripts

a	Acceleration field
av	Average
d	Discharge
eq	Equivalent
f	Friction
i	Inlet
ℓ	Liquid
m	Momentum
0	Evaluated at the wall
T	Total
v	Vapor
z	Evaluated at location z along the condensing length

SECTION 1

INTRODUCTION AND ABSTRACT

SECTION 1

INTRODUCTION AND ABSTRACT

INTRODUCTION

Condenser size and cooling air fan power consumption are two significant factors that limit the application of Rankine cycle power systems to automobiles. The Compact Condenser program recently completed by AiResearch (Reference 1) resulted in a substantial reduction in condenser size compared to that obtained using present day radiator technology. Reduction in fan power consumption is a definite possibility because a substantial increase in fan efficiency can be realized by using a sophisticated aerodynamic design.

The primary goal of this program is, therefore, to develop a high performance condenser and fan system for each of three Rankine cycle automotive power plants now under development by the Environmental Protection Agency. A condenser and fan package is to be delivered to each of three system contractors--Aerojet Liquid Rocket Company, Thermo Electron Corporation, and Steam Engine Systems--at the completion of the program.

This development program is supported by other tasks including: (1) the further optimization of the air-side perforated fin, (2) a measurement of the condensing heat transfer performance, and (3) a determination of the air-side pressure losses in a typical automobile installation.

ABSTRACT

The three condenser and fan assemblies were fabricated, leak checked, performance tested, and delivered to the three system contractors. Final specifications for each system are presented in Appendix A. The completed Aerojet assembly is shown on Figure 1-1, a front view, and Figure 1-2, a back view. A T-shaped design is used for the Aerojet unit to provide clearance between the condenser and the automobile frame rails. The assembly is designed to fit within the engine compartment of a 1972 Chevrolet Impala. A top view of the condenser assembly showing the flared vapor inlet duct is shown on Figure 1-3.

Photographs of the completed Thermo Electron condenser and fan assembly are shown on Figure 1-4, a front view, Figure 1-5, a top view, and Figure 1-6, a view of the back face. The assembly is designed to fit into the engine compartment of a 1972 Ford Galaxie.

The completed condenser and fan assembly built for Steam Engine Systems is shown on Figures 1-7 and 1-8. The assembly is designed to fit within a Plymouth "C" body engine compartment.

The optimization of the perforated air-side fin which was developed in the Compact Condenser program (Reference 1) was continued. Two additional surface geometrics were tested. Additional optimization studies were conducted to establish the optimum fin height and fins per inch for a given perforation geometry.

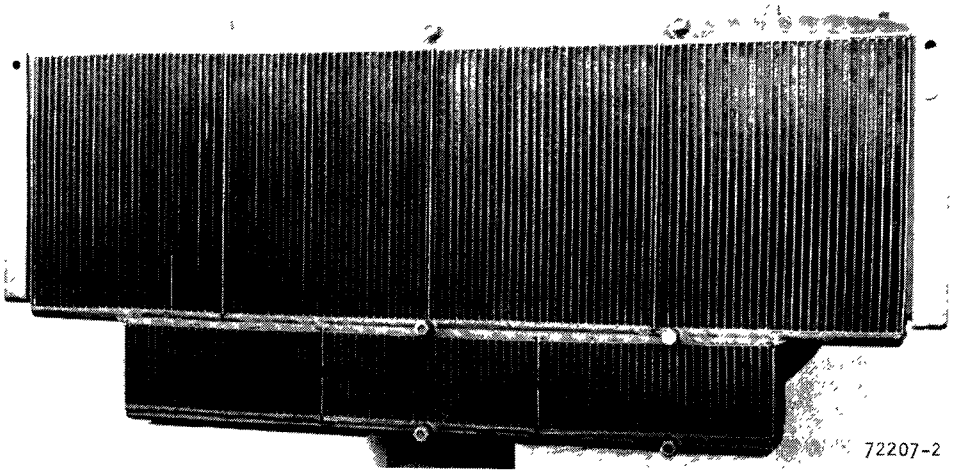

Figure 1-1. Aerojet Condenser and Fan Assembly (Front View)

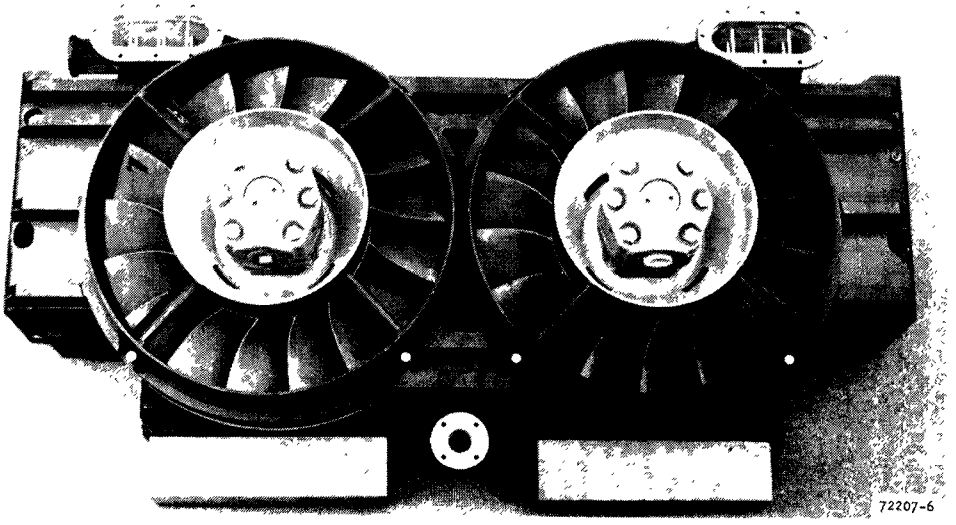

Figure 1-2. Aerojet Condenser and Fan Assembly (Back View)

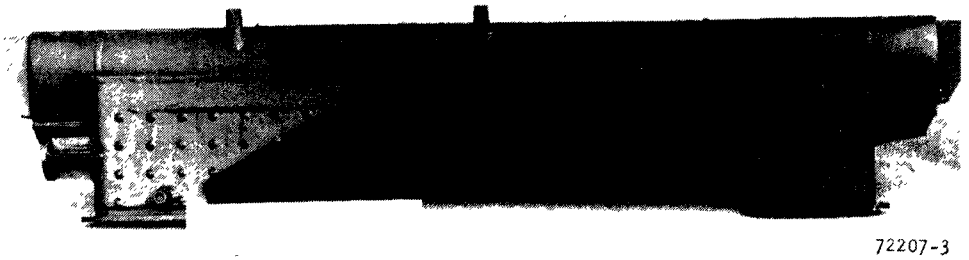

F-17491

Figure 1-3. Aerojet Condenser Assembly (Top View)

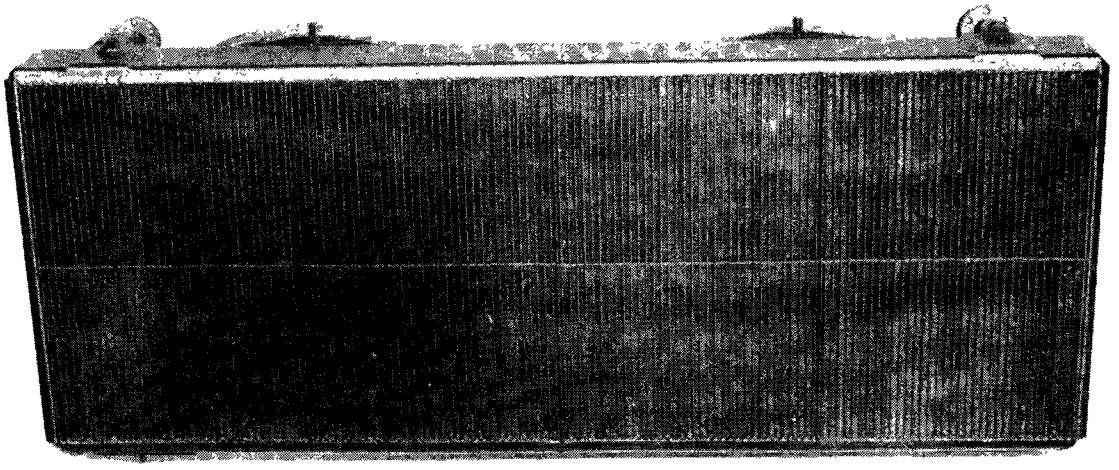

Figure 1-4. Thermo Electron Condenser and Fan Assembly (Front View)

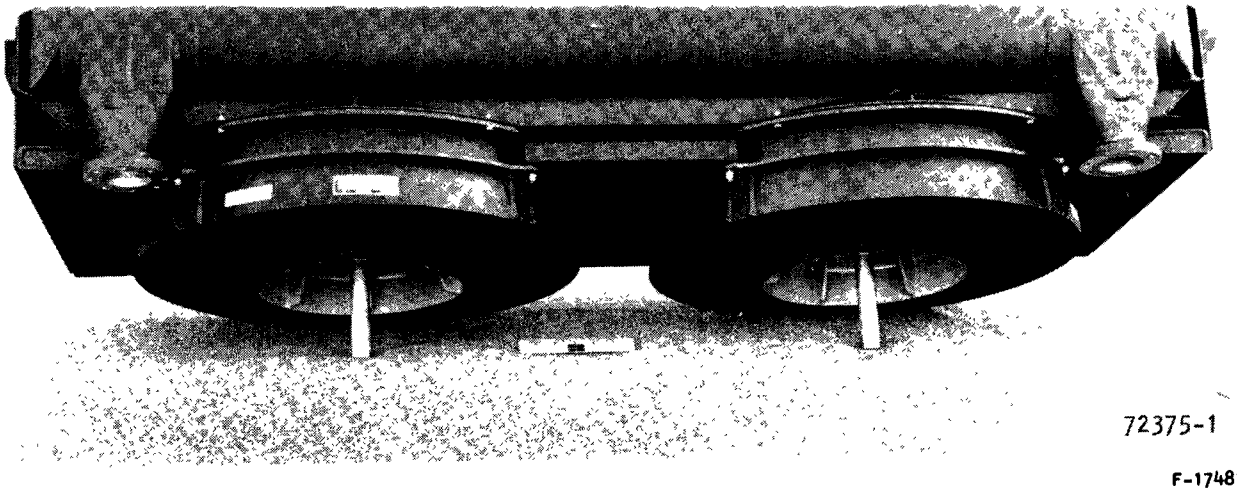

Figure 1-5. Thermo Electron Condenser and Fan Assembly (Top View)

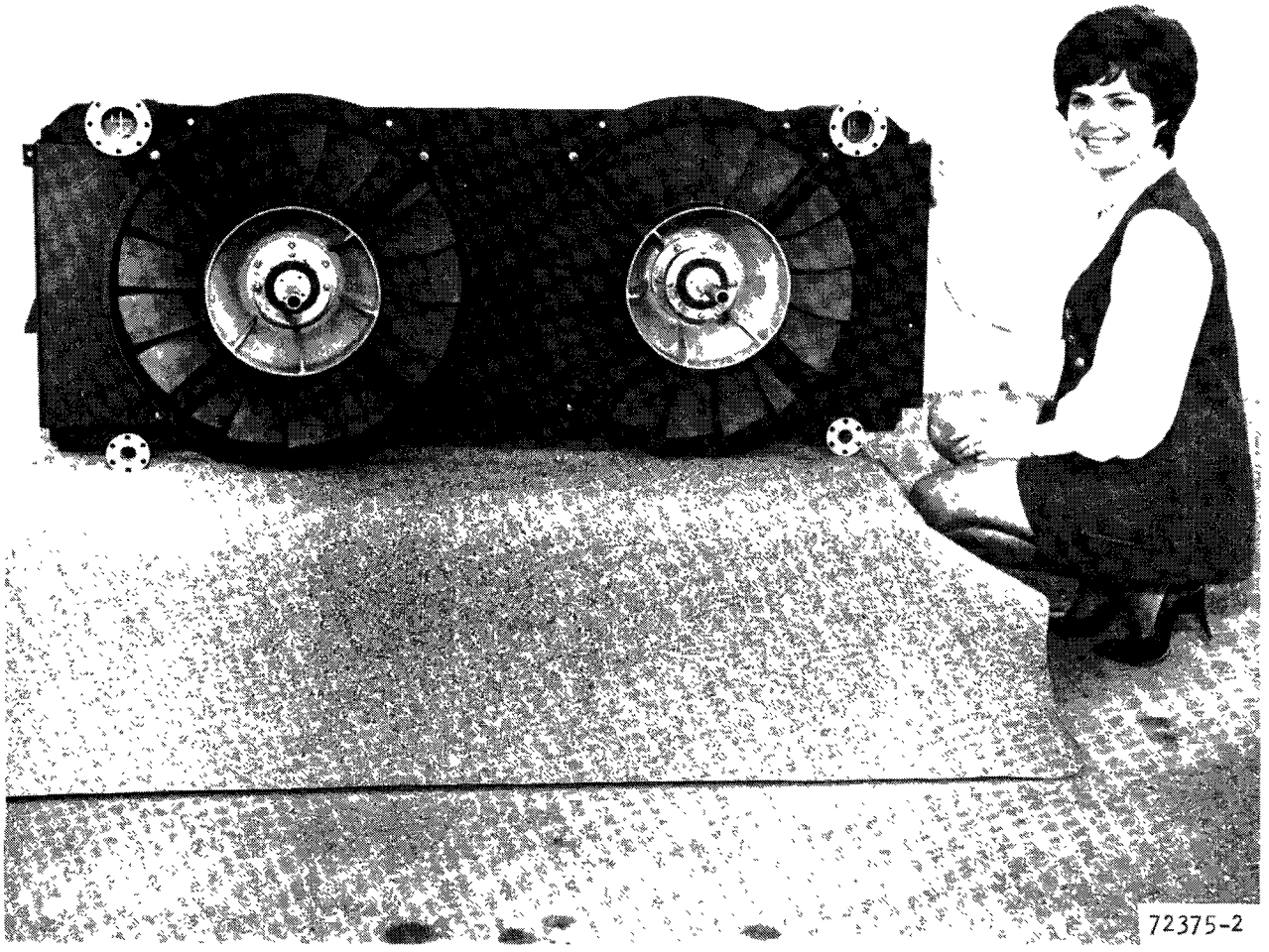

Figure 1-6. Thermo Electron Condenser and Fan Assembly (Back View)

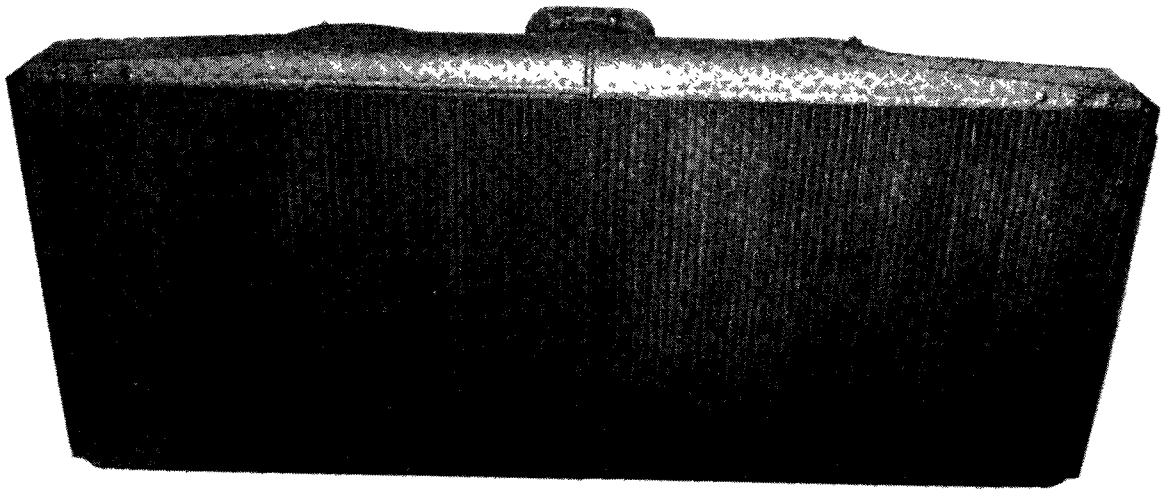

72423-2

Figure 1-7. Steam Engine Systems Condenser and Fan Assembly (Front View)

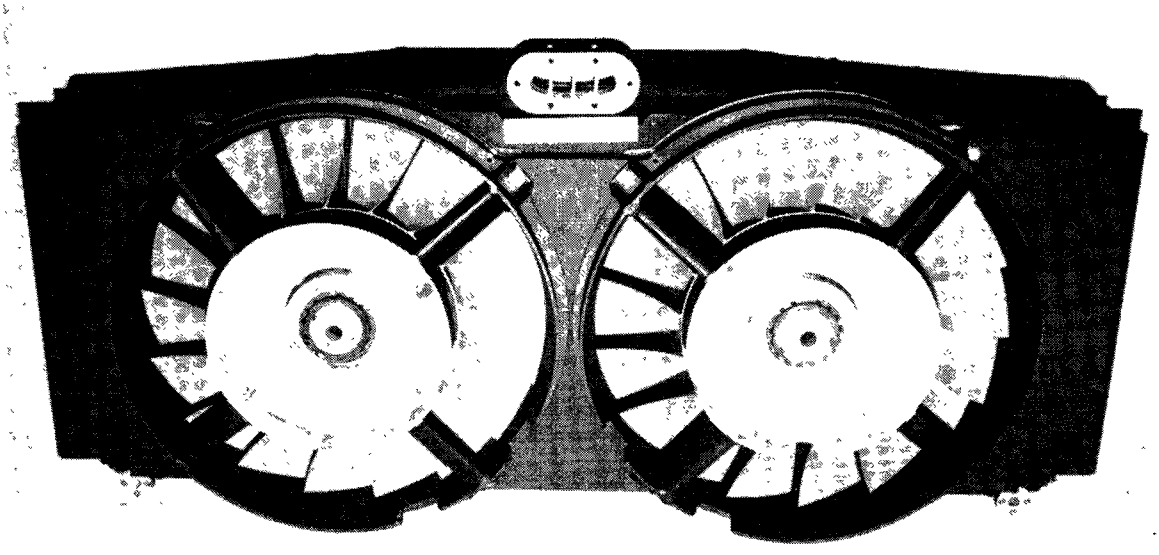

72423-1

F-17431

Figure 1-8. Steam Engine Systems Condenser and Fan Assembly (Back View)

Condensing heat transfer tests were performed using steam and Fluorinol-85, the TECO organic working fluid, condensing in three different vapor passage fin configurations. These tests were run primarily to establish the effect of a nonuniform condensation rate on the performance of a cross flow condenser.

Three different condensers were designed to meet the specific performance requirements of the three Rankine cycle engines. Each unit was configured to fit within the confines of the specified engine compartment. Detailed structual analyses were conducted to ensure that the units would withstand the expected pressure and temperature operating conditions. Analyses were also conducted to establish the required structure and mounting arrangement that would be necessary in a roadable design. An identical optimized perforated fin was used on the air-side of each condenser. The condenser core assembly was fabricated using a new fluxless brazing process to obtain a high level of cleanliness and structural reliability. All assemblies were treated with an epoxy ester coating to insure meeting a rigid vapor-side helium mass spectrometer leakage requirement.

All fans were designed to use a common high performance impeller design. The tip diameter and rotational speed were varied to meet the demands of three different installations. Aerodynamic performance and noise tests were performed on the completed fan assemblies.

Air flow tests were conducted on the Thermo Electron and Steam Engine Systems assemblies. The condensers were assembled with the fans and system airflow capability as a function of fan rotational speed was determined. Qualitative checks were made with regard to the system noise and vibration levels.

Cooling air flow through a Rankine cycle engine is about 3 to 5 times greater than that of a conventional IC automobile engine radiator. Thus, it was expected that the air-side pressure losses could become critical in a Rankine cycle engine installation. Since no test data was available, mockups of two of the Rankine cycle engines were installed in actual engine compartments and the pressure drop across the bumper and grille and through the engine compartment was experimentally determined.

SECTION 2

CONCLUSIONS AND RECOMMENDATIONS

SECTION 2

CONCLUSIONS AND RECOMMENDATIONS

CONCLUSIONS

Condenser and fan performance should meet all specification performance goals. The assemblies have been configured to fit within their respective engine compartments. The assemblies are not considered to be a fully roadable design, however, because additional structure and/or supports are required to withstand the expected vibration and shock environment. The installation could be modified at a later date to provide the required support.

Air flow tests performed on the condenser and fan assemblies revealed that the airflow through the Steam Engine Systems unit was slightly higher than predicted whereas the airflow through the Thermo Electron unit was nine percent lower than predicted over the fan speed range. The low performance in the TECO unit is attributed to the close spacing between the condenser and fans which was dictated by the engine compartment space limitations. The TECO design point airflow can be achieved, however, by merely increasing that fan speed and accepting a small increase in fan power consumption. Alternatively, the spacing between the condenser and fans could be increased.

The air-side perforated fin geometry appears to be close to optimum for this application. The selected fin height (0.326 in.) and fins per inch (22) result in a minimum in fan power consumption. The -13 rectangular slot perforation geometry as described in Section 3 was found to provide superior performance and should be used in the final condenser designs.

Vapor-side heat transfer performance should be as predicted based on the condensing heat transfer test results. The best vapor-side fin is the offset configuration because it permits redistribution of vapor flow as required to match the variable condensation rate in a crossflow condenser. A variable fin geometry designed to match the condensation rate could be used to obtain maximum performance but the small performance gain does not warrant the increased fabrication complexity. If vapor-side pressure drop is limited, then a perforated plain rectangular fin should be considered.

Fluxless brazing has been established as a practical fabrication method for the condenser plate-fin core assembly. A hydrostatic pressure test performed on a condenser core module reached a burst pressure of about 5 times the maximum operating pressure. The unit structural design is believed to be adequate. Braze and weld assembly of helium leaktight vapor passages will always present problems, especially with regard to detection and repair of individual leaks. It is believed that an epoxy ester coating as used on the present assemblies can be effectively used as a production technique to seal minute leaks and to provide a protective coating on the air-side fins.

The cooling air fans have met all performance requirements including air efficiency goal of greater than 70 percent. The measured noise levels were exceptionally low. It is expected that, if the fans are the major noise source on the engine, the EPA vehicle noise specifications can be met. The fan design is feasible for mass production and its cost can be minimized by injection molding of the fan impeller and by using a glass-filled nylon material.

Airflow pressure losses measured in the engine installation mockup were less than expected and, in fact, came reasonably close to meeting the specification allowance. These low losses were achieved by removing the grille from the 1971 Ford Galaxie and other vehicle modifications. The engine mockups were not complete and the addition of all equipment including wiring, instrumentation, and ancillary equipment would, no doubt, increase the pressure loss. However, by providing additional air flow exit area, e.g., louvers in the fender wells, the increase in flow restriction could be counteracted.

The Ford Galaxie had a high pressure drop and it must be modified to provide additional airflow area. It was found that small increases in airflow area such as obtained by removing 2 of the 4 vehicle headlights produce a significant reduction in pressure drop. The effect of undercar velocity as used to simulate vehicle motion on the compartment pressure drop was found to be minor--compartment pressure drop increased by only 15 percent when the undercar flow velocity increased from 0 to 60 mph. Qualitative observations indicated that the existing bumper design causes a significant flow maldistribution at the condenser inlet face and this effect will degrade the condenser performance.

RECOMMENDATIONS

Before road testing, the vehicle frame should be modified to provide a center support for the condenser and fan assembly. As an alternate and possibly better solution, the fans could be mounted to the vehicle frame with a flexible duct between the condenser and fans.

A specific test should be run to evaluate the full-size condenser heat transfer and pressure drop performance. A 1/4 section of the condenser could be used for this purpose. This data would be of value in determining the condenser behavior after it is installed in the vehicle.

Flow blockage at the fan discharge should be minimized. Engine equipment should be relocated to avoid blockage insofar as possible because the velocity maldistribution caused by blockage will significantly affect fan performance.

Because of the limited space within the engine compartment, an axial flow fan will always be subjected to flow blockage. It does appear that a radial flow or centrifugal machine would fit the installation better. Less axial length is required and a diffuser section can be incorporated to recover a portion of the swirl energy. The fan can be designed independent of the rest of the engine because the outlet diffuser directs the flow down and away from the engine. The installed efficiency would be higher than that of an axial machine because there would be no flow blockage effects. A centrifugal machine

turns slower than any other type of fan, and hence, it is more quiet. It is recommended that the system contractors review the results of their initial tests and determine the effectiveness of the installed axial flow fans. If performance is lacking then a radial flow machine should be considered.

The existing bumpers and grille should be modified to reduce flow blockage at the condenser inlet.

SECTION 3

PERFORATED FIN DEVELOPMENT

SECTION 3

PERFORATED FIN DEVELOPMENT

SURFACES

During the previous program (Reference 1) perforated fins with 0.015-, 0.030-, and 0.060-in. wide slots and open area ratios of 12.5 and 25.0 percent were tested, and the best overall performance was obtained for the 0.030-in. slots at 25.0 percent open area. This particular core was designated as the -13 configuration; details of the perforation geometry are shown in Table 3-1. On the basis of this work, it was decided to test the same 0.030-in. slot width at open area ratios of 16.7 and 33.3 percent during the current program. The 22 fins/in., 0.326-in. fin height and 0.004-in. fin thickness of the previous cores were maintained.

TABLE 3-1

FIN PERFORATION GEOMETRIES

Core	Slot Width, in.	Slot Length, in.	Slot Spacing, in.	Theoretical Open Area, percent	Actual Open Area, percent
-13	0.030	0.250	0.120	25.0	22.0
-21	0.030	0.250	0.180	16.7	16.0
-23	0.030	0.250	0.090	33.3	32.0

The theoretical percent open area values are for the perforations in an infinite heat exchanger where edge effects are negligible. The actual percent open area values are for the perforations in the test cores where the perforations had to be in a total airflow length of 3.38 in. and the air fin actually consisted of two separate pieces, each 1.69-in. long. Figure 3-1 shows the perforation layout for the -21 and -23 fins.

It was originally planned to select a third perforation geometry on the basis of a study of heat transfer from perforated plates at the University of Michigan (Contract No. 68-04-0019). Based on a meeting held in December of 1971 with Dr. Wen-Jei Yang, who conducted the study, it was concluded that one of the two geometries already selected represented very nearly the optimum geometry (fin spacing and percent open area) indicated by the results of the University of Michigan study.

Therefore, it was decided to conduct a heat exchanger optimization study to obtain the fin geometry (fin height and fins/in.) yielding minimum fan air horsepower for a typical condenser problem statement and set of envelope limitations. The purpose of this study was to determine whether it would be profitable to test one of the previously tested perforation geometries in a configuration involving either a new fin height or a different number of fins/in. The design conditions used for this analysis were essentially those of the TECO problem statement as listed in Table 3-2. The -13 fin perforation geometry was used, since this was found to be optimum in the Reference 1 study.

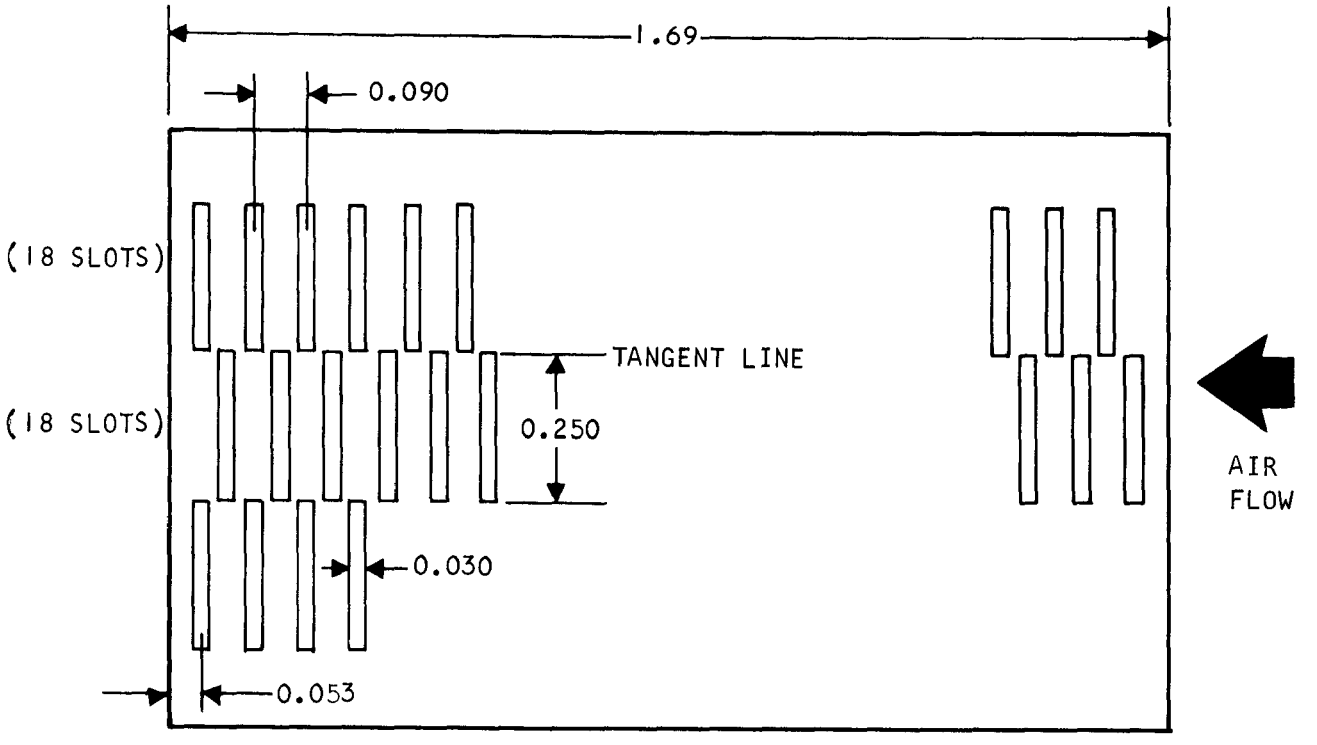

(a) -23 FIN SHEET

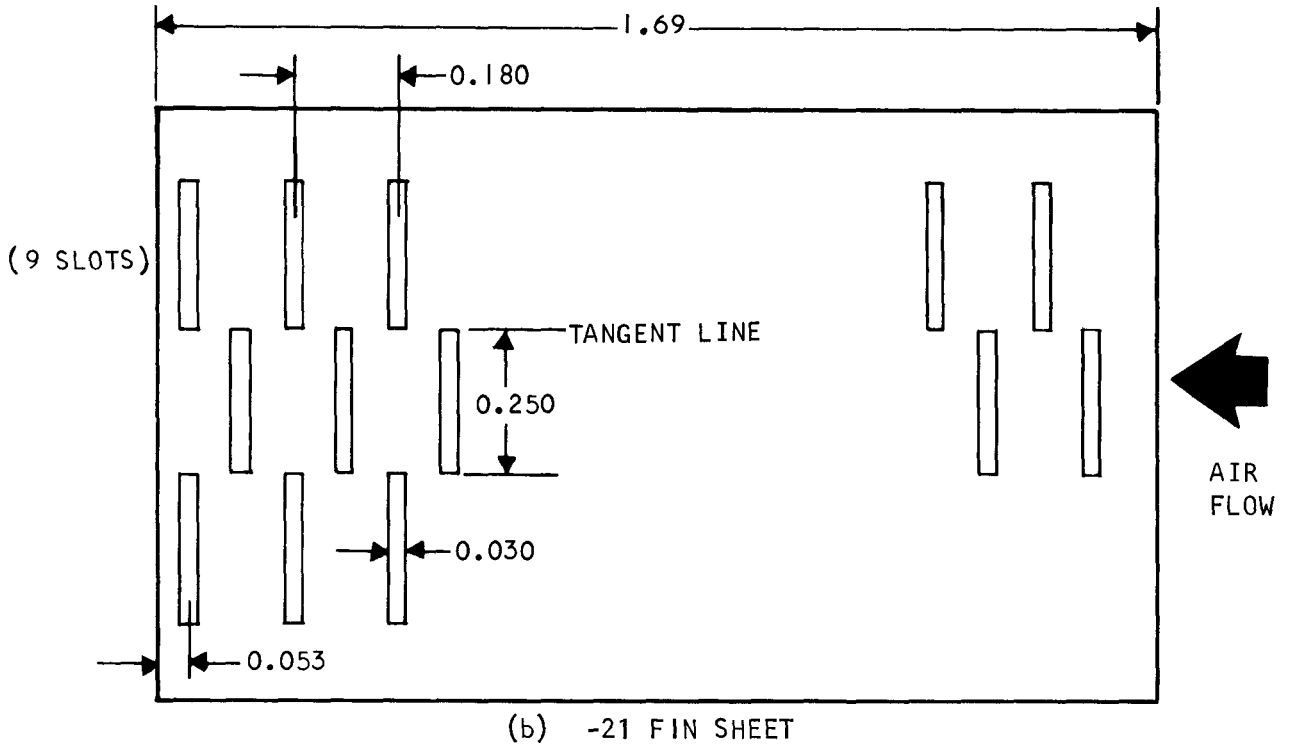

(b) -21 FIN SHEET

NOTE: ALL DIMENSIONS ARE IN INCHES

S-68091

Figure 3-1. Perforated Fin Materials For Cores -21 and -23

TABLE 3-2

DESIGN CONDITIONS FOR FIN OPTIMIZATION STUDY

Working fluid	Fluorinol 85
Total heat rejection	1.88×10^6 Btu/hr
Condensing temperature	$213^{\circ}F$
Air inlet temperature	$85^{\circ}F$
Working fluid flow rate	9860 lb/hr
Condenser core frontal area	8.46 sq ft

The fin configuration in the condensing side passage was a 0.050 in. high rectangular offset surface with twenty 0.004-in. thick aluminum fins/in. An average condensing heat transfer coefficient of 640 Btu/hr sq ft $^{\circ}F$ was used and the analysis was based upon a "no UA margin" design. The air side effectiveness and the air side fin height and number of fins/in. were varied. The experimental f and j from the -13 perforated fin were used for all the air side fins analyzed. At each air side effectiveness, air side fin height, and number of fins/in., the condenser flow length and air ΔP were calculated. The pressure drop associated with getting the air out of the engine compartment, $\Delta P_{installation}$, was calculated at each value of air side effectiveness from

$$\Delta P_{installation} = 2.80 \times \left(\frac{W}{1277}\right)^2 \text{ in. } H_2O$$

where W is the airflow rate through the condenser in lb/min. The TECO design point is at a vehicle speed of 90 mph which gives a ram pressure rise (assuming 100 percent recovery) of 3.73 in. H_2O. The required fan pressure rise was calculated as the condenser air side ΔP plus $\Delta P_{installation}$ minus the ram ΔP. The fan air horsepower could then be calculated from the fan pressure rise and the air volumetric flow rate. The results of the analysis were plotted as fan air horsepower vs condenser flow length. A typical plot is shown in Figure 3-2 for a fin height of 0.326 in. It is seen that with an increasing air-side effectiveness (decreasing airflow) the power requirement decreases at the expense of increased condenser airflow length. At a particular condenser length, the power requirement decreases with increasing number of fins/in. over the range analyzed. Similar data were generated for fin heights of 0.250 in. and 0.400 in. and cross-plotted to obtain the required fan air horsepower as a function of fin height, as shown in Figure 3-3. The comparison in Figure 3-3 is made at a flow length of 4.25 in. as this was the design objective for the TECO condenser. It is seen that for 22 or 26 fins/in., there is no horsepower

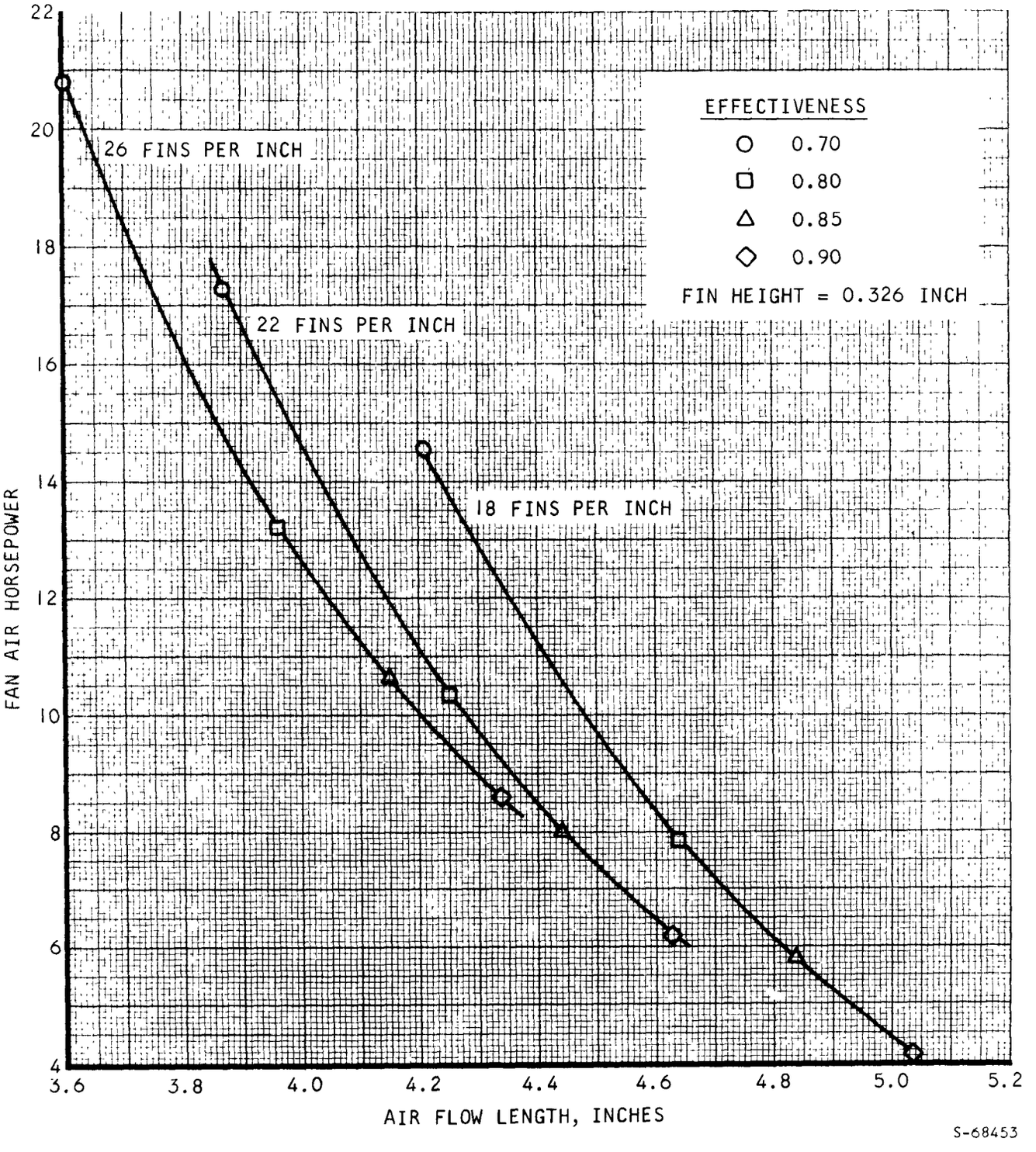

Figure 3-2. Effect of Air Side Fin Geometry on Condenser Length and Required Fan Air Horsepower

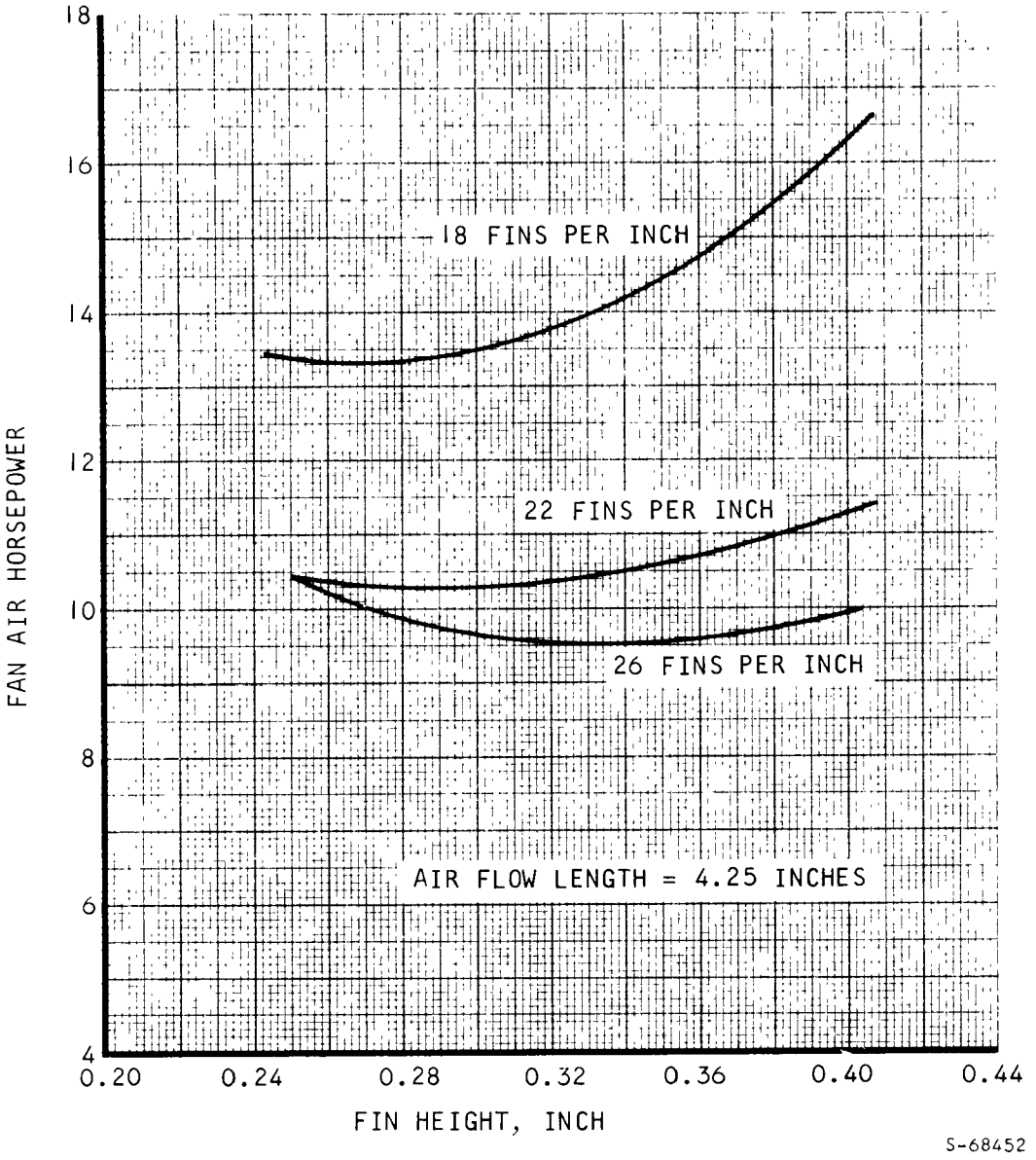

Figure 3-3. Effect of Fin Height on Fan Air Horsepower at a Fixed Condenser Size

incentive to go to fin heights other than the baseline 0.326 in. At 18 fins/in. slightly less power is required at a fin height of 0.250 in. than at 0.326 in. As noted above, the required power decreases with increasing number of fins/in., but because of the potential problems of contamination and plugging of the condenser fins, it was decided that the 22 fins/in. baseline should not be exceeded. On the basis of the 22 fins/in. limit and the horsepower-fin height relationship of Figure 3-3, it was concluded that the baseline fin (22R-.326-PERF(-13)-.004 Al) was still optimum. Based on these results, it was decided not to test a third fin.

TEST CORES

As a result of the considerations discussed above, two cores were tested. The cores were tested without and with turbulence upstream of the core.

A typical perforated fin aluminum test core is shown in Figure 3-4. The flow configuration is single-pass crossflow. The core is constructed from ten air-side sandwiches using the selected perforated rectangular fin surface and eleven water-side sandwiches using a 20 fin/in. offset rectangular fin surface.

As in the case of the eleven previous cores, the test data were reduced on the basis of a solid fin both in heat transfer area and in fin efficiency. In addition, the small variations between cores were neglected and the same dimensions were used for all the cores. As a result, the curves can be compared directly. That is, at the same Reynolds number, the airflow in each core would be the same and the heat transfer and friction factors can be used to compare the heat transfer conductances and the pressure drops, respectively. It would be impossible to make such direct comparisons if the effect of the perforations on the hydraulic diameter and the heat transfer area was included in the curves. Since the principal purpose of this study is to obtain the best air side surface, this procedure is indicated.

TEST PROCEDURE

Figure 3-5 is a schematic of the test setup. The air source was a blower instead of the pressurized air supply used in the previous program.

The air weight flow rate was determined upstream of the core by a square-edged orifice plate in a 4-in. diameter pipe flow measuring section; both met the requirements of the 1959 ASME Power Test Code for this type of flowmeter. Four orifice diameters were used: 3.0, 2.5, 2.0 and 1.5 in. The inlet air temperature was measured by two thermocouples, and the outlet air temperature was measured by four thermocouples after the air had been mixed in an insulated mixing device.

On the water side, the water was pumped from an open sump through a heat exchanger where it was heated by steam. The water then passed through a filter and a mixing device to the unit. After flowing through the core, the water passed through another mixing device and through a weighing system back to the sump. The weight flow was determined by the weight-time method where the flow time for a specific weight of water was determined automatically to 0.01 sec.

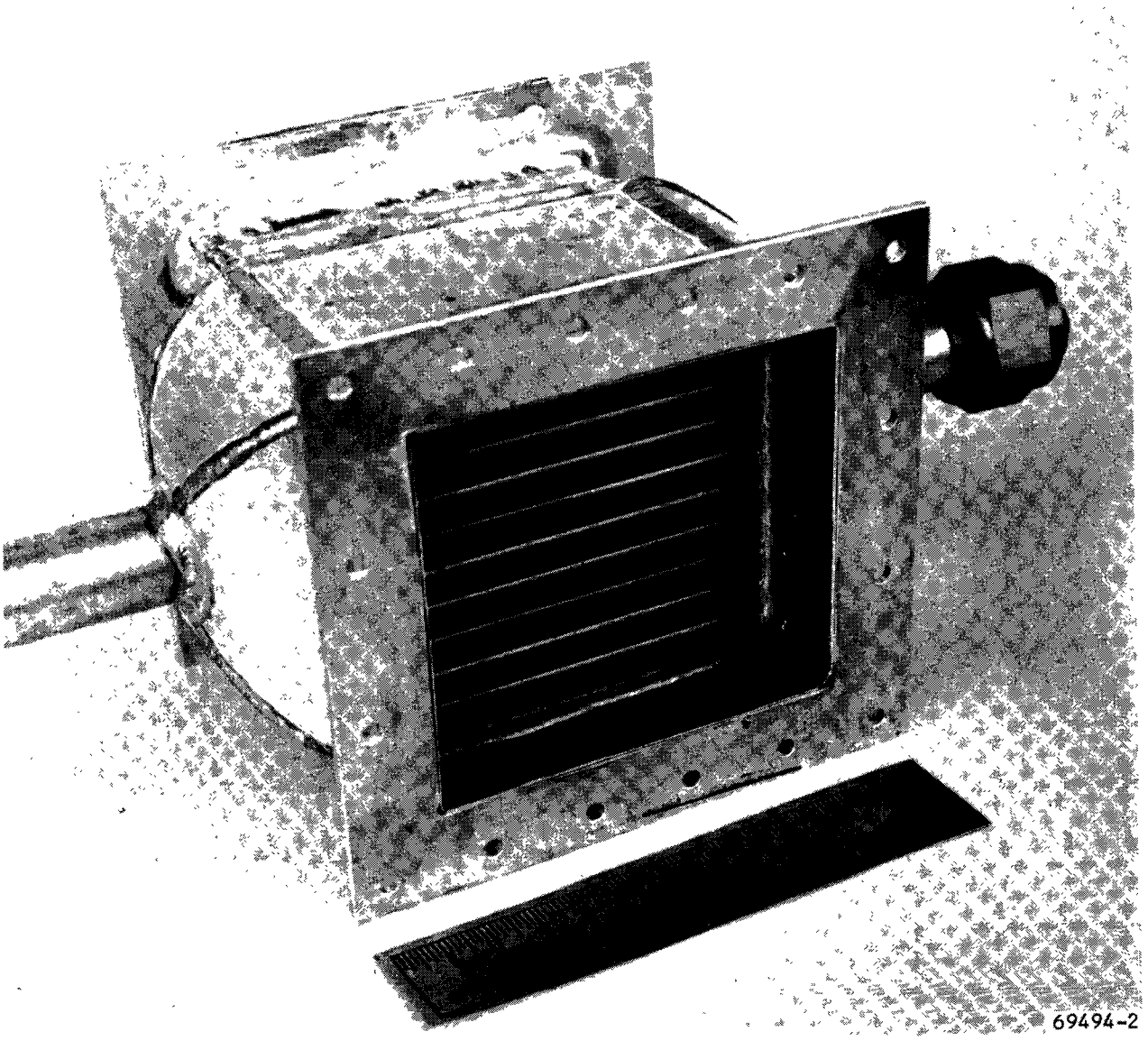

Figure 3-4. Typical Test Core for f and j Factors (22 Fins per Inch, Perforated, 0.004-in. Aluminum Material)

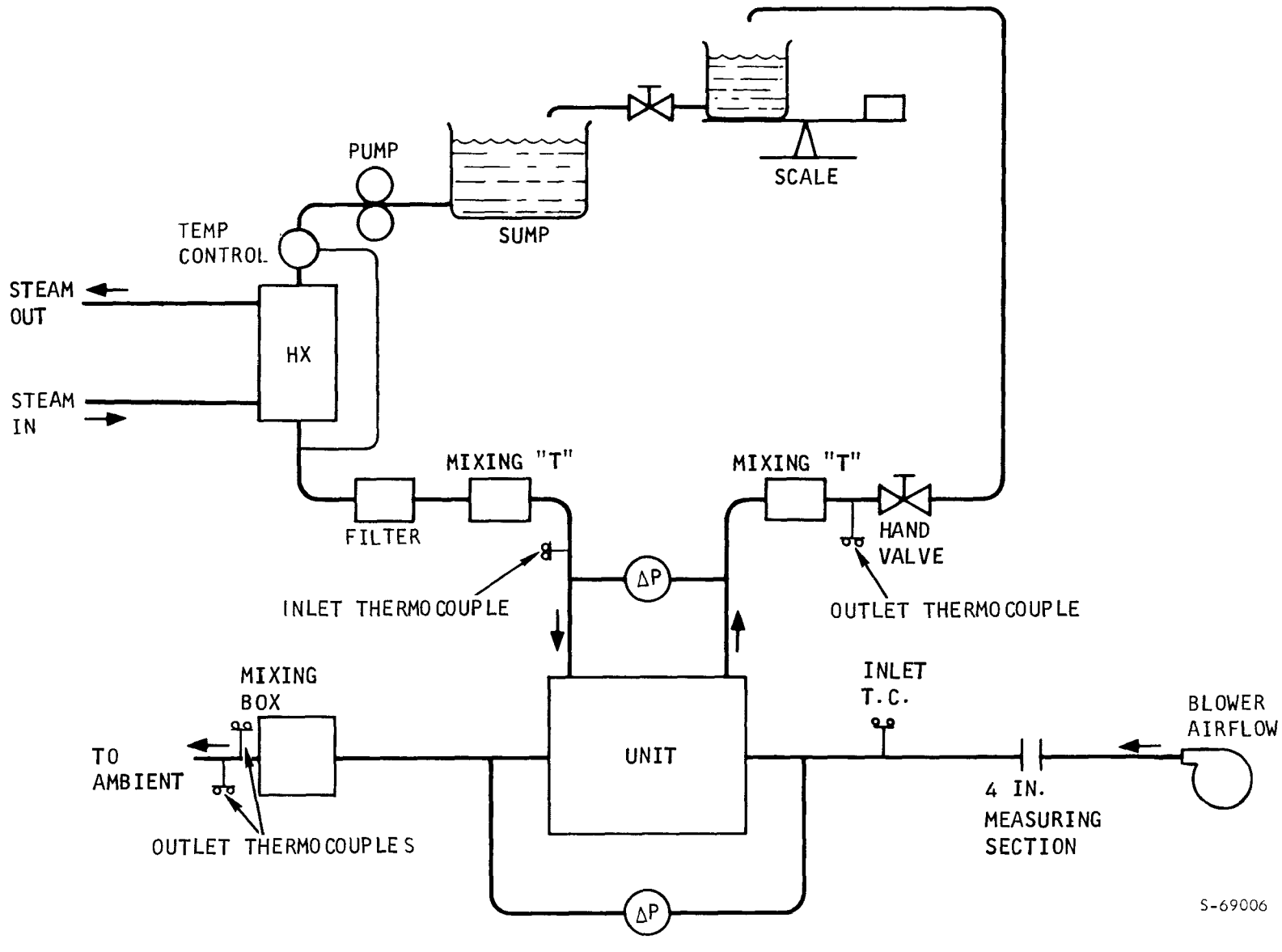

Figure 3-5. Typical Heat Exchanger Test Setup Schematic

Thermocouples were of special grade copper-constantan, which has an allowable tolerance of $\pm 0.75^{\circ}F$. Temperatures were read in millivolts by a potentiometer. Water temperature drop was measured by a differential thermocouple in most runs.

Air inlet static pressure and static pressure drops were measured by water manometers; inclined manometers were used to read all but the highest pressure drops to an accuracy of 0.01 in. of water. Wall pressure taps were located 3.0 in. upstream and 5.0 in. downstream of the faces of the test cores. Two taps located on opposite sides of the duct were used at each location and were connected to a common manometer to average the pressures. Water-side pressure drops were measured in inches of water by differential pressure gauges and were used in the data reduction to calculate the frictional heating of the water.

Accuracy of the data was indicated by the heat balances achieved. For all airflows except one, at least one run was obtained with a heat balance of not over 2.7 percent. Average heat balance for all runs was approximately 1.6 percent.

The test setup did not have the traversing pressure probes upstream of the core or the thermocouple grid downstream of the core as in the previous tests. In addition, the orifice pipe measuring section was changed. Photographs of the previous test setup are presented in Figures 3-6 and 3-7.

In the tests to determine the effect of turbulence, turbulator rods were installed upstream of the test section to determine the effect of turbulence on fin performance. Three 1/2-in.-diameter rods were placed 4 in. upstream of the face of the core as shown in Figure 3-8. The size and spacing of the turbulator rods were selected on the basis that the wakes of the air stream would be intersecting upstream of the test unit, resulting in a minimum variation in air velocity at the face of the core.

TEST RESULTS

Figures 3-9 and 3-10 present the heat transfer factors (j) and friction factors (f) for the two perforated surfaces. As previously, the surface identification, 22R-.326-PERF( )-.004(Al), is based on the AiResearch system for plate-fin surfaces where the 22 refers to the fins/in., the R is for rectangular fin, the .326 is the plate spacing in inches, PERF refers to a perforated fin, .004 is the fin thickness, and Al is the fin material. In addition, for the purposes of this work, the perforated core identification is placed in the parentheses after PERF. Fluid properties including the density were evaluated at the bulk average temperature. The heat transfer area, hydraulic radius, and fin efficiency are based on those of a solid fin of the same geometry. The hydraulic diameter (D_h) is 0.07345 in., the area density (β) is 589 sq ft/cu ft and the fin area-to-total area ratio (A_f/A_t) is 0.886.

With upstream turbulence, the two cores had lower friction factors and equal or higher heat transfer factors than the original or no-upstream-turbulence runs, except for the Reynolds number of 1200 in the -21 core where the test point was essentially the same for the two cases. The -21 core curves in the 800 to 1200 Reynolds number range are not well defined in this transition range due to the lack of sufficient data points.

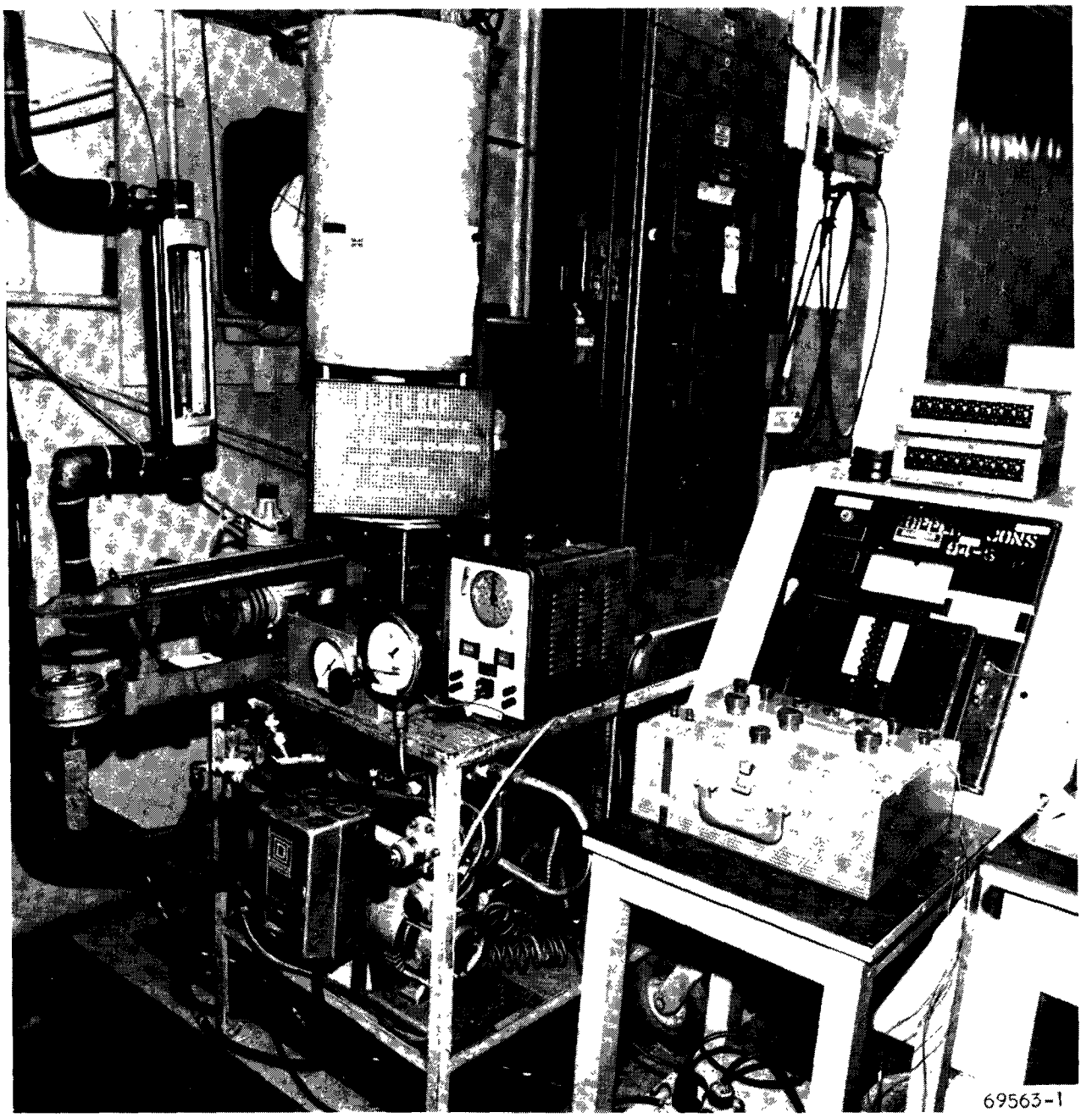

Figure 3-6. Test Setup Showing Water Flowrate Measuring System and Thermocouple Measuring Apparatus

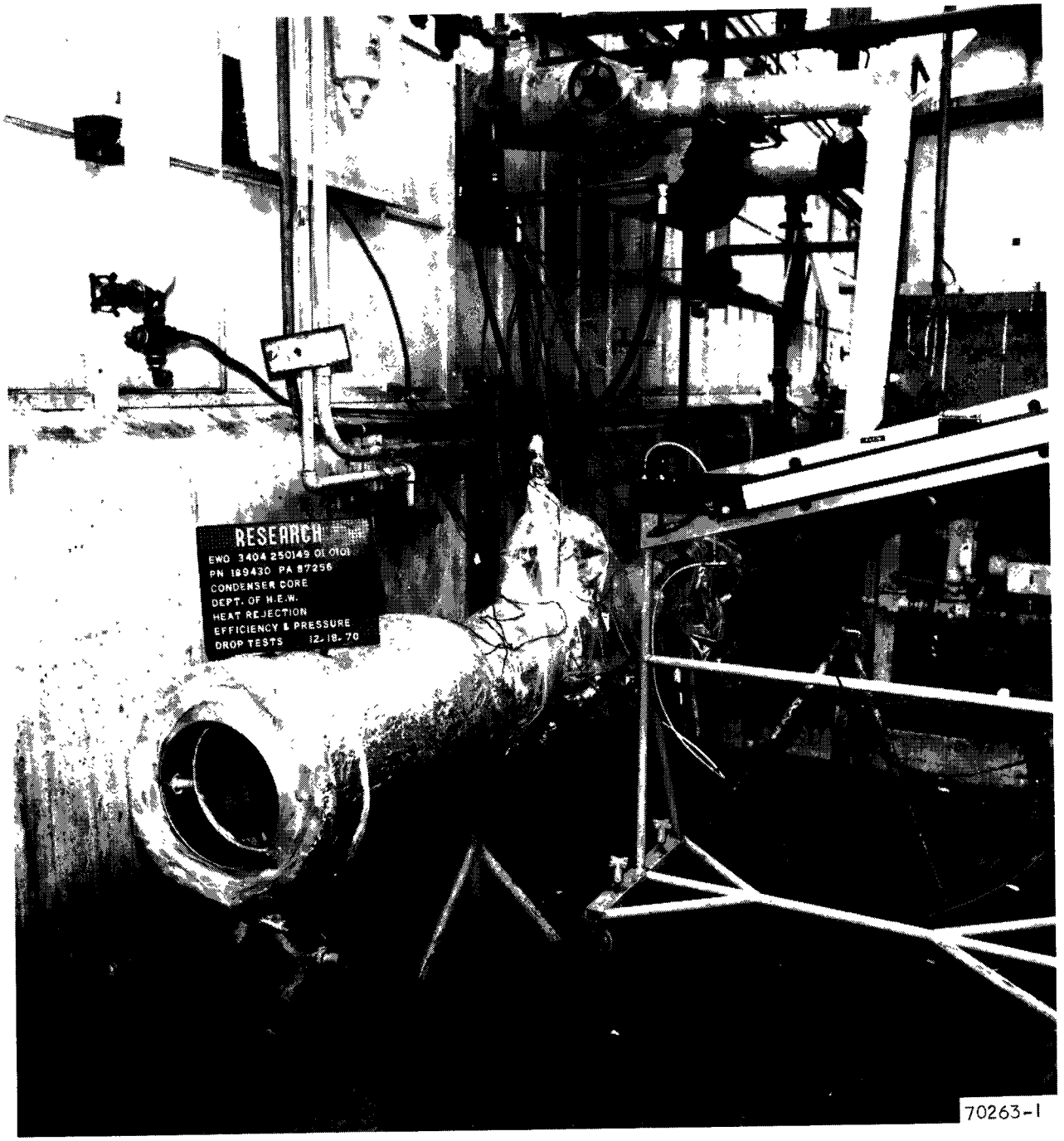

Figure 3-7. Test Setup Showing Test Core Mounted in Ducting

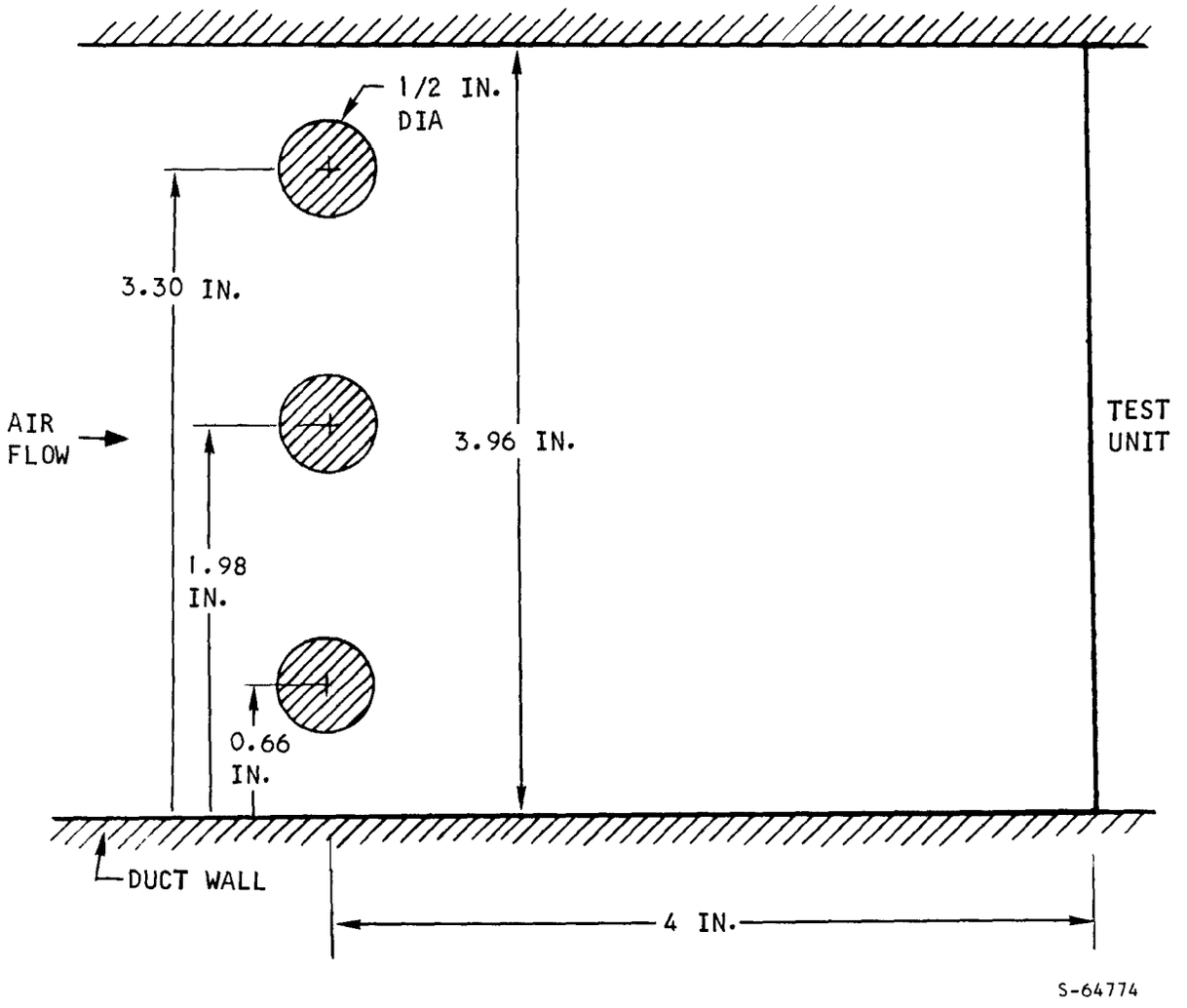

Figure 3-8. Turbulator Rods Design

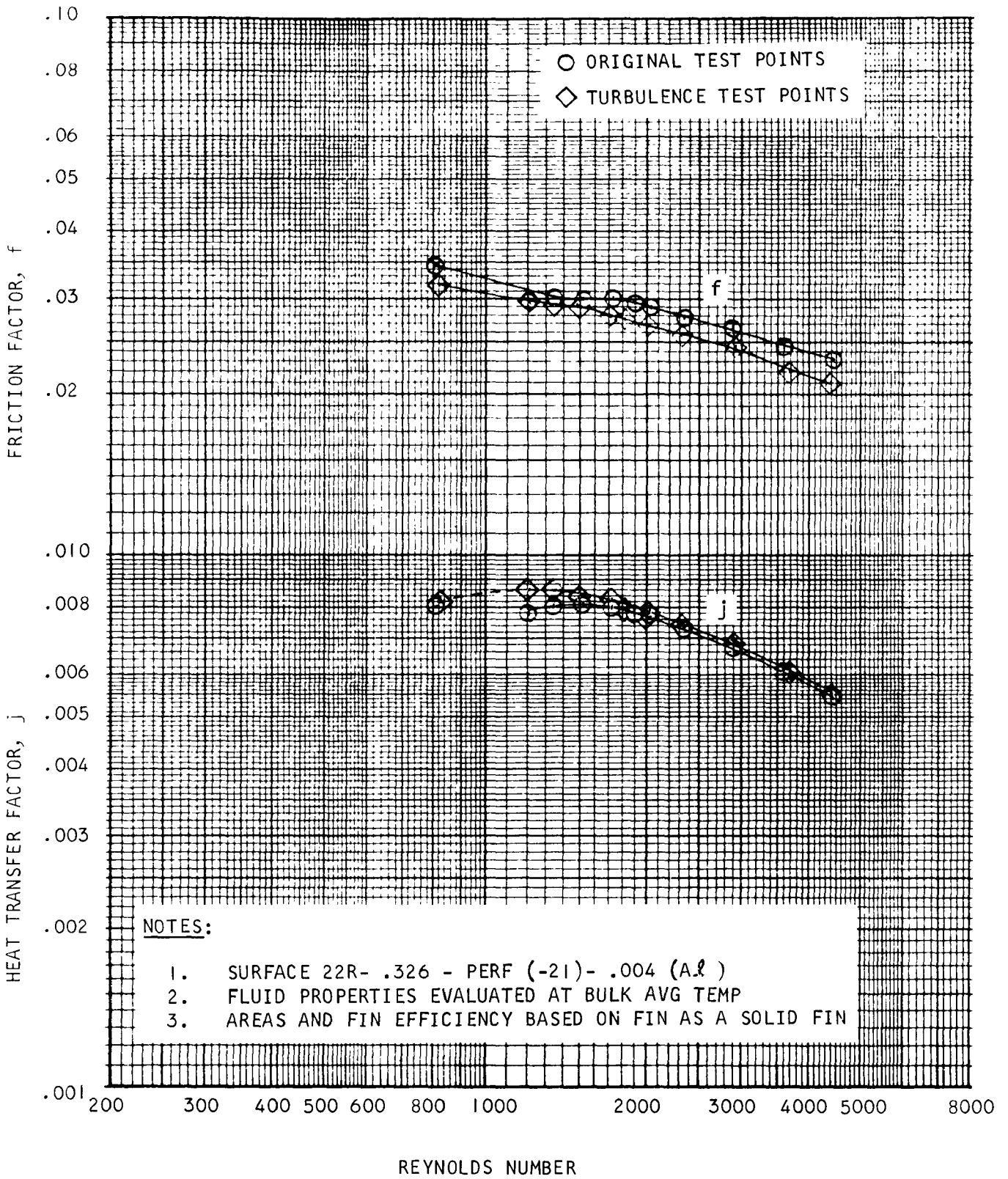

Figure 3-9. Performance Parameters for the -21 Perforated Fin

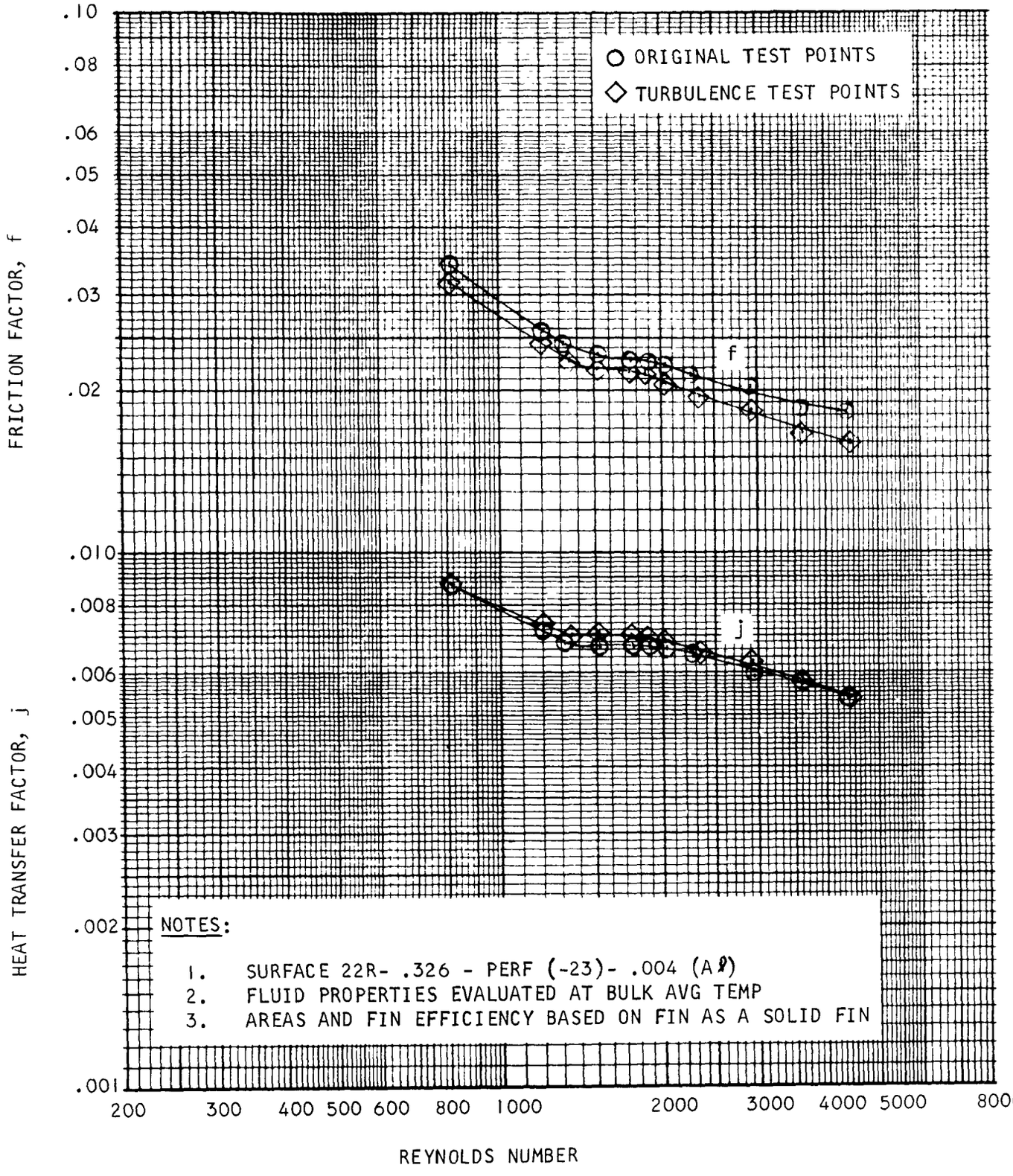

Figure 3-10. Performance Parameters for the -23 Perforated Fin

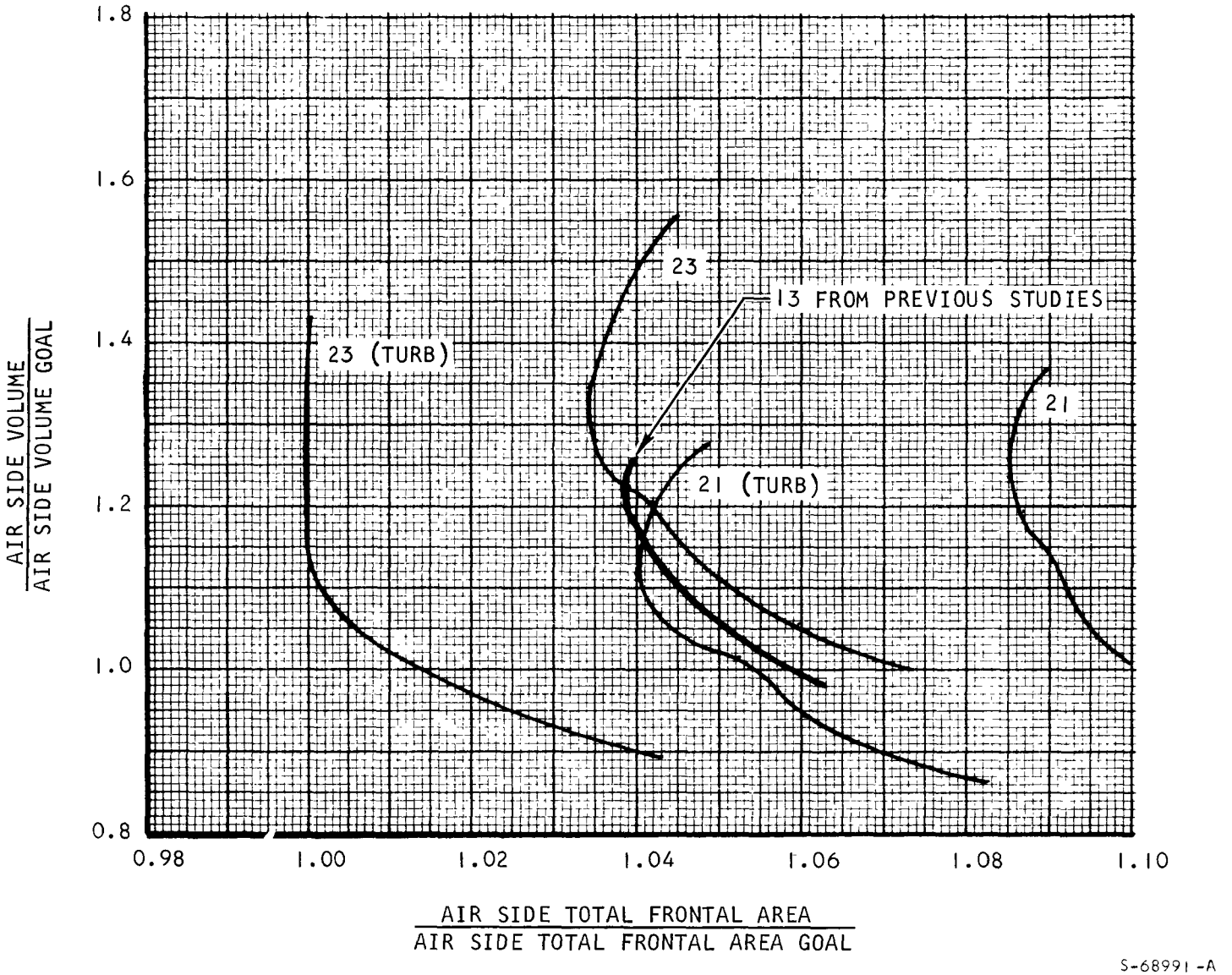

Figure 3-11. Condenser Solutions for Tested Fins

The f and j data were used to size condensers at the previous parametric study (Reference 1) design point heat rejection of 1.5×10^6 Btu/hr. The non-dimensionalized core sizes are shown in Figure 3-11. The cores were non-dimensionalized by dividing the air total frontal area and the air side volume by the area and volume design goals, respectively. The variation of volume with frontal area for each fin geometry is obtained by varying airflow and air pressure drop in such a way as to maintain a constant air power requirement of 9.0 hp.

The selection of the best fin involves a tradeoff between air frontal area and air volume because a larger volume means a longer airflow length, which is not desirable due to the restricted space available for the fan and condenser. As shown in Figure 3-11, there are many combinations of air frontal area and volume which will yield condensers for the given heat load and air horsepower requirement. For designs that lie near the minimum frontal area solution, it is possible to achieve significant decreases in volume with small increases in air frontal area by operating at somewhat higher airflows.

Introduction of upstream turbulence improved the fin performance such that slightly smaller condensers are obtained. However, there is some uncertainty in the turbulent data results in that (1) the reason for the decreased f and higher j with turbulence is not fully understood, (2) it is possible that the lower f was partly due to the pressure tap being located in the wake of the middle turbulence generating rod so that a lower than actual upstream pressure was measured, and (3) the changes in f and j in the range of interest for this program are estimated to be in the order of the experimental uncertainty of the data. Therefore, for conservatism, the no-turbulence data were used in the design of the condensers for this program.

On the basis of the no-turbulence data, the -13 core is still the best core for this application. The -21 core does not merit any consideration. The -23 core has a smaller minimum frontal area than the -13 core but the difference is less than 0.5 percent. For frontal areas above the minimum, the -13 core has a significantly smaller volume (and thus shorter airflow length) than the -23 core. The smaller volume characteristic of the -13 core is definitely preferred for this application due to the critical envelope restriction on overall fan/condenser airflow length.

SECTION 4

CONDENSING HEAT TRANSFER TESTS

SECTION 4

CONDENSING HEAT TRANSFER TESTS

TEST OBJECTIVES

As the result of a condensing heat transfer analysis, it was revealed that a large degree of uncertainty existed in the prediction of overall condenser performance due to a variation in condensation rate with axial position within the heat exchanger. This variation occurs because the temperature differential between condensing fluid and air decreases by a factor of five (corresponding to an air-side effectiveness of 0.80) between the air inlet face and the air outlet face. As a result, there is a tendency for the outlet vapor flow to be subcooled in the passages nearer the air inlet face and partially uncondensed in the downstream passages. This situation, which leads to a lower overall heat transfer rate for a given vapor inlet temperature, may be partially offset by vapor flow redistribution, vapor crossflow (if the vapor fins are offset or perforated), axial conduction of heat in the airflow direction, and condensation of vapor on liquid in the outlet manifold. Because of the complexity involved in trying to account for each of these effects analytically, the condensing heat transfer tests were oriented toward establishing the magnitude of the loss in overall condenser performance as a result of variable condensation. In addition, tests were performed to determine the improvement in condensing performance obtained by using a variable flow resistance on the vapor side.

TEST CORE DESCRIPTIONS

Three test cores were tested. Each core incorporated three vapor-side passages alternating with four air-side passages. The interior air-side passages were of double-sandwich configuration, whereas the passages forming the core sides were single-sandwich and thus contained half the heat transfer area of the interior passages. This arrangement provides essentially uniform cooling of each of the vapor passages. The air-side fin sandwiches were 16R-0.153-0.143(O)-0.004(A1) (16 rectangular fins/in., 0.153 in. high, 0.143 in. offset length, 0.004 in. fin thickness, aluminum).

Each of the three cores incorporated a different vapor-side fin configuration. A plain rectangular fin (20R-0.050-Plain-0.040) was used in the first core, an offset rectangular fin (20R-0.050-0.100(O)-0.004) was used in the second core, and the third core incorporated a variable-fin geometry designed to the SES problem statement. Each core was 18.0 in. long in the vapor flow direction and 4.25 in. long in the airflow direction. A picture of one of the completed test core assemblies is shown on Figure 4-1. Large, cylindrical manifolds are incorporated at each end of the assembly to provide uniform air flow distribution across the face of the test core.

The design of the vapor passages in the variable fin geometry core is shown in Figure 4-2. In this design, which is based on the SES problem statement, the steam-side fin geometry is varied in such a manner as to obtain a steam flow distribution that matches the steam-to-air temperature differential.

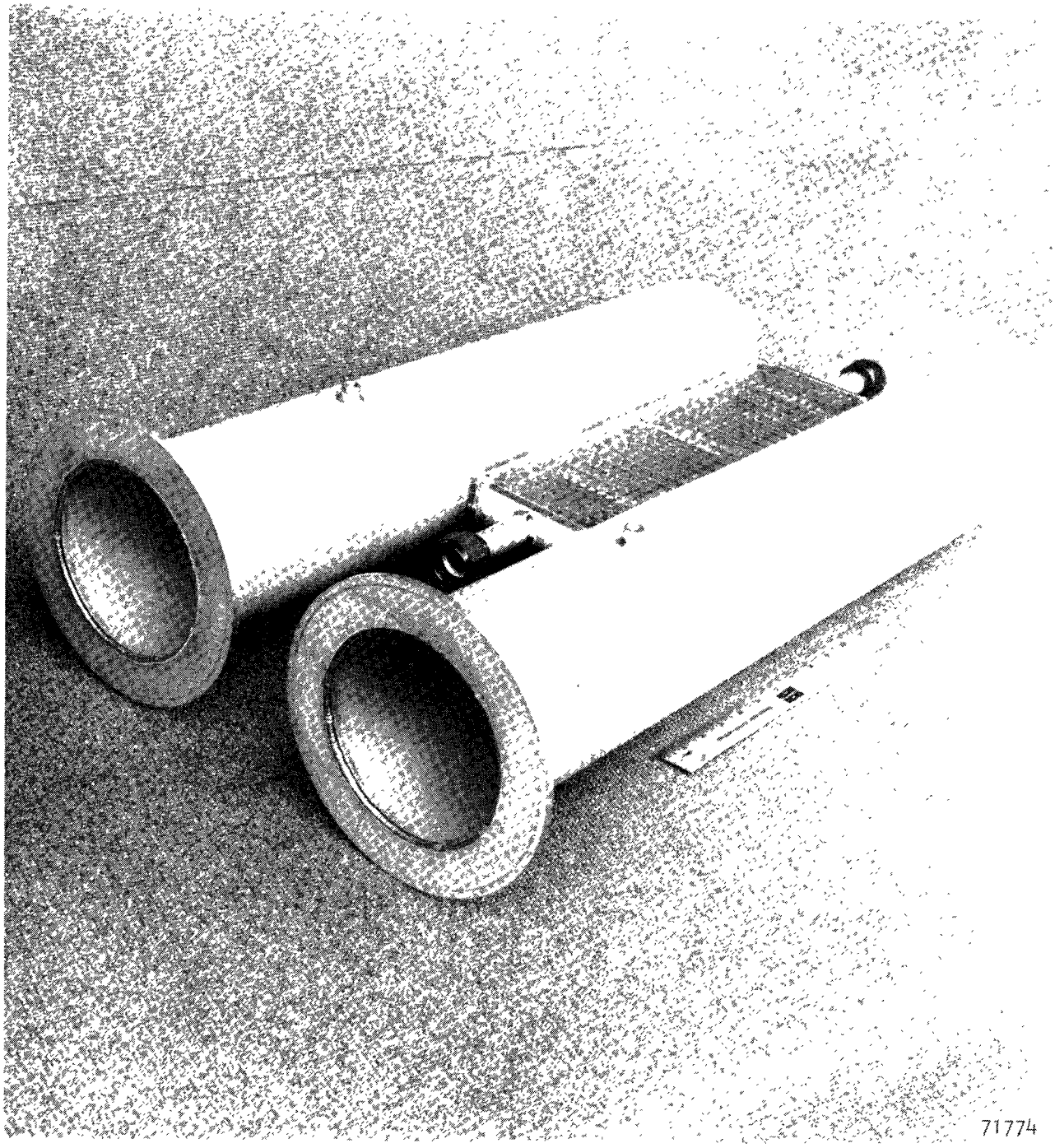

Figure 4-1. Test Core Assembly Condensing Heat Transfer Test

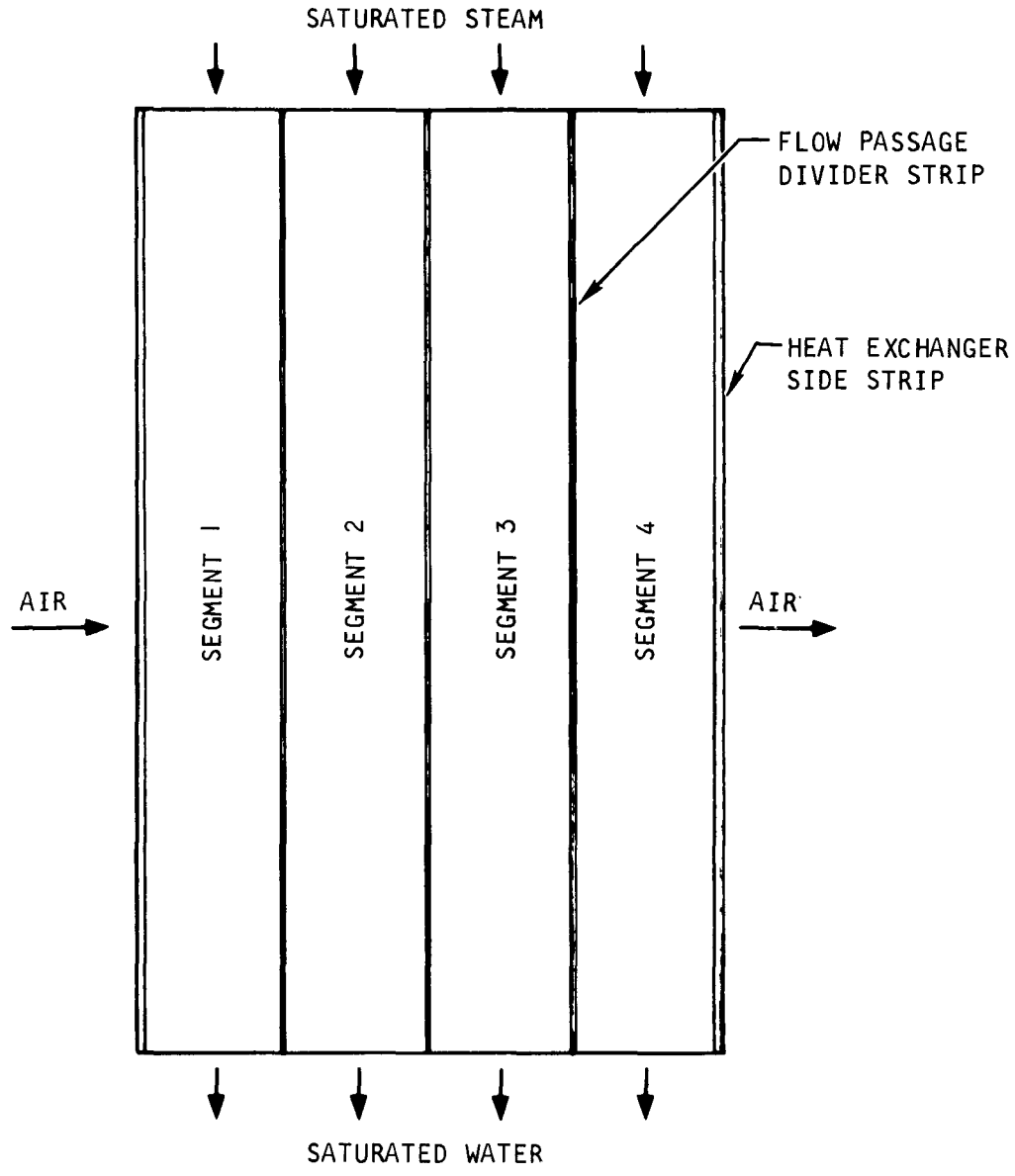

Segment	Fins/In.	Fin Offset Length (in.)	Fin Height (in.)	Fin Thickness (in.)
1	10	None	0.050	0.004
2	12	0.500	0.050	0.004
3	16	0.125	0.050	0.004
4	28	0.100	0.050	0.004

Figure 4-2. Steam-Side Fins in Variable Geometry Test Core

The heat exchanger is divided into four parallel passages of equal width, and a different fin geometry is selected for each passage. The variation in flow resistance obtained by varying fins per inch and fin offset length is sufficient to obtain a steam flow rate ratio of approximately three to one from the first to the last passage. Figure 4-3 shows the variation in pressure loss with flow rate for each of the parallel passages. The design point flow in each passage is obtained from the requirements that (1) the pressure drops in all four passages must be equal, and (2) the total flow rate must equal the design flow of 21.33 lb/min. These two requirements define the dashed line labelled "Equilibrium ΔP" in Figure 4-3, and the intersections between dashed and solid lines yield the flow rates in each passage. Figure 4-4 shows both the desired steam flow distribution, which is proportional to the steam-to-air temperature differential, and the calculated actual distribution obtained with the variable fin geometry. The actual is very close to the desired distribution and should yield a nearly uniform fluid state at the steam-side outlet.

Two series of tests were conducted, the first in an open-system test setup utilizing steam as the vapor-side fluid, and the second in a closed-system test setup utilizing Fluorinol 85 as the condensing fluid. The open- and closed-system tests are discussed below.

OPEN-SYSTEM TESTS

Test Setup and Procedure

The open-system test setup is shown schematically in Figure 4-5 and a picture of the completed setup in Figure 4-6. Steam was drawn from the plant steam system and regulated to an inlet pressure of approximately 15 psig. Because the plant steam is wet, a superheater was installed upstream of the core. The superheater used hot air as the energy source and was adjusted to provide 10° to 25°F of superheat. A calibrated sight glass was installed in the steam line downstream of the test core, followed by a valve for back-pressuring the system. During operation, this valve was adjusted to maintain the vapor-liquid interface at an approximately constant level in the sight glass. Downstream of the valve, the water was cooled and then weighed in a weigh tank. The flow rate, as measured by the weigh tank, was corrected by the measured change in the sight-glass liquid level between the start and finish of each test run.

The cooling fluid was air at ambient temperature. Instrumentation was installed to obtain test core inlet and outlet pressures and temperatures on both the steam and air sides. Airflow rate was measured using a standard orifice section.

Testing was conducted on each core over a range of airflows (approximately 15 to 80 lb/min) corresponding to an air-side effectiveness range of about 0.70 to 0.90. The data were reduced to obtain test UA at each set of flow conditions, based on measured air-side inlet and outlet temperatures, the measured inlet temperature and average pressure on the vapor side, and the assumption of saturated liquid conditions at the vapor-side outlet. The

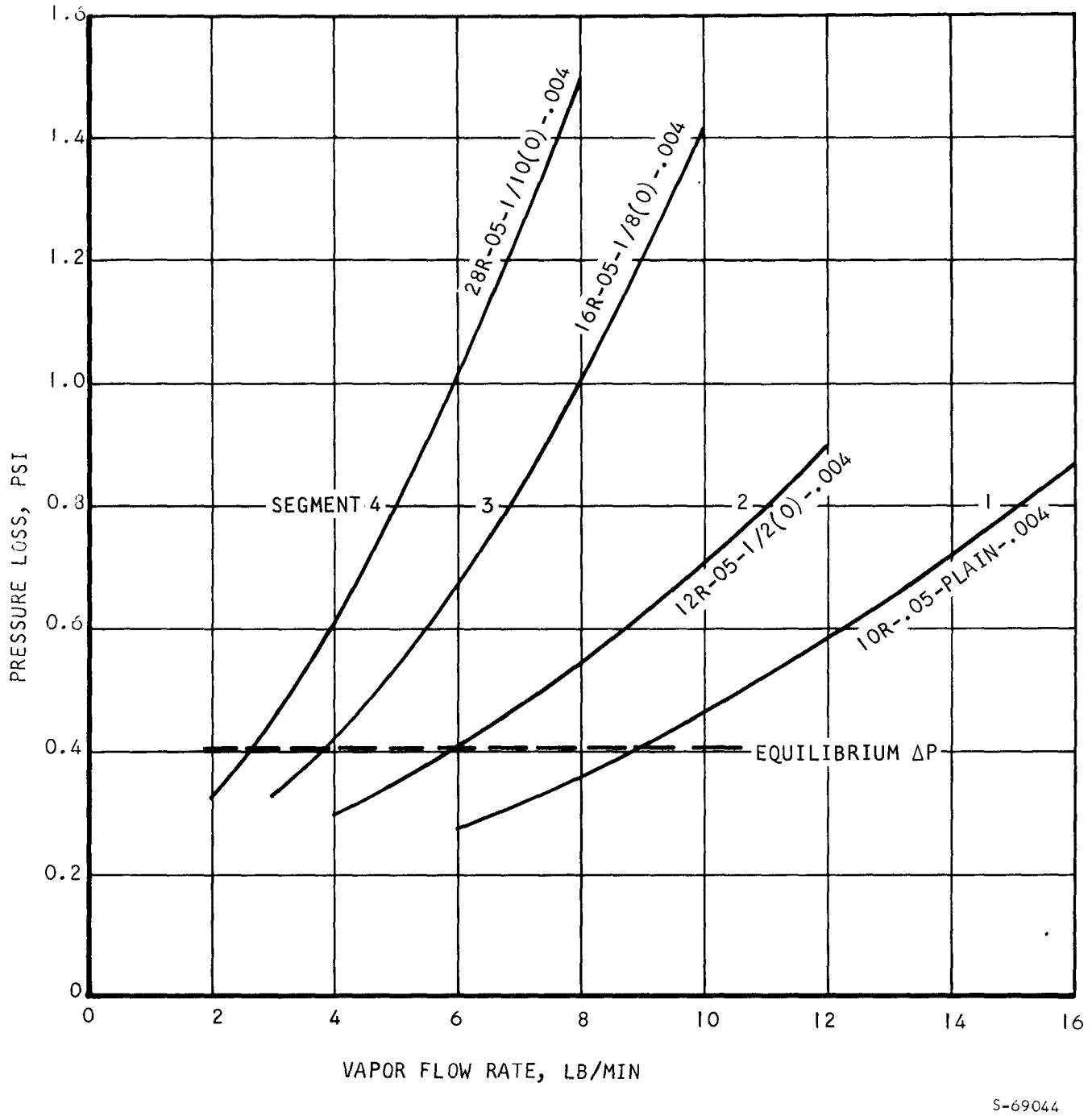

Figure 4-3. Condensing Pressure Loss vs Flow Rate in Each Condenser Segment of Variable Geometry Core

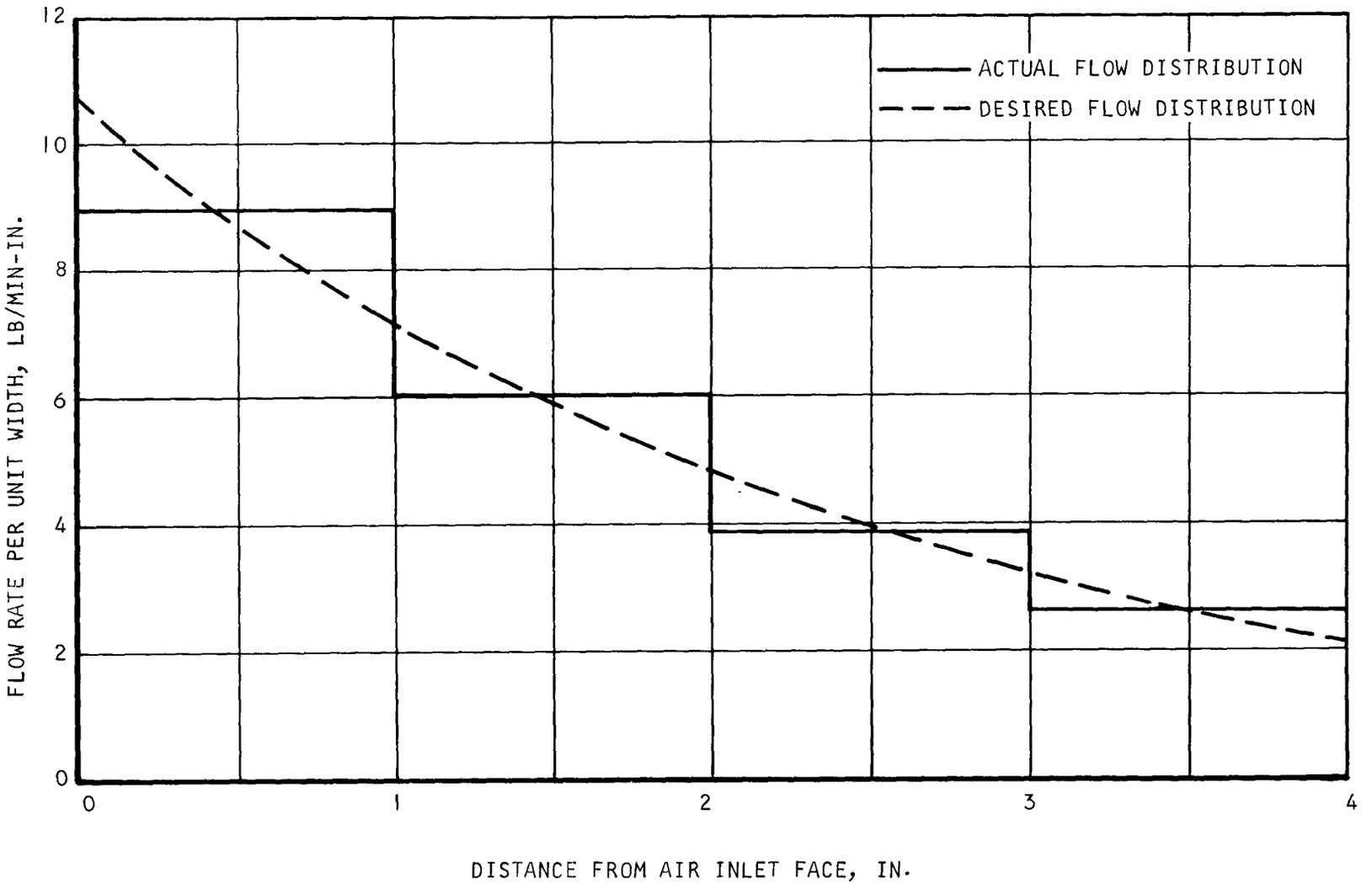

Figure 4-4. Distribution of Vapor Flow Rate in Variable Geometry Core

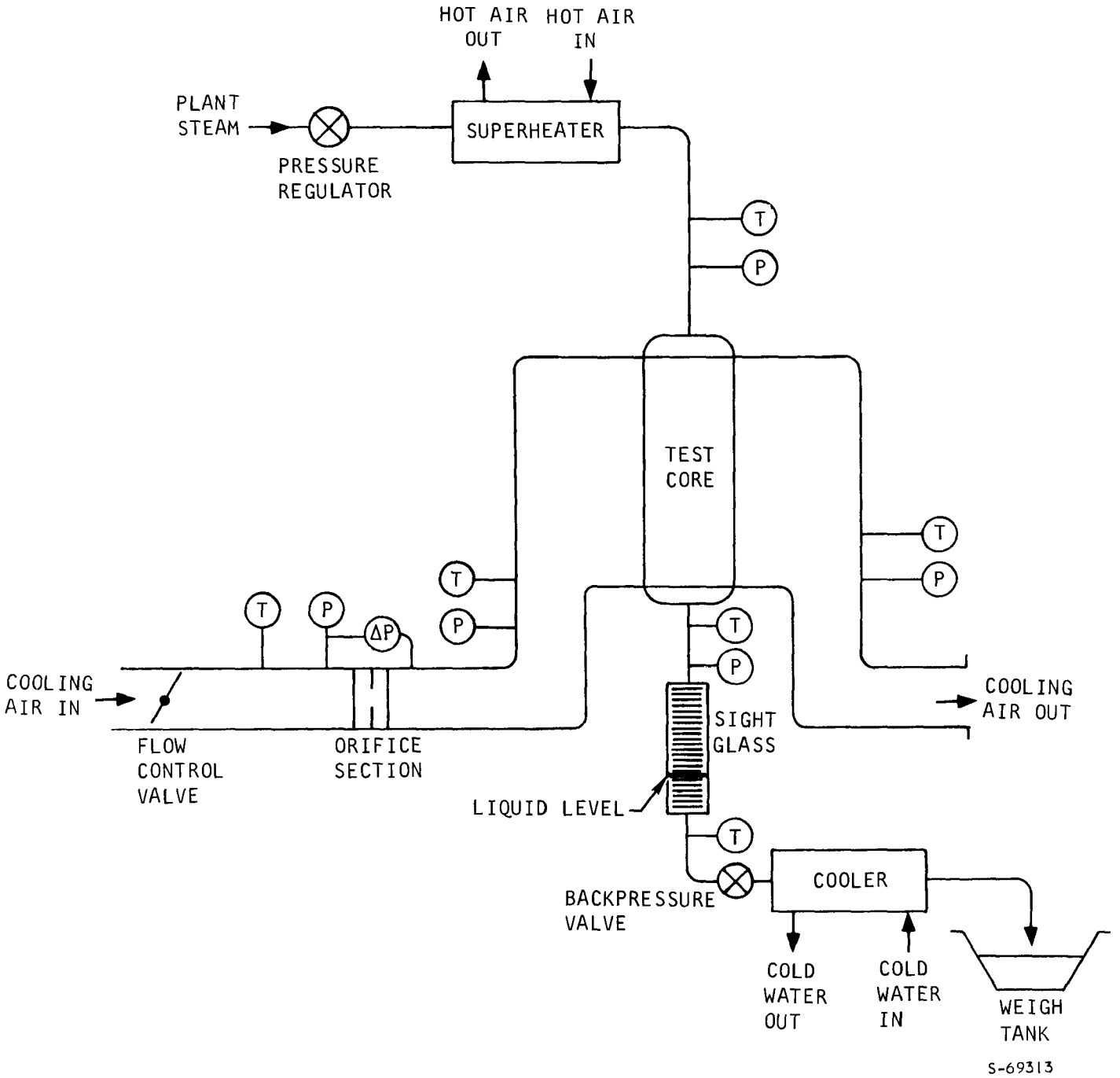

Figure 4-5. Open-System Test Schematic

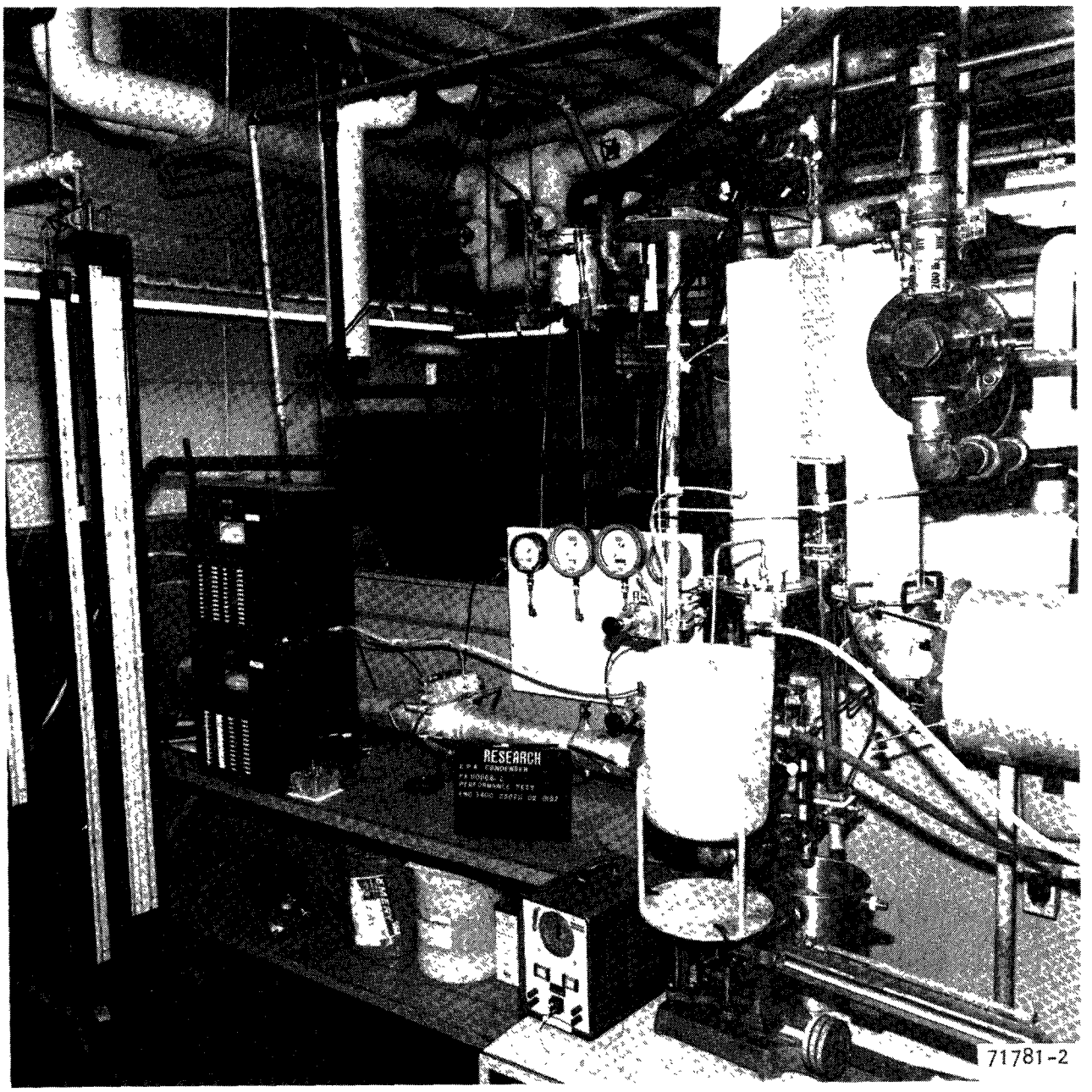

Figure 4-6. Test Setup Used for Open-System Condensing Test

latter assumption, by ignoring the possibility that portions of the condenser passages may be filled with liquid and therefore act as subcoolers, results in the calculation of an equivalent (rather than actual) UA. The equivalent UA defines the cooling capacity of the heat exchanger based on the assumption that the total core is used for desuperheat and condensing.

Results and Discussion

Results of the tests, plotted as (Test UA)÷(Predicted UA) versus air-side effectiveness, are shown in Figure 4-7. Of a total of 29 test data points taken on the three cores, five were rejected due to poor heat balances (greater than five percent difference between calculated heat rates in the hot and cold streams). Of the remaining 24 test points, four exhibited a high degree of subcooling (greater than 50°F) in the outlet liquid and are shown circled with subcooling as noted on Figure 4-7. The remaining 20 points were used in drawing the curves of condenser performance for each of the three units.

These curves show that the variable-fin core has the best performance, with a test UA ten percent greater than predicted at the design air-side effectiveness of 0.80. The offset-fin core is shown to be almost as good, with a test UA eight percent greater than predicted at design airflow; the plain-fin core exhibits the poorest performance, with a test UA three percent above predicted at design. All three cores show a rapid decrease in test UA as a percent of predicted UA at air-side effectiveness above 0.8. This is believed to be due to the increasing variation in condensation rate across the vapor flow passage as air-side ΔT increases. In addition, the variable-fin core shows a slight tendency toward reduced performance at lower air-side effectiveness, as can be expected because this core achieves optimum vapor flow distribution at only the design effectiveness of 0.80.

A possible explanation of the poor performance of the high subcooling points of Figure 4-7 is that there was a buildup of noncondensible gases above the liquid-vapor interface in these runs. The presence of noncondensibles in the core would reduce performance, and noncondensibles in the outlet manifold and sight glass could increase the measured subcooling by preventing uncondensed vapor from exiting the core and condensing on the liquid. The buildup of noncondensibles was minimized by flushing the system with steam prior to each test run data point.

No definite explanation can be given as to why the measured performance was generally higher than predicted. The high conductance ratio (vapor side÷ air side) of these cores, which ranged from about 15-to-1 to 40-to-1 over the test flow ranges, precludes the possibility that this could be due to better-than-predicted condensing coefficients. The measured air-side pressure drop, however, was 30 to 40 percent above predicted, which could be consistent with an eight to ten percent increase in heat transfer performance if this were due to irregularities in the air-side fins. To expedite fabrication of the test cores, an available offset fin was used on the air side. A perforated air-side fin, as is used on the preprotytype condensers, is still expected to meet predicted performance based on previous tests.

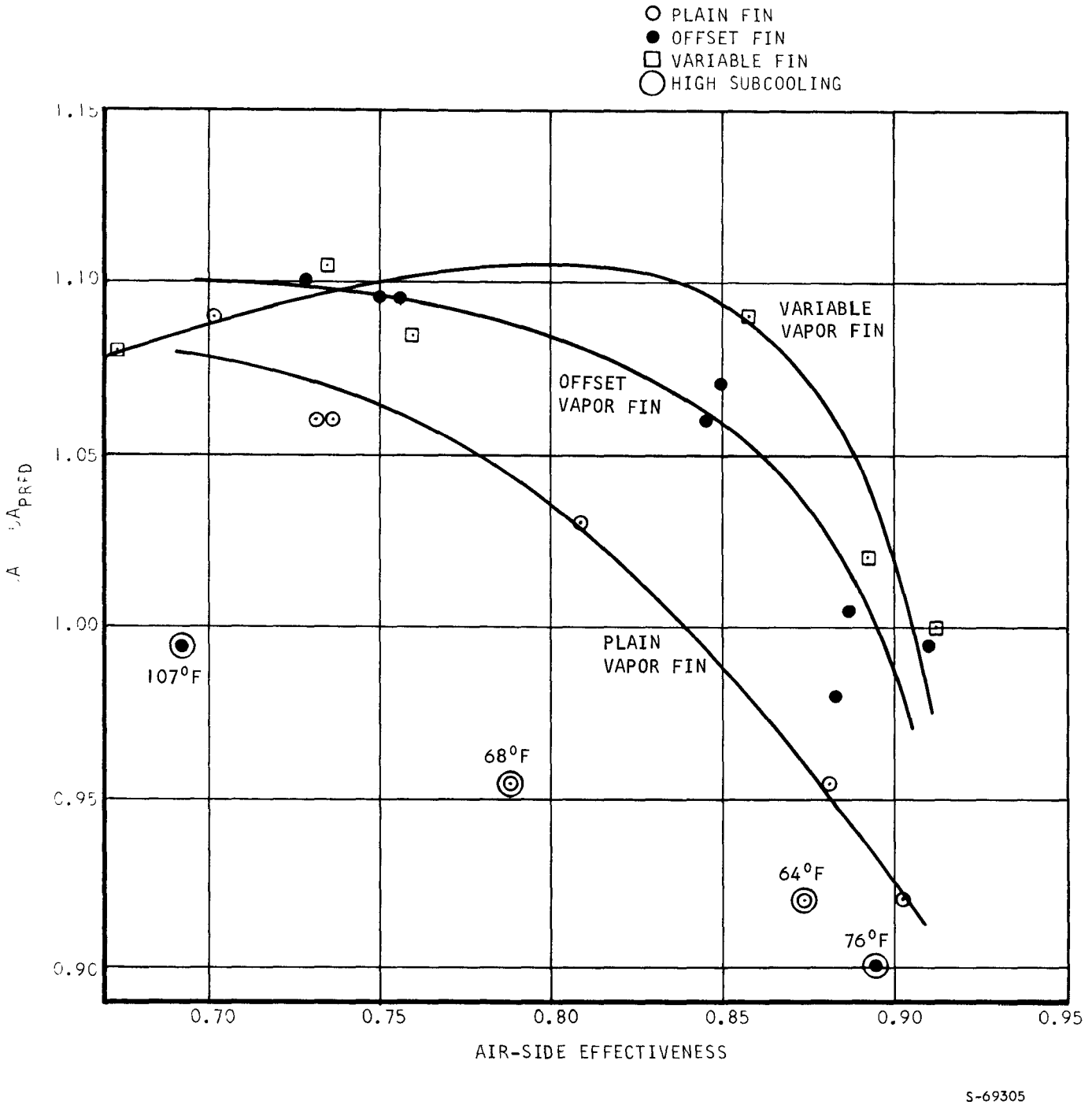

Figure 4-7. Open-System Performance of Condenser Test Modules

Based on the open-system test results, the following conclusions were drawn:

(a) The offset vapor fin performs as well or nearly as well as the variable fin in the flow range of interest and should therefore be used in the SES and TECO condenser designs.

(b) The plain vapor fin exhibits a performance penalty at design effectiveness that is probably due to variable condensation and resultant liquid fill-up of portions of individual passages. A penalty of approximately seven percent in heat rejection capability (at design flow) would be expected if this fin were used in the Aerojet condenser. The use of an offset or perforated fin in the Aerojet design would be a way of reducing this penalty.

CLOSED-SYSTEM TESTS

Test Setup and Procedure

The test setup for the closed-system condenser module tests with Fluorinol 85 as the vapor-side fluid is shown in the schematic diagram in Figure 4-8. The completed setup is depicted in Figure 4-9. The cold Fluorinol 85 fluid was pumped through a calibrated turbine flowmeter to a boiler that evaporated the liquid. The vapor was superheated approximately 50° to 60°F by a superheater before the dry vapor entered the test core. Both the boiler and the superheater were heated by hot air. A sight glass was in the Fluorinol 85 line downstream of the test core, and one was used for the boiler. During operation, a valve downstream of the test core sight glass was adjusted to maintain the liquid level at an approximately constant level in the sight glass. After passing the sight glass and control valve, the vapor was subcooled in a cooler by water before the condensate returned to the pump. The air side of the system was the same as in the open-system test where ambient air was used. The airflow was measured by a square-edged orifice section installed in accordance with the ASME power test code. Test core inlet and outlet temperatures and pressures were obtained on both the Fluorinol 85 and cooling air sides.

Testing was conducted on each of the three test cores over a range of airflows (approximately 17 to 86 lb/min) corresponding to an air-side effectiveness range of about 0.52 to 0.93. After the desuperheat portion was calculated and deducted from the core performance, the data was reduced to obtain test UA at each set of flow conditions, based on measured air-side inlet and outlet temperatures, the measured inlet temperature and average pressure on the vapor side, and the assumption of saturated liquid conditions at the vapor-side outlet. The latter assumptions, by ignoring the possibility that portions of the condenser passages may be filled with liquid and therefore act as subcoolers, results in the calculation of an equivalent (rather than actual) UA. The equivalent UA defines the cooling capacity of the heat exchanger based on the assumption that the total core less the desuperheat portion is used for condensing.

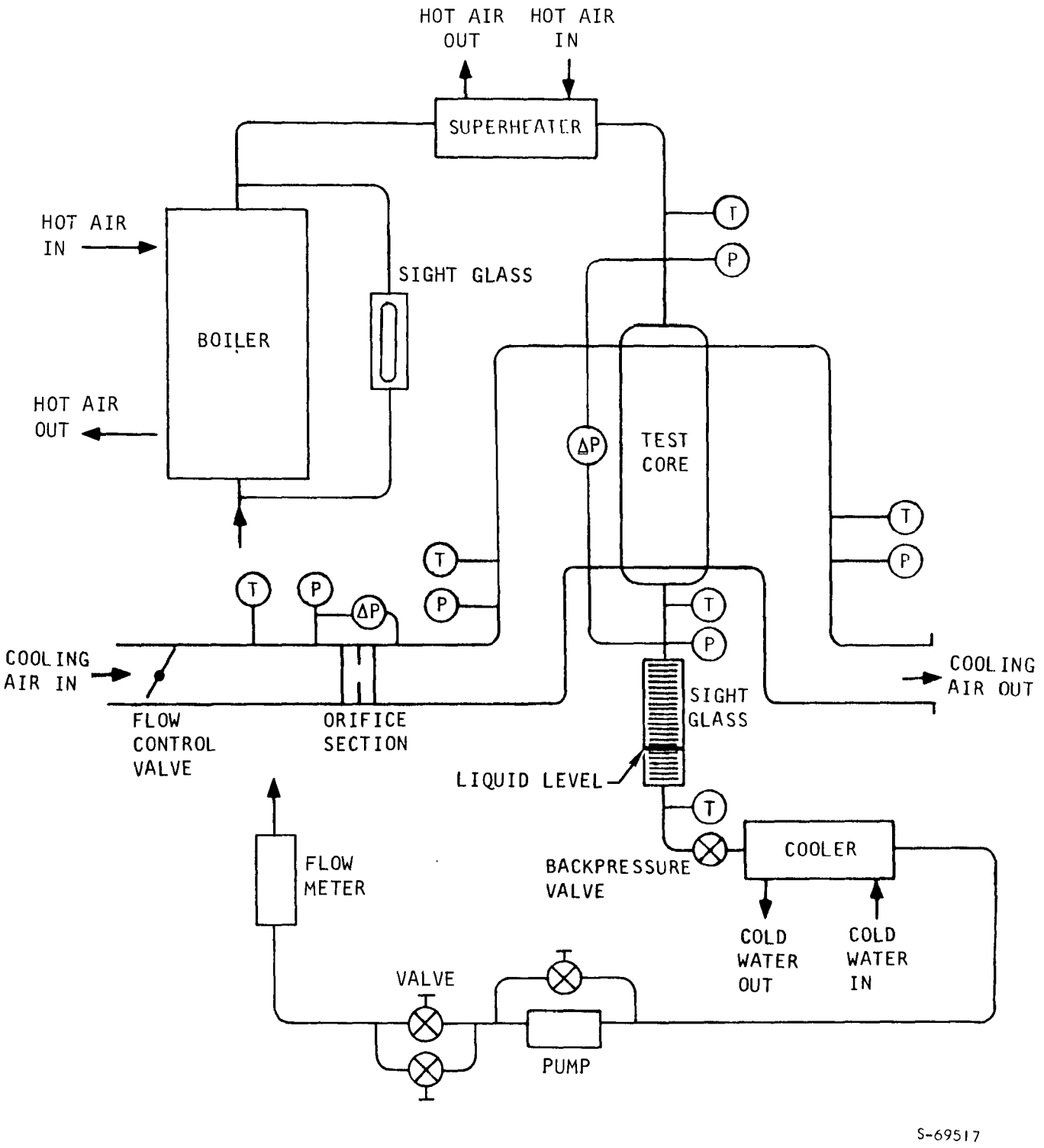

Figure 4-8. Closed-System Test Schematic

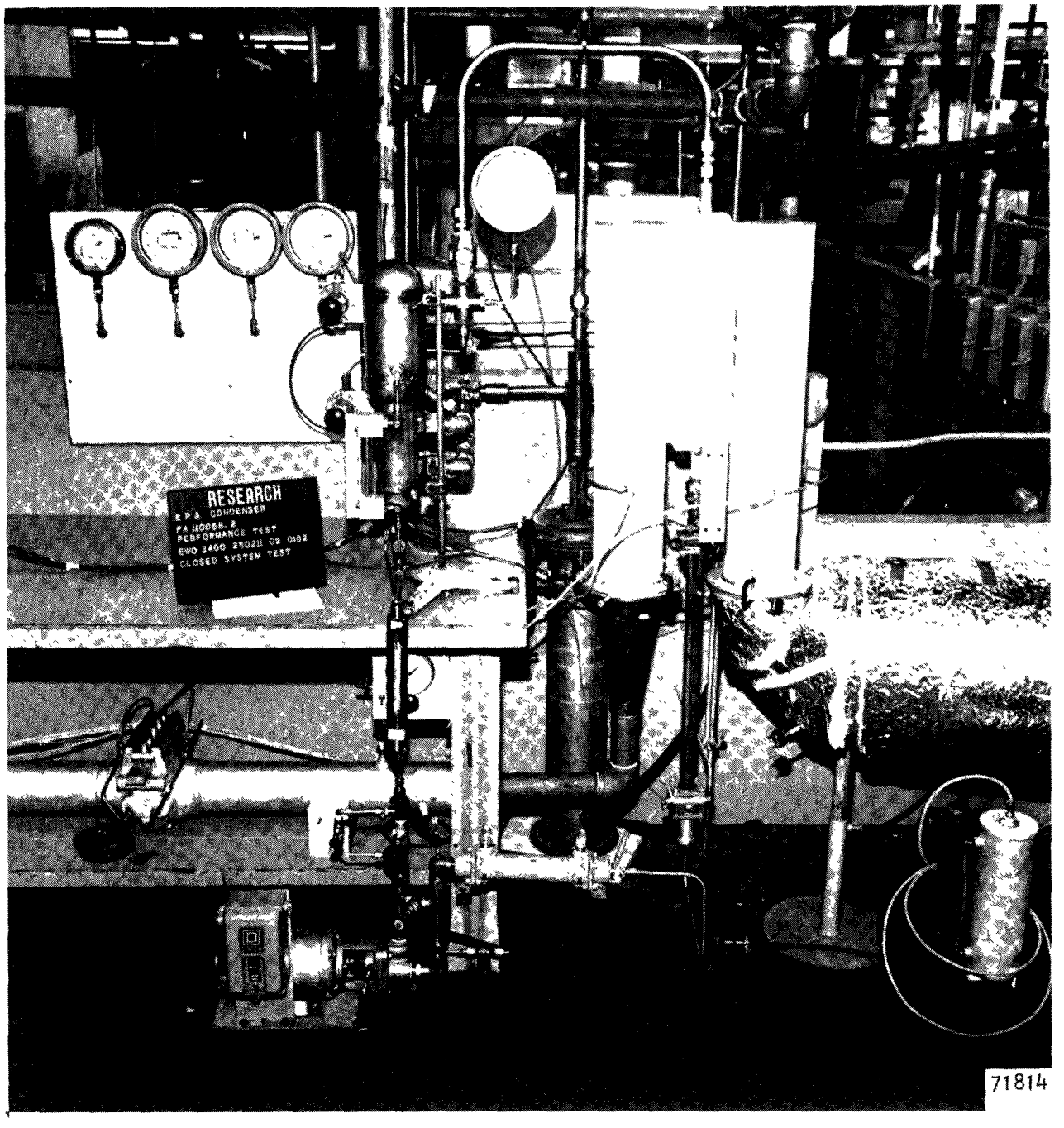

Figure 4-9. Test Setup Used for Closed System Condensing Tests

Results and Discussion

Figure 4-10 shows the test results as (Test UA)÷(Predicted UA) plotted against air-side effectiveness. A total of 16 points were taken on the three cores. One was rejected because of a very poor heat balance due to an extremely low Fluorinol 85 flow. All of the remaining 15 points were plotted; although two had heat balances between 5 and 6 percent, they plotted satisfactorily compared to the rest of the data. The curves are not similar to the curves for the open-system tests. These curves are concave instead of convex, are lower at low effectiveness rather than high effectiveness, are higher at high effectiveness, and the plain vapor fin results are farther above the predicted values than the other two fins. At the design air-side effectiveness of 0.8, the offset and variable fin results are essentially as predicted, but the plain fin results are nearly 12 percent higher than the prediction.

The amount of subcooling of the condensate was higher than in the open-system tests. To check this effect, the data points of Figure 4-10 were plotted in Figure 4-11 as a function of the subcooling. The offset fin curve of Figure 4-11 is smoother than that of Figure 4-10, although exactly the same values are plotted. Since the other two fins do not cover as wide a range of subcooling and are not as smooth, curves are not drawn through the data for these two. Figure 4-11 shows that the spread between these points is due to the difference in air-side effectiveness, which corresponds to the difference in airflow.

It is not clear why the test performance was so much higher than predicted at the high air-side effectiveness. The high air-side effectiveness points correspond to low airflows and low Fluorinol 85 flows. At airflows corresponding to the design point effectiveness of 0.8, the heat transfer conductance ratio (vapor-side divided by air-side) is on the order of 3-to-1 for the plain fin and 5-to-1 for the other two. In the case of the plain fin at high effectiveness, the Fluorinol 85 flow is in the range where the Nusselt equation for laminar condensation, as modified by McAdams, gives higher heat transfer conductances than the Soliman correlation (Reference 2). The calculated condensing heat transfer coefficient (based on Soliman) therefore could be conservative in this range of air-side effectiveness for the plain fin.

Factors influencing the data points are airflow, Fluorinol 85 flow, inlet temperature, condensing temperature, amount of subcooling, and heat balance. The curves shown in Figure 4-11 are at attempt to reduce the effect of the first four parameters. This plot involves an estimate of the desuperheat portion that varied from 8 to 13 percent of the core in the closed-system tests. Control of the subcooling was attempted by regulating the liquid level in the sight glass at the core outlet. While most of the test points had heat balances under 5 percent, heat balance is still a significant factor at the high air-side effectiveness because a 5 percent difference in the design point effectiveness of 0.80 would be 0.04, which would significantly affect the calculated test UA.

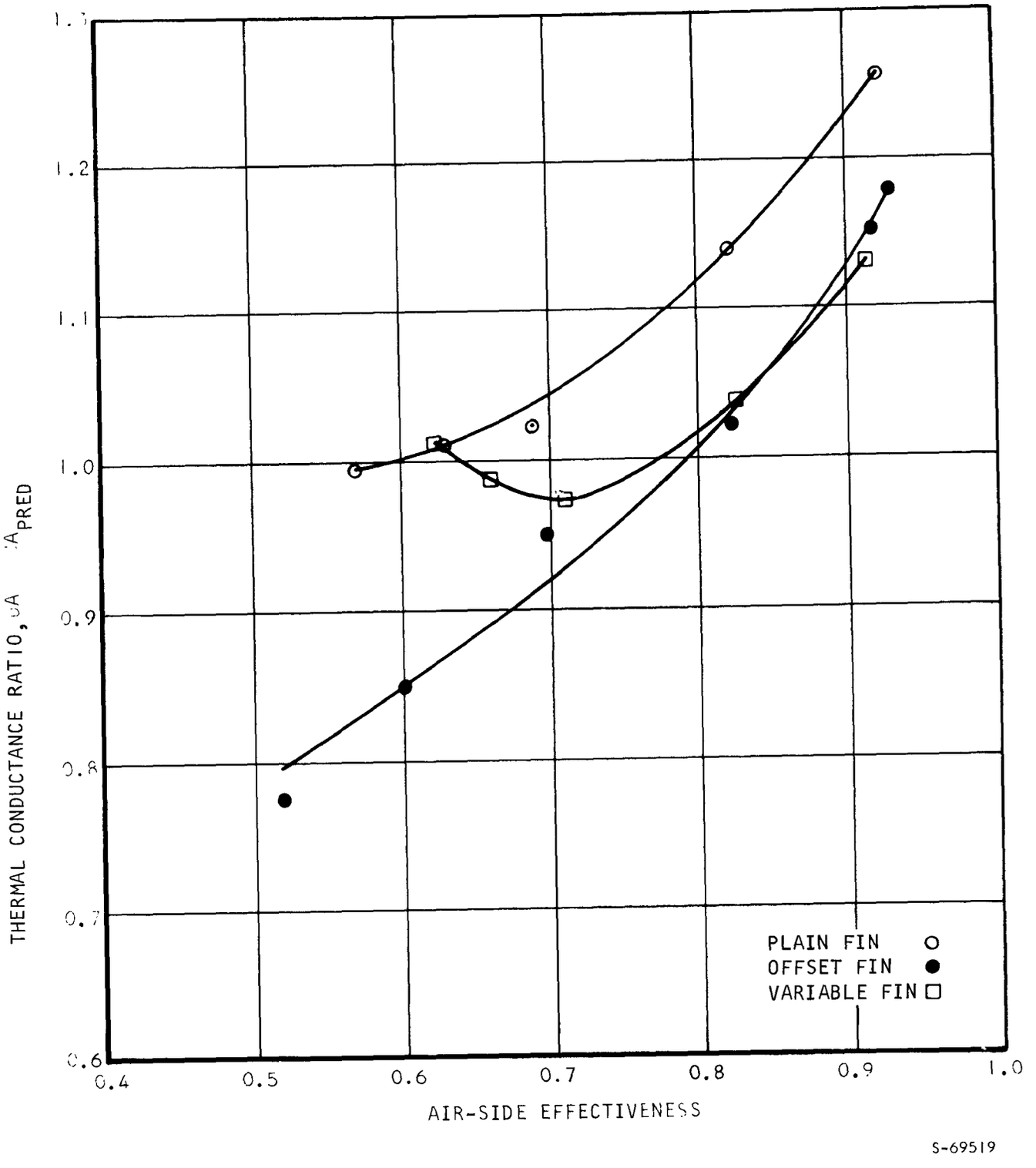

Figure 4-10. Closed-System Performance of Condenser Test Modules as a Function of Effectiveness

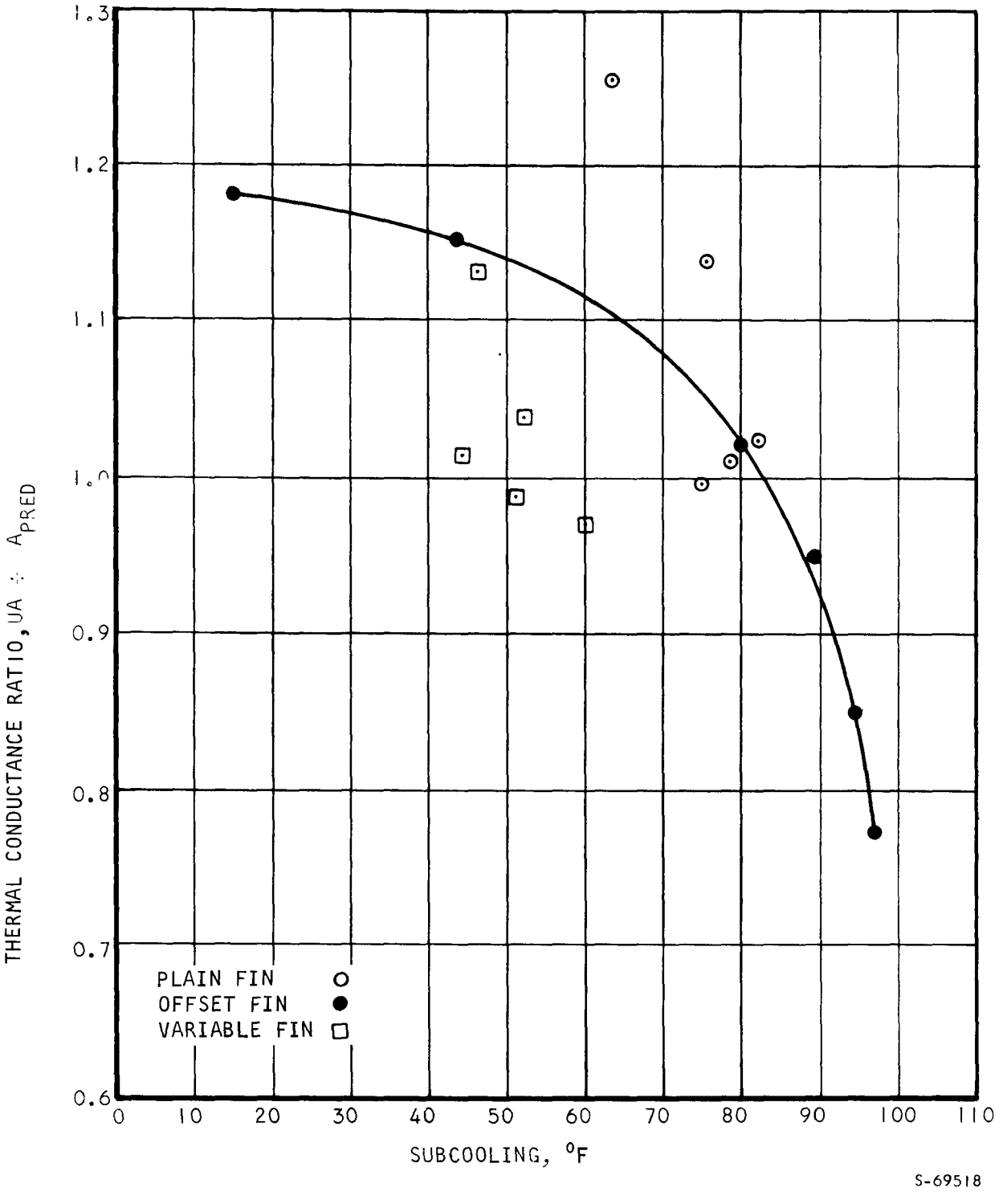

Figure 4-11. Closed-System Performance of Condenser Test Modules as a Function of Subcooling

Although the plain fin overall thermal conductance ratio, UA/UA_{PRED} is higher than that for the other two fin configurations, the overall heat transfer performance of all the fins is about the same. Consider the following test data for an airflow that yields approximately the same air-side effectiveness as that at the design point:

Vapor Fin	Airflow, lb/min	F-85 Flow, lb/min	Average Heat Transfer,* Btu/min	Initial Temperature Difference,** ^{o}F	Average Heat Transfer ÷ Initial Temperature Difference, (Btu/min)/^{o}F
Plain	27.1	3.06	667	173.5	3.84
Offset	27.0	3.28	733	189	3.88
Variable	26.8	3.40	716	186	3.85

*Total of desuperheating, condensing, subcooling
**F-85 inlet temperature - air inlet temperature

As shown in the last column, the heat transfer rate per unit temperature difference at the heat exchanger inlet is about the same for all fins. That is, overall thermal conductance, UA, of the heat exchanger is not affected by the vapor fin configuration. This result is somewhat surprising since it was believed that the offset fin would yield the best performance based on the known performance of plain and offset fins in air.

While the shape of the curves in Figure 4-10 cannot be completely explained on the basis of present theory, two factors are obviously important. In the closed-loop tests, as opposed to the open-system steam tests, the ratio of vapor-side to air-side conductance is such that an error in prediction of condensing film coefficient could lead to a significant error in predicted overall UA. Since the Soliman condensing heat transfer correlation is believed to be increasingly conservative at low flow (dropping below the laminar film prediction at a vapor flow of about 2 lb/min in the offset fin core), the UA prediction at high effectiveness is probably significantly in error from this effect. Secondly, the relatively high subcooling experienced at high vapor flow, while not explicable by present theory, is sufficient to significantly reduce performance in the low effectiveness region. An unknown in these tests is the amount of noncondensible gas in the system, which could affect both condenser performance and amount of subcooling. Since the tests were generally run in order of increasing airflow, a consistent buildup of noncondensibles would have the greatest effect on the high-flow, low-effectiveness points. Since both of the above sources of error (i.e., the effect of inaccurate condensing heat transfer prediction and the possible presence of noncondensibles) were minimized during the open-system steam tests, it is believed that the

open-system test results represent the more accurate prediction of the effect of variable condensation rate on condenser performance. The closed-loop tests serve to verify that predicted performance is obtained at the design effectiveness of 0.80 but are less useful in identifying the effect of a single factor such as variable condensation.

SECTION 5

CONDENSER DESIGN, FABRICATION, AND TEST

SECTION 5

CONDENSER DESIGN, FABRICATION, AND TEST

HEAT TRANSFER DESIGN

Condenser design requirements as established by the system contractors are summarized in Table 5-1. Based on the requirements, a specific condenser was designed for each contractor, accounting for the differences in working fluids, heat rejection rates, operating temperatures and pressures, and installation requirements.

A computer program for the calculation of condensing heat transfer coefficients and two-phase pressure drop was written. This program was then combined with an existing AiResearch performance prediction program to provide a tool for analysis and design of condensing heat exchangers.

All three condensers utilize the same perforated fin on the air side, its selection being based on the test results presented in Section 3 in conjunction with the previous testing reported in Reference 1. The air-side fin has a fin pitch of 22 fins per in., a fin height of 0.326 in., a fin thickness of 0.004 in., and the -13 perforation geometry. The -13 perforations are rectangular slots with a slot width of 0.030 in. and a slot spacing such that an open area of approximately 25 percent is obtained. Reference 1 should be consulted for a complete description of the geometry and heat transfer performance of this surface.

Selection of the condensing side fin geometry was based on obtaining maximum heat transfer performance within the allowable pressure drop specified for each condenser. In addition, the condensing test described in Section 4 indicated the desirability of using a surface that allows some transverse flow (crossflow) of the vapor within the heat exchanger core. Vapor crossflow improves overall heat exchanger performance by increasing the rate at which vapor is supplied to the areas of high condensation rate (i.e., passages near the air inlet face). For the TECO and SES condensers, an offset fin was found to be optimum for this application. For the Aerojet condenser, where pressure drop is limiting, a perforated fin is used in the condensing section and an offset is used in the subcooler.

The following paragraphs present a discussion of the condenser computer program that was written during this task, the heat transfer analysis, and the design of each of the three condensers.

Condensing Heat Transfer and Pressure Loss

This program for the calculation of condensing coefficients and two-phase flow pressure drop was written using the correlation of Soliman et al (Reference 2). Correlations presented in the referenced paper are used in the program to calculate local and average condensing coefficients with modifications for plate fin heat exchanger applications. A brief description of the program is given in the following paragraphs.

TABLE 5-1

CONDENSER DESIGN REQUIREMENTS

System Contractor	Aerojet	Thermo Electron	Steam Engine Systems
Vapor Side			
Working fluid	AEF-78	Fluorinol 85	Water
Total heat rejection, Btu per hr	1.50×10^6	1.88×10^6	1.21×10^6
Flow, lb/hr	20,000	9,860	1,285
Inlet temperature, ^oF	241	238	258
Inlet pressure, psia	32.7	40.0	34.0
Condensing temperature (avg), ^oF	235	212	256
Condensing pressure (avg), psia	31.3	36.4	33.3
Liquid outlet temperature, ^oF	192.5	193	256
Subcooling, ^oF	38.5	17.0	0.0
Core pressure drop, psi	2.8	2.6	0.6
Over-all pressure drop, psi	3.1	5.0	1.0
Maximum operating conditions	50 psig at 300^oF	100 psig at 300^oF	35 psig at 280^oF
Maximum allowable leakage, std cc per sec of helium	1×10^{-6}	1×10^{-6}	No visible leakage
Air Side			
Flow, lb/hr	52,000	75,300	38,200
Inlet temperature, ^oF	85	85	85
Inlet pressure, psia	14.7	14.7	14.7
Outlet temperature, ^oF	205	189	217
Temperature effectiveness	0.80 Condenser 0.62 Subcooler	0.80	0.763
Overall core pressure drop, in. H_2O	4.0	4.1	2.1

The heat transfer and pressure drop equations are as follows:

$$h_z = 0.036 \frac{k_\ell \rho_\ell^{1/2}}{\mu_\ell} Pr_\ell^{0.65} F_o^{1/2} \tag{1}$$

$$F_o = F_f + F_m + F_a \tag{2}$$

$$F_f = \left(\frac{G_T^2}{2\rho_v}\right) f_v \left[x^{1.80} + 5.7 \left(\frac{\mu_\ell}{\mu_v}\right)^{0.0523} (1 - x)^{0.47} x^{1.33} \left(\frac{\rho_v}{\rho_\ell}\right)^{0.261} + 8.11 \left(\frac{\mu_\ell}{\mu_v}\right)^{0.105} (1 - x)^{0.94} x^{0.86} \left(\frac{\rho_v}{\rho_\ell}\right)^{0.522} \right] \tag{3}$$

f_v = friction factor evaluated at Re_T
[For round tube, $f_v = 0.045 (Re_T)^{-0.2}$]

$$F_m = - \left(\frac{G_T^2}{2\rho_v}\right)\left(\frac{D}{2Lo}\right) \left[2(1 - x) \left(\frac{\rho_v}{\rho_\ell}\right)^{2/3} + \left(\frac{1}{x} - 3 + 2x\right) \left(\frac{\rho_v}{\rho_\ell}\right)^{4/3} + (2x - 1 - 1.25x) \left(\frac{\rho_v}{\rho_\ell}\right)^{1/3} + \left(2.5 - \frac{1.25}{x} - 1.25x\right) \left(\frac{\rho_v}{\rho_\ell}\right)^{5/3} + 0.5(x - 1) \left(\frac{\rho_v}{\rho_\ell}\right) \right] \tag{4}$$

$$F_a = g \sin \theta \, (\rho_\ell - \rho_v)(1 - \alpha) \frac{D}{4} \tag{5}$$

$$\alpha = \frac{1}{1 + \left(\frac{1 - x}{x}\right) \left(\frac{\rho_v}{\rho_\ell}\right)^{2/3}} \tag{6}$$

$$\frac{dP}{dz} = - \frac{4}{g_c D} F_o(z) \tag{7}$$

For the derivation of the above equations reference may be made to the original paper.

The average condensing heat transfer coefficient is calculated by integrating the local coefficient between the inlet and exit qualities.

$$h_{av} = \frac{1}{(x_2 - x_1)} \int_{x_1}^{x_2} h_z dz \qquad (8)$$

This program can be used as an individual program and has also been incorporated as a subroutine into the AiResearch plate-fin heat exchanger performance program. The resultant program, called HI000, was used for final sizing of the three condensers.

Effect of Oil Film

In the Thermo Electron and Steam Engine Systems designs, a small amount of oil is expected to blow by the pistons in the expander and become entrained in the condenser inlet vapor. It is expected that this oil will form a film on the condenser surfaces thereby introducing an additional thermal resistance on the condensing side. An analysis was performed to estimate the oil film thicknesses and the magnitude of the additional resistance.

With an oil film present in the condensate, the wall shear stress $F_o(x)$ given in Equation 2 is assumed at the interface between the oil film and the condensate. Figure 5-1 shows the model used in the analysis.

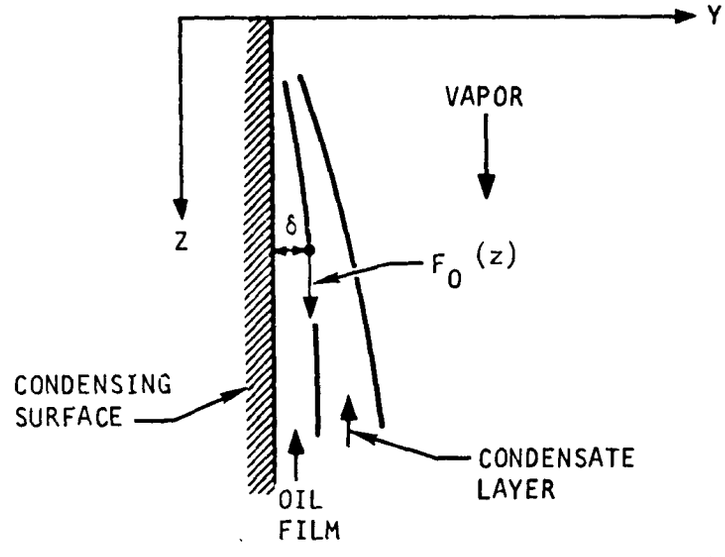

Figure 5-1. Model Used in Oil Film Analysis

A force balance on the oil film gives

$$F_o + (\delta - y)\, \rho_{oil}\, g \sin\theta = \mu_{oil} \frac{du}{dy} \quad .$$

or

$$u = \frac{F_o}{\mu_{oil}} y + \frac{\rho_{oil}\, g \sin\theta}{\mu_{oil}} \left(\delta y - \frac{1}{2} y^2\right)$$

The oil film flow rate at any location z is

$$W_{oil\ film} = \rho_{oil}\, S \int_o^{\delta} u\, dy$$

or

$$W_{oil\ film} = \rho_{oil}\, S \left[\frac{F_o\, \delta^2}{2\mu_{oil}} + \frac{\rho_{oil}\, g \sin\theta\, \delta^3}{3\mu_{oil}}\right] \qquad (9)$$

The local oil film flow rate is a function of the total oil flow (W_{oil}) entering the condenser which must be given in the problem statement. There are two assumptions made in relating the total oil flow to the local oil film flow rate:

(a) Constant oil film flow rate ($W_{oil\ film} = W_{oil}$): This model assumes that all the oil mist is separated from the vapor at the inlet of the condensing channel. This will give a maximum calculated oil film thickness.

(b) Constant oil deposite rate [$W_{oil\ film} = (1 - z)W_{oil}$]: This model assumes that the oil mist is completely mixed with the condensing vapor at the entrance to the condenser. The deposit rate of the oil mist is assumed to be equivalent to the vapor condensing rate.

Calculation of the oil film thickness was incorporated into the condensing computer program. The program calculates oil film thicknesses and equivalent condensing heat transfer coefficients which account for the oil film based upon both of the above assumptions.

The average equivalent heat transfer coefficient is

$$h_{av,eq} = \frac{1}{x_2 - x_1} \int_{x_1}^{x_2} h_{z,eq}\, dz \qquad (10)$$

where

$$\frac{1}{h_{z,eq}} = \frac{1}{h_z} + \frac{\delta_{oil}}{k_{oil}} \qquad (11)$$

The program was used to calculate the average oil film thickness and the average equivalent heat transfer coefficient as a function of the percentage of oil in the inlet flow for the Thermo Electron and Steam Engine Systems preliminary condenser designs. The results are shown in Figures 5-2 and 5-3. The oil film thickness is shown for both of the assumptions regarding local oil film flow rate. The average equivalent heat transfer coefficients are shown with and without oil films. The actual percentage of oil in the inlet vapor has not been established but it is thought to be less than 0.1 percent. The analysis predicts reduction in condensing coefficients of 10 to 20 percent at this oil concentration.

TECO Condenser

The final problem statement for the TECO condenser is shown in Table 5-1. The Fluorinol-85 working fluid enters the condenser as superheated vapor at 238°F and 40 psia and leaves as subcooled liquid at 193°F. The total heat load of 1.88×10^6 Btu/hr is divided into approximately 0.065×10^6 Btu/hr desuperheat, 1.70×10^6 Btu/hr condensing, and 0.118×10^6 Btu/hr subcooling (referred to the initial condensing pressure of 40 psia). In addition to the thermodynamic design requirements of Table 5-1, packaging requirements impose dimensional limits of 22.5 in. on the height, 58 in. on the width, and 4.5 in. on the airflow length of the condenser.

The fractions of the condenser required for desuperheat, condensing, and subcooling were determined from separate performance calculations of each section. The performance calculations were made for a constant airflow length of 4.25 in. and assumed maximum total core frontal dimensions of 58 in. by 20.8 in. (allowing 1.7 in. for the Fluorinol-85 manifolds). Results of the calculations were plotted as (UA-calculated) ÷ (UA-required) vs the condensing section fraction, as shown in Figures 5-4 and 5-5. The intersection points in these figures provide the estimated ratios of condensing section size to desuperheat section size and condensing section size to subcooling section size. Combining the results from the two figures yields a desuperheat fraction of 0.042, a condensing fraction of 0.879, and a subcooling fraction of 0.079.

Having established that 87.9 percent of the vapor-side flow length is available for condensing, the condenser performance was calculated as a function of condenser airflow length. The results are plotted in Figure 5-6.

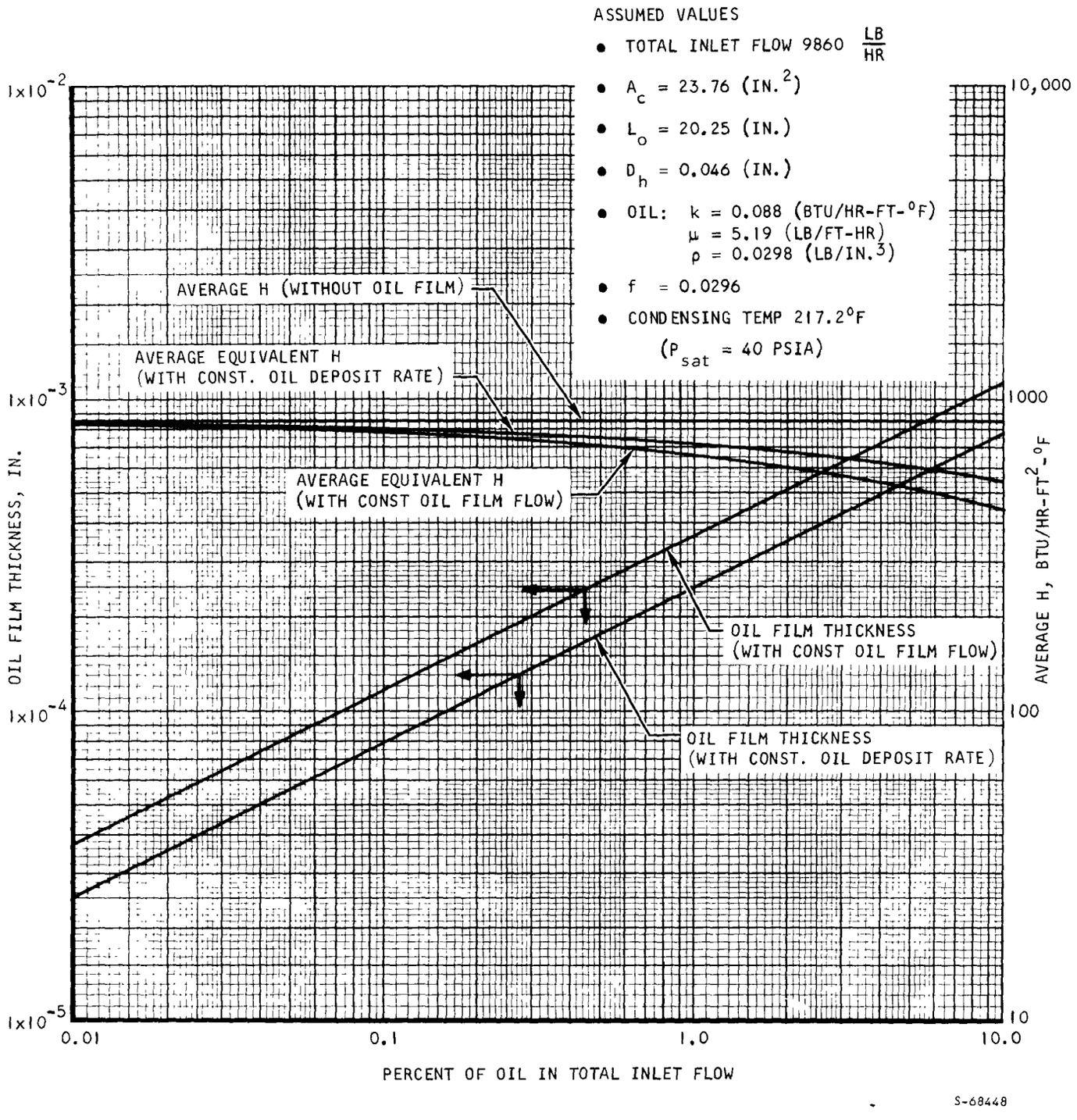

Figure 5-2. Estimated Condensing Heat Transfer Coefficient and Oil Film Thickness for Fluorinol-85 Condenser with/without Oil Film

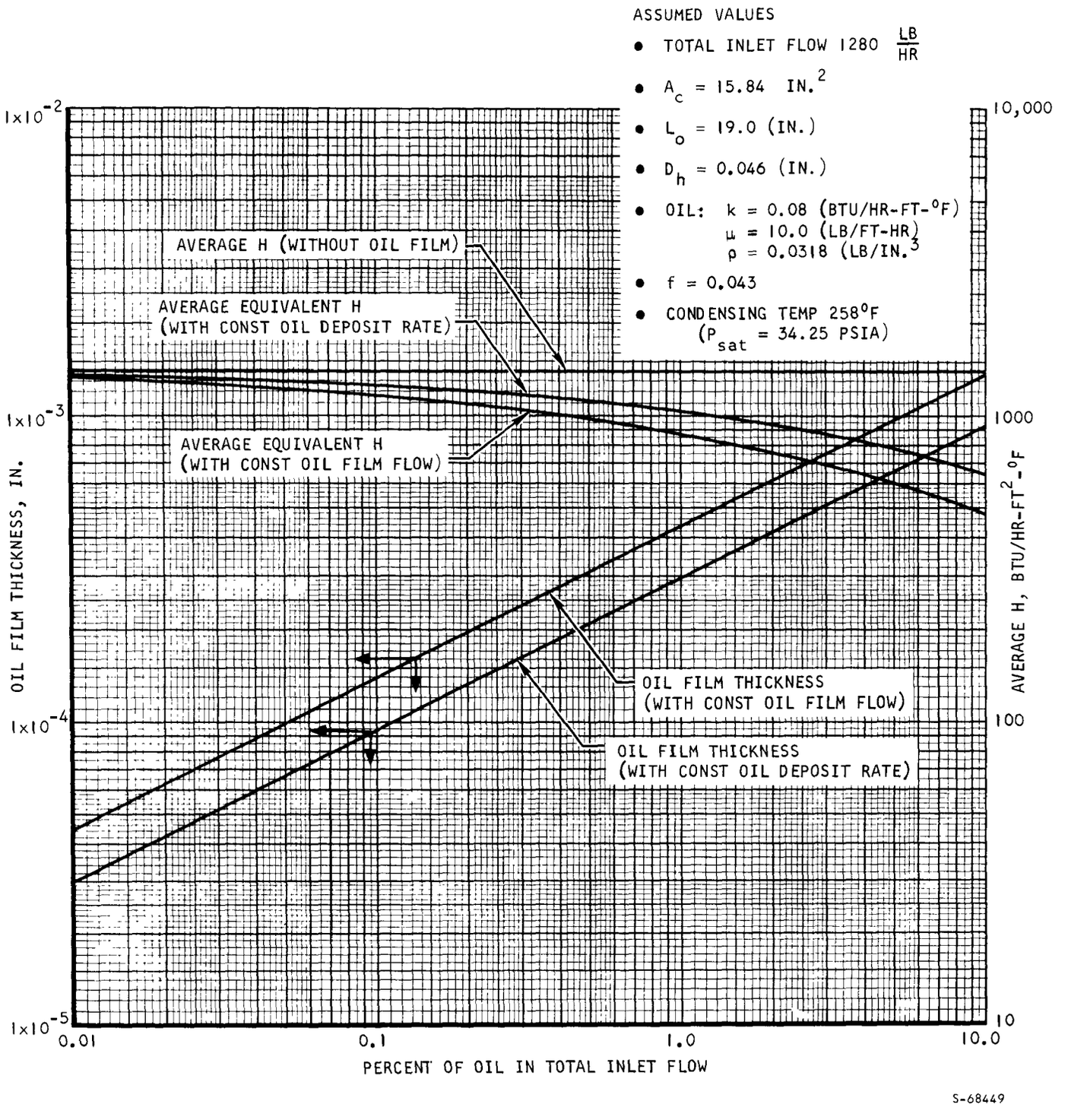

Figure 5-3. Estimated Condensing Heat Transfer Coefficient and Oil Film Thickness for Steam Consenser with/without Oil Film

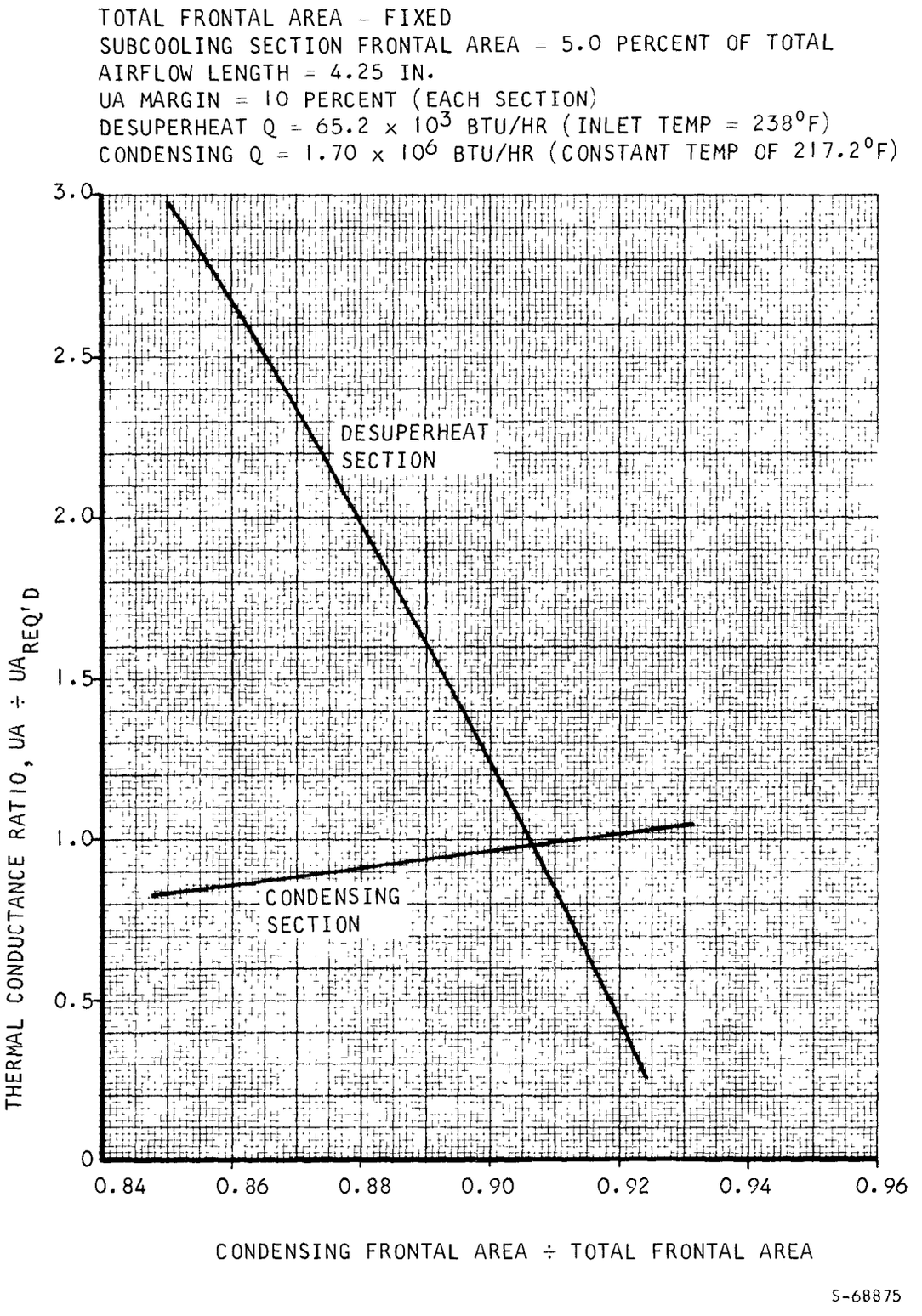

Figure 5-4. TECO Condenser Performance Calculations, Desuperheat and Condensing Section

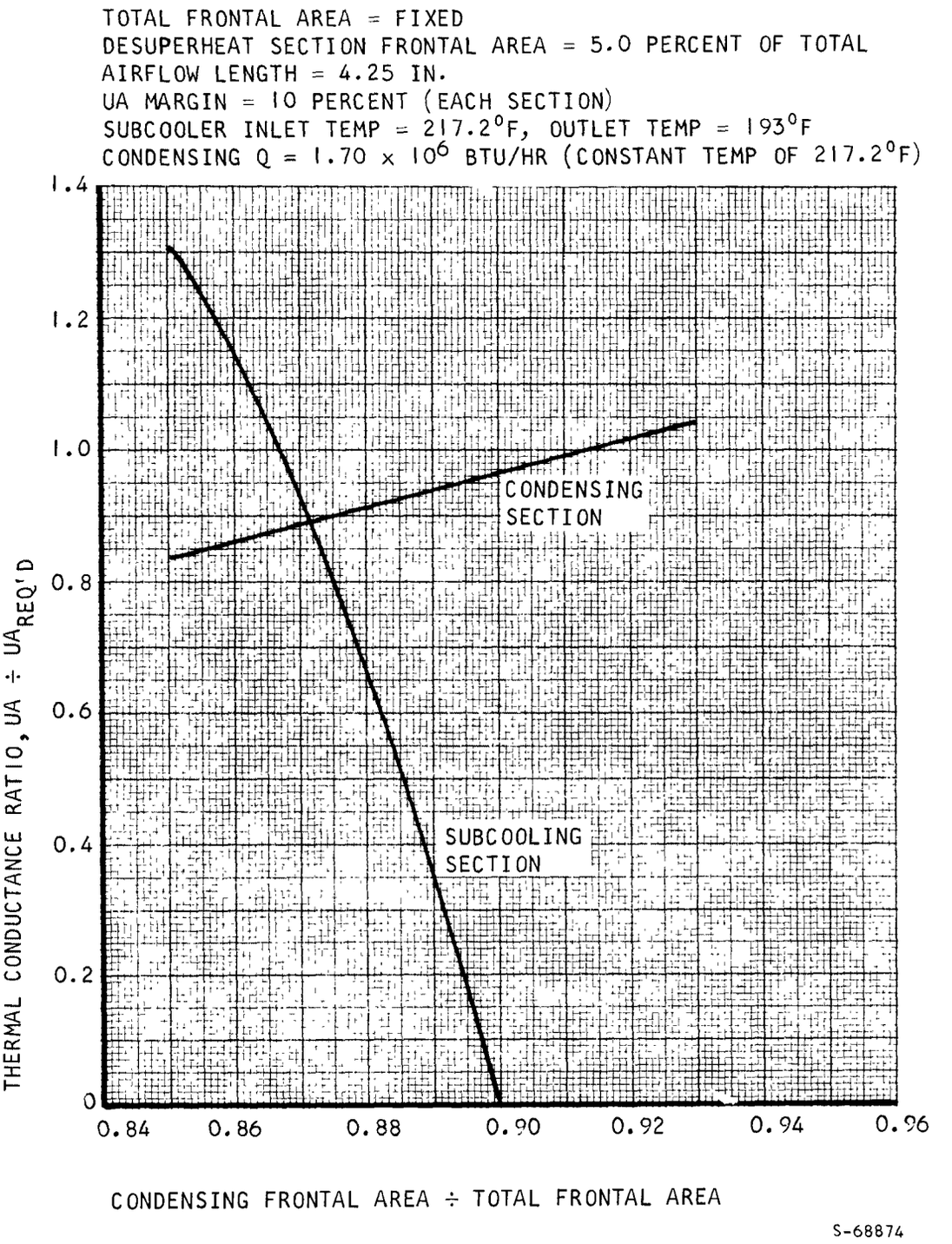

Figure 5-5. TECO Condenser Performance Calculations, Condensing and Subcooling Sections.

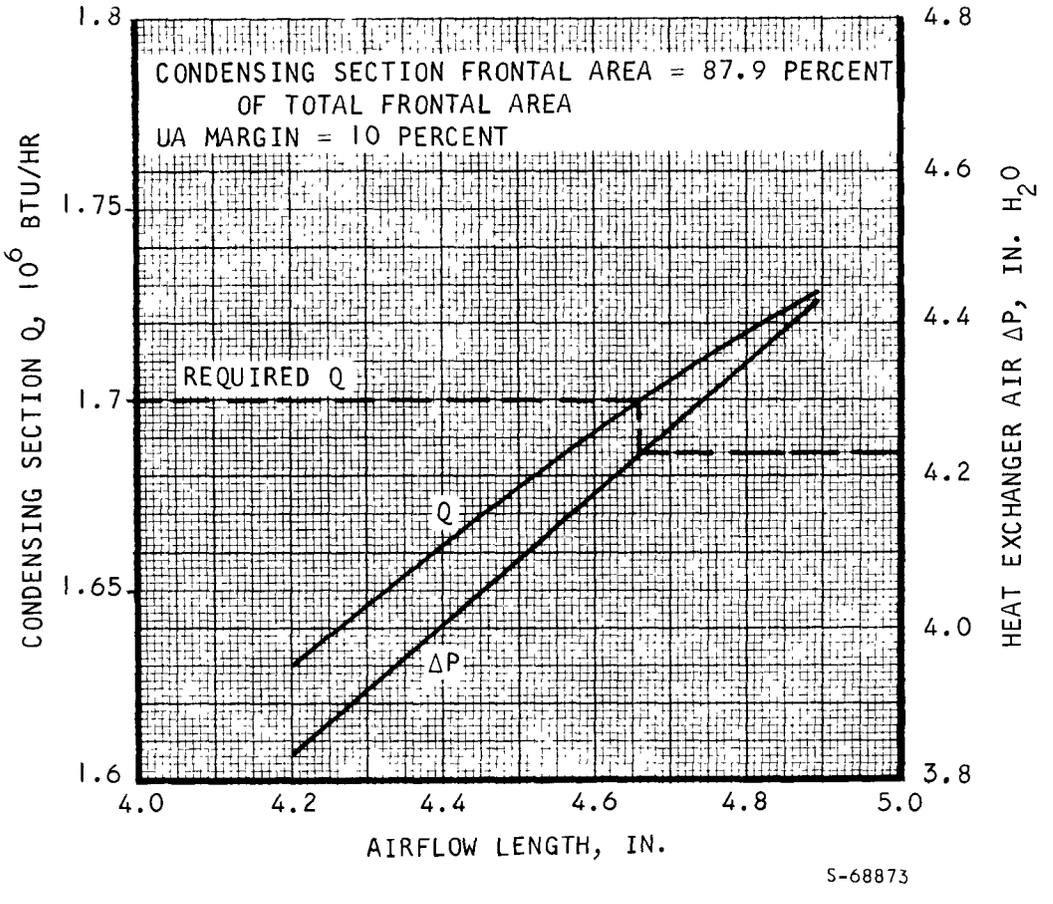

Figure 5-6. Variation of Heat Rejected with Airflow Length for Condensing Section of TECO Condenser

With a required condensing heat load of 1.70×10^6 Btu/hr, the required airflow length is 4.66 in. and the air pressure drop is 4.23 in. H_2O. The required airflow length of 4.66 in. exceeds the specified envelope and it was therefore decided to reduce this dimension to the specified maximum length of 4.50 in. A performance analysis of the 4.50-in. condenser indicates that it meets performance on a theoretical basis but does not contain the amount of UA margin usually required to compensate for such factors as flow maldistribution and manufacturing tolerances. As a result, it is considered marginal as to whether this condenser will reject the full required heat load of 1.88×10^6 Btu/hr under specified design conditions. The indicated heat rejection rate is instead 1.68×10^6 Btu/hr for the condensing section alone and 1.85×10^6 Btu/hr total.

The final design of the TECO condenser is summarized in Table 5-2. The Fluorinol-85 core pressure drop in this design is 2.6 psi and the estimated manifold loss (vapor plus liquid) is 2.3 psi, yielding a total Fluorinol-85 pressure drop of 4.9 psi. The air pressure drop, from Figure 5-6, is 4.09 in. H_2O. The values of air pressure drop given here and for the other condensers include a one-half velocity head loss at the inlet face and an exit loss based on on an exit duct area equal to the frontal area of the core.

TABLE 5-2

TECO CONDENSER DESIGN SUMMARY

Airflow length	4.50 in.
Vapor-side flow length (core only)	20.8 in.
Width	57.8 in.
Air-side fins (nominal)	Perforated (-13)
Height	0.326 in.
Thickness	0.004 in.
Fins/in.	22
Vapor-side fins	Offset rectangular
Height	0.050 in.
Thickness	0.004 in.
Fins/in.	20

Aerojet Condenser

The Aerojet condenser consists of two separate units, arranged to form a T-shaped frontal area, with the upper unit sized for the condensing load only, with no subcooling, and the lower unit sized to have the same airflow length as the condenser and utilize the maximum available air-side frontal area. The problem statement for the condenser is given in Table 5-1. The AEF 78 enters as saturated vapor at 241°F and 32.7 psia. The condensing heat load is 1.25 x 10^6 Btu/hr, and a minimum subcooling of 38°F is required at the outlet from the subcooling unit.

Detail design of the Aerojet condensers resulted in the adoption of a modular approach to accommodate manufacturing requirements. The condenser was brazed as four separate modules and the modules welded together to form a single unit. Similarly, the subcooler consists of three modules. Each module in the condenser consists of alternating air and vapor sandwiches. The passage heights are 0.326 in. and 0.050 in. for air and vapor, respectively, with the exception that the passages adjacent to the module side plates are air passages with a height of 0.163 in. (i.e., 22R-.163-Perf (-13)-.004). For calculation purposes, the equivalent sandwich structure was assumed to be 116 vapor sandwiches and 116 air sandwiches of nominal height. Each module in the subcooler consists of alternating air and liquid sandwiches, with air sandwiches of half nominal height (i.e., 22R-.163-Perf (-13)-.004) again adjacent to the side plates. The equivalent sandwich structure for calculating subcooler performance was taken as 87 vapor sandwiches and 87 air sandwiches of nominal height.

Based on the results of the Task 2 tests, it was decided to use a perforated fin for the vapor-side heat transfer surface in the condenser. This fin provides open area for transverse vapor flow redistribution with less of a pressure drop penalty than would be incurred with the use of an offset fin. The perforation geometry used is the -15 geometry (Reference 1), which has a slot width of 0.030 in. and an open area of approximately 12.5 percent. In the subcooler, where pressure drop is less critical, an offset fin is used.

The airflow length for the final design, as required to reject the condensing load in the condenser, is 4.65 in. With this airflow length, the liquid outlet temperature from the subcooler is 192.5°F. Vapor-side pressure drops are 2.64 psi in the condenser and 0.06 psi in the subcooler. Additional manifold losses are estimated to be approximately 0.3 psi, resulting in a total heat exchanger pressure loss of 3.0 psi and an outlet pressure of 29.7 psia. The saturation temperature corresponding to this outlet pressure is 231°F, giving a subcooling ΔT of 38.5°F. Air-side pressure loss is 3.95 in. H_2O. The final design of the Aerojet condenser is summarized in Table 5-3. Total heat rejection at design conditions is 1.50 x 10^6 Btu/hr, including 0.25 x 10^6 Btu/hr in the subcooler.

TABLE 5-3

AEROJET CONDENSER DESIGN SUMMARY

Condensing Unit	
Airflow length	4.65 in.
Vapor flow length (core only)	14.65 in.
Width	48.24 in.
Air-side fins (nominal)	Perforated (-13)
Height	0.326 in.
Thickness	0.004 in.
Fins/in.	22
Vapor-side fins	Perforated (-15)
Height	0.050 in.
Thickness	0.004 in.
Fins/in.	20
Subcooling Unit	
Airflow length	4.65 in.
Vapor flow length (core only)	4.90 in.
Width	36.22 in.
Air-side fins (nominal)	Perforated (-13)
Height	0.326 in.
Thickness	0.004 in.
Fins/in.	22
Vapor-side fins	Offset rectangular
Height	0.050 in.
Thickness	0.004 in.
Fins/in.	20

SES Condenser

The SES design requirements are shown in Table 5-1. The steam enters the condenser as saturated vapor and leaves as saturated liquid, with no subcooling called for by the problem statement. Subcooling is not desirable in this system due to the possibility of freezing that would occur with the existence of a liquid level in the condenser core. The absence of any subcooling poses the requirement for a uniform fluid state (saturated liquid) at the fluid outlet, independent of transverse position. The vapor-side fin geometry shown in Figure 4-1 was proposed as one method of achieving this result. The variable flow resistance of the Figure 4-1 passage is such that the transverse vapor flow distribution matches to the vapor-to-air ΔT variation, resulting in a vapor flow in each parallel flow path proportional to the local heat rejection rate in that path. By matching local vapor flow rate to local heat rejection rate, uniform fluid conditions are obtained at the fluid outlet. It was inferred from the condensing heat transfer test results, however, that with the use of a single offset fin on the vapor side there is a sufficient amount of transverse redistribution of vapor flow within the core to accomplish essentially the same result. For this reason, an offset fin geometry was selected in preference to the more complex variable geometry of Figure 4-1.

The overall heat exchanger design is summarized in Table 5-4. Steam-side pressure drop for this design is 0.6 psi for the core and approximately 1.0 psi total. Air-side pressure loss is 2.09 in. H_2O.

TABLE 5-4

SES CONDENSER DESIGN SUMMARY

Airflow length	4.0 in.
Vapor-side flow length (core only)	19.0 in.
Width	48.0 in.
Air-side fins (nominal)	Perforated (-13)
Height	0.326 in.
Thickness	0.004 in.
Fins/in.	22
Vapor-side fins	Offset rectangular
Height	0.050 in.
Thickness	0.004 in.
Fins/in.	20

STRUCTURAL CONSIDERATIONS

A structural analysis was performed on the three system condensers. This structural analysis consisted of the following elements:

(a) Pressure containment

(b) Thermal stresses

(c) Supporting structure

The information on each of the condensers is presented in the following paragraphs:

Pressure Containment

Pressure containment strength has been based on the maximum operating temperature and pressure in the condenser. The strength criteria for design based on short-time material properties were that stresses at proof pressure not exceed the material yield strength and that the stresses at burst pressure not exceed the material ultimate strength. For creep limited design, the long-term load conditions are compared with the life of the material based on a Larson-Miller plot of the material stress rupture at the operating temperature. The design of the condensers was based on the following conditions for the three condensers:

(a) Aerojet condenser (190390)

Maximum operating pressure = 50 psig at 300°F

Proof pressure = 100 psig at 70°F

(b) TECO condenser (190370)

Maximum operating pressure = 85 psig at 300°F

Proof pressure = 183 psig at 70°F

(c) SES condenser (190640)

Maximum operating pressure = 35 psig at 280°F

Proof pressure = 86 psig at 70°F

The calculated pressure stresses for the three condensers are summarized in Tables 5-5 through 5-7.

1. Aerojet Condenser (190390)

A structural schematic of this condenser is shown in Figure 5-7. For the normal operating conditions of 18 psig at 241°F for a life of 3500 hr, the highest operating stresses are 5.4 ksi in the middle pan and 3.1 ksi in the flat inlet duct. For these low operating stresses at 241°F, the creep stresses will have a factor of safety of 6.5 on the stresses and a factor of better than 100 to 1 on the operating life of the condenser.

TABLE 5-5

SUMMARY OF PRESSURE STRESSES IN THE
190390 CONDENSER FOR AEROJET

PROOF PRESSURE STRESSES, 100 PSIG AT 70°F

Part (See Figure 5-7)	Aluminum Alloy and Dimensions in.	Load	Stress ksi**	Min. F_{ty} ksi*	Margin of Safety
Top pan at weld	6061 T4 t = 0.10	Weld Tension	4.0	18.0	3.5
Top tie bar at weld	6061 T4 0.05 x 0.15	Tension and Bending	16.7	18.0	0.08
Top header bar at weld	6061 T4 0.12 x 0.326	Tension and Bending	3.6	18.0	4.0
Bottom pan at weld	6061 T4 t = 0.37	Tension and Bending	11.6	18.0	0.55
Middle pan away from weld	6061 T6 t = 0.23	Tension and Bending	30.0	33.2	0.11
Flat inlet duct away from weld	6061 T4 t = 0.10	Tension and Bending	16.9	18.0	0.07
Inlet duct tie rods at weld	6061 T4	Tension	15.9	18.0	0.13
High pressure fins	3003-0 t = 0.004	Tension	2.3	6.0	1.60
Tube sheets	No. 22 Brazed Stock t = 0.020	Tension	0.3	14.4	Adequate
Header bars	No. 22 Brazed Stock 0.12 x 0.12	Tension	0.4	18.0	Adequate

*MIL-Hdbk-5A Values of F_{ty} after a soak at 300°F for 1000 hr

**Weld joint efficiency factor of 0.70 used to modify stress where relevant

TABLE 5-6

SUMMARY OF PRESSURE STRESSES IN THE TECO CONDENSER

PROOF PRESSURE STRESSES, 183 PSIG AT 70°F

Part (See Figure 5-8)	Aluminum Alloy and Dimensions, in.	Load	Stress ksi**	Min F_{ty} ksi*	Margin of Safety
Top pan and weld	6016-T4 t = 0.125	Weld Tension	4.9	18.0	2.67
Top tie bar at weld	6061-T4 0.05 x 0.15	Tension and Bending	12.6	18.0	0.43
Top header bar at weld	6061-T4 0.12 x 0.326	Tension and Bending	5.31	18.0	2.39
Bottom pan at outlet port	6061-T4 t = 0.50	Tension and Bending	15.11	18.0	0.19
Bottom pan at center	6061-T6 t = 0.31	Tension and Bending	31.4	35.0	0.118
Bottom pan at undercut for thermal relief	6061-T6 t = 0.20	Tension and Bending	30.8	35.0	0.14
Flat inlet duct at span center	6061-T4 t = 0.128	Tension and Bending	15.3	18.0	0.19
Inlet duct tie rods at weld	6061-T4 d = 0.1875	Tension	17.0	18.0	0.06
High pressure fins	3003-0 t = 0.004	Tension	4.2	6.0	0.43
Tube sheets	No. 22 brazed stock t = 0.020	Tension	0.6	14.0	Adequate
Header bars	No. 22 Brazed stock 0.12 x 0.12	Tension	0.7	18.0	Adequate

*MIL-Hdbk-5A Values of F_{ty} after a soak at 300°F for 1000 hr

**Weld joint efficiency factor of 0.70 used to modify stress where relevant

TABLE 5-7

SUMMARY OF PRESSURE STRESSES IN THE SES CONDENSER

PROOF PRESSURE STRESSES, 86 PSIG AT 70°F

Part (See Figure 5-9)	Aluminum Alloy and Dimensions, in.	Load	Stress ksi**	Min F_{ty} ksi*	Margin of Safety
Top and bottom pan at weld	6016-T4 t = 0.100	Weld Tension	2.88	18.0	5.26
Tie bar at weld	6061-T4 0.05 x 0.15	Tension and Bending	5.93	18.0	2.04
Header bar at weld	6061-T4 0.12 x 0.326	Tension and Bending	2.50	18.0	6.20
Inlet duct at span center	6061-T4 t = 0.100	Tension and Bending	15.5	18.0	0.16
Inlet duct tie rods at weld	6061-T4 OD = 0.200 ID = 0.150	Tension	9.8	18.0	0.84
High pressure fins	3003-0 t = 0.004	Tension	1.98	6.0	2.03
Tube sheets	No. 22 Brazed Stock t = 0.020	Tension	0.29	14.0	Adequate
Header bars	No. 22 Brazed Stock 0.12 x 0.12	Tension	0.34	18.0	Adequate

*MIL-Hdbk-5A Values of F_{ty} after a soak at 300°F for 1000 hr

**Weld joint efficiency factor of 0.70 used to modify stress where relevant

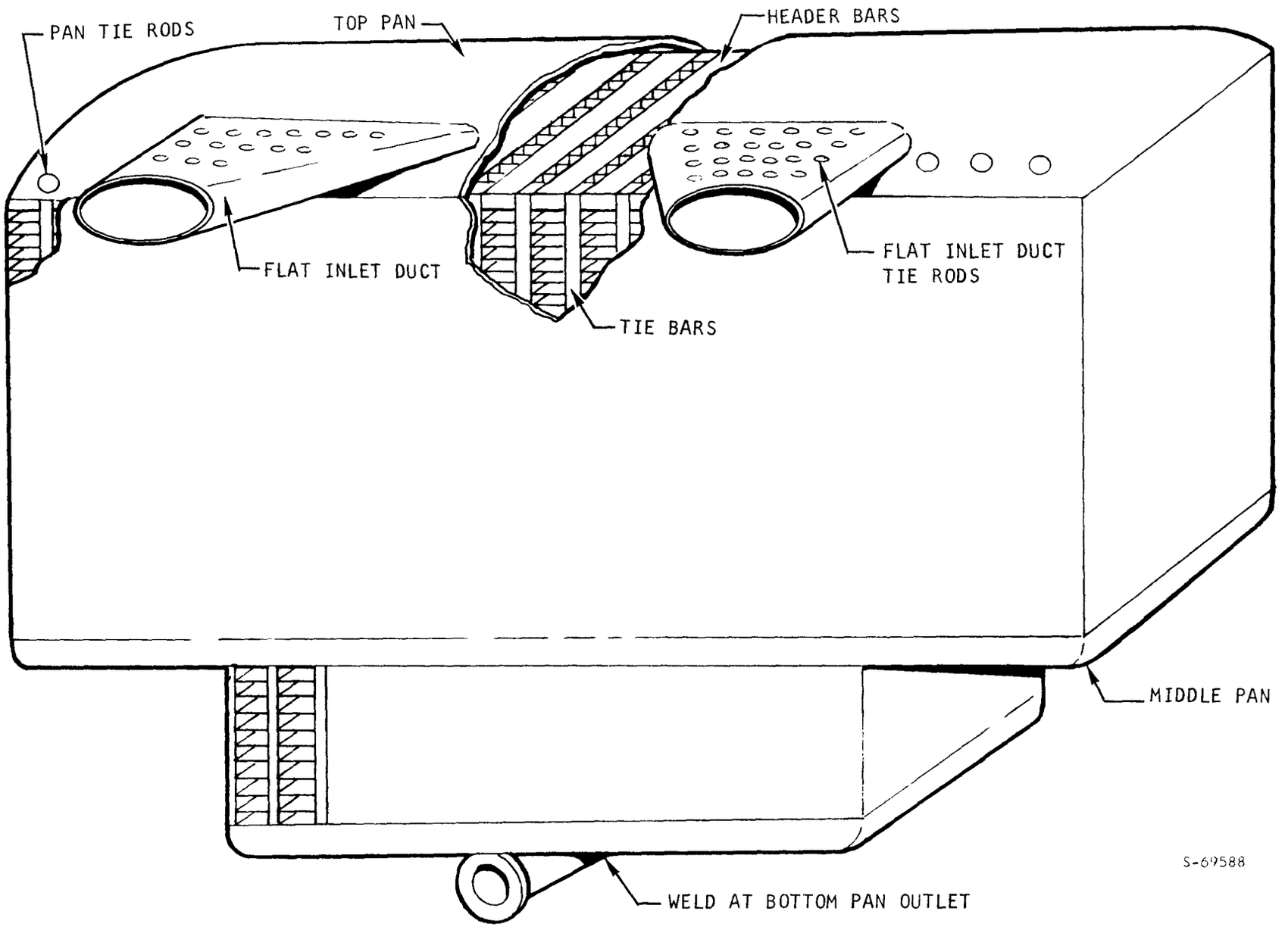

Figure 5-7. Aerojet Condenser (190390) Structural Schematic

2. TECO Condenser (190370)

A structural schematic of this condenser is shown in Figure 5-8. For the normal operating conditions of 25 psig at 238°F for a life of 3500 hr, the highest operating stresses are 2.33 ksi in the tie rod and 2.3 ksi in the flat inlet duct. For these low operating stresses at 238°F, the creep stresses will have factors of safety of at least 6.5 on the stresses and a factor of better than 100 to 1 on the operating life of the condenser.

3. SES Condenser (190640)

A structural schematic of this condenser is shown in Figure 5-9. For the normal operating conditions of 20 psig at 258°F for a life of 3500 hr, the highest operating stresses are 2.3 ksi in the tie rod and 3.6 ksi in the flat inlet duct. For these low operating stresses at 258°F, the creep stresses will have a factor of safety of at least 5.0 on the stresses and a factor of better than 100 to 1 on the operating life of the condenser.

Thermal Stresses

Temperature differences are developed within the condensers which produce thermal strains. The maximum normal operating transient temperature difference between the bar and tube sheet is calculated to be 20°F for 1000 cycles and 15°F for 2000 cycles. A design life of 3500 cycles was selected for the design point under normal condenser operating conditions. The condensers have adequate life capability for this requirement, however, some further thought should be given to the possibility of higher metal temperature differentials occurring when a hot condenser core is subjected to a cold water splash condition.

Supporting Structure

An analysis was conducted on the support structure for the three condenser and fan assemblies. The support structures were analyzed for a 10-g shock load in three axes and a 2.0-g vibration input load in three axes with a response of 5 times the input to give a maximum vibratory response output os 10 g. The structures should be provided with isolators to limit the vibratory response to 10 g.

The strength criteria for shock loads are that the stresses do not exceed the ultimate strength of the material. For vibratory loads, the structure should be designed so that the alternating stresses do not exceed the allowable endurance limit fatigue properties of the material.

The component weights listed in Table 5-8 were used in this analysis.

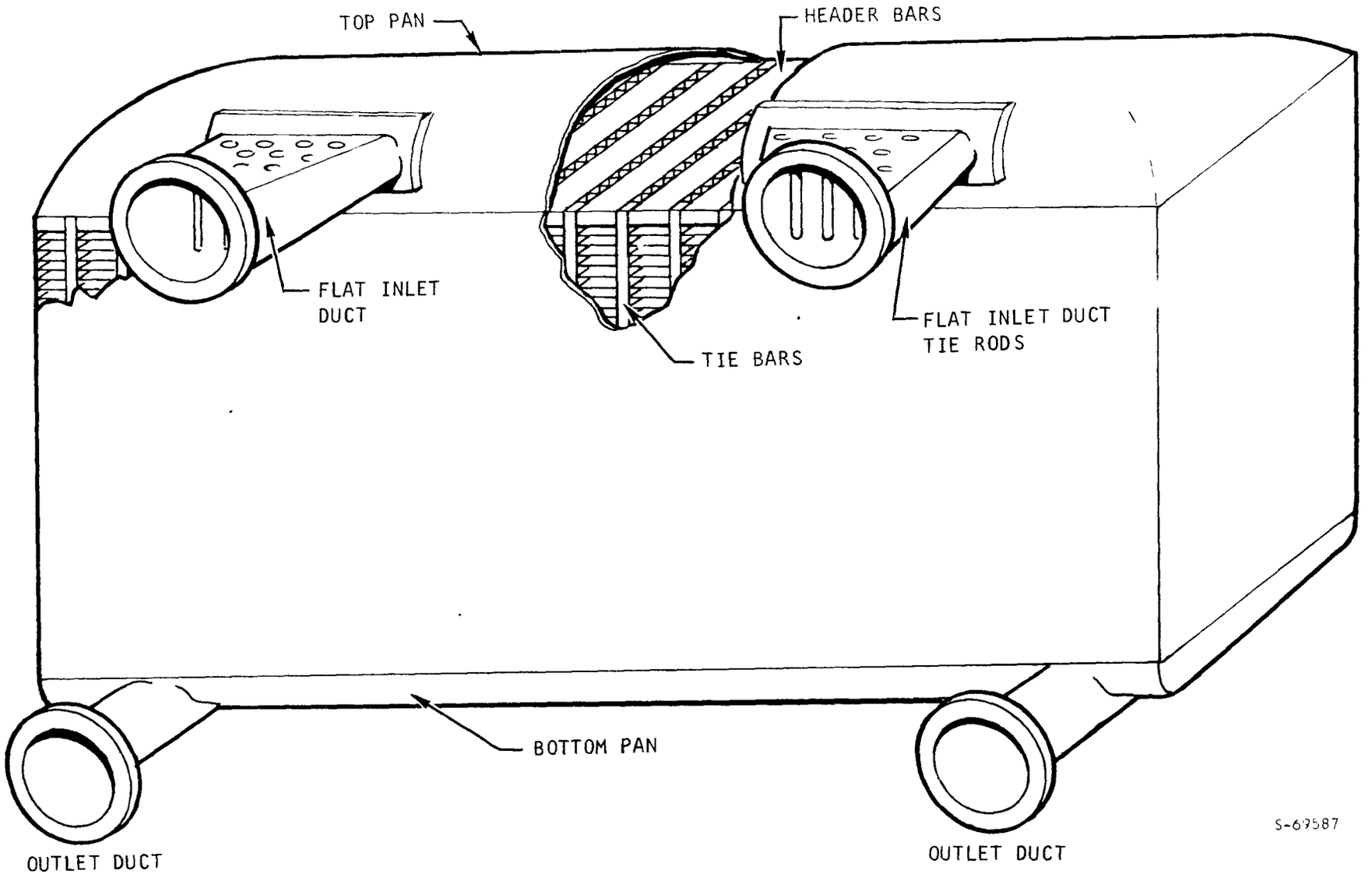

Figure 5-8. TECO Condenser (190370) Structural Schematic

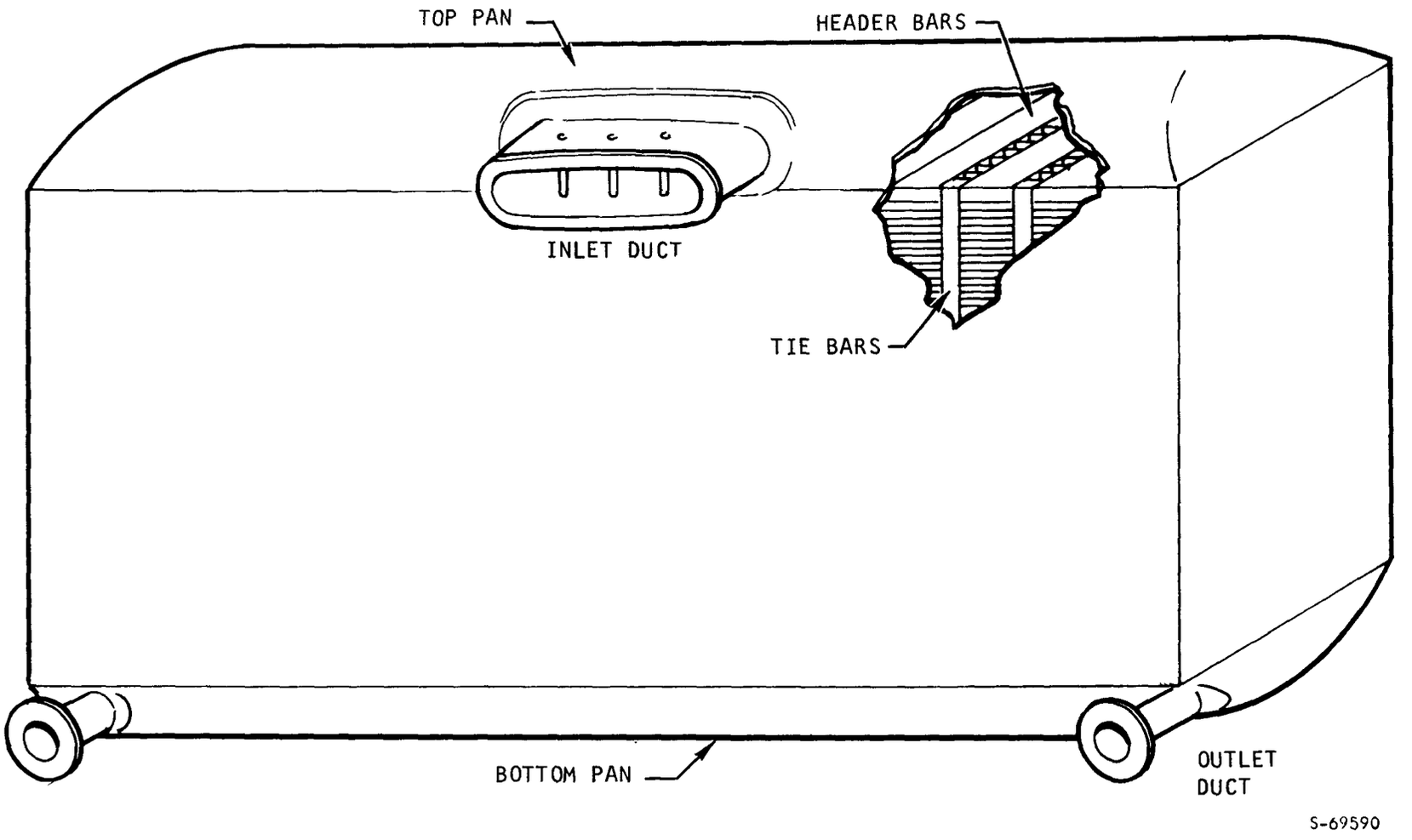

Figure 5-9. SES Steam Engine Condenser (190640) Structural Schematic

TABLE 5-8

COMPONENT WEIGHTS

Part	TECO 190370 Weight, lb	Aerojet 190390 Weight, lb	SES 190640 Weight, lb
Condenser	137	80	93
Subcooler assembly	0	27	0
Liquid in condenser	10	0	11
Liquid in subcooler	0	18	0
Wet weight of condenser	147	125	104
Two motors	0	70	0
Two fans	70	46	66
Support structure	17	24	20
Fan and structure	89	140	86
Total weight condenser and fan	236	265	190

1. Heat Exchangers

Vibration isolators equivalent to the Lord BTR elastomeric mountings, HT2-80 or 200P-45, should be used to limit the maximum response output to 10 g. The heat exchanger fins are very flexible and are not capable of supporting the heat exchanger core weight in either the vertical or the longitudinal direction of the airflow. For vertical loads the air fins act as very flexible guided cantilever beams since the thickness per fin is 0.004 in. For longitudinal loads, the fluid fins act in a similar manner; the thickness per fin is also 0.004 in. As a result, the top and bottom pans are not capable of acting as an integrated beam due to insufficient shear carrying ability of the core.

The top and bottom pans must act as separate beams to support the longitudinal and vertical loads. For three isolator supports on each side of the heat exchanger and no middle support, the unsupported pan beam span will be 50.0 in. for the Aerojet, 60.19 in. for the TECO, and 51.62 in. for the SES units. The top and bottom pans are insufficient in themselves to carry the 10-g vibratory loads in the vertical direction for all three designs.

To make the heat exchanger core more rigid and to reduce the vibration amplitude and strengthen the structure so that its alternating stresses will be less than the endurance limit of the material, a truss structure shown for

the Aerojet condenser in Figure 5-10 is recommended, and a similar truss may be used for the other condensers. This truss may be located in the discharge shroud of the condenser or it may be located at the inlet to the condenser. If the truss is located in the shroud between the condenser and fan, this shroud will have to be lengthened to prevent obstruction of airflow through the outer sides of the shroud. For the best structural design, the truss should be located as close as practical to the core.

An alternate and preferred structural design is to provide the condenser core with at least one support at its middle. This support is shown with an isolator in Figure 5-10 (adjacent to liquid outlet port). Use of the center mount eliminates the need for a truss structure. This will divide the beam span in half and reduce the alternating bending stresses to one quarter such that these stresses would be less than the endurance limit of the material.

The top and bottom pans and cores of the TECO, Aerojet, and SES condensers are sufficiently rigid and strong to take the 10-g vibratory loads in the longitudinal direction so the condenser core may be supported on three vibration isolators at each end. An additional longitudinal truss must be provided between the cores to strengthen the middle pan in the Aerojet condenser to carry the longitudinal ±10-g vibratory loads. By using this structural configuration, the alternating stresses in the components of the Aerojet unit will be less than the endurance limit of the material. No additional reinforcing is required to carry longitudinal vibratory loads in the TECO and SES units.

To isolate the condenser and fan package from external vibration inputs and to maintain compatibility with the isolation mounting, the inlet ducts to the condenser must be provided with flexible connections. Also, the outlet duct and the motor lines must be flexible to eliminate vibration input through these lines.

2. Frame Assembly

For automotive installations with a 10-g response output, the condenser and fan frame assembly should be reinforced as follows: on the frame assembly for the Aerojet condenser and fan, the top of the two support rings (which are machined away to provide for the inlet ducts to the condenser) should be fabricated as solid 0.625-in. by 1.75-in. rectangular rings, and the inlet ducts should be indented to accommodate the rings. As shown in Figure 5-11, these solid rectangular rings should have a tapered thickness which increases from 0.625 in. at station (1) to 1.00 in. at station (2). This tapered thickness is necessary to support the torsional stresses that are transmitted through the upper arches of these support rings. Also, to carry the torsional stresses through the lower arches of the rings, rectangular box sections must be incorporated between stations (4) and (6).

For the automotive installation of the TECO condenser, the fan annulus support ring, spokes, and hub act as an integrated structure for supporting the fan and belt loads. The channel ring section between the upper support bolts should be a rectangular box section to prevent excessive twist of the fan annulus which will occur when subjected to vibratory loads. Likewise, the channel ring section between the lower support bolts should be a rectangular box section.

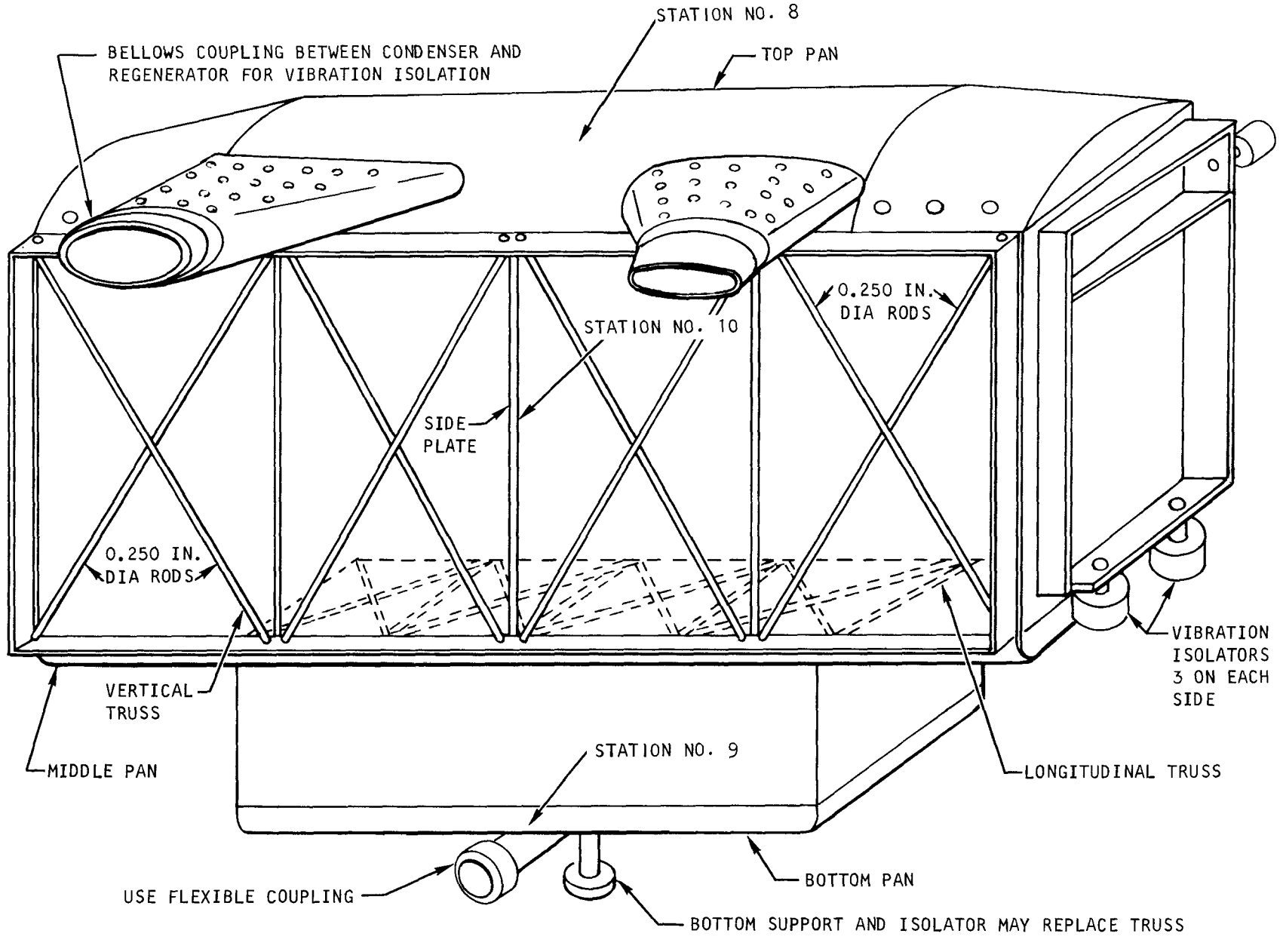

Figure 5-10. Aerojet Condenser with Truss

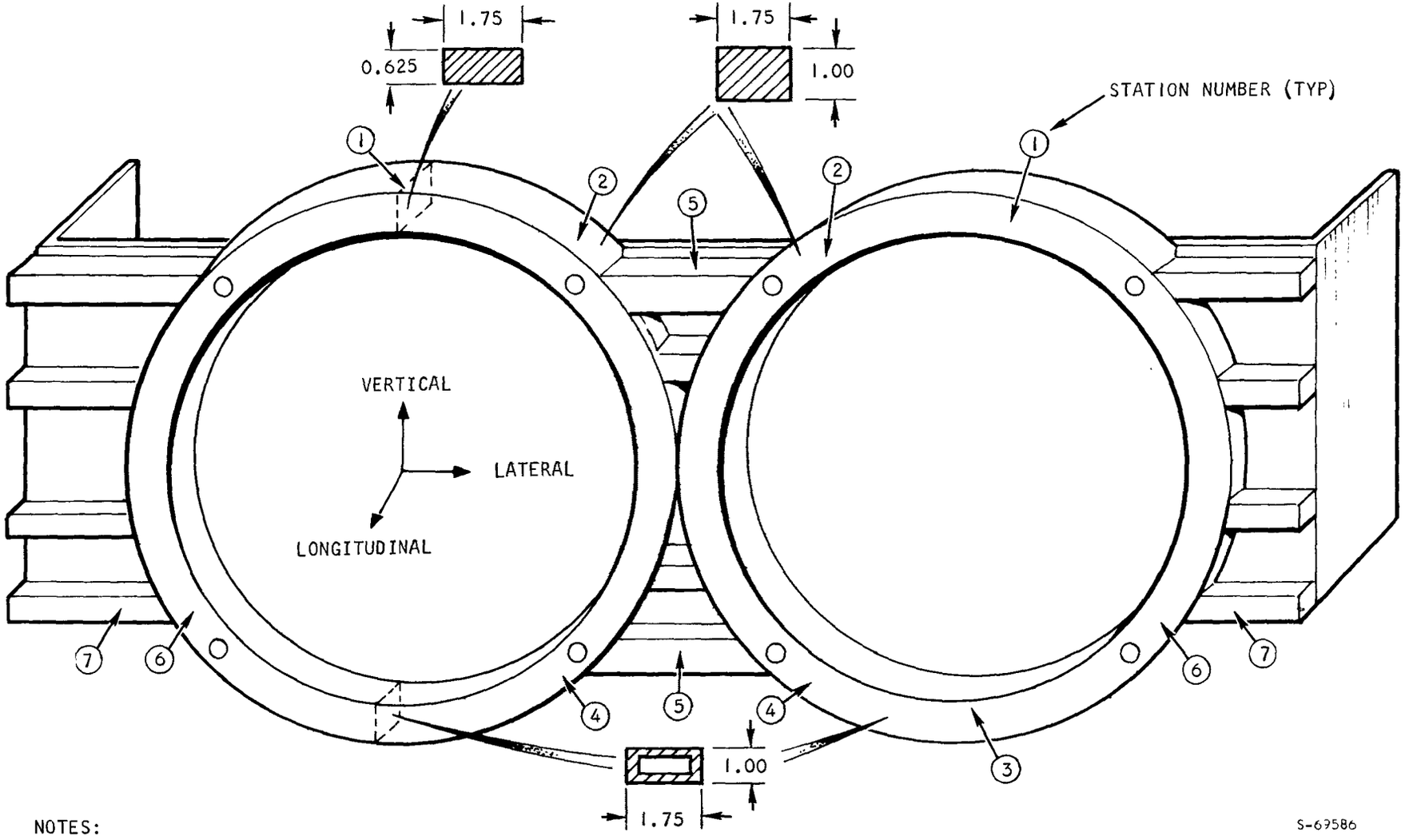

NOTES:

- STATION NUMBERS ARE CIRCLED
- DIMENSIONS IN INCHES

Figure 5-11. Aerojet Support Frame for Fans

Table 5-9 summarizes the alternating stress calculations for the various structural components in the Aerojet unit. Vibratory stresses in the TECO and SES units are approximately the same.

TABLE 5-9

SUMMARY OF STRUCTURAL DYNAMIC STRESS IN THE 190390 AEROJET CONDENSER

2-g input with a response of 5-to-1 to yield a 10-g maximum response output

Station	Direction of Load	Part (Refer to Figure 5-10 and 5-11)	Type Stress	Vibratory Stress ksi
1	Longitudinal	Ring at upper center	Bending	10.45
2	Longitudinal	Ring at upper center bolt	Principal Shear	7.98
2	Longitudinal	Ring at upper center bolt	Principal Tension	11.00
3	Longitudinal	Ring at lower center	Bending	10.45
4	Longitudinal	Ring at lower center bolt	Principal Shear	7.60
4	Longitudinal	Ring at lower center bolt	Principal Tension	12.00
5	Longitudinal	Center of truss	Bending	9.25
6	Longitudinal	Ring at lower outer edge	Shear	6.50
7	Longitudinal	Lower outer beam	Bending	9.60
8	Longitudinal	Top pan at center	Bending	2.48
9	Longitudinal	Bottom pan at center	Bending	1.00
10	Vertical	1/4-in. dia truss rods	Tension	10.00

For 6061-T4 Al the endurance limit F_e = 12.00 ksi

Structural Summary

1. Aerojet Condenser (190390)

The 190390 condenser and subcooler meets the strength criteria for design based on short-time material properties, and the stresses at proof pressure will not exceed the material yield strength. The normal operating stresses are low and the maximum long-term operating temperature is only 241°F; therefore, it should not rupture during the 3500 hour operating life because it has a factor of safety of 6.5 on creep stress and a factor of 100 on creep life based on a Larson-Miller plot of the material stress rupture at the operating temperature. The thermal stresses are low and in the elastic range of the material.

The Aerojet condenser inlet ducts may take static loads of 500 lb in the longitudinal and lateral axes and 150 lb in the vertical direction for handling and installation; however, these ducts are not designed to take any dynamic loads and should be provided with bellows or a flexible coupling which has a spring rate of 1000 lb per inch or less in the three axes with a maximum displacement capability of 0.50 in. In the static systems test program of the Aerojet condenser, the above handling loads should not be exceeded.

To limit the maximum response output to 10 g or less, vibration isolators should be utilized.

The present condenser core and pan structure of all three units needs to be reinforced to support a vertical vibratory response of 10 g if no midspan mount is provided. One of the following structural changes is recommended:

(a) The recommended installation is to provide all three units with a midspan support of the condenser core with vibration isolators at all supports, as shown by Figure 5-10.

(b) In lieu of (a) above, an alternate design would be to provide the condenser core with a truss structure, as shown in Figure 5-10. Additional space may be required in the shroud between the condenser and the grille to reduce the cooling airflow losses.

(c) The least desired alternate design would be to weld gussets and plate beams on the top, middle, and bottom pans. This would be an expensive and heavy alternative.

For the automotive installation of the Aerojet condenser and fan frame assembly, the top two support rings should be fabricated as solid 1.75-in.-wide rectangular rings having a tapered thickness that increases from 0.625 in. at station (1) to 1.00 in. at station (2) of Figure 5-11. The lower ring arches between stations (4) and (6) of Figure 5-11 should be fabricated as a box section.

2. TECO Condenser (190370)

The 190370 condenser and subcooler meets the strength criteria for design based on short-term material properties, and the stresses at proof pressure will not exceed the material yield strength. The condenser was not analyzed for a burst pressure because no definition for the burst requirement is specified. The normal operating stresses are low and the maximum long-term operating temperature is only 238°F; therefore, it should not rupture during the design life of the engine (3500 hr) because it has a factor of safety of 3.0 on creep stress and a factor of 45 on creep life based on a Larson-Miller plot of the material stress rupture at the operating temperature. The thermal stresses are low and in the elastic range of the material.

As outlined in the Aerojet condenser discussion, the TECO condenser and fan annulus support rings should be fabricated as rectangular box sections on the upper and lower segment to prevent excessive twist of the fan annulus due to the 10 g response output loads.

For the automotive installation of the TECO condenser, spring loaded idler pulleys should be provided on the belt between the fan pulley and the drive pulley on the automobile frame. These idler pulleys should be designed to take up a racking motion between the fan and auto frame.

3. SES Condenser (190640)

This condenser and subcooler meets the strength criteria for design based on short-time material properties, and the stresses at proof pressure will not exceed the material yield strength. The normal operating stresses are low and the maximum long-term operating temperature is only 258°F; therefore, it should not rupture during the 3500-hr design life of the engine because it has a factor of safety of 5.0 on creep stress and a factor better than 100 on creep life based on a Larson-Miller plot of the material stress rupture at the operating temperature. The thermal stresses are low and in the elastic range of the material. The same comments made for the support frame of the TECO condenser also apply to the SES condenser.

DETAIL DESIGN

Aerojet

Outline dimensions for the condenser and subcoder assembly are shown on Drawing 190391. For manufacturing purposes the condenser case consists of four separate brazed modules which are subsequently welded together. Likewise, the subcooler sections consists of three separate modules.

The vapor inlet ducts are designed to mate directly to the engine recuperator. The ducts are tapered to provide a constant flow area. Tension tie rods extend across the inlet ducts to minimize the stresses in the flat sections of the duct. The inlet face of the duct is subject to a final machining operation to ensure that the face is parallel to the front face of the condenser (engine installation requirement). The ends of the vapor inlet manifold are tapered to clear the vehicle hood.

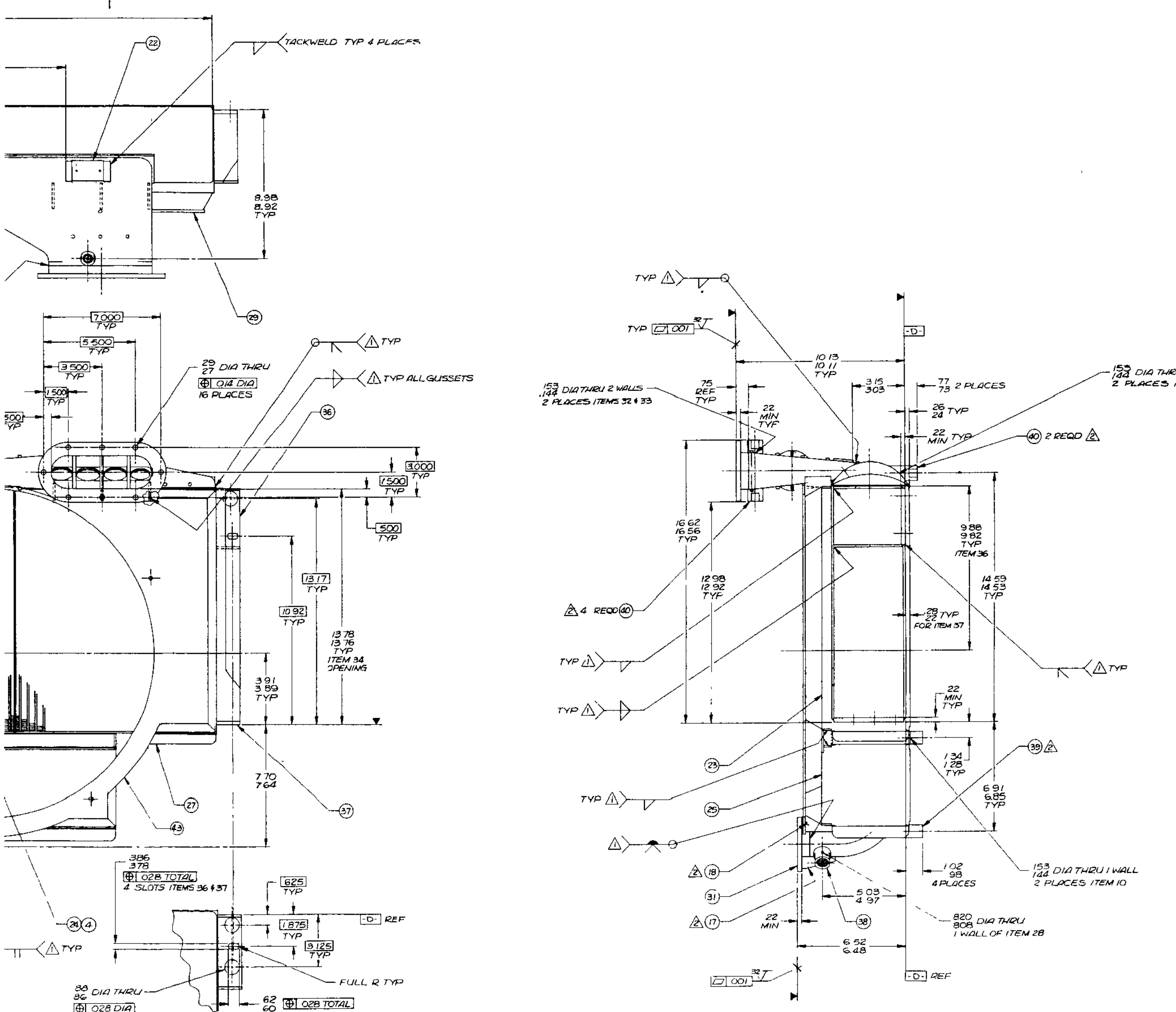

QTY REQD -11	-9	-7	-5	-3	-1	ITEM NO	CODE IDENT NO.	PART OR IDENTIFYING NO	NOMENCLATURE OR DESCRIPTION	SYM	ZONE
					AR	43		FP73F04		4	4
			6			40		187577-1	BOSS, UPPER		2,3
			4			39		187576-1	BOSS, LOWER		2
			1			38		187522-1	BOSS, DRAIN		2
			2			37		187487-1	BRACKET ASSY, LOWER		4
			2			36		187486-1	BRACKET ASSY, UPPER		4
			1			35		187459-1	FLANGE, DUCT		6
		2				34		187458-1	FLANGE, INLET		6
		1				33		187453-2	DUCT ASSY		5
		1				32		187453-1	DUCT ASSY		6
			1			31		187449-1	FLANGE, SUBCOOLER		3
		1				30		187422-1	MANIFOLD ASSY, CONDENSER		5
			1			29		187419-1	SHROUD		4
			1			28		187418-1	MANIFOLD ASSY, LOWER		6
			2			27		187417-1	MANIFOLD		4
1						26		187415-2	CORE ASSY, SUBCOOLER		5
2						25		187415-1	CORE ASSY, SUBCOOLER		3
	2					24		187414-2	CORE ASSY, CONDENSER		5
	2					23		187414-1	CORE ASSY, CONDENSER		3
		1				22		89195	MOUNT, NAMEPLATE		4
			1			18		-37	GUSSET, .100SH, 1.93×2.62 AL ALY QQ-A-250/11 6061-T6		3
			1			17		-35	GUSSET, .100SH, .75×2.00 AL ALY QQ-A-250/11 6061-T6		3
			2			15		-31	GUSSET, .100SH, .69×1.59 AL ALY QQ-A-250/11 6061-T6		7
			4			14		-29	GUSSET, .100SH, 1.25×1.59 AL ALY QQ-A-250/11 6061-T6		7
			4			13		-27	GUSSET, .100SH, .60×2.50 AL ALY QQ-A-250/11 6061-T6		6
			2			12		-25	CORNER, .100SH, 1.00×1.44 AL ALY QQ-A-250/11 6061-T6		8
			2			11		-23	END, .100SH, .53×1.00 AL ALY QQ-A-250/11 6061-T6		8
			2			10		-21	STRIP, .100SH, .88×36.25 AL ALY QQ-A-250/11 6061-T6		8
			1			5		-11	WELDED ASSY		5
			1			4		-9	WELDED ASSY		5
			1			3		-7	WELDED ASSY		5
				1		2		-5	WELDED ASSY		6
					1	1		-3	MACHINED ASSY		6

PARTS LIST

6 HELIUM LEAK CHECK CONDENSER FOLLOWING PROOF PRESSURE TEST. LEAKAGE SHALL NOT EXCEED 1×10⁻⁶ SCC/SEC

5 PROOF PRESSURE TEST VAPOR SIDE TO 85 PSIG AT ROOM TEMPERATURE. PRESSURE TO BE HELD FOR 5 MIN. NO PERMANENT DEFORMATION ALLOWED

4 APPLY TO EXTERNAL SURFACES ONLY

3 SURFACES MARKED ▼ HAVE .12 MACHINING STOCK ALLOWANCE

2 TRIM TO FIT ON ASSEMBLY

1 WELD PER AIRESEARCH SPEC WBS-18

NOTES: UNLESS OTHERWISE SPECIFIED

QTY REQD	NEXT ASSY	USED ON
1 (-1)	190390	190390-1

APPLICATION

UNLESS OTHERWISE SPECIFIED BURR CONTROL PER SC085
IDENTIFICATION MARKING PER MCM, CLASS IV A
STD INTERPRETATIONS PER PS

HEAT TREATMENT: COND T4 MIN PER MIL-H-6088

DR 7-10-72
CHK 7-10-72
APPD 7-20-72

AIRESEARCH MANUFACTURING COMPANY

CONDENSER AND SUBCOOLER ASSY

SIZE J | CODE IDENT NO. 70210 | DWG NO. 190391

SCALE 1/2 | SHEET 1 OF 1

REVISIONS: A — SEE ENGINEERING ORDER

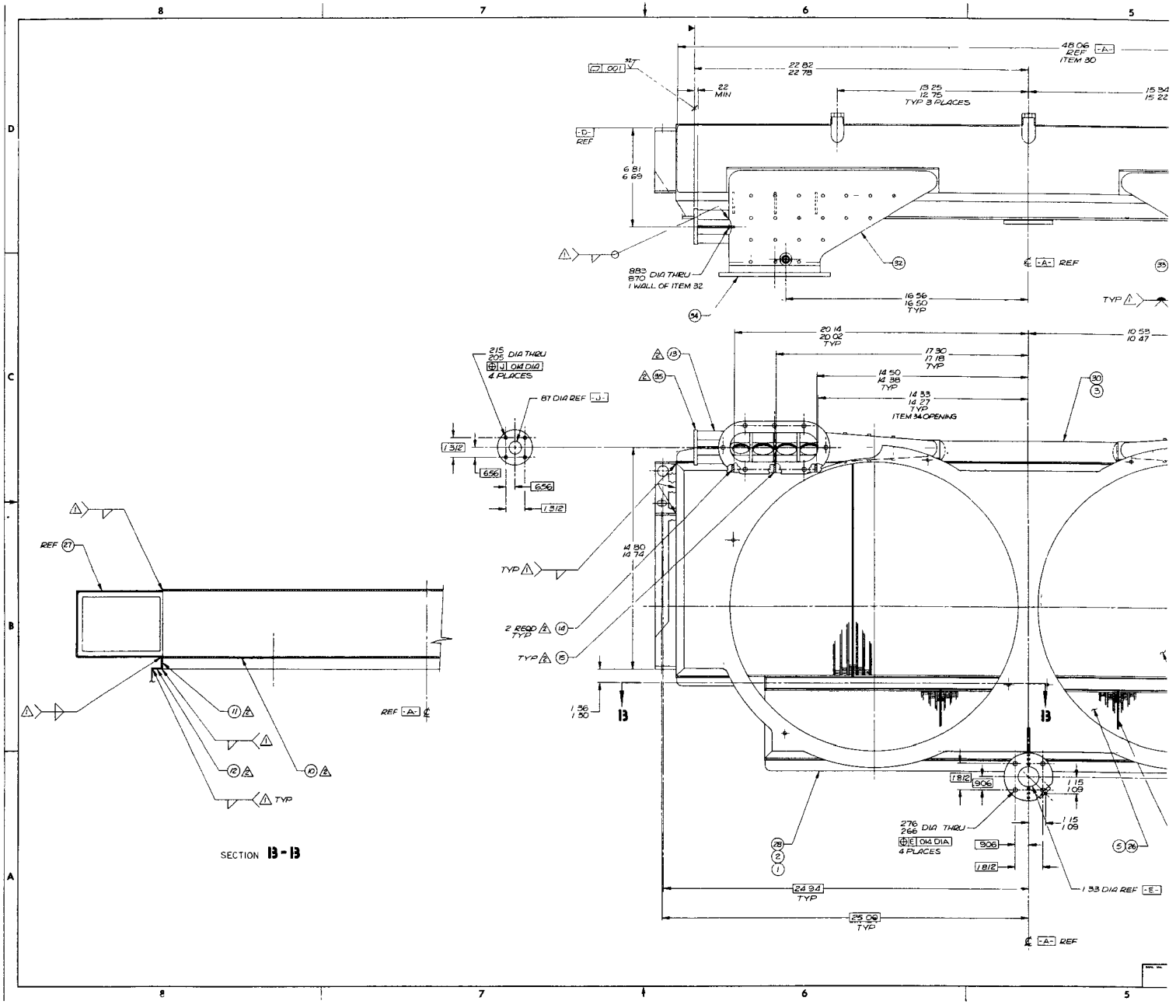
48.06
REF
ITEM 30
-A-
22.82
22.78
.001 M
22
MIN
13.25
12.75
TYP 3 PLACES
15.34
15.22
-D-
REF
6.81
6.69
8.83
8.70
DIA THRU
I WALL OF ITEM 32
32
-A- REF
35
16.56
16.50
TYP
34
TYP
20.14
20.02
TYP
10.59
10.47
17.30
17.18
TYP
14.50
14.38
TYP
14.33
14.27
TYP
ITEM 34 OPENING
30
3
2.15
2.05
DIA THRU
.014 DIA
4 PLACES
J
8.7 DIA REF -J-
1.312
.656
.656
1.312
18
36
14.80
14.74
TYP
2 REQD TYP
14
TYP
15
1.56
1.50
B
B
REF 27
11
12
10
TYP
REF -A-
SECTION B-B
1.812
.906
1.15
1.09
2.76
2.66
DIA THRU
.014 DIA
4 PLACES
E
28
2
1
.906
1.812
1.15
1.09
5
26
1.33 DIA REF -E-
24.94
TYP
25.06
TYP
-A- REF

Mounting brackets are welded directly to the sides of the condenser core assembly. The threaded bosses which are welded to the manifolds are for instrumentation purposes. A single liquid outlet is utilized.

The manifolds are designed to minimize the overall condenser height and thus, the intermediate and liquid outlet manifolds are flat rather than round as would be desired to minimize metal thickness. The flat intermediate and liquid outlet manifolds are machined from plate stock and are a maximum of 3/8 in. thick as required to withstand the specified operating pressure.

The condenser-to-fan shroud is designed to be welded to the back face of the condenser.

Outline dimensions of the final condenser and fan assembly are shown on Dwg No. 190390. A separate aluminum alloy frame assembly is used to mount the fan assemblies to the condenser. The weight of the two fan and hydraulic motor assemblies was estimated to be 110 lb, and hence, a robust structure is required to withstand the expected operating loads. A rubber pad is used at the bottom mounting surface to absorb the differential thermal expansion between the frame and condenser. A description of the fan assemblies is presented in Section 6.

Thermo Electron

Outline dimensions of the condenser assembly is shown on Dwg No. 187532. For manufacturing purposes the core is designed to be brazed in four separate modules which are welded together to form the complete assembly in a subsequent operation.

The vapor inlet ducts are tapered to minimize area changes and tension ties are used to reduce the stress in the flat portion of the duct. Mounting brackets are welded directly to the sides of the core. As specified by TECO, two vapor inlets and two liquid outlets are incorporated in the design. The liquid outlet manifold was designed to be flat to reduce the overall height of the condenser. The condenser-to-fan shroud is welded directly to the back face of the condenser.

Outline dimension of the final condenser and fan assembly are shown on Dwg No. 190370. For this design, a three-piece frame is used to mount the fans to the condenser. A center piece is used to join to two fans together; two side pieces secure the frame to the condenser. The side pieces incorporate the vehicle mounts. A 1/4-in. thick pad of closed-cell foam silicone rubber is placed between the fan front flange and the condenser-to-fan shroud to prevent air in-leakage. No provisions are made for a center bottom support although a cradle type of mount could be used to help support the assembly in the actual automobile installation. A description of the fan assembly is presented in Section 6.

Steam Engine Systems

The condenser assembly is shown on Dwg No. 187562. The design is similar to the TECO unit except that a single vapor inlet duct is used. The ends of the inlet manifold are tapered to clear the vehicle hood. The outlet manifold is cylindrical and incorporates a threaded bosses on each end which are designed to mate with the SES noncondensible gas vent manifold.

Outline dimensions of the condenser and fan assembly are shown on Dwg No. 190640. The assembly is similar to the TECO unit and uses a three-piece frame assembly to mate the fans with the condenser. Location of the fan drive pulley and V-belts is shown for reference. A description of the fan assembly is presented in Section 6.

FABRICATION

Conventional aluminum heat exchangers are fabricated using a salt bath brazing technique, which requires a flux during the brazing process for removing the oxide film from the aluminum parts. Such fluxes are corrosive, and it is necessary to wash the parts thoroughly to remove both residual flux and brazing salts. Even minute quantities of entrapped salt and flux will cause severe corrosion.

Techniques for salt bath brazing are well developed at AiResearch and thousands of units are in the field and successfully operating. It was recognized, however, that due to the very small vapor passages in the EPA condensers (0.050 in. high), that salt entrapment would be likely. It was decided, therefore, to use a relatively new vacuum fluxless brazing process.

The key to the vacuum fluxless brazing process is the use of a clad brazing sheet. The clad sheet consists of a proven heat exchanger core alloy, type 3003 or 6951, which is clad on both sides with an Al-Si-Mg alloy. Total clad thickness is 5 to 15 percent of the brazing sheet thickness, depending on gage or application.

Silicon lowers the melting point of the clad to below that of the core alloy, allowing parts to bond without thermal distortion under proper conditions of clamping force, temperature, and vacuum. In the furnace environment, the protective oxide film on the aluminum surface breaks up, exposing the clean surface essential for brazing. Magnesium in the clad also vaporizes under these conditions, helping to disrupt the oxide film. Oxygen in the furnace atmosphere preferentially combines with the magnesium, preventing reoxidation of the clean aluminum. The clad melts and wets joint surfaces thus forming the brazed joint.

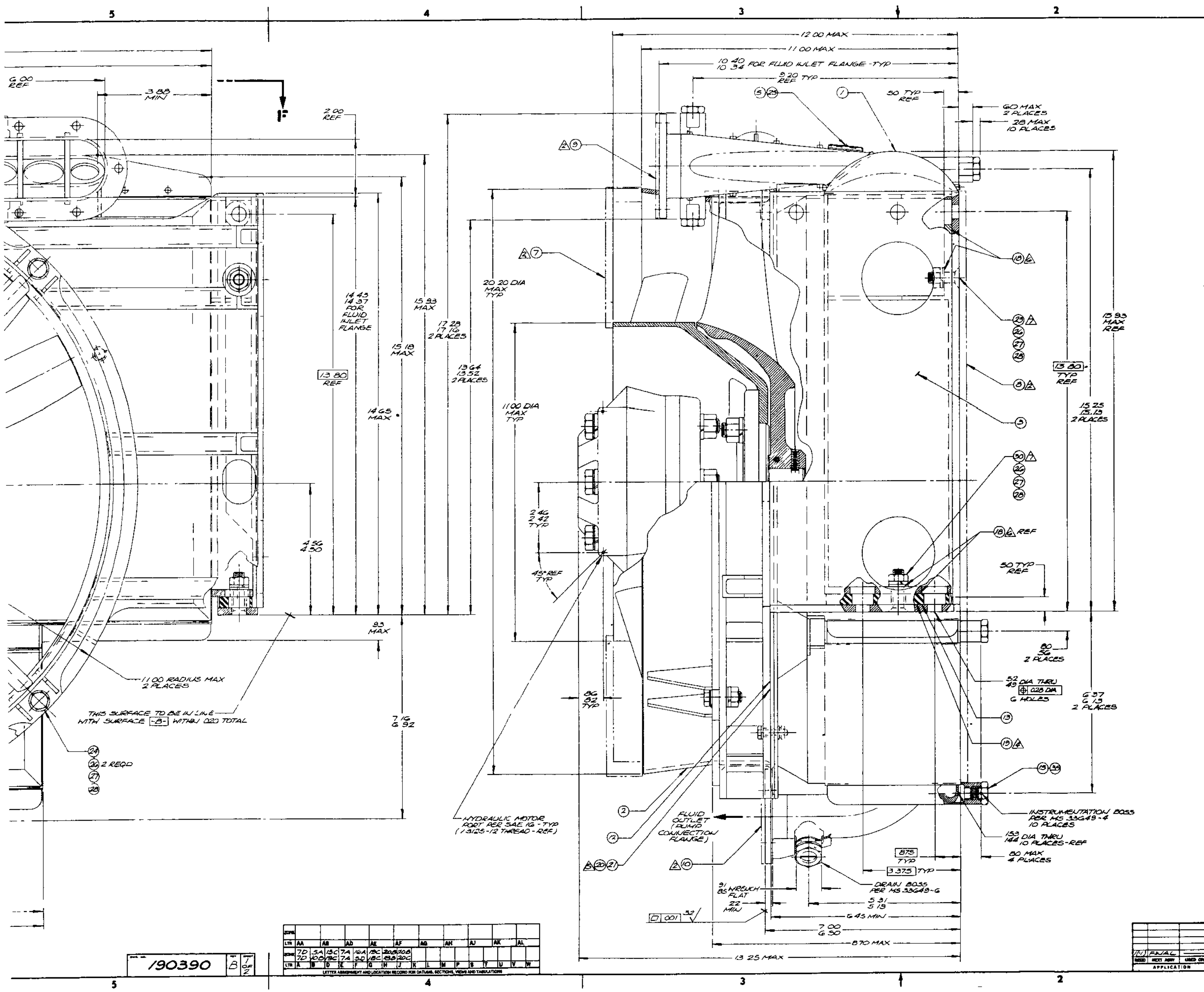

11 UNIT CALCULATED WEIGHT (DRY) 250 LBS.

9 THIS UNIT IS DESIGNED TO WITHSTAND 15 PSIG PROOF PRESSURE AT ROOM TEMPERATURE

8 LEAKAGE MUST BE LESS THAN 1×10^{-6} SCC/SEC OF HELIUM

⚠7 TORQUE TO 250 IN/LBS AND BACK-OFF HALF TURN TO ALLOW FOR THERMAL MOVEMENT.

⚠6 LUBRICATE FRAME AND CONDENSER SURFACES IN CONTACT WITH EACH OTHER (INCLUDING MTG SLOTS AND WASHERS) USING ITEM 18, GREASE AS REQD.

⚠5 APPLY PER AIRESEARCH SPEC RS-159

⚠4 APPLY PER AIRESEARCH SPEC RS-60.

⚠3 VENDOR ITEM - SEE SPEC CONTROL DWG

⚠2 ATTACH PROTECTIVE COVERS WITH SHIPPING TAPE AS REQUIRED

1 ALL OPENINGS ARE PROVIDED WITH PROTECTIVE COVERS. REMOVE ONLY AT TIME OF INSTALLATION.

NOTES UNLESS OTHERWISE SPECIFIED.

PARTS LIST

QTY REQD	ITEM NO.	CODE IDENT NO.	PART OR IDENTIFYING NO.	NOMENCLATURE OR DESCRIPTION		
AR	39		MS 33540	[illegible]		7
AR	38		MS 20995C32	WIRE, LOCK		7
7	36		AN814-10DL	PLUG		7
10	35		AN814-4D	PLUG		2
6	33		AN315-3R	NUT, HEX		6
6	32		MS35338-43	WASHER, SPLIT LOCK		6
6	31		AN960-10	WASHER, PLAIN		6
2	30		MS24694-S56	SCREW, FLAT HD		2
6	29		AN3-7A	SCREW, HEX HD		6
2	28		AN315-6R	NUT, HEX		
2	27		MS 35338-46	WASHER, SPLIT LOCK		
2	26		AN960-616	WASHER, PLAIN		
2	25		MS 24629-1	SCREW, TAPPING		3
8	24		AN6-11A	SCREW, HEX HD		
2	23		MS 24694-S82	SCREW, FLAT HD		2
AR	21		MIL-A-25457	ADHESIVE		3
AR	20		358-024-5001	PRIMER	⚠	3
AR	19		105-010-5001	ADHESIVE	⚠	2
AR	18		358-042-5001	GREASE	⚠	2
1	16		S9028A906	PACKING		7
10	15		S9028A904	PACKING		2
2	13		187537-1	PAD		2
2	12		187536-1	GASKET		3
1	11		187527-3	COVER, PROTECTIVE		13
1	10		187527-2	COVER, PROTECTIVE		3
2	9		187527-1	COVER, PROTECTIVE		4
1	8		187525-1	COVER, PROTECTIVE		2
2	7		187528-1	COVER ASSY, PROTECTIVE		4
1	5		187526-1	PLATE, IDENTIFICATION		3
1	3		187416-1	FRAME ASSY		2
2	2		603972-1	FAN, HYD MTR DRIVEN		3
1	1		190391-1	CONDENSER & SUBCOOLER ASSY		3

-1 ← ASSY

APPLICATION: -1 FINAL

CONDENSER AND FANS ASSY, RANKINE CYCLE TURBINE ENGINE - (ORGANIC WORKING FLUID)

SIZE J | CODE IDENT NO. 70210 | DWG NO. 190390

SCALE 1/1 | SHEET 1 OF 2

REVISIONS: A SEE ENGINEERING ORDER; B SEE ENGINEERING ORDER

190390 B 1 OF 2

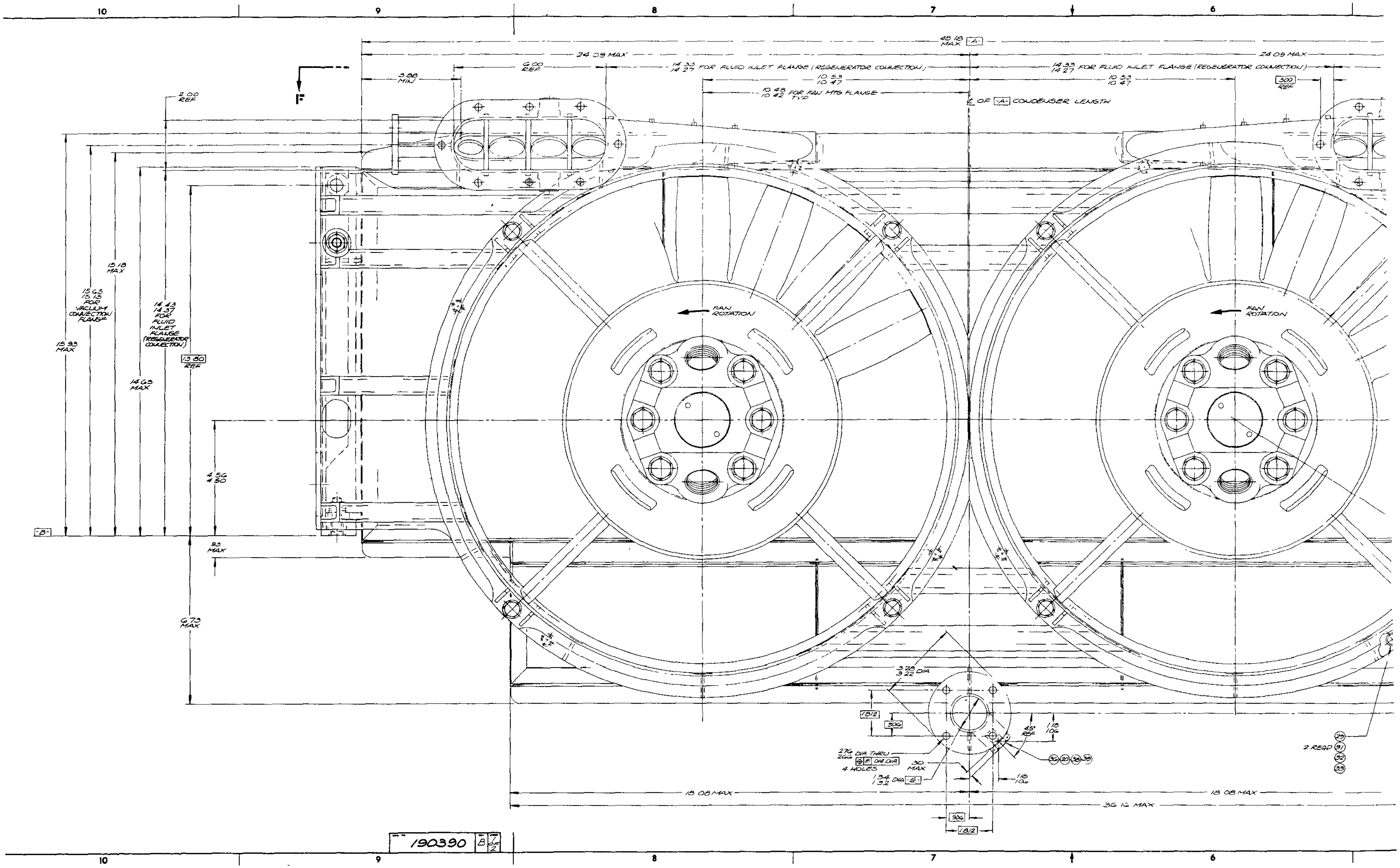
FAN ROTATION
FAN ROTATION
24.09 MAX
FOR FLUID INLET FLANGE (REGENERATOR CONNECTION)
FOR FAN MTG FLANGE
CONDENSER LENGTH
18.08 MAX
18.08 MAX
36.16 MAX
2 REQD
4 HOLES

190390 B

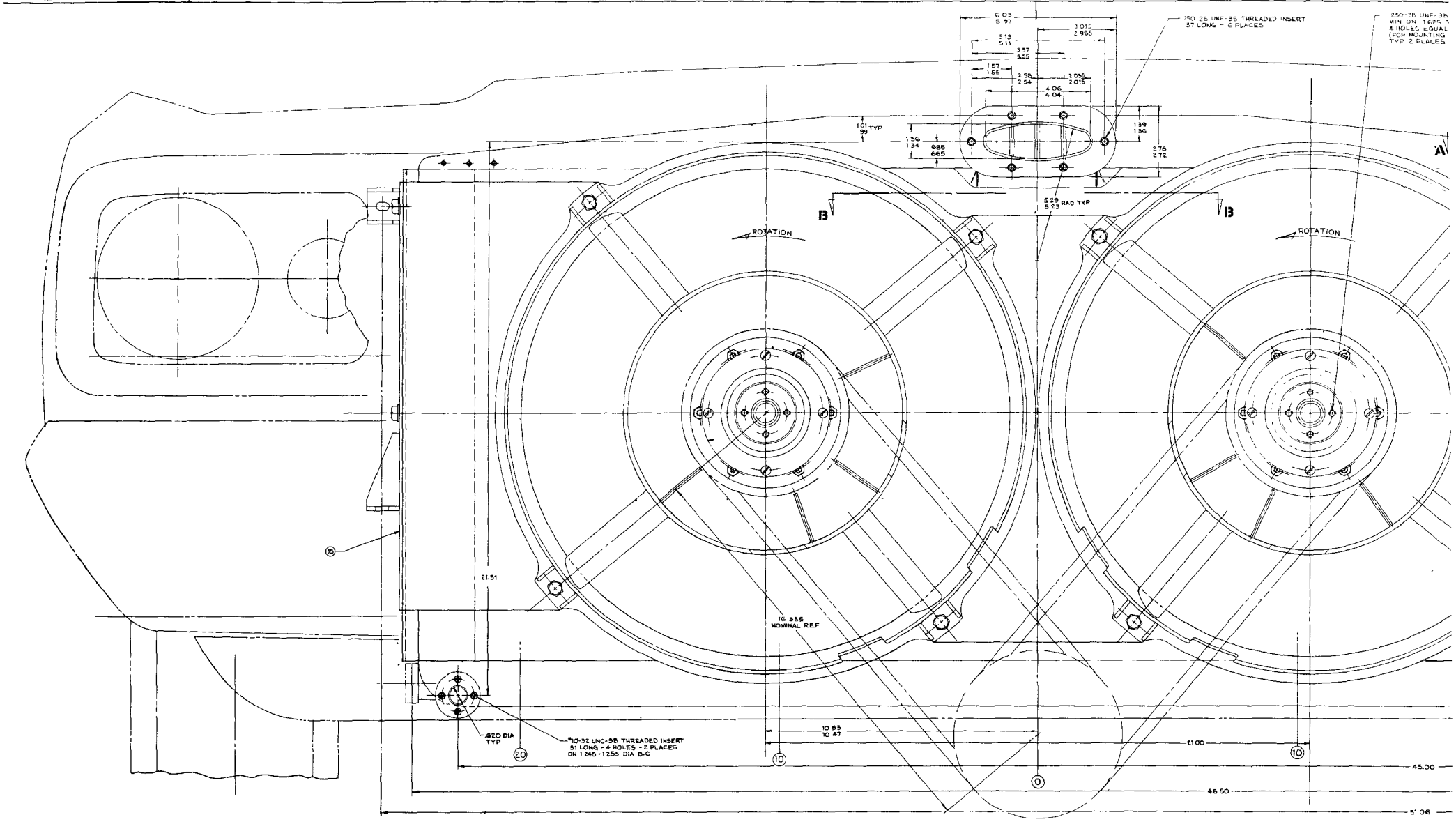
6.03
5.97
3.015
2.985
5.13
5.11
3.57
3.55
1.57
1.55
2.58
2.54
2.035
2.015
4.06
4.04
.101 TYP
.099
1.36
1.34
.685
.665
1.39
1.36
2.78
2.72
250-28 UNF-3B THREADED INSERT
.37 LONG - 6 PLACES
.250-28 UNF-3B
MIN ON .1625 D
4 HOLES EQUAL
FOR MOUNTING
TYP 2 PLACES
5.29
5.23 RAD TYP
B
B
ROTATION
ROTATION
A
21.31
16.335
NOMINAL REF
.820 DIA
TYP
#10-32 UNC-3B THREADED INSERT
.31 LONG - 4 HOLES - 2 PLACES
ON 1.245 - 1.255 DIA B.C
10.53
10.47
21.00
45.00
48.50
51.06
190640
A
1 OF 1
12
11
10
9
8

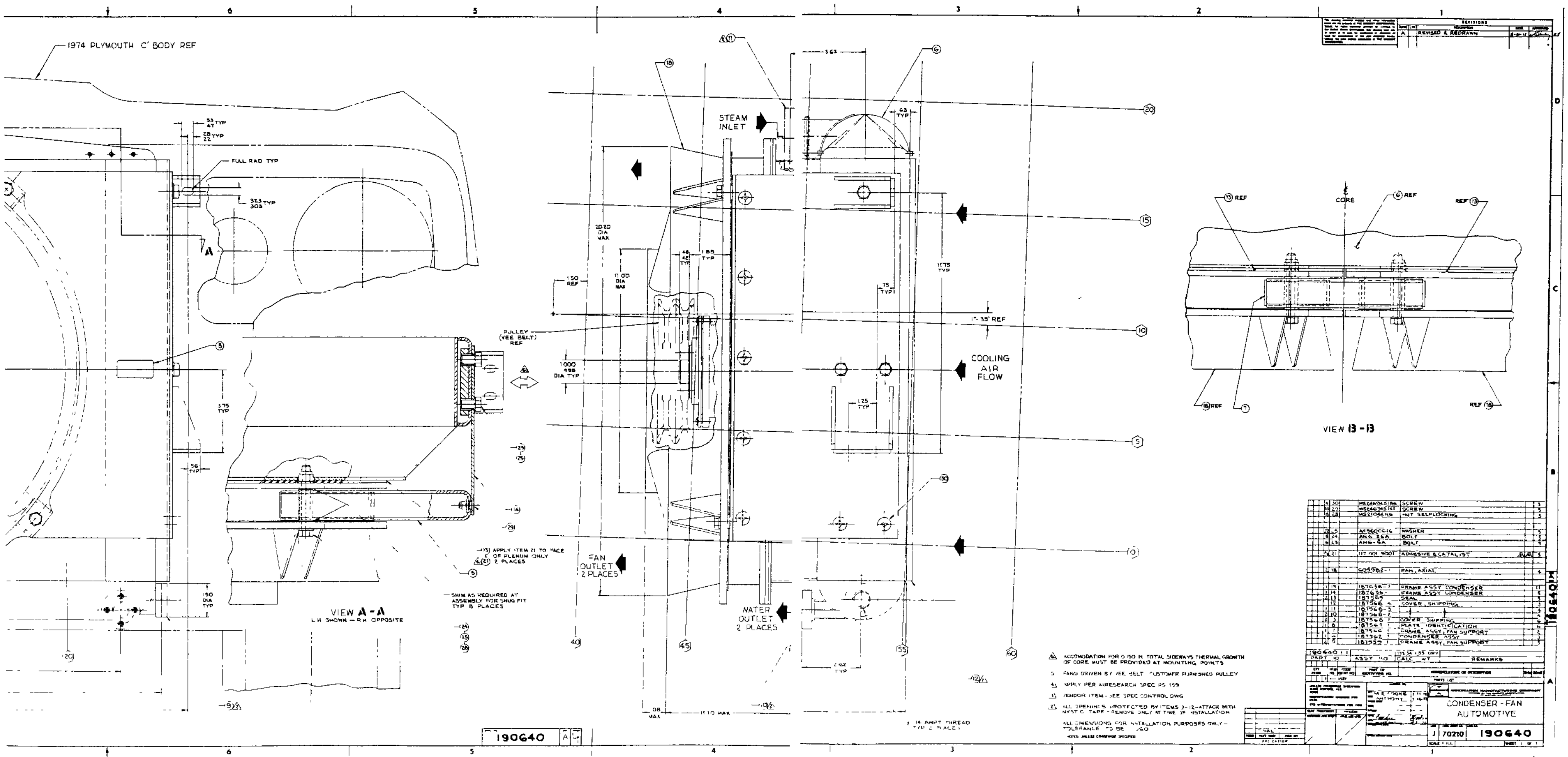
1974 PLYMOUTH C' BODY REF
STEAM INLET
COOLING AIR FLOW
FAN OUTLET 2 PLACES
WATER OUTLET 2 PLACES
PULLEY (VEE BELT) REF
VIEW A-A
L.H. SHOWN – R.H. OPPOSITE
VIEW B-B
CORE
SHIM AS REQUIRED AT ASSEMBLY FOR SNUG FIT TYP 8 PLACES
ACCOMODATION FOR 0.150 IN. TOTAL SIDEWAYS THERMAL GROWTH OF CORE MUST BE PROVIDED AT MOUNTING POINTS
FANS DRIVEN BY VEE BELT CUSTOMER FURNISHED PULLEY
APPLY PER AIRESEARCH SPEC PS 159
VENDOR ITEM - SEE SPEC CONTROL DWG
ALL OPENINGS PROTECTED BY ITEMS 3-12-ATTACH WITH MYSTIC TAPE - REMOVE ONLY AT TIME OF INSTALLATION
ALL DIMENSIONS FOR INSTALLATION PURPOSES ONLY
NOTES: UNLESS OTHERWISE SPECIFIED
FRAME ASSY CONDENSER
SEAL
COVER, SHIPPING
PLATE IDENTIFICATION
FRAME ASSY, FAN SUPPORT
CONDENSER ASSY
FAN, AXIAL
ADHESIVE & CATALYST
WASHER
BOLT
NUT SELFLOCKING
SCREW
PARTS LIST
CONDENSER - FAN
AUTOMOTIVE
70210
190640
REVISED & REDRAWN

For the three EPA condensers the following specific alloys were selected for the tube plates:

Aerojet and SES

Reynolds MD-133 Alloy, 0.020 in. thick, 15 percent cladding thickness (0.003 in.). This alloy consists of type 3003 core with type X4003 cladding which contains 7.5 percent Si and 2.5 percent Mg.

Thermo Electron

Reynolds MD-151 alloy (present designation is XS), 0.020 in. thick, 15 percent cladding thickness (0.003 in.). This alloy consists of type 6951 core with type X4003 cladding which contains 7.5 percent Si and 2.5 percent Mg.

A heat treatable alloy, MD-151, was specified for the TECO core because of its higher working pressure. All other alloys used in the condenser were conventional heat exchanger aluminum alloys.

Core Assembly

All units were basically similar and used a conventional bar-and-plate construction technique. To facilitate brazing, the condenser was divided into four separate modules. After completing module brazing, the four units were weld-assembled to form the complete condenser. The identical -13 perforated air side fin was used on all assemblies and is shown on Figure 5-12. The offset vapor fin used in the TECO and SES assemblies is shown in Figure 5-13 and the perforated plain fin as used in the Aerojet assembly is shown in Figure 5-14, Figure 5-15 shows a completed core module assembly (TECO condenser), and Figure 5-16 shows a closeup of the core construction.

The air-side and vapor-side fins were fabricated from type 3003 alloy; the header and reinforcement bars from type 6951 core alloy; and the tube sheets from Reynolds MD alloys.

When the first core modules were brazed, a considerable amount of distortion was observed as a result of random movement of the header bars from their normal vertical orientation. There was also extensive leakage at the tube-to-header joints. The cores were mechanically straightened in a press and TIG weld repairing was used to achieve a near leak-tight condition. The cores successfully passed a proof pressure test after these operations.

After extensive weld repair, some of the core modules still exhibited a series of minute header bar-tube sheet joint leaks. The leaks were discernible as streams of approximately 0.030 in. dia bubbles when the cores were pressurized to approximately 40 psig. At a pressure less than 40 psig, there were no bubbles. It was obvious that the module would not pass the required helium mass spectrometer leak test without additional repair.

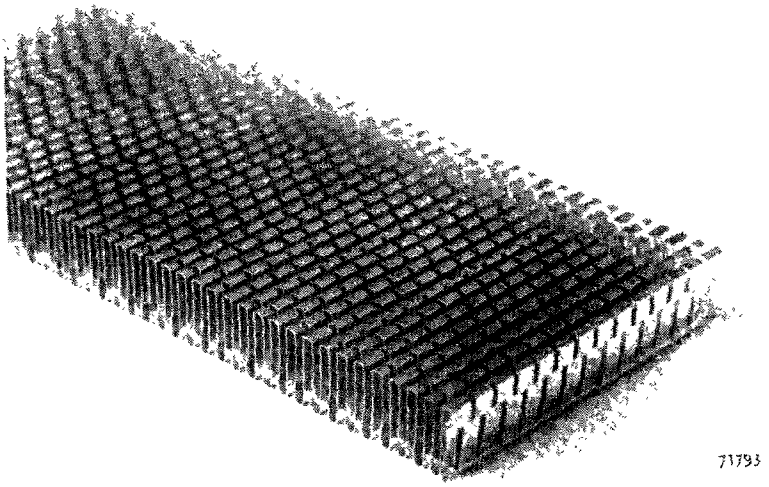

Figure 5-12. Air Side Perforated Fin (-13)

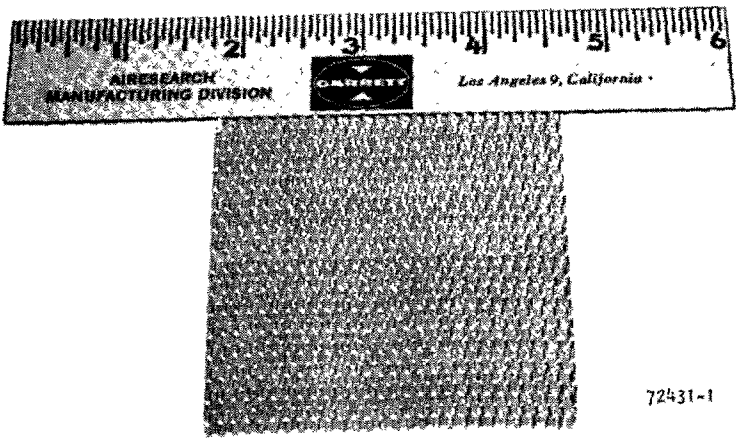

Figure 5-13. Vapor Side Offset Fin (TECO and SES)

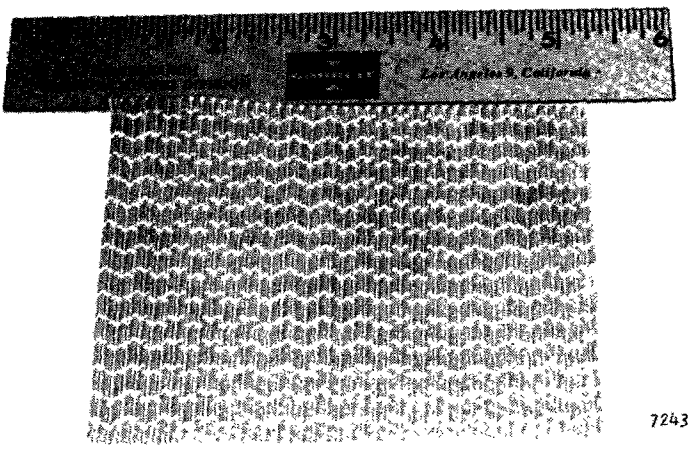

Figure 5-14. Vapor Side Perforated Plain Fin (Aerojet)

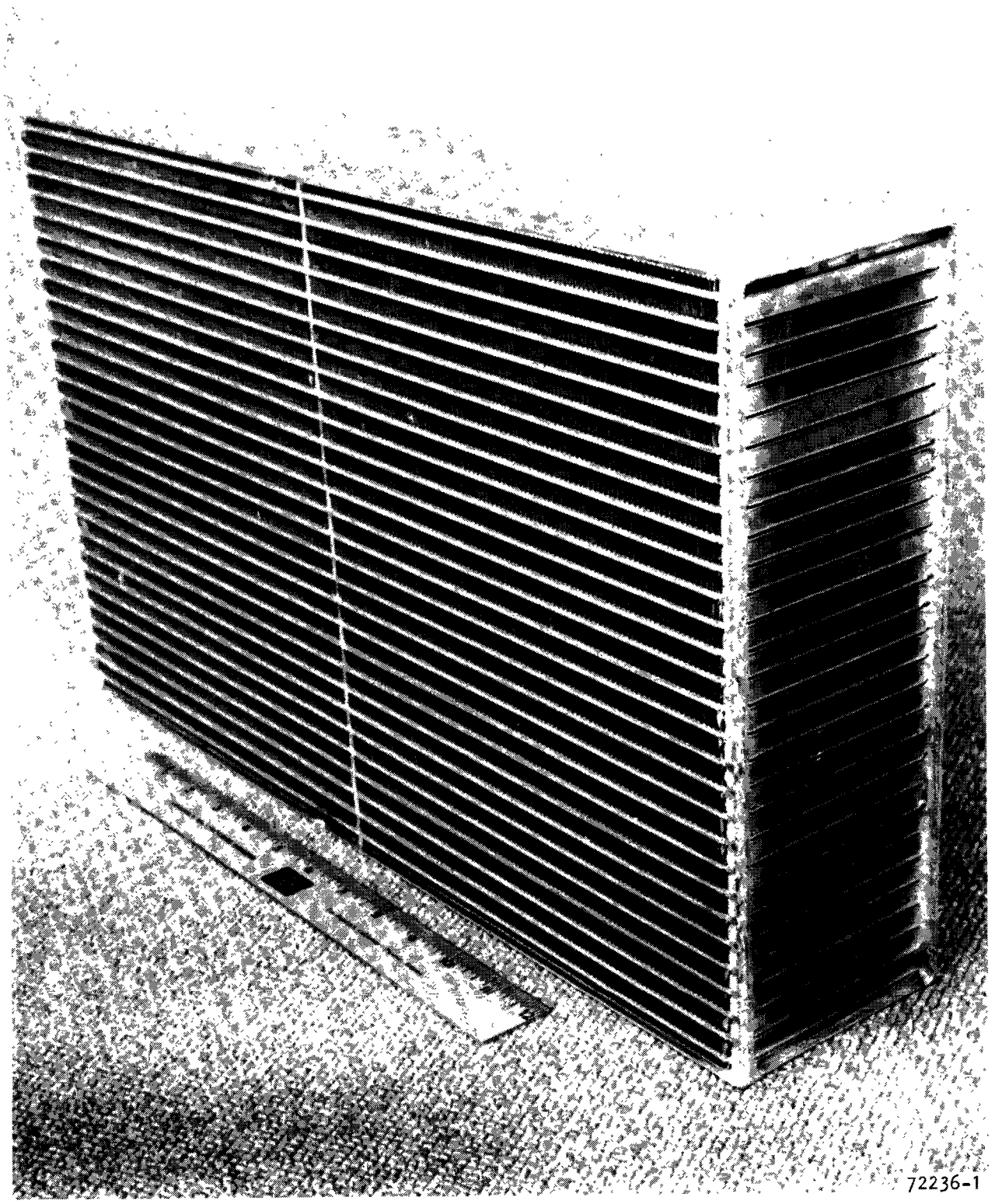

Figure 5-15. Condenser Core Module

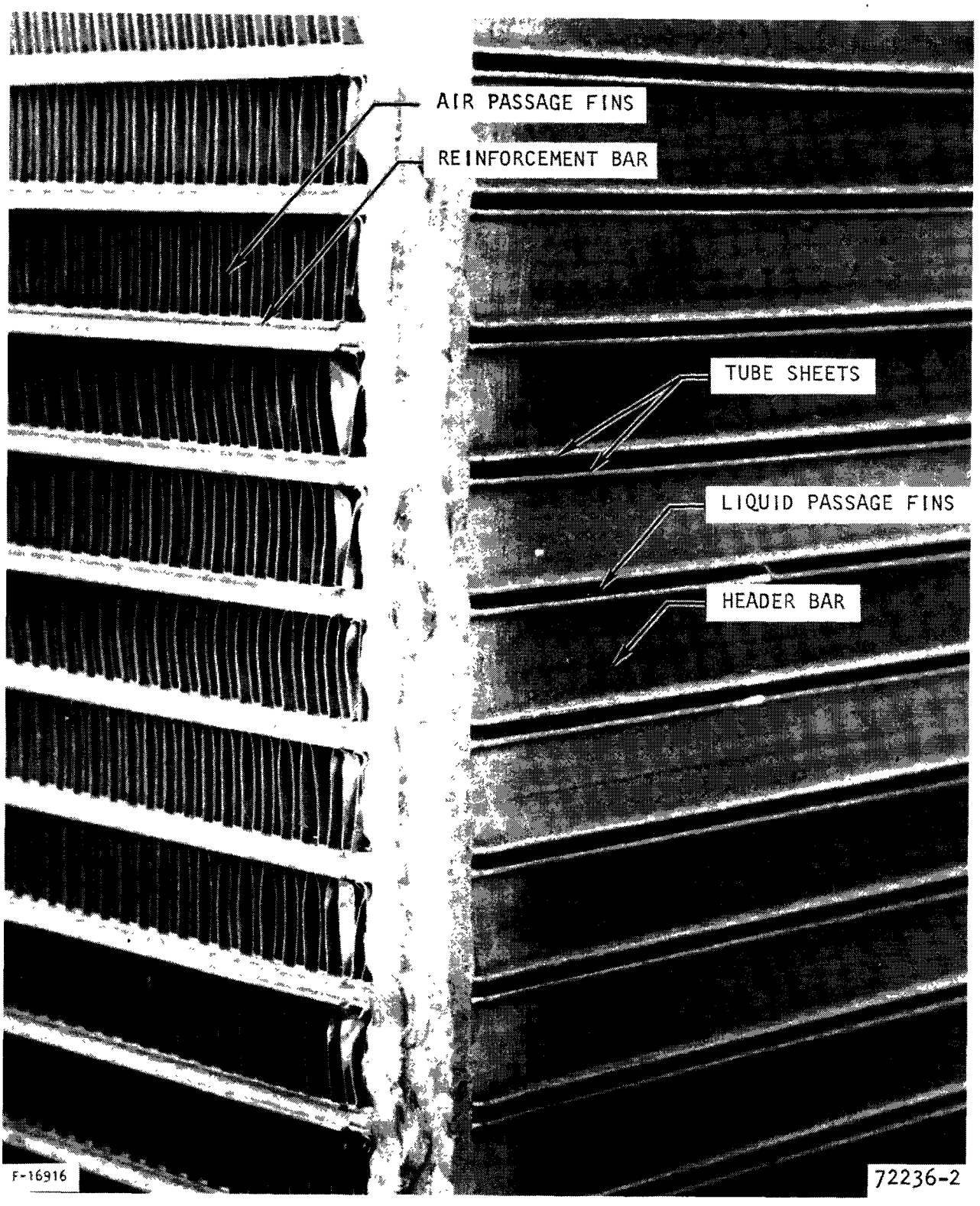

Figure 5-16. Condenser Core Module Detail Component Arrangement

The cores were believed to be structually sound and useable except for the minute leakage. Accordingly, the following repair procedure was used on one of the leaking cores. After the outside surfaces of the core were treated by a chem-film process, it was dipped in a thinned epoxy ester bath while a vacuum was induced in the coolant passages in accordance with AiResearch Process Specification FP-36. After this treatment, the core was thoroughly drained and the epoxy was then cured at 275°F; two coats of epoxy, each approximately 0.00005 in. thick, were applied in this manner. The unit was then leak-tested, using a mass spectrometer. A hard vacuum was drawn inside the core while a helium atmosphere was maintained outside. Under these conditions, a leakage of 8×10^{-8} scc of helium per sec was measured. This leak rate was well below the maximum allowable condenser leakage of 1×10^{-6} scc of helium per sec.

The epoxy ester repair procedure was successful and was subsequently adapted for use on all units. AiResearch has accumulated considerable experience in the field with this coating and it has been found to be extremely durable. In addition to sealing minute leaks, the coating provides excellent corrosion protection for the air-side fins. The coating does not add a measurable amount of resistance to heat transfer.

To verify the structural integrity of the module core assembly braze joints, the epoxy treated core assembly was subjected to a room temperature hydrostatic burst test. The assembly withstood a pressure of 475 psig without leakage. At this pressure, the joint between the pan and core failed. No failure or distortion was observed in the braze joints. Figure 5-17 is a photograph of the failed module. The failure is adjacent to dial indicator No. 5.

Proof pressure for the Aerojet assembly is 85 psig while the maximum proof pressure requirement is 183 psig for the TECO assembly. Because of the margin of safety demonstrated by the specimen, no additional tests were performed.

Subsequent development of the brazing operation eliminated the problems associated with core distortion and gross leakage. To ensure meeting the helium leakage requirement, it was necessary, however, to coat the external surfaces of the final condenser assembly with epoxy ester as previously described.

Aerojet

Final assembly of the Aerojet condenser consisted of the following tasks:

(a) Weld assembly of the four condenser core modules and three subcooler core modules and testing of the weld joints.

(b) Welding of the inlet and outlet pan assemblies and shroud to the core. The appearance of the unit at this stage of assembly is shown by Figure 5-18.

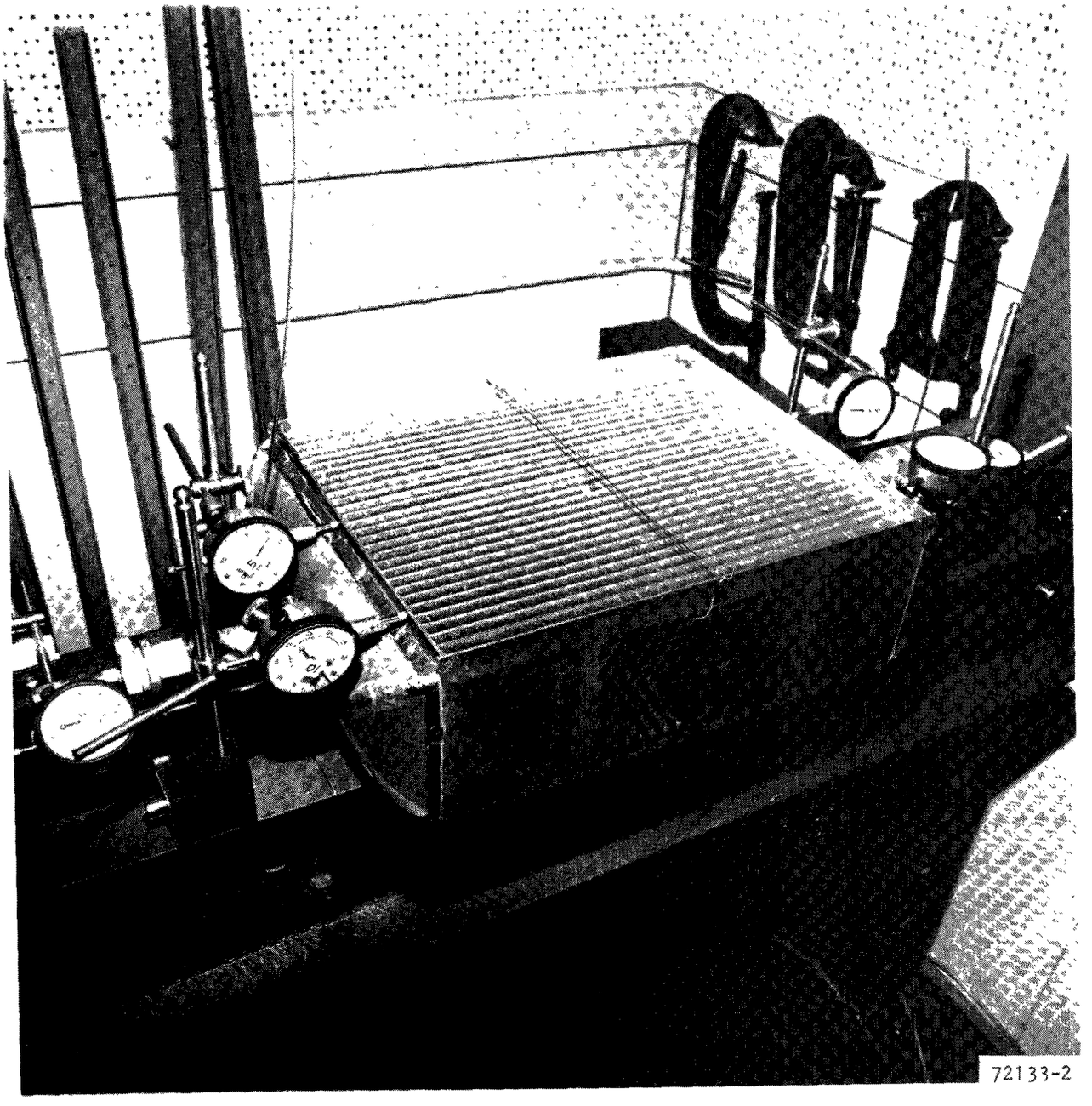

Figure 5-17. Failed Module

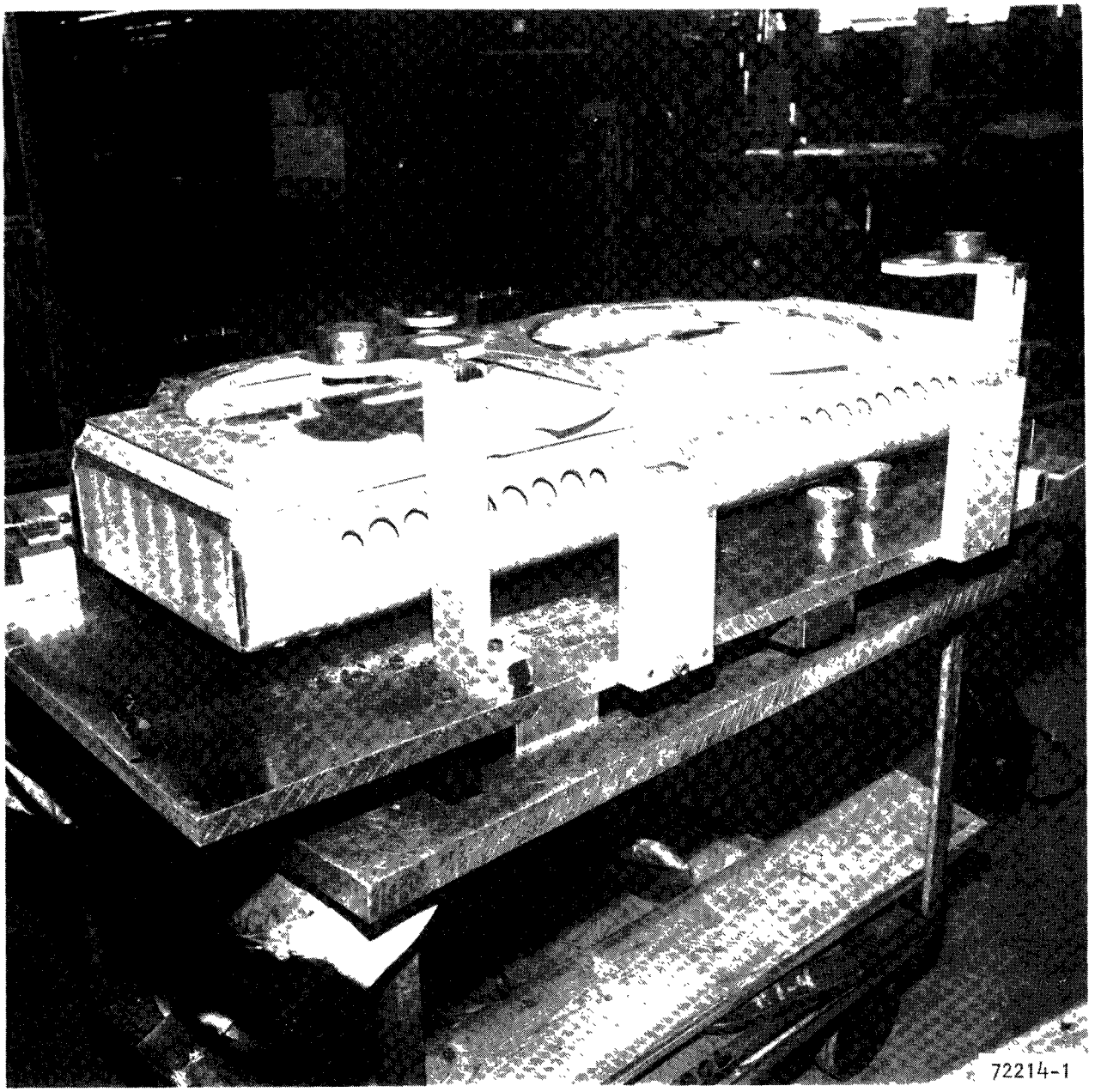

Figure 5-18. Aerojet Condenser, Partially Assembled

(c) Welding of the support bracket to the sides of the cores and the flanged ducts to the inlet and outlet pans.

(d) Machining of flange faces and brackets.

(e) Leak testing with air at 50 psig and proof pressure testing at 85 psig. At this point, all external joints were bubble-free at 50 psig; however, there were minute leaks at three of the core module tube header joints. These leaks were not evident at approximately 10 psig.

(f) Epoxy ester coating of the exterior surfaces of the core and helium leak testing. The measured leakage, with a vacuum inside the vapor passages and a helium atmosphere outside was 1.2×10^{-5} scc of helium per sec.

(g) Weld assembly of the fan support frame.

(h) Painting and final assembly of the condenser and support frame.

Figure 5-19 is a photograph of the front view of the completed Aerojet condenser assembly showing the core assembly. Figure 5-20 is a back view showing the inlet and outlet ducts and the condenser-to-fan shroud. Figure 5-21 is a back view of the condenser assembly showing the inlet manifold assembly. Figure 5-22 shows the final fan support frame of the condenser.

Thermo Electron

A similar assembly sequence was followed for the TECO assembly as for the Aerojet unit. The completed assembly was subjected to a 185 psig proof pressure and leak tested. Helium leakage, measured with a vacuum inside the vapor passages and helium outside, was 4.8×10^{-9} scc per sec. Figure 5-23 shows the front view of the completed assembly and Figure 5-24 shows the back view. The three-piece fan support frame, assembled with the two fans, is shown in Figure 5-25.

Steam Engine Systems

A similar assembly sequence was followed for the SES assembly as for the Aerojet unit. The completed assembly was subjected to an 85 psig proof pressure test. Before final painting, the condenser was subjected to a helium leak test and the final leakage value was 4.8×10^{-5} scc per sec. A front view of the completed assembly is shown on Figure 5-26. Figure 5-27 is the back view of the completed assembly. The three-piece fan support frame, assembled with two fans is shown in Figure 5-28.

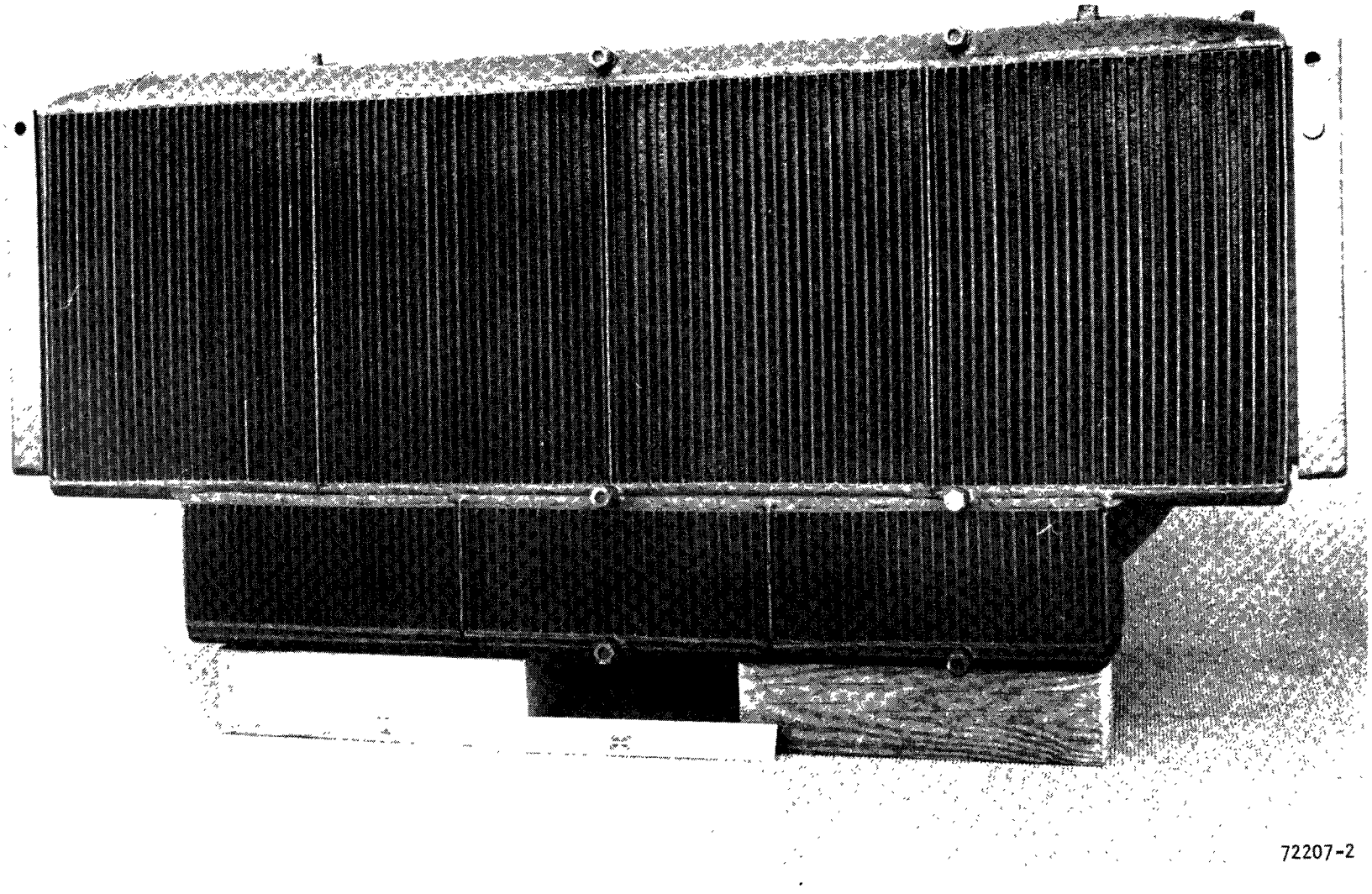

Figure 5-19. Aerojet Condenser Assembly--Front View

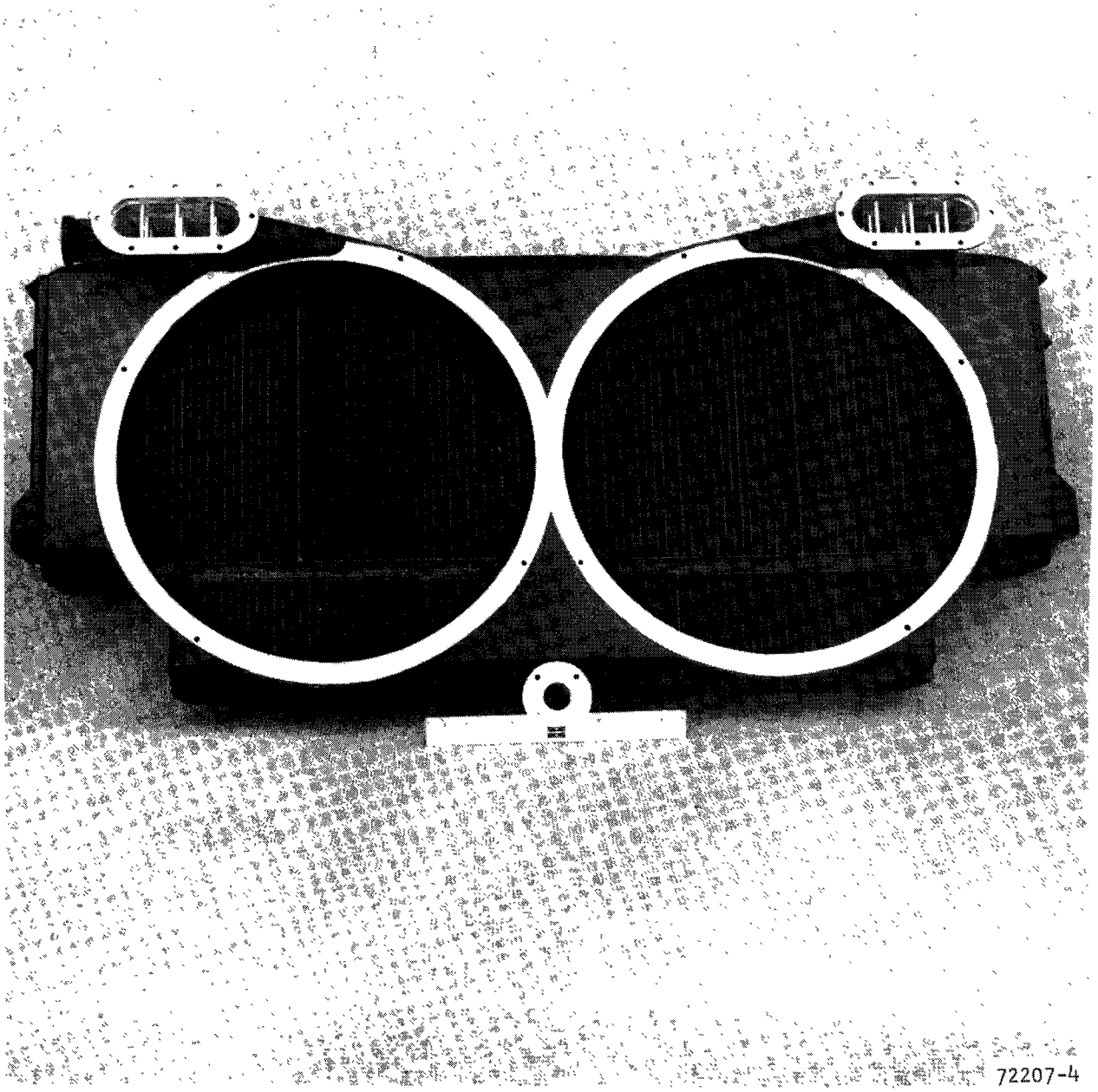

Figure 5-20. Aerojet Condenser, Back View

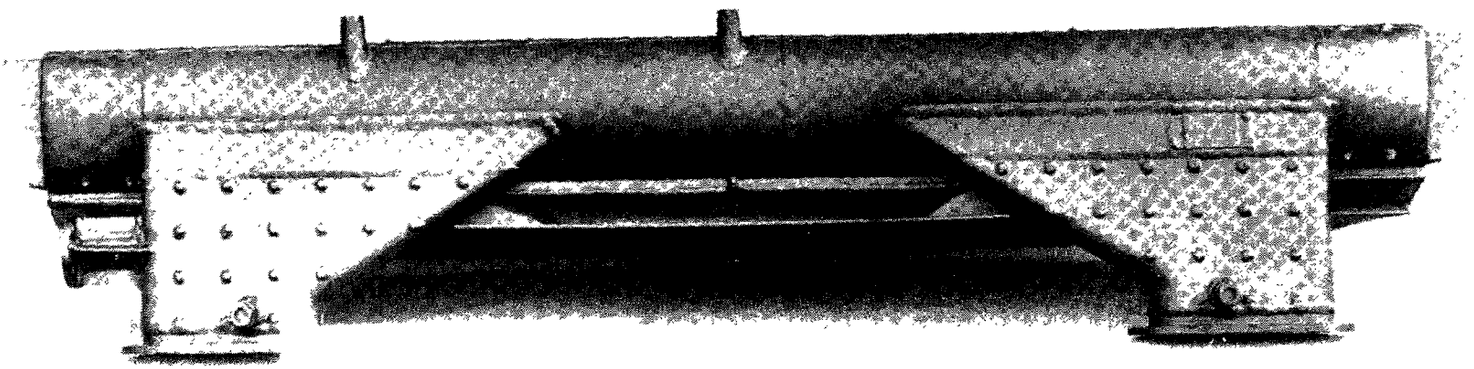

72207-3

Figure 5-21. Aerojet Condenser--Top View

Figure 5-22. Aerojet Condenser--Fan Support Frame

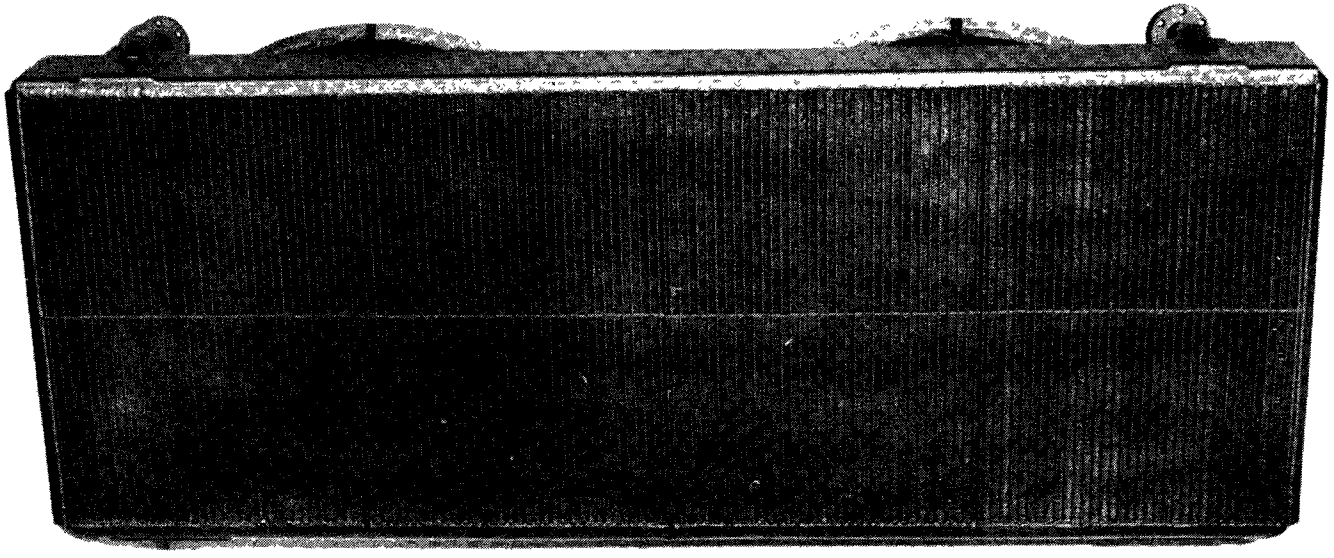

72375-4

Figure 5-23. Thermo Electron Condenser--Front View

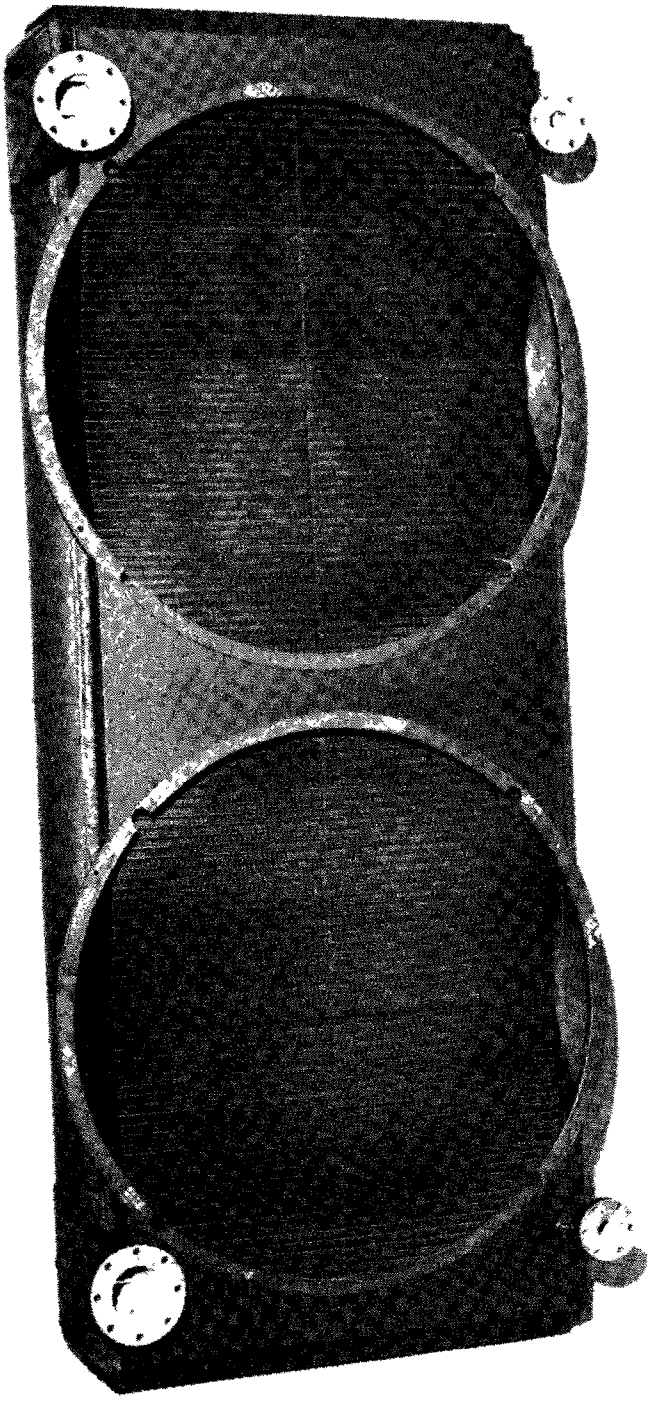

72375-6

Figure 5-24. Thermo Electron Condenser - Back View

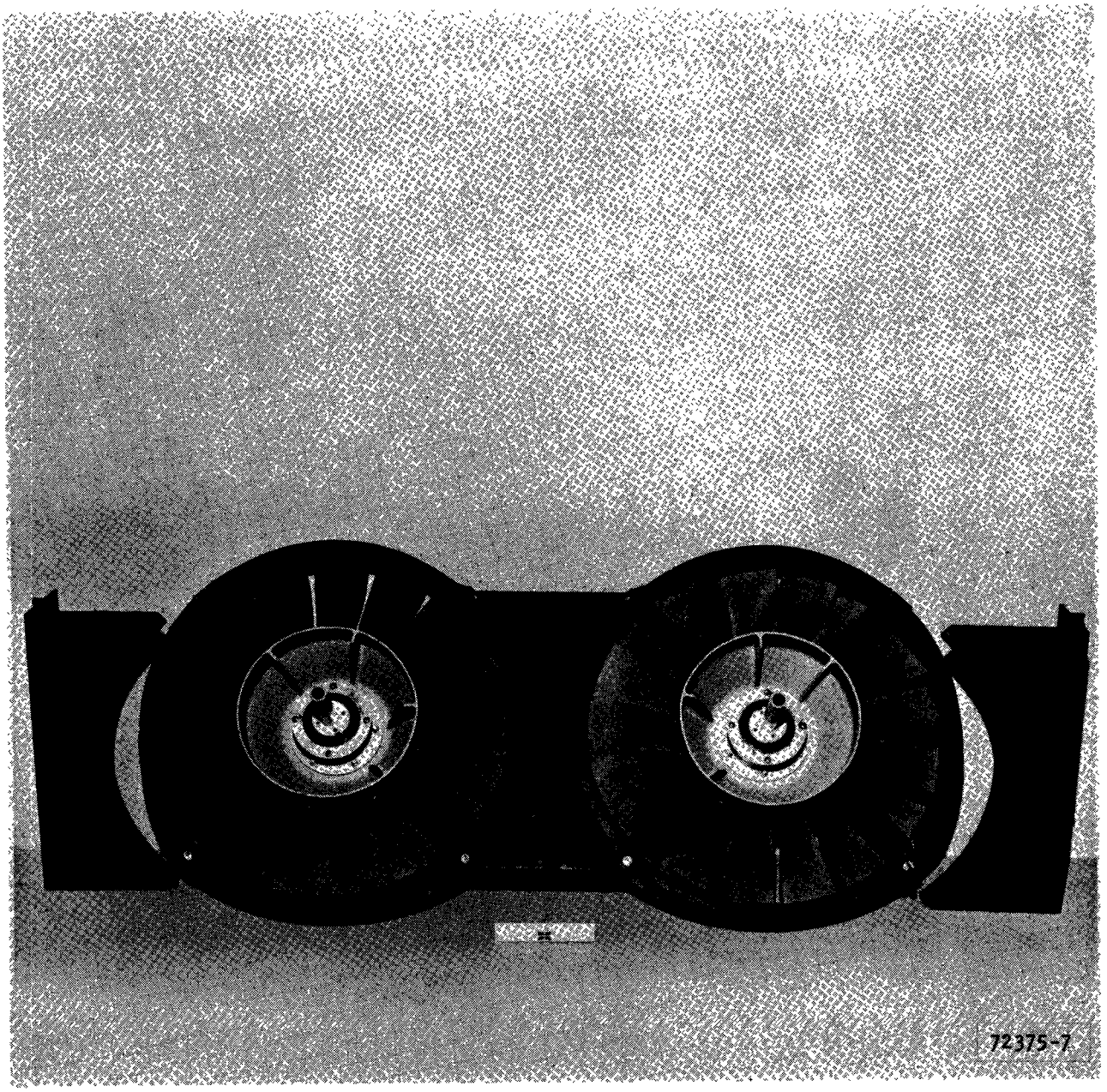

Figure 5-25. Thermo Electron Condenser--Three-Piece Fan Support Frame

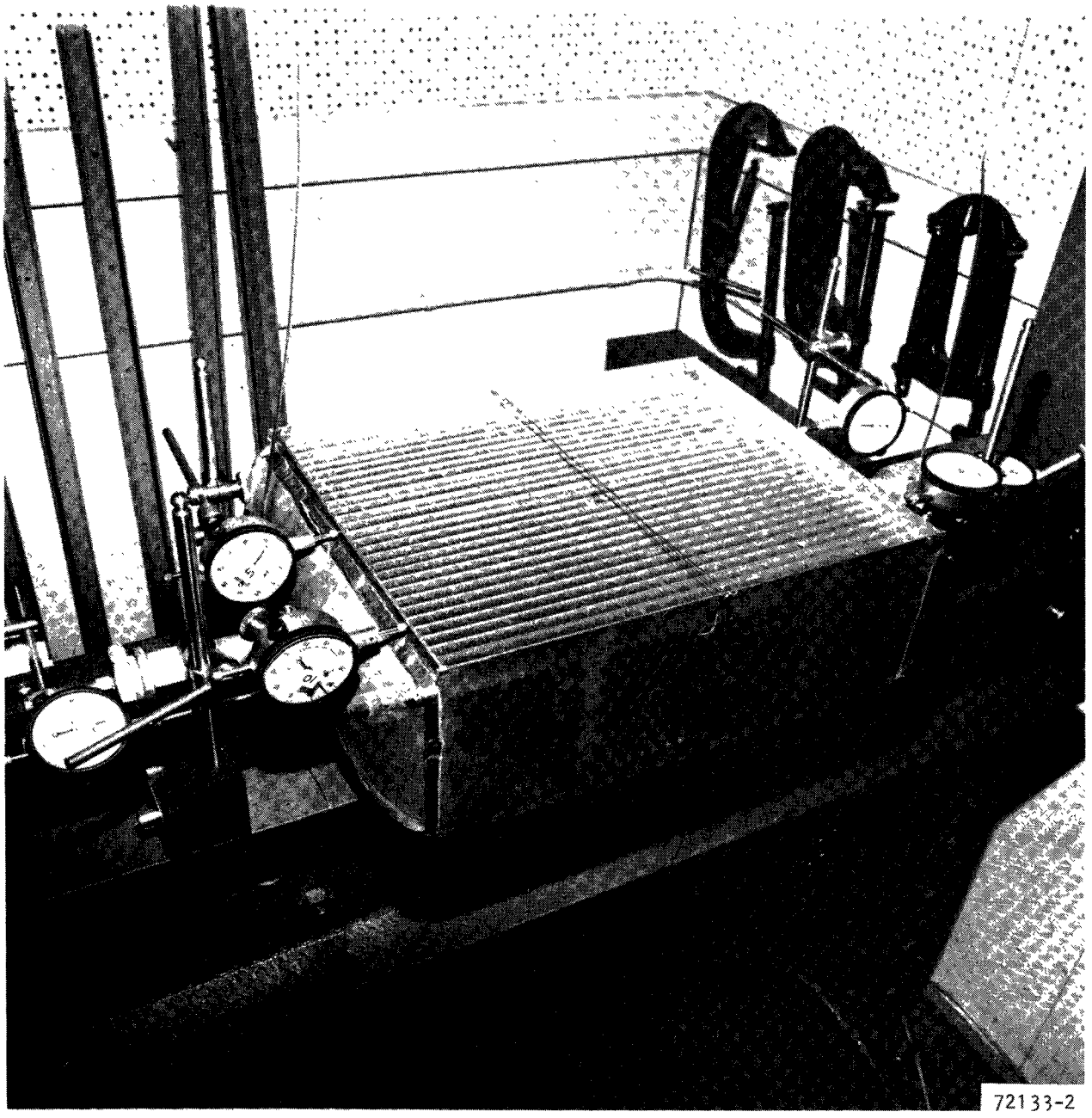

Figure 5-26. Core Module Structural Test

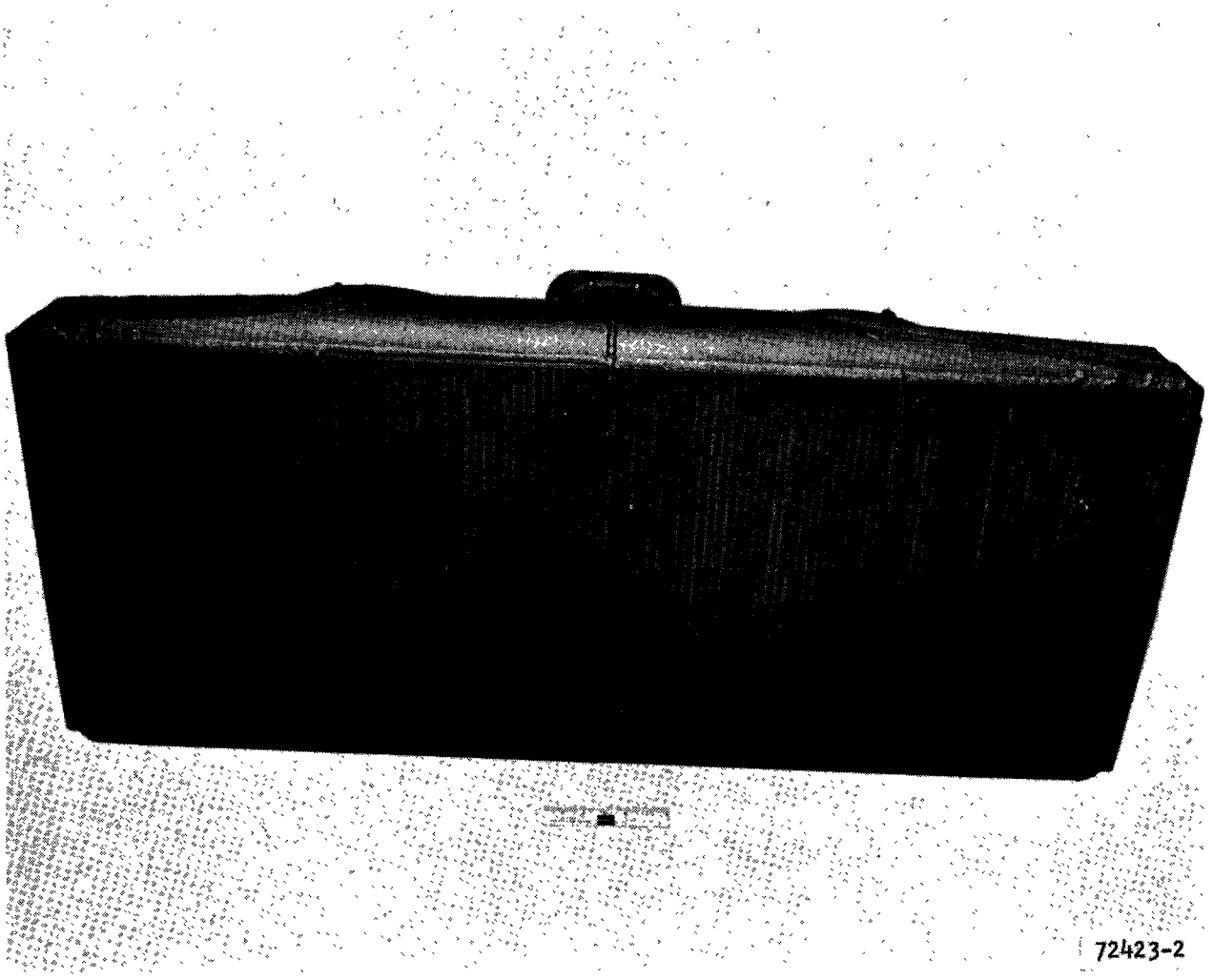

Figure 5-27. Steam Engine Systems Condenser--Front View

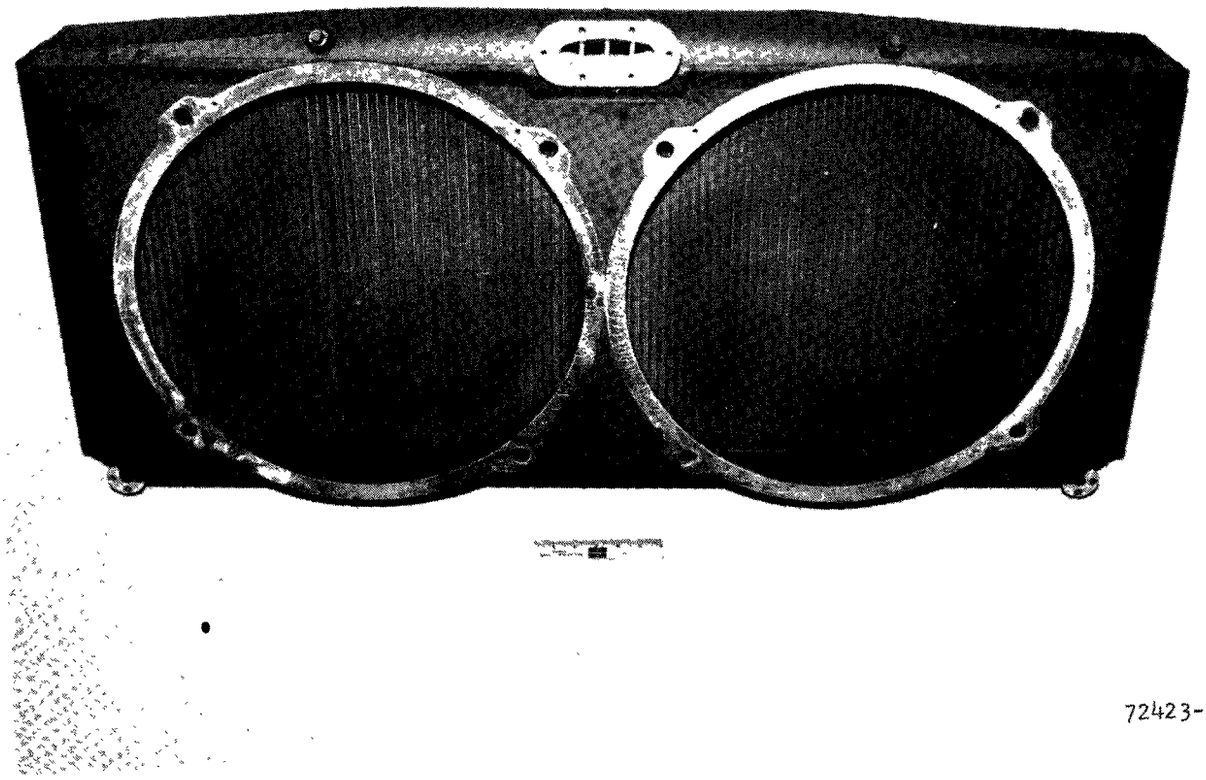

72423-3

Figure 5-28. Steam Engine Systems Condenser--Back View

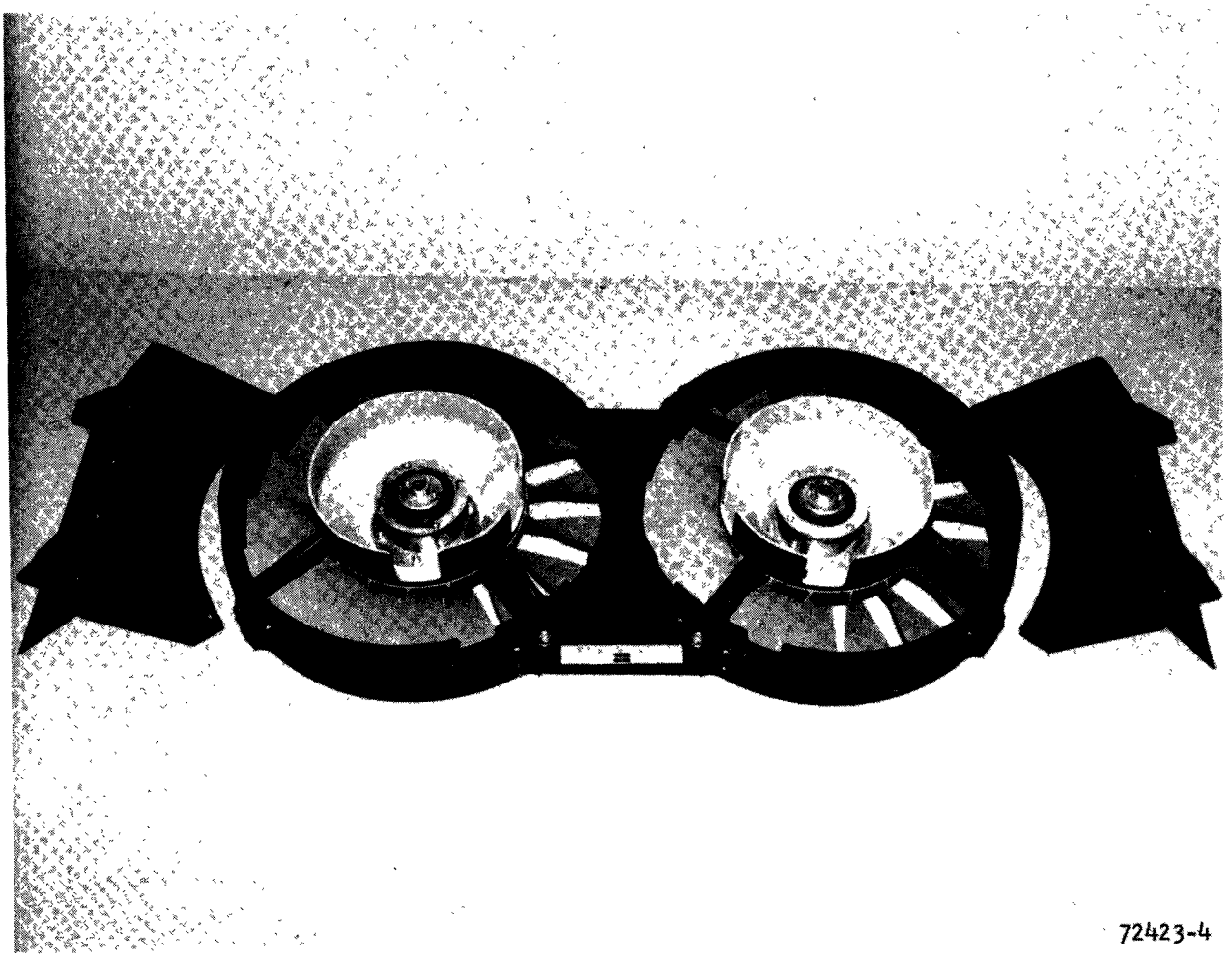

Figure 5-29. Steam Engine Systems Condenser--Three Piece Fan Support Frame

HEAT TRANSFER PERFORMANCE TEST

Condenser heat transfer performance can be established by testing a section or module of the full-size condenser in striaght crossflow. The full-size condensers for all three systems actually consists of four separate modules which are welded together to form a complete assembly. Thus, if production type detail parts, i.e., fins, header bars, and tube plates are utilized in the module (1/4 section of the full condenser), then the module test results can be considered as fully representative of the full-size condenser performance. Module testing is considered wise since a separate test unit can be utilized rather than risk contaminating or damaging a deliverable assembly.

To minimize test cost it was decided to eliminate testing with the organic working fluids (AEF-78 and Fluorinol-85) and to utilize steam or hot water as the working fluid. This procedure is believed to be reasonable because most of the heat transfer resistance is on the air-side of the unit and any change in the condensing-side performance would have only a small effect on the overall performance. The condensing side resistance is calculated to range from 4 percent (steam) to 18 percent (Fluorinol-85) of the overall resistance. Moreover, the condensing side performance has been determined as described in the condensing heat transfer test, Section 4.

Thus, the remaining item to be verified is the air-side performance. The condenser design is based on the results of the -13 test core as previously described. This data was originally obtained using s small 4 in. by 4 in. face area test core which utilized preprototype perforation tooling. It was considered to be wise to test a full-size module which utilized all of the production-type detail parts and fluxless brazing processer.

Test Unit

A SES module was selected to represent the typical condenser section. A sketch of the module design is shown in Figure 5-29. Figure 5-30 is a photograph of the completed assembly. The unit was designed to utilize high velocity steam as the heat source. Thus, a fan-shaped steam inlet duct was specified to provide uniform steam distribution across the inlet face of the test module. Flanges, designed to mate with the laboratory air ducts, are incorporated on the air side of the test module. The test module finishing operations, chemical film, epoxy dip, and paint, are identical to those used for the full-size condenser.

Performance Test

This task was terminated after completing the test unit fabrication. No performance tests were conducted.

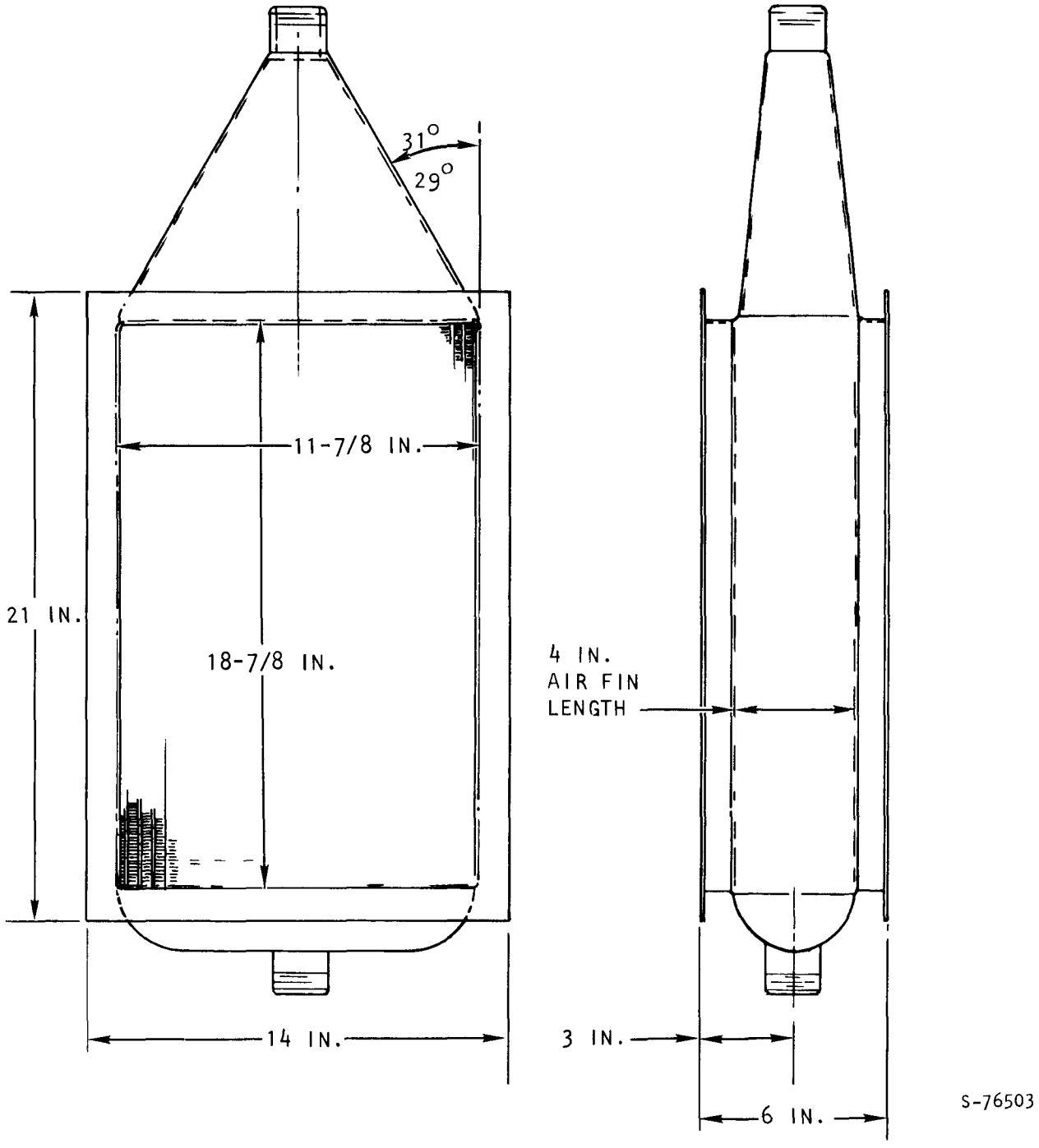

Figure 5-30. Heat Transfer Performance Test Module

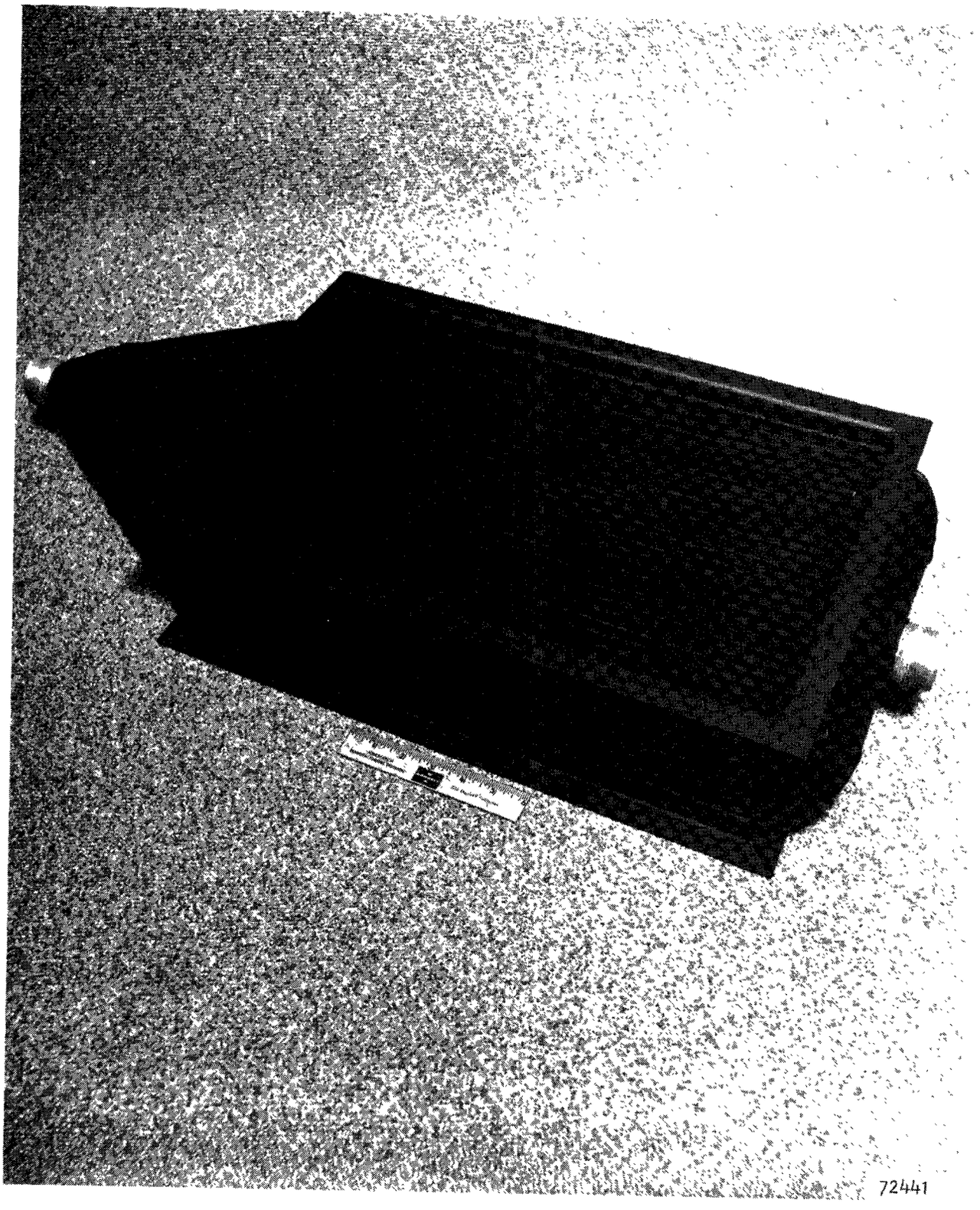

Figure 5-31. Heat Transfer Performance Test Module

SECTION 6

FAN DESIGN, FABRICATION, AND TESTING

SECTION 6

FAN DESIGN, FABRICATION, AND TESTING

DESIGN

Fan design requirements as generated by the three system contractors are summarized on Table 6-1. Installation drawings supplied by the system contractors all depicted a tube-axial fan configuration because of the severe axial length restrictions in the engine compartment: i.e., space was alloted for the fan impeller but no axial length was allowed for the inclusion of stator vanes for removing the swirl velocity component from the fan discharge air.

After a detailed review of the fan problem statements, the following fan design philosophy was adopted:

(a) Design a high performance tube-axial fan to meet the specified performance. A sophisticated aerodynamic design will be essential to meet the high efficiency requirement.

(b) If possible, use a single basic aerodynamic design for all applications. Close to optimum performance would be achieved by varying the tip diameter and rotational speed. This procedure was considered essential to minimize program cost since a single aerodynamic design would require only one impeller casting.

(c) Maximize fan diameter consistent with the installation dimensions to improve condenser effectiveness and minimize the fan dump loss.

(d) Incorporate a slight radial component in the fan discharge velocity (conical flow) to help reduce the fan sensivity to flow blockage

(e) Minimize rotational speeds to reduce swirl losses and acoustic noise

(f) Select a design that can be produced using high volume, low cost processes.

(g) Provide ample stall margin to allow for a probable increase in the installation pressure loss.

(h) Design for minimum axial length to fit within the alloted space

TABLE 6-1

FAN DESIGN REQUIREMENTS

System Contractor	Aerojet	Thermo Electron	Steam Engine Systems
Total number of fans	2	2	2
Design point vehicle speed, mph	50	90	32
Ambient temperature, ^{o}F	14.7	14.7	14.7
Ambient pressure, psia	14.7	14.7	14.7
Air temperature at fan inlet, ^{o}F	205	189	217
Total airflow, lb/hr	52,000	75,300	38,198
Volumetric airflow per fan, cfm	7,250	10,300	5440
Inlet flow dynamic pressure, in. H_2O	1.17	3.79	0.44
Inlet recovery factor, per cent	78	100	100
Net ram pressure rise, in. H_2O	0.91	3.79	0.44
Predicted condenser air-side pressure drop, in. H_2O	3.95	4.09	2.09
Installation loss, in. H_2O (1)	1.67	2.80	1.22
Required fan total pressure rise, in. H_2O	4.71	3.10	2.87
Calculated air horsepower	5.4	5.0	2.5
Specified efficiency, percent	70	70	Not Specified
Fan rotation (2)	ccw	ccw	ccw
Fan drive mechanism (3)	Hydraulic Motor	V-belt	V-belt
Maximum overall length	6.4	4.0	Not specified
Fan noise level, dbA maximum	(4)	(4)	(4)

(1) Installation loss includes losses across the bumper, grille, transition section between condenser and fans, and the engine compartment.

(2) Fan rotation as viewed from drivers seat

(3) Hydraulic motors and V-belt drive mechanisms are supplied by the system contractor.

(4) Fan noise levels have not been specified. However, the overall vehicle noise level, of which the fans are probably a major portion, shall not exceed 77 dbA at 50 ft according to the EPA vehicle specifications.

Impeller Design

The basic fan impeller design was based on the TECO requirements because it had the longest blades. The NACA 65 series blade section thickness distribution was used because experience has shown this section to be superior to the older circular arc and parabolic arc sections for this class of tube axial fan. A hub shape previously found effective on this class of machine was used and the maximum permissible tip diameter of 22 in. used. The maximum number of blades for trouble-free casting, 17, was selected. By iteration, the hub diameter and approximate chord length were established. The flow paths at various blade sections were obtained by electrical analog assuming a uniform pressure at the blade trailing edge. The velocity triangles presented in Figure 6-1 were obtained from this approach. The estimated rotational speed was 2500 rpm.

Each individual blade section was carefully analyzed to allow for maximum surge margin without compromising too much on negative stall. This results in the selection of slightly negative incidence angles for sections near the tip where the flow angles are very high. Blade parameters are summarized on Table 6-2.

The rotational speeds for the TECO and SES fans were selected to produce the pressure rise required by the problem statements in the areas of maximum efficiency and the impeller tip diameters were calculated to reduce the flow area to that required for the specified flow rate. It was recognized that minor speed changes could be made on prototype units to make final adjustments to performance.

A stress analysis of the impeller was conducted on the 22 in. impeller for a rotational speed of 4000 rpm. Effective stress levels in the blades and hub are presented in Figures 6-2 and 6-3. All stresses were well within the allowable stresses for the impeller material. A blade vibration study indicated that the first bending mode occurs at approximately the twelfth harmonic of blade frequency at operating speed. Results of that study are presented in Figure 6-4. Additionally, it was found that at 4000 rpm the forward movement of the blade tip of a 22 in. impeller would not exceed 0.015 in. max. In the interests of safety, it was decided to limit fan operating speed to 3600 rpm.

Housing Design

In order to insure maximum fan efficiency, the impeller to housing clearance must not be so close as to cause excessive boundary layer drag, nor so great as to permit significant leakage. For fans of this class, that value is approximately 0.030 in., which is the nominal value used for the three designs. Clearances of this magnitude dictated that the impeller had to be accurately positioned relative to the outer housing (shroud). Thus, four struts were used to support the centerbody which carried the rotating assembly. The impeller hub diameter was matched to the centerbody diameter to minimize turbulence, thus reducing turbulence induced noise. The number of struts does have an integer relationship to the number of impeller blades, so noise was minimized by having only one blade wake striking a support strut

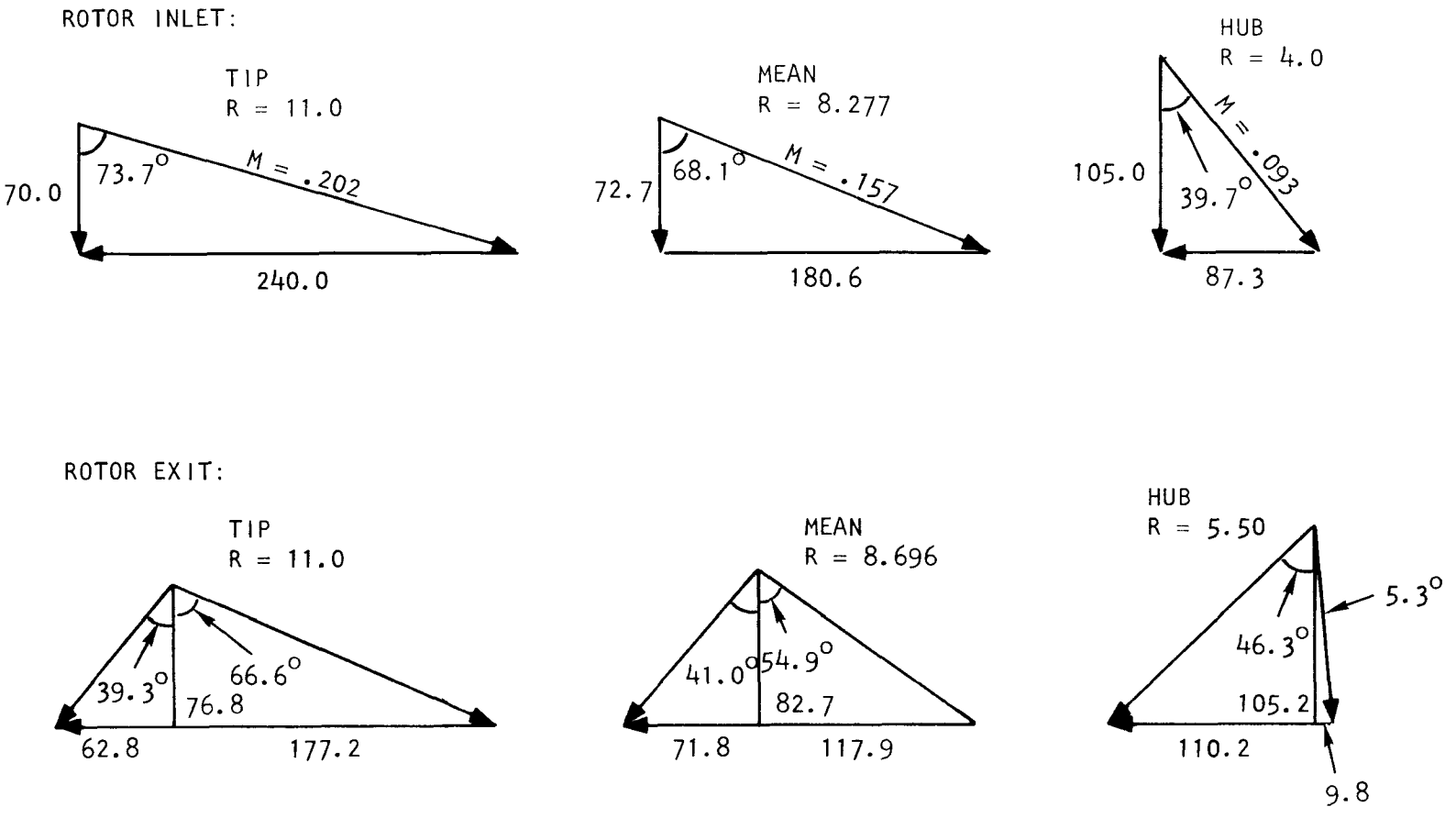

Figure 6-1. Fan Velocity Triangles

TABLE 6-2

FAN BLADE PARAMETERS

Streamline	Hub	Mean	Tip
Leading edge radius, in.	4.0	8.3	11.0
Trailing edge radius, in.	5.5	8.7	11.0
Camber angle, deg	45.0	19.4	11.9
Chord along streamline, in.	3.48	3.77	3.84
Thickness, percent	12.0	8.5	6.0
Incidence angle, deg	-3.8	1.1	-0.8
Stagger angle, deg	21.0	57.3	68.6

Number of blades = 17

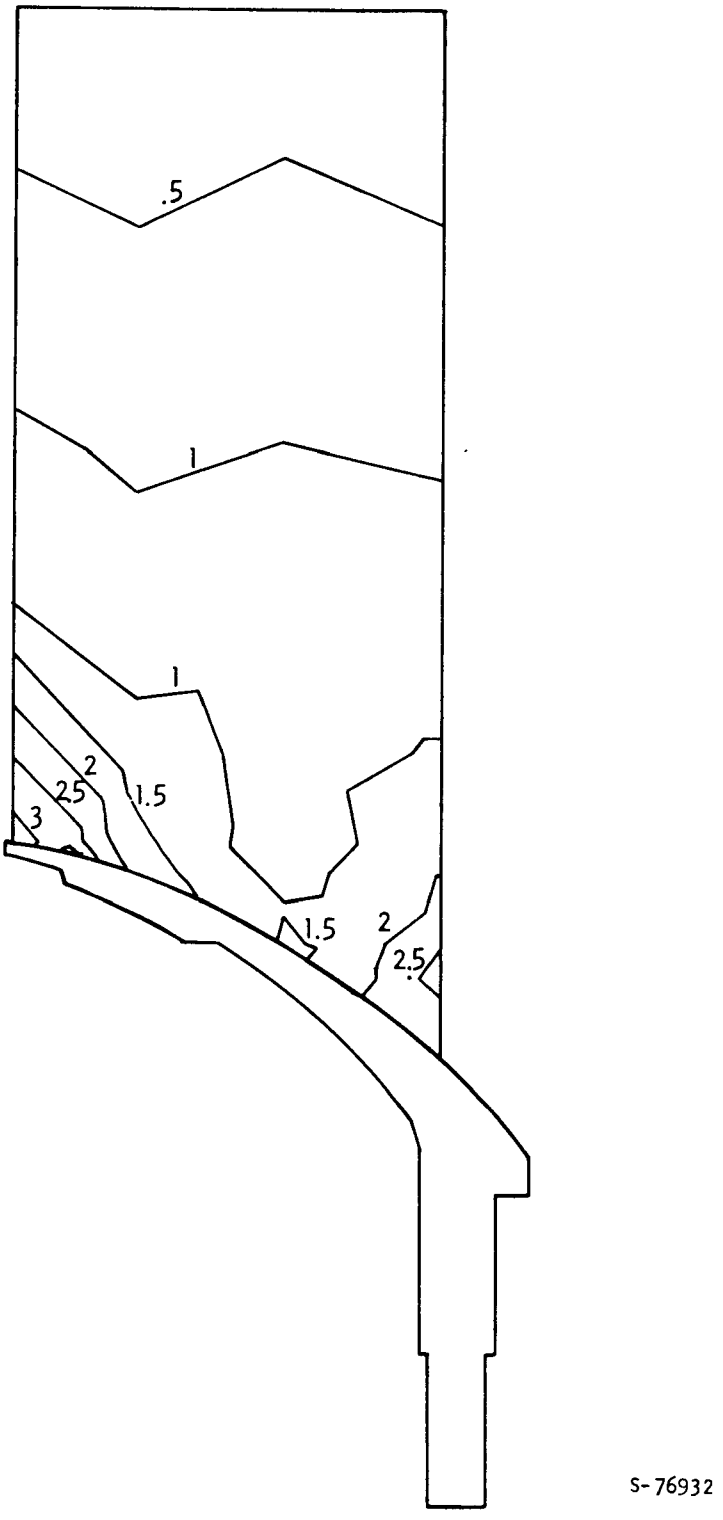

Figure 6-2. Effective Stresses (KSI) on Plate at 4000 RPM

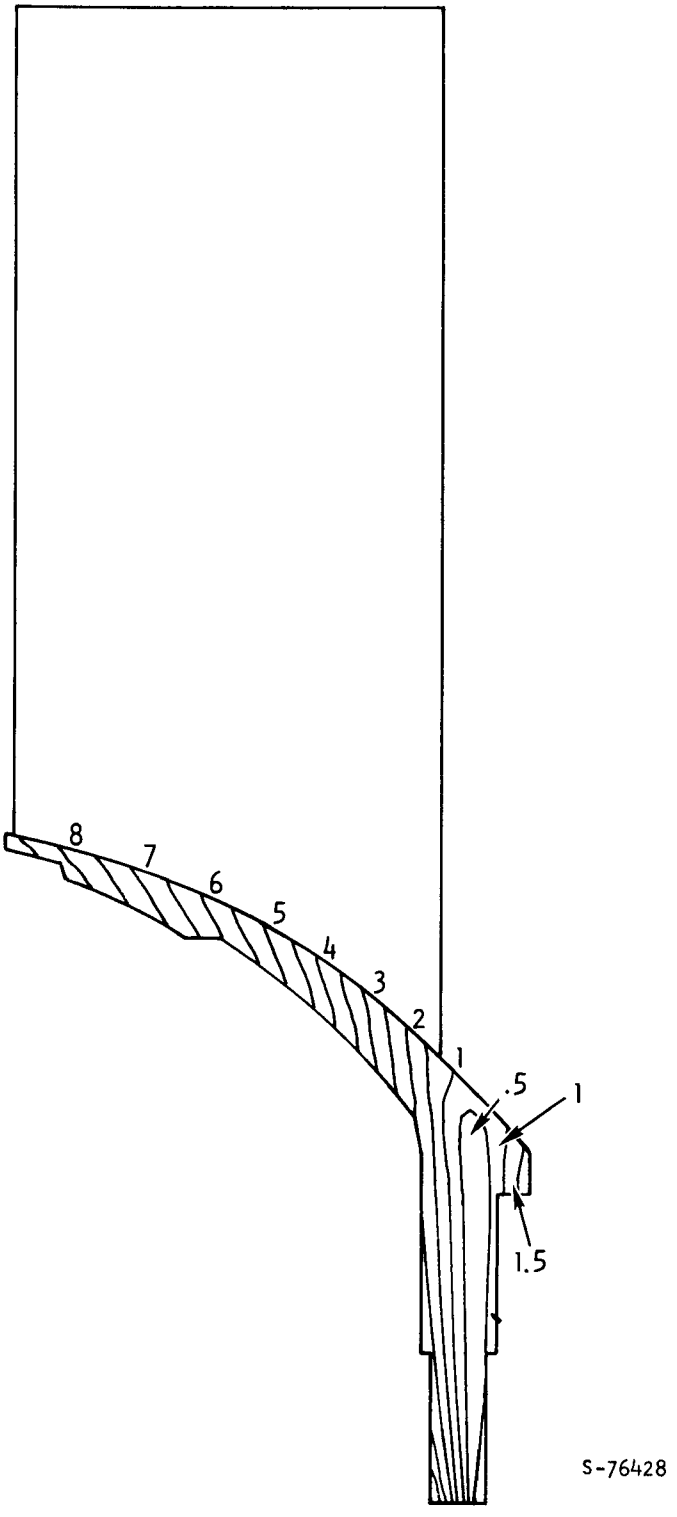

Figure 6-3. Effective Stresses (KSI) on Disk at 4000 RPM

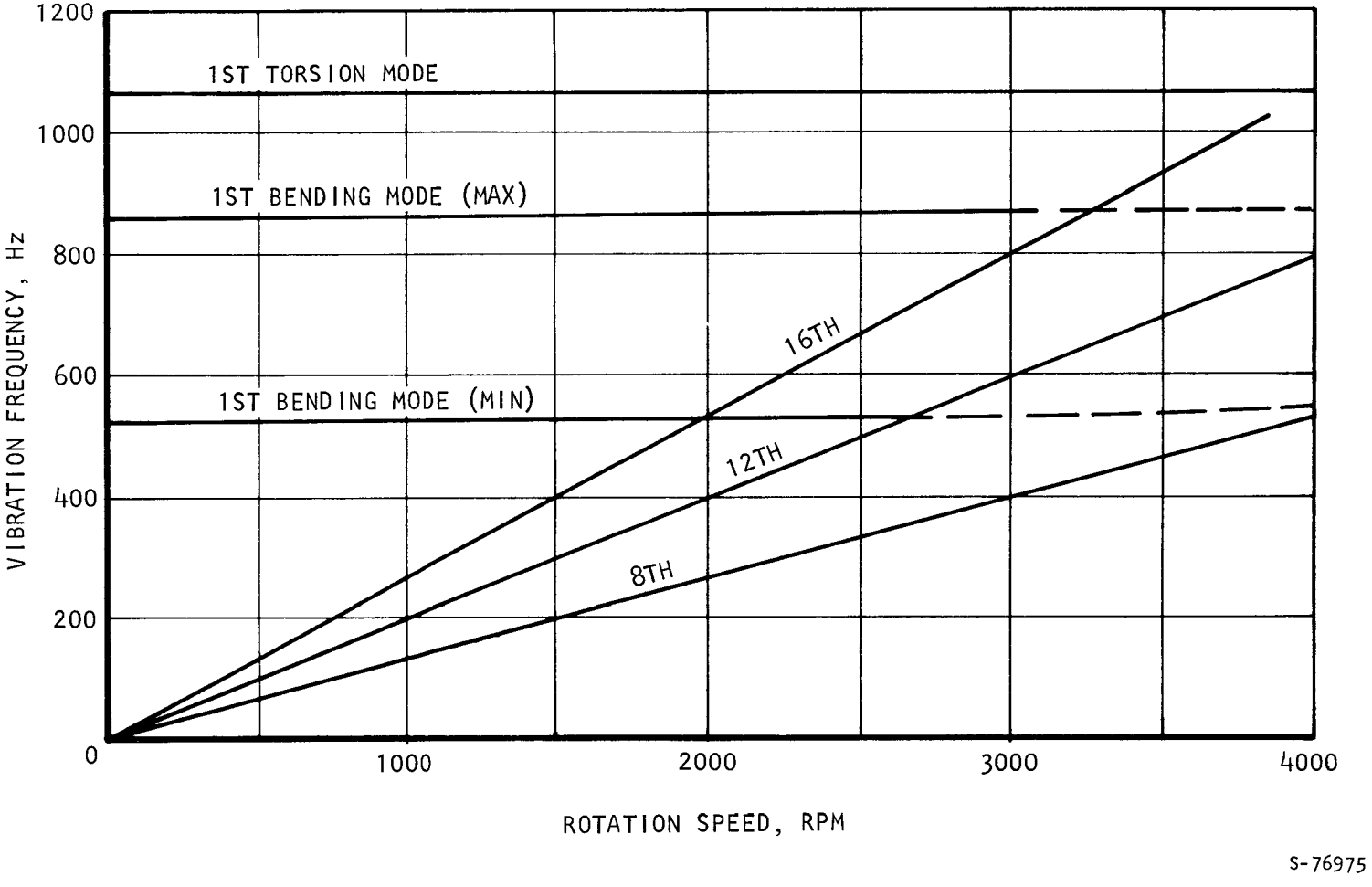

Figure 6-4. Blade Vibration Interference Diagram (22.0 In. OD)

at any given instant in time. There is a direct load path from the centerbody through the struts to the mounting holes. The support struts were aligned with the average air angle leaving the impeller. There was no possibility of trying to recover the rotational (swirl) component of velocity, so the struts were aligned to present a minimum of flow resistance.

Fan designs are summarized on Table 6-3.

TABLE 6-3

FAN DESIGN SUMMARY

	System Contractor		
	Aerojet	TECO	SES
Volumetric airflow per fan, cfm	7,250	10,300	5,440
Total pressure rise, in. water	4.7	3.1	2.9
Inlet temperature, ^{o}F	205	189	217
Number of blades	17	17	17
Tip diameter, in.	19.2	22.0	18.85
Speed, rpm	2,980	2,400	2,360

Detail Design

Outline dimensions of the Aerojet fan are shown on Dwg No. 605972. In this case, the fan impeller is directly mounted on the hydraulic motor output shaft; the bearing assembly is contained within the motor. The hydraulic motor is a commercial product, developed by Hydraulic Products Incorporated, Sturtevant, Wisconsin. The motor ratings are: 11 gpm flow at 2800 rpm producing 220 ft-lb torque at 2000 psi. All shaft seals are Viton elastomer. The unit is a standard design except that the output shaft diameter was ground to 0.8740-0.8742 in. diameter to provide a closer fit with the fan impeller. The impeller is secured to the shaft using a 0.250 in. square key and a setscrew. The hydraulic motors were purchased by Aerojet and supplied to AiResearch for installation on the fan assembly.

Outline dimensions of the TECO and SES fans are shown on Dwg Nos. 605977 and 605982, respectively. Both fans are designed to be belt driven. Slots were cut in the housing to permit belt clearance. Large diameter, sealed, grease packed, deep groove ball bearings with maximum separation between the impeller end and pulley end bearings are provided. Based on a 3000 hr life, these bearings are designed to support maximum side loads of from 775 lb applied at the face of the drive shaft step to 225 lb applied 4 in. back of the fan centerbody (i.e., the end of the 605977-1-1 driveshaft). The bearings

are lubricated with Unitemp 500A, a high temperature grease, and do not require additional lubrication during the estimated 3000 hr life. The bearings are mechanically preloaded and locked to preserve the preload and ensure maximum bearing life.

FABRICATION

The prototype fan impellers were cast using aluminum alloy 356 because of its excellent casting properties and previous AiResearch experience with the alloy in similar applications. The impeller was cast using a plaster mold process and heat treated to the T6 condition. Additional material was provided in two planes of the hub which could be removed during the balancing process. The entire housing assembly was fabricated of type 6061 aluminum alloy and heat treated to the T6 condition.

After balancing was completed, each impeller was oversped by a factor of 1.5 times the maximum rated speed of 3600 rpm, or 5400 rpm.

The completed Aerojet fan assembly is shown in Figures 6-5 and 6-6; the TECO fan assembly in Figure 6-7 and the SES fan assembly in Figure 6-8.

TESTING

Three separate tests were run to calibrate the fan assemblies prior to shipment. Tests consisted of hydraulic motor performance calibrations for the Aerojet unit and laboratory unit, aerodynamic performance tests of all three fan assemblies, and a noise test which was performed on the Aerojet and TECO assemblies. Details of these tests are described below.

Hydraulic Motor Calibration

The HPI hydraulic motor was removed from the Aerojet fan and was calibrated with hydraulic fluid per MIL-H-5606A. The test setup was as shown in Figure 6-9. The inlet and outlet oil pressure, outlet oil temperature, and the motor shaft torque were measured at 3000 rpm and the results are shown on Figure 6-10. The motor torque was found to be a linear function of pressure drop across the motor and no significant variation with speed was noted.

A similar test was performed to calibrate a Vickers laboratory motor which was used to drive the TECO and SES fan assemblies. The results of this calibration are shown in Figure 6-11. The Vickers motor torque is again a linear function of pressure drop across the motor.

These motor calibrations were used during the subsequent fan performance tests to establish the shaft power input to the fans.

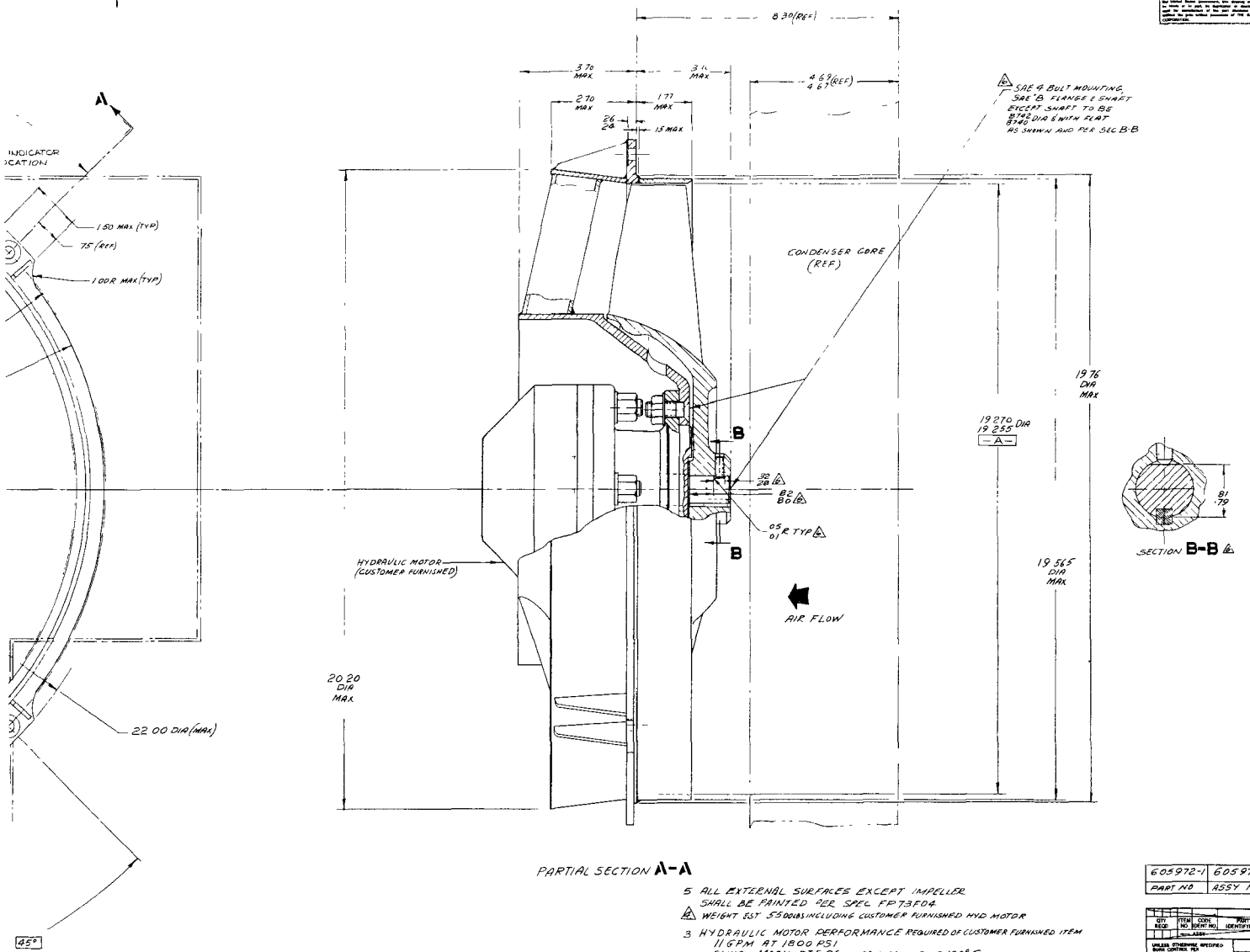

PARTIAL SECTION A-A

5 ALL EXTERNAL SURFACES EXCEPT IMPELLER SHALL BE PAINTED PER SPEC FP73F04

4 WEIGHT EST 5500 LBS INCLUDING CUSTOMER FURNISHED HYD MOTOR

3 HYDRAULIC MOTOR PERFORMANCE REQUIRED OF CUSTOMER FURNISHED ITEM
11 GPM AT 1800 PSI
FLUID: MOBIL DTE 26 OR EQUIVALENT AT 100°C

2 FAN RATING 7250 CFM @ 4 67 IN H_2O
TOTAL PRESSURE RISE
AIR DENSITY 0596 LB/FT³

1 ALL DIMENSIONS ARE FOR INSTALLATION PURPOSES ONLY

NOTES UNLESS OTHERWISE SPECIFIED

3 THESE DIMENSIONS ARE FOR THE HYDRAULIC MOTOR FLANGE & SHAFT REQUIREMENTS FOR THE CUSTOMERS INFORMATION ONLY INSPECTION AT THIS LEVEL NOT REQUIRED

605972-1	605973-1	
PART NO	ASSY NO	REMARKS

PARTS LIST

AIRESEARCH MANUFACTURING COMPANY

FAN OUTLINE, TUBE AXIAL, HYDRAULIC MOTOR DRIVEN

SIZE J | 70210 | 605972

SCALE 1/1 | WT EST | SHEET 1 OF 1

605972 REV A

972

Page 6-11

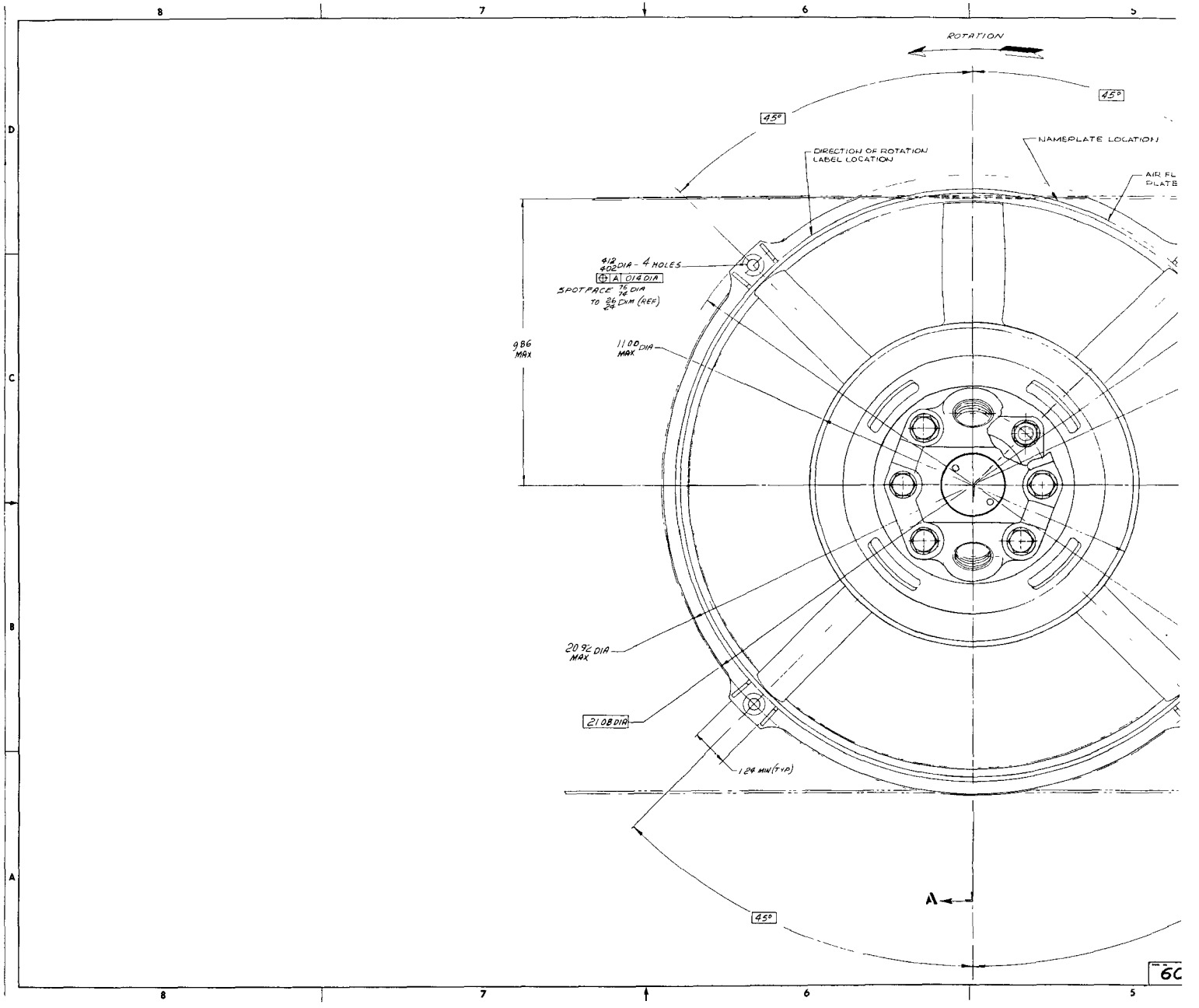
ROTATION
45°
45°
DIRECTION OF ROTATION LABEL LOCATION
NAMEPLATE LOCATION
AIR FL
PLATE
9.40 4.02 DIA - 4 HOLES
⌖ A .014 DIA
SPOTFACE 7.6 7.6 DIA
TO 2.6 2.4 DIM (REF)
9.86 MAX
11.00 DIA MAX
20.92 DIA MAX
21.08 DIA
1.24 MIN (TYP)
45°
A
8
7
6
5
D
C
B
A

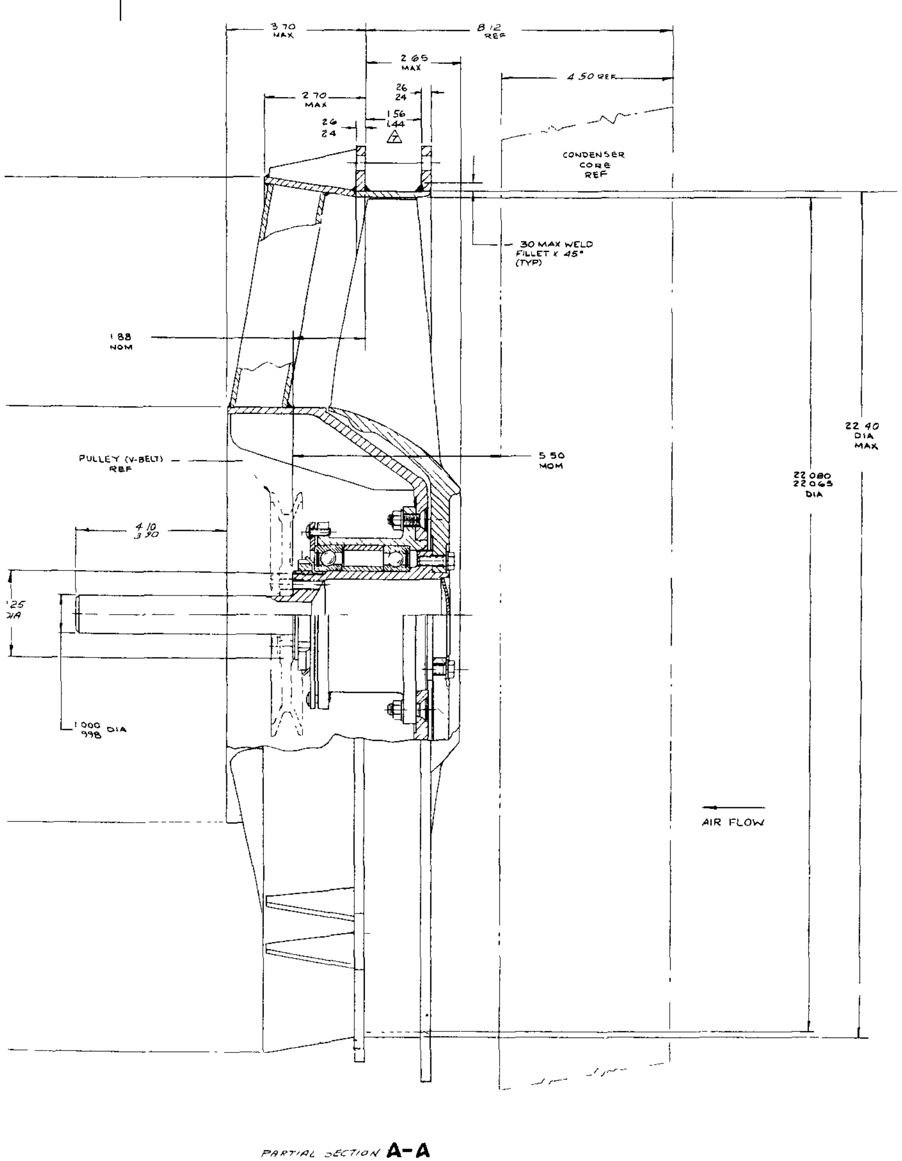

7. AT TIME OF INSTALLATION, MATING PARTS TO BE SHIMMED TO PRECLUDE BENDING OF FLANGES

6. ALL EXTERNAL SURFACES EXCEPT IMPELLER SHALL BE PAINTED PER SPEC FP73F04

5. FAN DRIVEN BY VEE BELT, CUSTOMER FURNISHED PULLEY

4. INPUT HORSEPOWER 7.2 HP UNDER CONDITIONS SPECIFIED IN NOTES 2 & 3

3. APPROXIMATE ROTATIONAL SPEED 2500 RPM

2. FAN RATING 10,300 CFM OF AIR AT 29.9 IN HG ABS AND 189°F WITH 3.1 INCHES OF WATER TOTAL PRESSURE RISE

1. ALL DIMENSIONS ARE FOR INSTALLATION PURPOSES ONLY

NOTES UNLESS OTHERWISE SPECIFIED

PART NO	ASSY NO	REMARKS
605977-1	605978-1	

ZONE	LTR	DESCRIPTION	DATE	APPROVED
	A	SEE ENGINEERING ORDER		
	B	SEE E.O.		

AIRESEARCH MANUFACTURING COMPANY

FAN OUTLINE, TUBE AXIAL, BELT DRIVEN

SIZE J | CODE IDENT NO 70210 | DWG NO 605977

SCALE 1/1 | WT EST 32 LBS | SHEET 1 OF 1

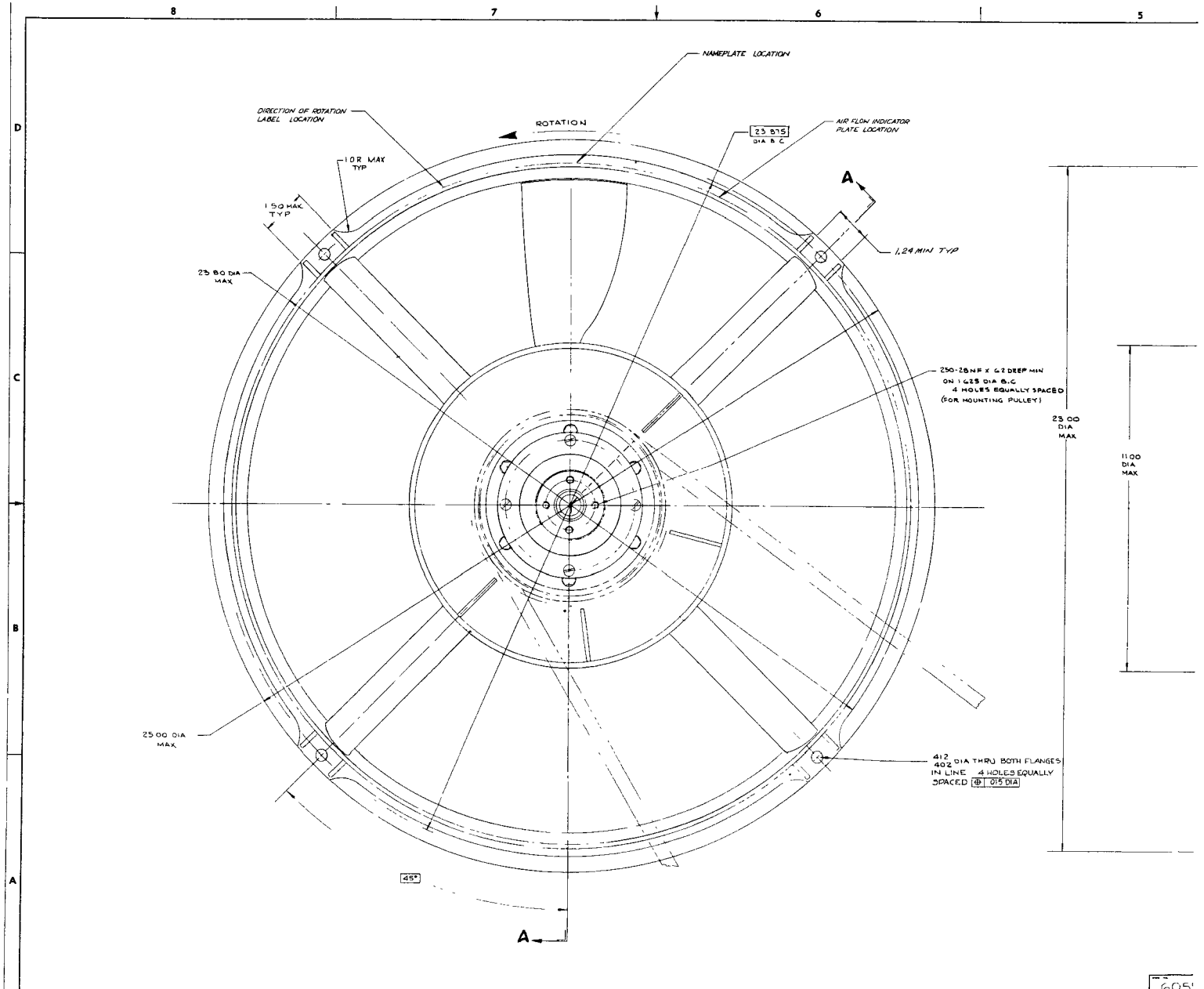
NAMEPLATE LOCATION
DIRECTION OF ROTATION LABEL LOCATION
ROTATION
23 875 DIA B.C
AIR FLOW INDICATOR PLATE LOCATION
.10R MAX TYP
.150 MAX TYP
A
1.24 MIN TYP
23.80 DIA MAX
250-28 NF X .62 DEEP MIN ON 1.625 DIA B.C 4 HOLES EQUALLY SPACED (FOR MOUNTING PULLEY)
23.00 DIA MAX
11.00 DIA MAX
25.00 DIA MAX
.412 .402 DIA THRU BOTH FLANGES IN LINE 4 HOLES EQUALLY SPACED ⌖ .015 DIA
45°
A

605

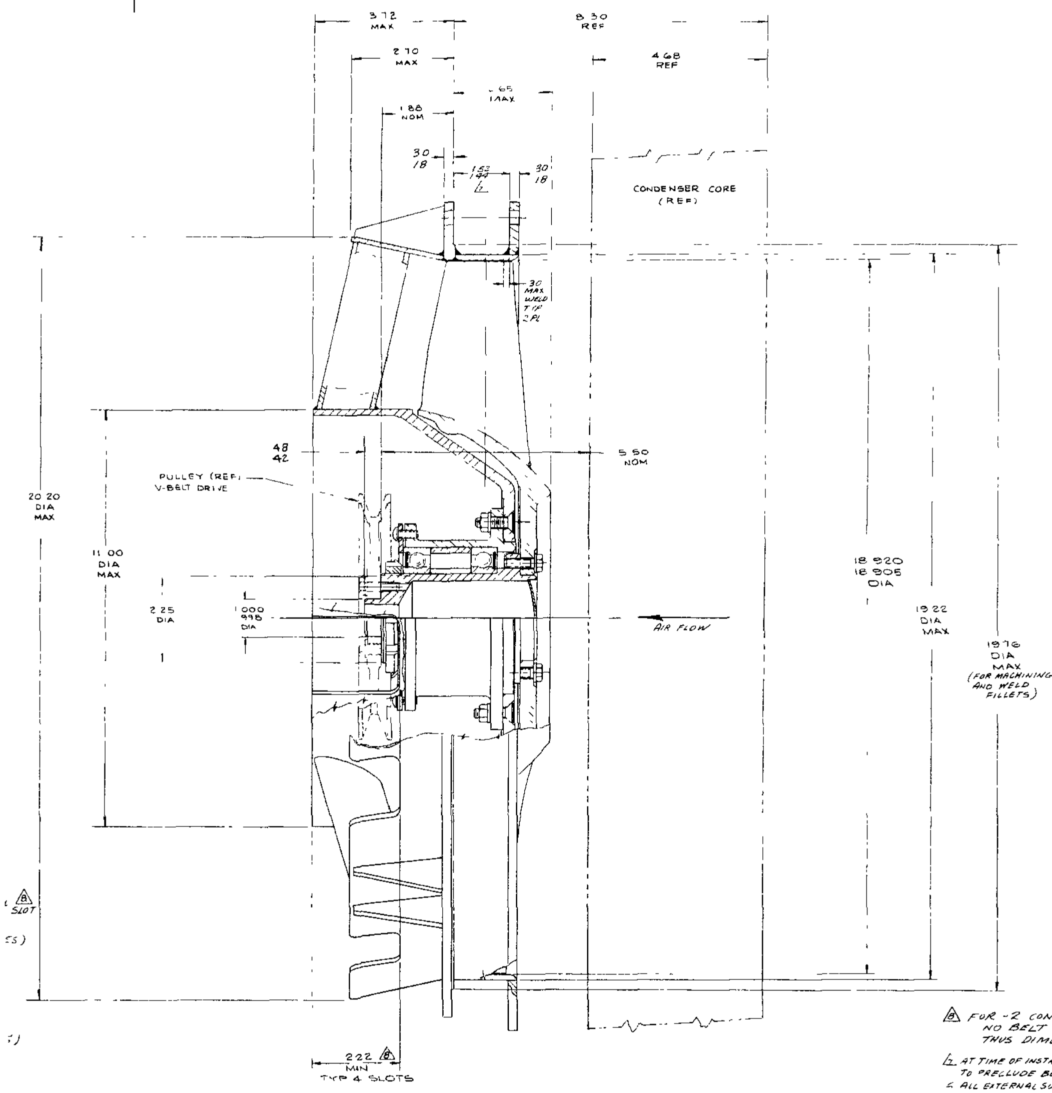

10 MAXIMUM PERMISSIBLE SPEED 3600 RPM

9 MAXIMUM PERMISSIBLE BELT TENSION 600 LB

(B) FOR -2 CONFIGURATION ONLY~ NO BELT SLOTS ARE PROVIDED THUS DIMENSIONS NOTED ARE NOT APPLICABLE

7 AT TIME OF INSTALLATION, MATING PARTS TO BE SHIMMED, TO PRECLUDE BENDING OF FLANGES

6 ALL EXTERNAL SURFACES EXCEPT IMPELLER SHALL BE PAINTED PER SPEC FP73F04

5 FAN DRIVEN BY VEE BELT CUSTOMER FURNISHED PULLEY

4 INPUT HORSEPOWER 3.5 HP UNDER CONDITIONS SPECIFIED IN NOTES 2 & 3

3 DESIGN ROTATIONAL SPEED 2360 RPM

2 FAN RATING 2410 CFM AT 29.8 IN Hg ABS AND 217°F WITH 2.86 INCHES OF WATER TOTAL PRESSURE RISE

1 ALL DIMENSIONS ARE FOR INSTALLATION PURPOSES ONLY

NOTES UNLESS OTHERWISE SPECIFIED

PART NO	ASSY NO	REMARKS
605982-2	605983-2	SEE NOTE (B)
605982-1	605983-1	

AIRESEARCH MANUFACTURING COMPANY

FAN OUTLINE, TUBE AXIAL BELT DRIVEN

SIZE J | CODE IDENT NO 70210 | DWG NO 605982

SCALE 1/1 | WT EST 32 LBS | SHEET 1 OF 1

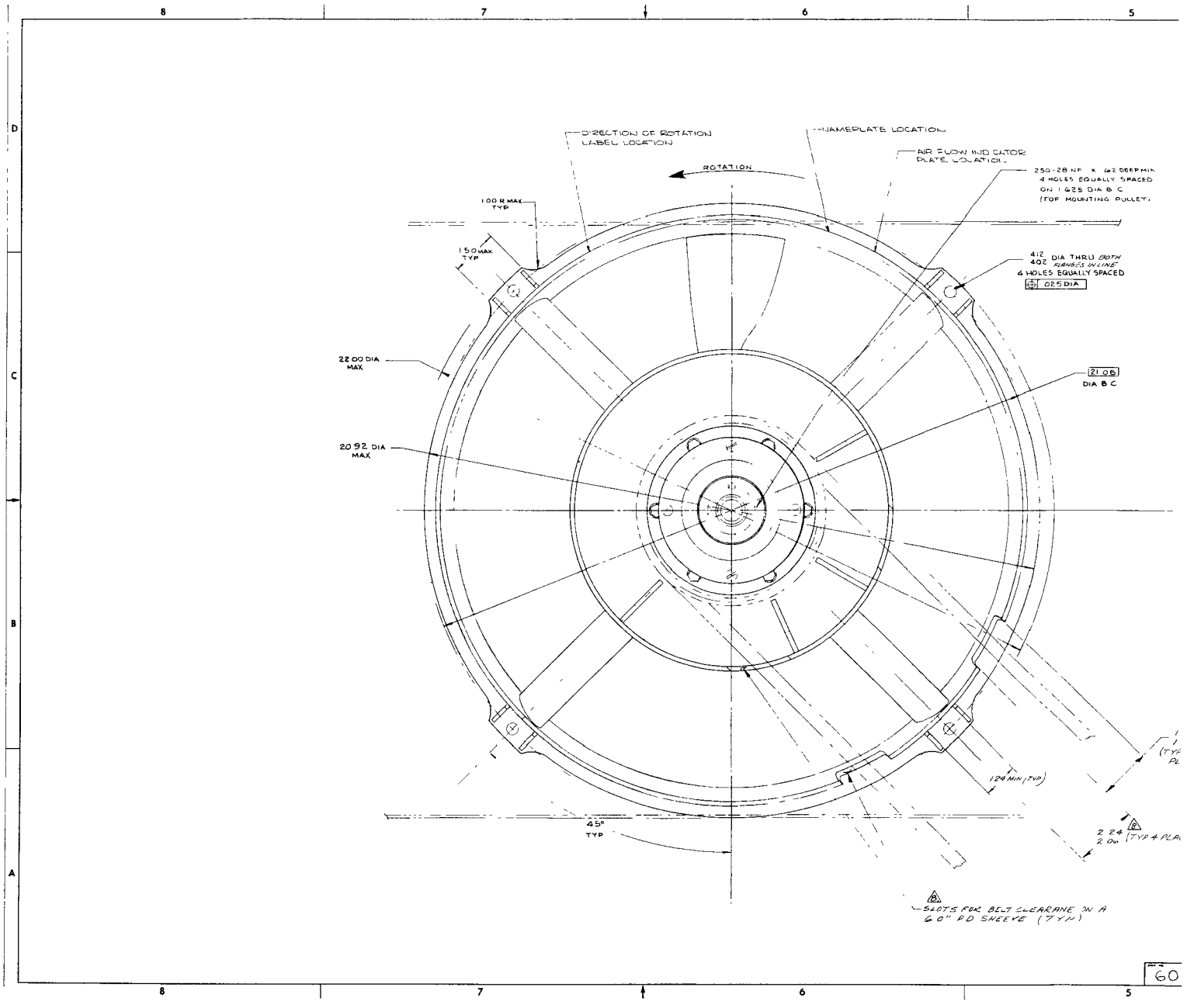
DIRECTION OF ROTATION LABEL LOCATION
NAMEPLATE LOCATION
AIR FLOW INDICATOR PLATE LOCATION
ROTATION
250-28 NF x .62 DEEP MIN 4 HOLES EQUALLY SPACED ON 1.625 DIA B.C. (FOR MOUNTING PULLEY)
100 R MAX TYP
150 MAX TYP
.412 DIA THRU BOTH .402 REAMED IN LINE 4 HOLES EQUALLY SPACED
.025 DIA
2200 DIA MAX
2092 DIA MAX
21.06 DIA B.C.
.120 MIN (TYP)
45° TYP
2.24
2.04 (TYP 4 PLA
SLOTS FOR BELT CLEARANCE IN A 6.0" PD SHEEVE (TYP)

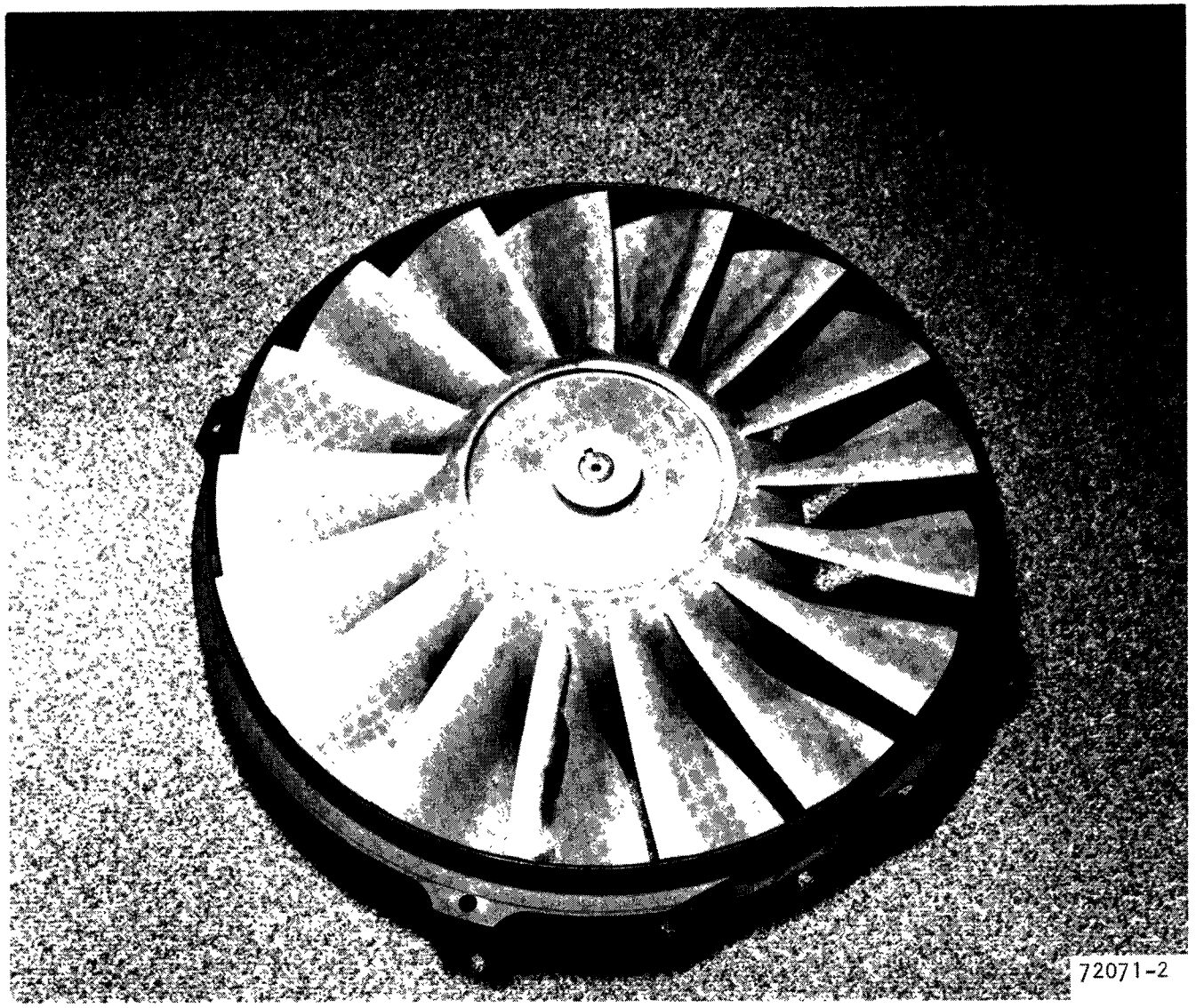

Figure 6-5. Aerojet Fan Assembly

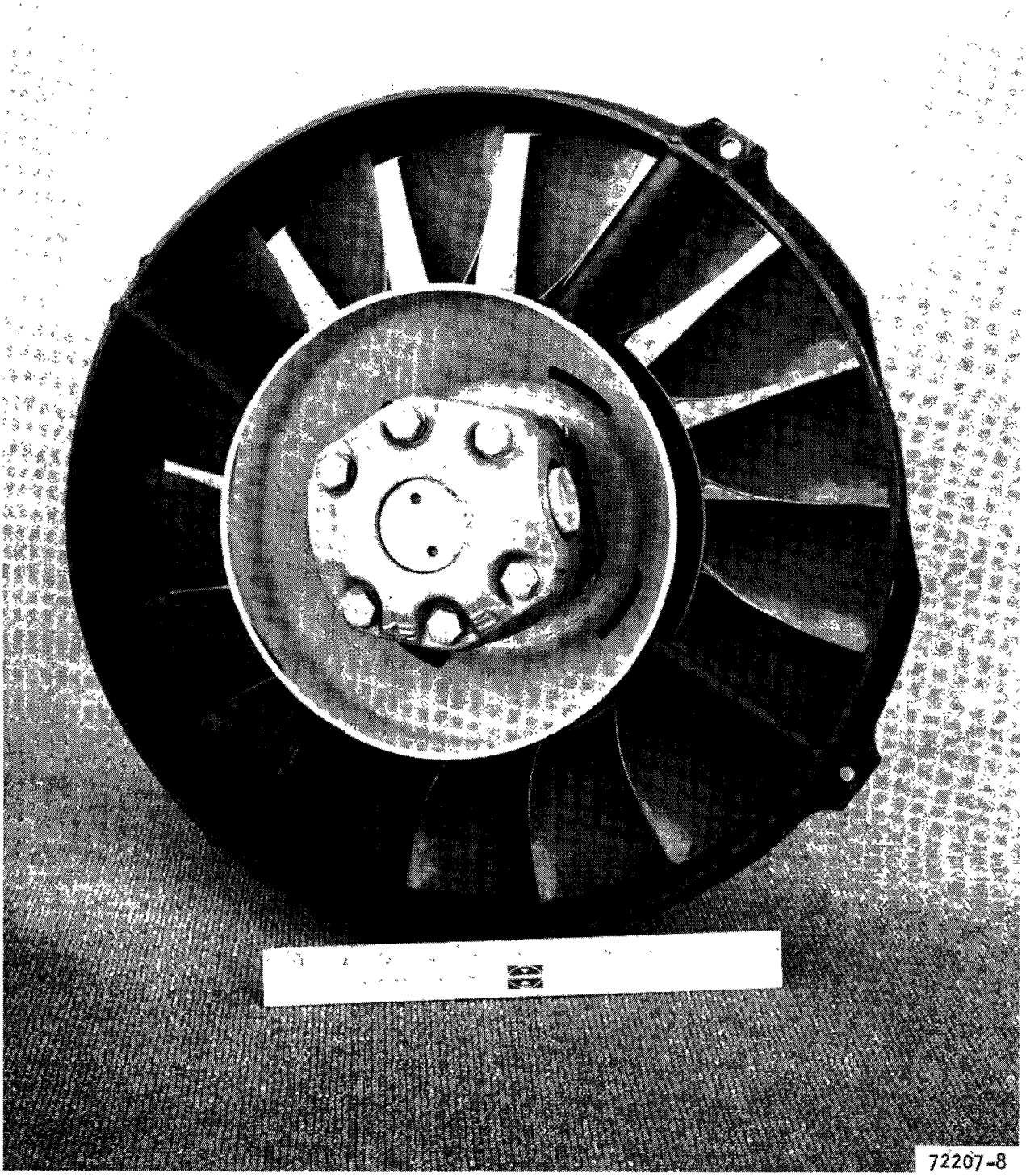

Figure 6-6. Aerojet Fan Assembly

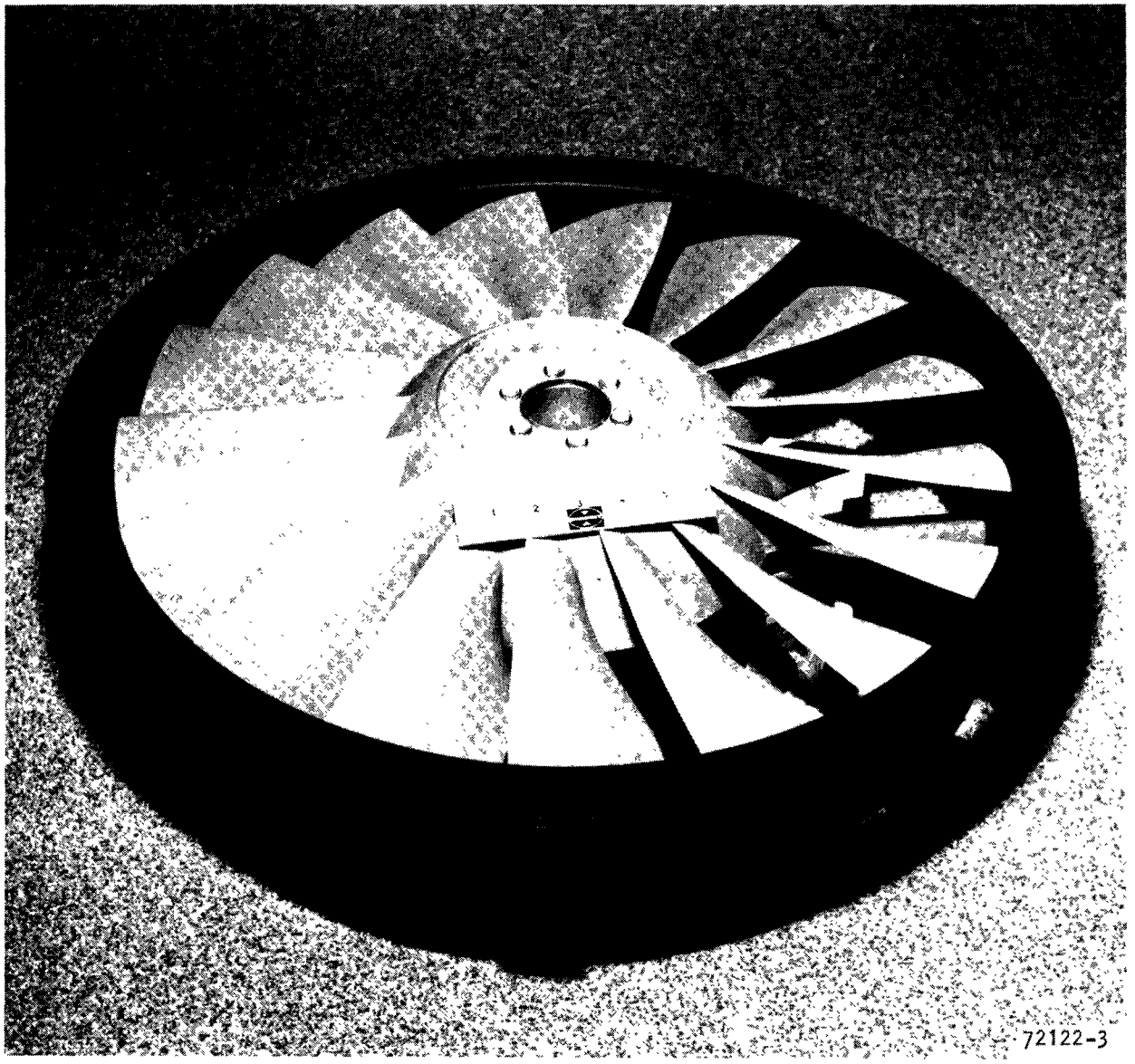

Figure 6-7. Thermo Electron Fan Assembly

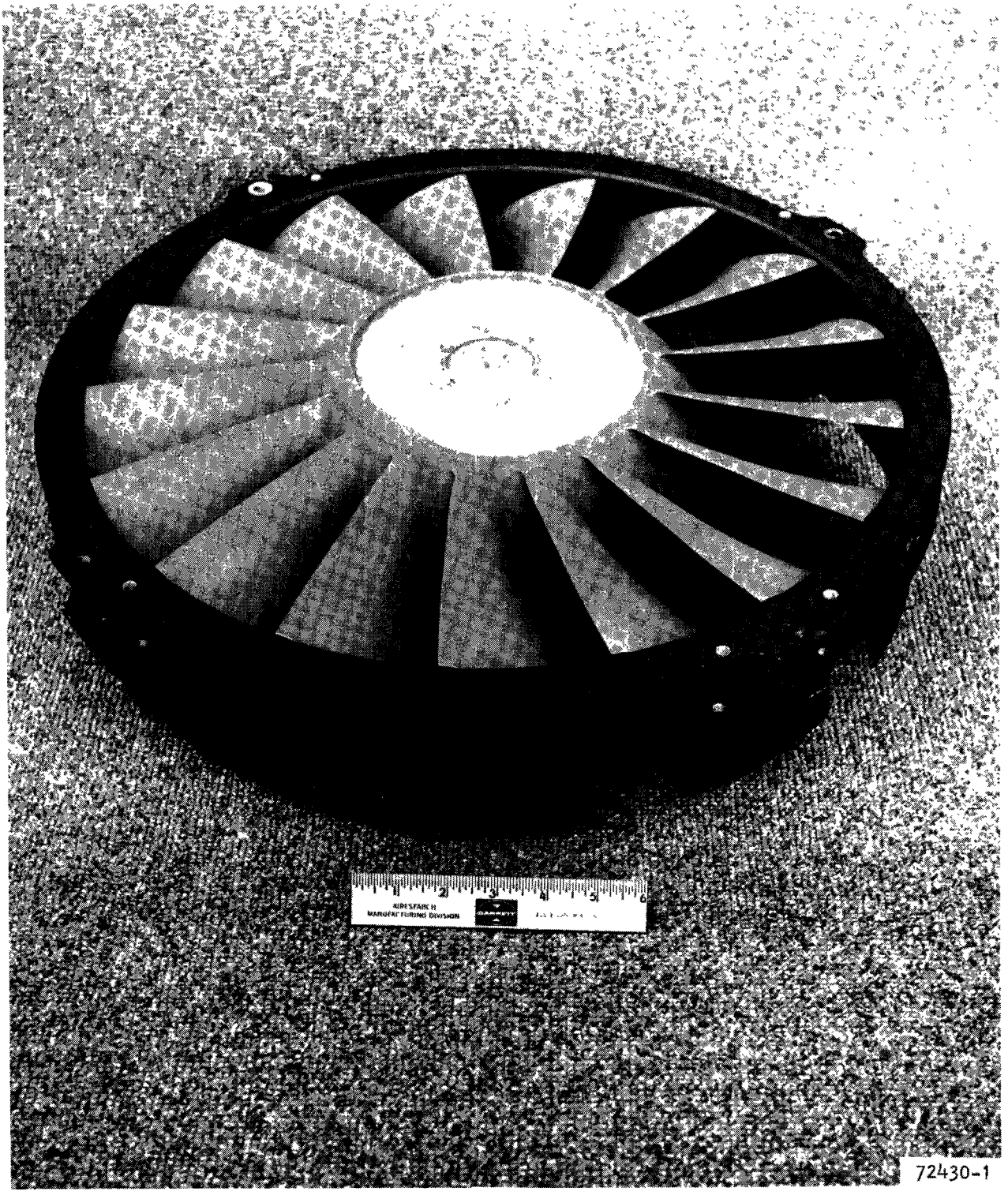

Figure 6-8. Steam Engine System Fan Assembly

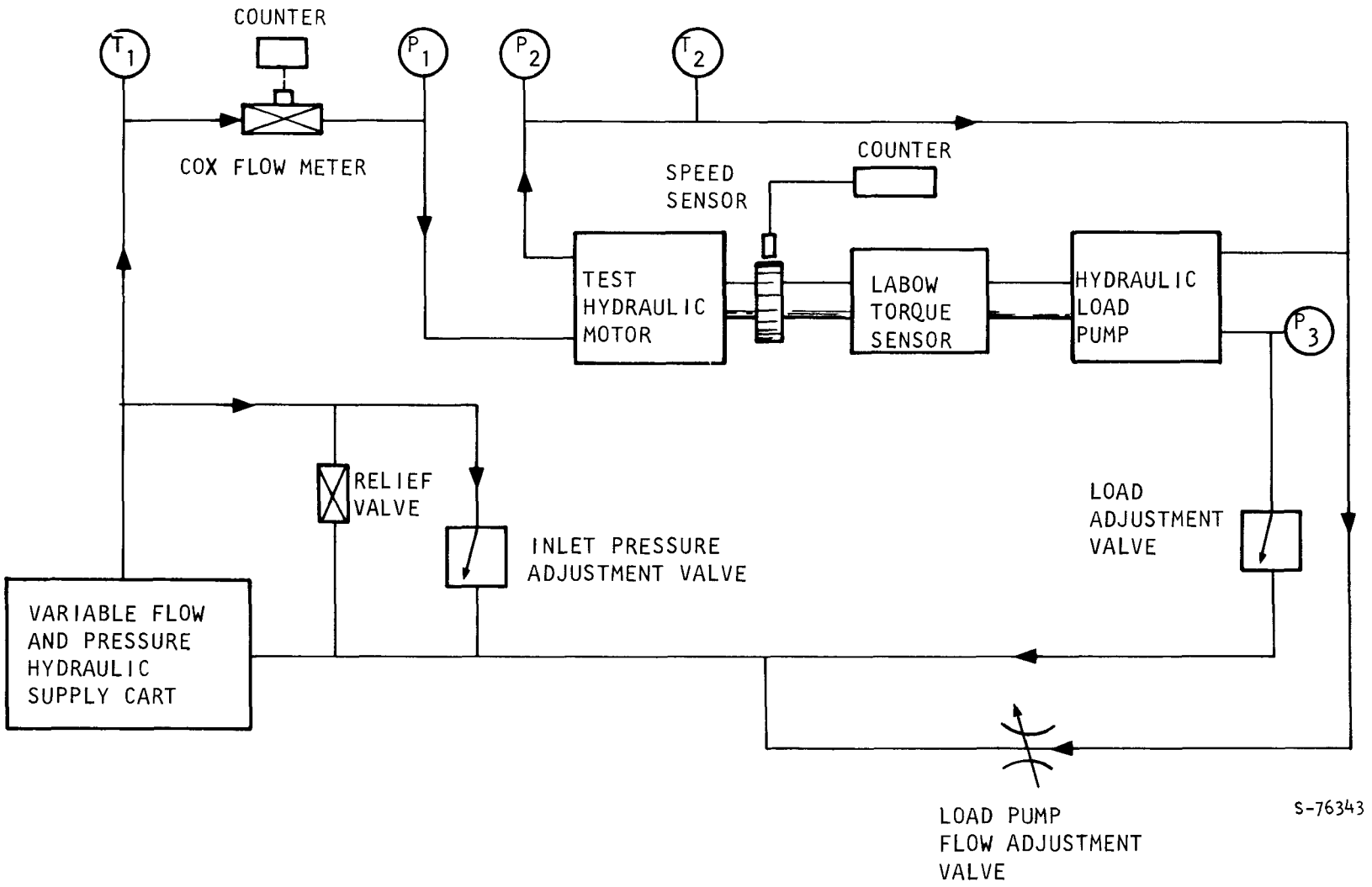

Figure 6-9. Hydraulic Motor Calibration Test Setup

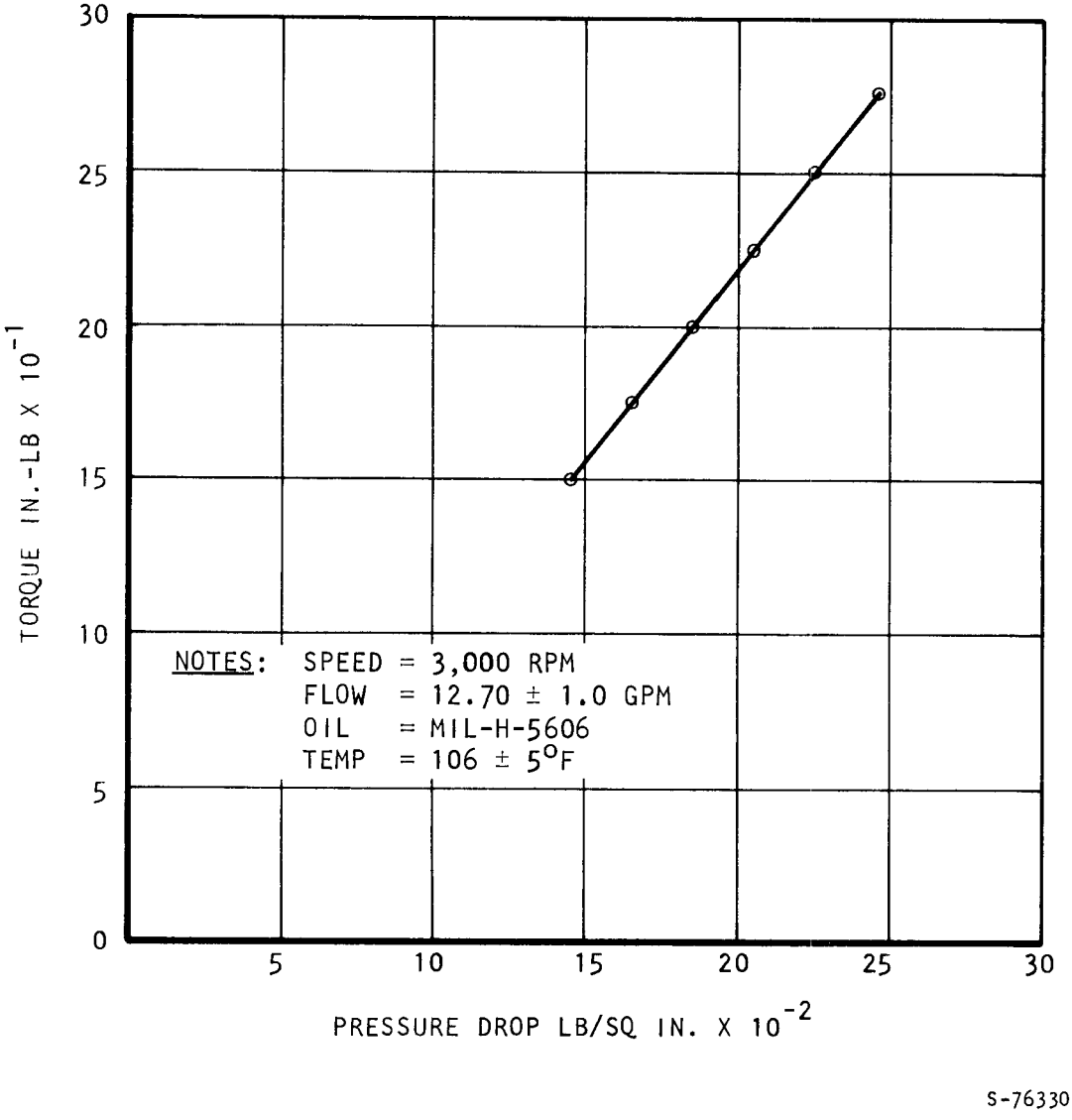

Figure 6-10. Motor Calibration--HPI PN M20-90155-01, SN 20047

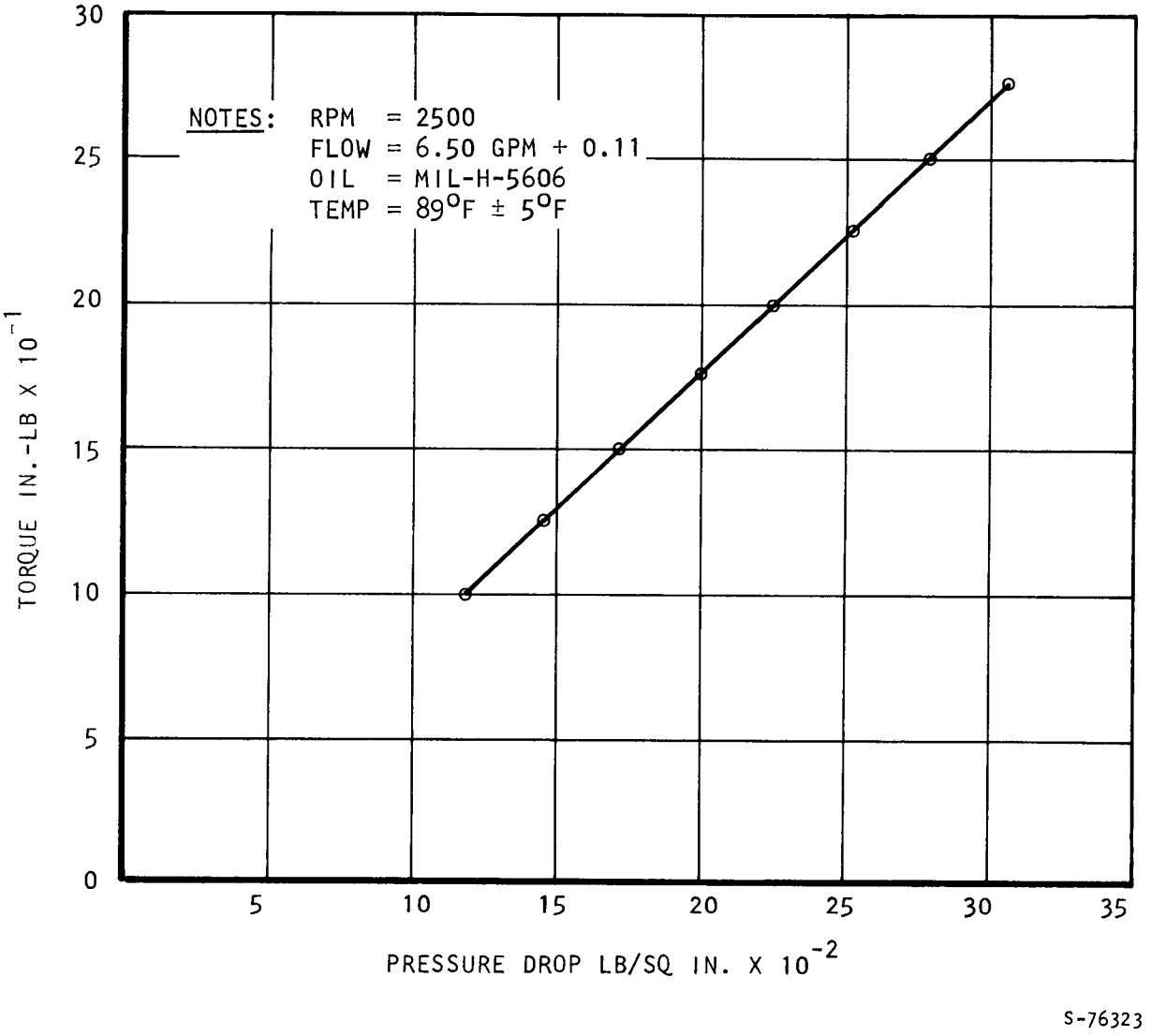

Figure 6-11. Motor Calibration--Vickers Motor, Model No. 3911-30

Fan Performance

Fan aerodynamic performance was determined using a setup as shown in Figure 6-12. Figure 6-13 is a picture of the Aerojet fan installed in the performance test rig. The duct leading to the fan was designed to be the same diameter as that at the fan exit. Because the fan exit duct is conical, the laboratory inlet duct diameter was slightly larger than that at a fan inlet and, hence, a fairing was used to provide a smooth entrance to the fan. Duct length from the fan inlet to the flow measuring orifice section was equal to at least 20 duct diameters to ensure uniform flow at the fan inlet. The fan discharged directly to atmosphere as is the case in the actual installation.

A hydraulic motor was used to drive the fan. The Aerojet fan used the HPI motor that is part of the fan assembly. The TECO and SES fans used a laboratory supplied Vickers hydraulic motor. Both motors were calibrated as previously described.

During the test, the fan speed and suction pressure were varied until the flow and pressure rise as specified by the fan design point conditions were achieved. This speed was considered to be the actual fan design point speed. This speed was then held constant and the flow varied from full flow to an aerodynamic stall condition. The fan static pressure rise and hydraulic motor flow and pressure drop over the range of air flow was then recorded.

Fan total pressure rise is defined as

$$\Delta P_T = P_{T_d} - P_{T_i} \tag{6-1}$$

where $$P_T = P_s + P_v \tag{6-2}$$

and $$P_v = \frac{\rho}{2g_c}\left[\frac{Q}{60\ \pi\ D^2/4}\right]^2 \tag{6-3}$$

Equation (6-1) can now be written as

$$\Delta P_T = P_{s_d} + P_{v_d} - \left(P_{s_i} + P_{v_i}\right) \tag{6-4}$$

If the discharge and inlet fan duct diameters are equal the dynamic pressures, P_{v_d} and P_{v_i}, are identical neglecting the small difference in air density across the fan. Thus, Equation 6-4 becomes

$$\Delta P_T = P_{s_d} - P_{s_i} \tag{6-5}$$

but, $$P_{s_d} = P_{amb} \tag{6-6}$$

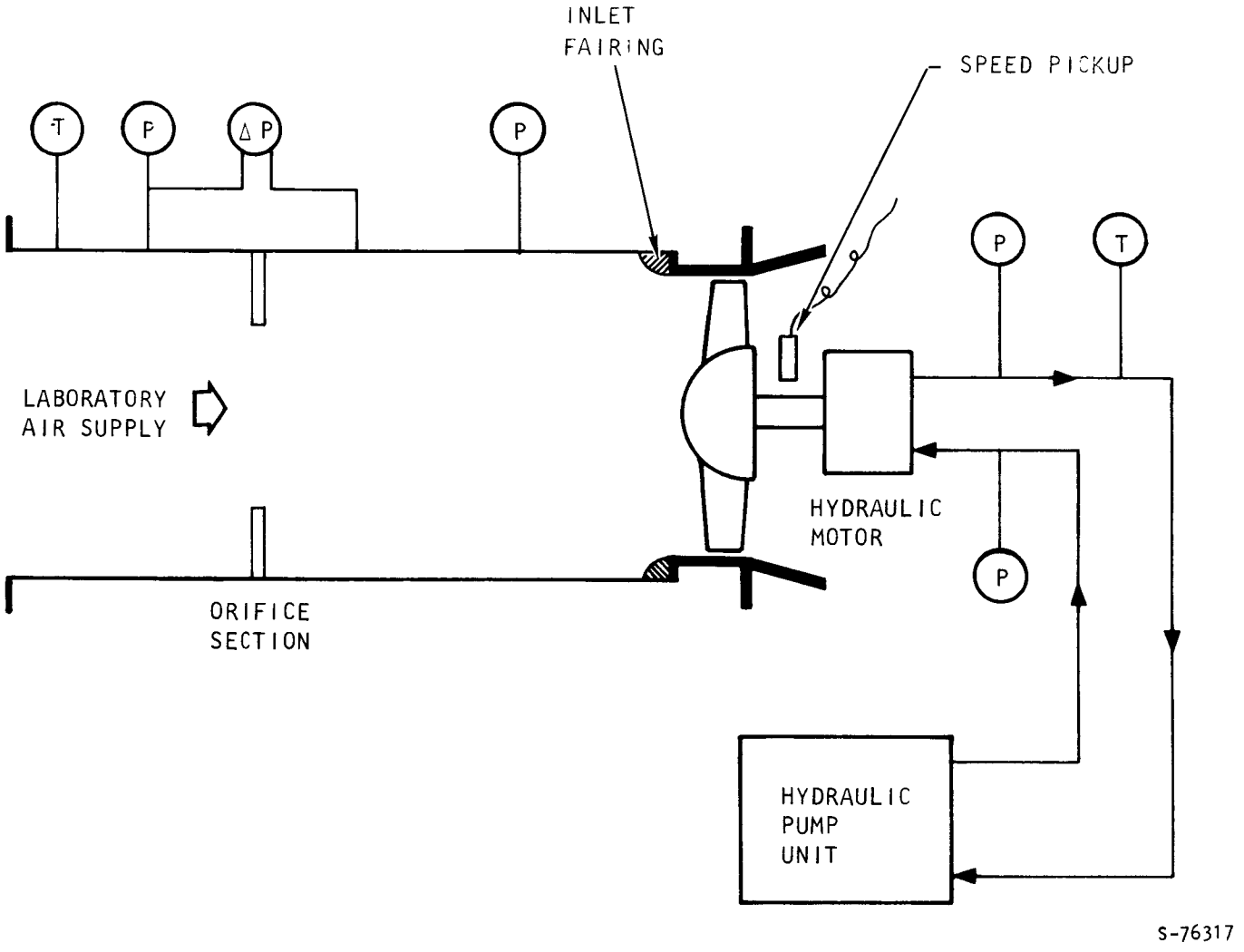

Figure 6-12. Fan Aerodynamic Performance Test Setup

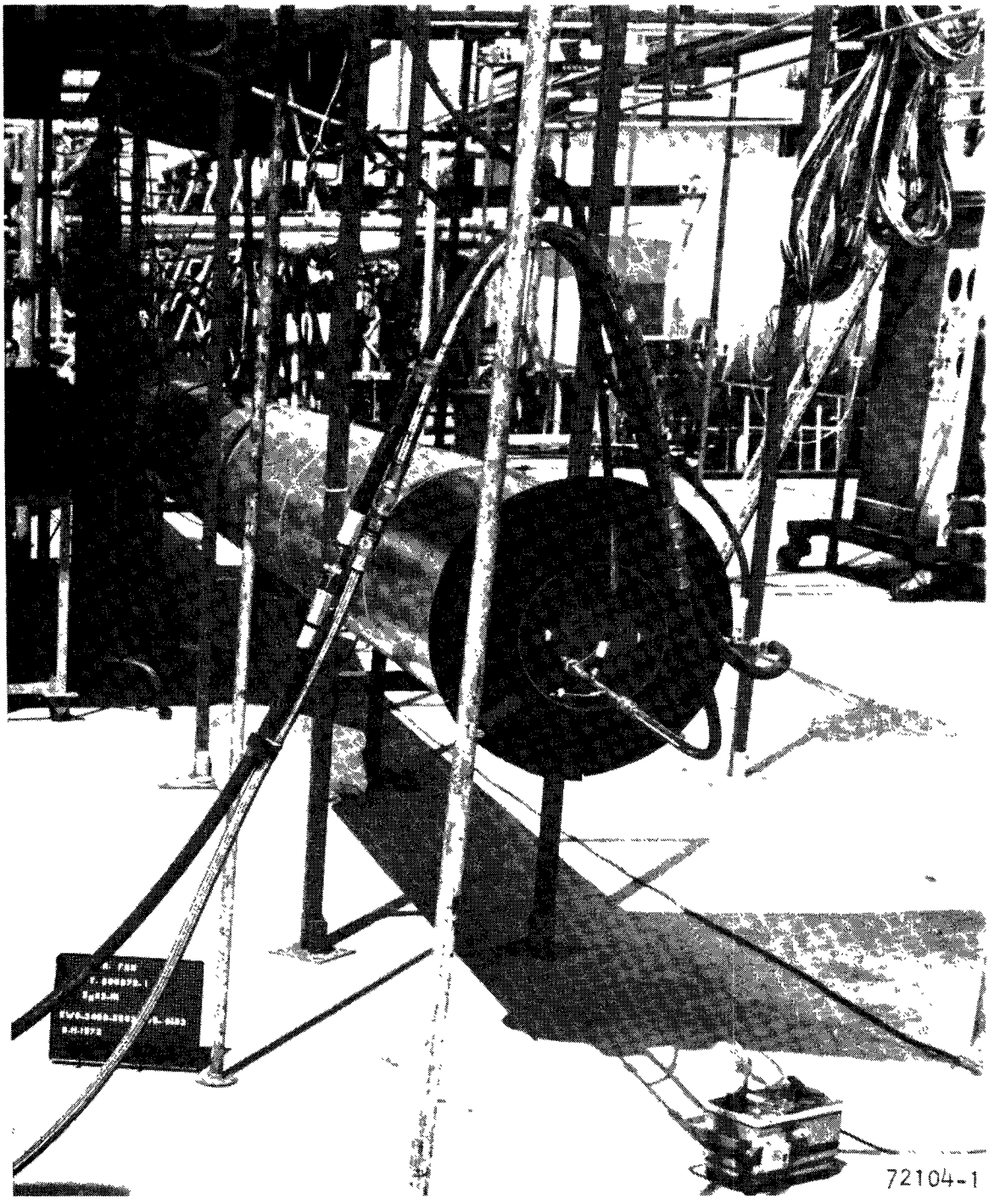

Figure 6-13. Aerojet Fan Calibration Test Setup

and thus, $\Delta P_T = P_{amb} - P_{s_i}$ (6-7)

Using the setup shown on Figure 6-12 the fan total pressure rise can be determined by measuring the inlet static pressure and the barometric pressure.

The fan efficiency is defined as

$$\eta_f = \frac{\text{Total Air hp Out}}{\text{Shaft hp in.}} \quad (6\text{-}8)$$

where $\text{Air hp} = 1.57\ Q\Delta P_T \times 10^{-4}$ (6-9)

and $\text{Shaft hp} = \frac{2\pi\ N\ M_t}{33{,}000 \times 12}$ (6-10)

Substituting in Equation 6-9 the following expression for fan efficiency is obtained.

$$\eta_f = \frac{(.99)\ Q\Delta P_T}{N\ M_t} \quad (6\text{-}11)$$

Equations 6-7 and 6-11 were used to reduce the test data. The final performance plots for the Aerojet, TECO, and SES fans are shown on Figures 6-14, 6-15, and 6-16, respectively. The following fan efficiencies were achieved at the design point flow:

System Contractor	Design Point Flow, CFM	Efficiency, Percent
Aerojet	7,250	71.2
TECO	10,300	73.5
SES	5,440	70.2

All fans met the 70 percent design goal efficiency.

Noise Tests

Testing was conducted in a chamber which had been treated to reduce background noise with the fans operating at their respective design point conditions. Each fan was set up in the chamber in an arrangement similar to its automobile installation with the inlet restricted and the fan discharging directly to atmosphere. Figure 6-17 is a sketch of the test setup. Seven points, 45 deg apart, were established with reference to the fan centerline and each point is five ft from the fan. These points were the microphone positions for measuring the sound pressure level generated by the fan. A wind shield was placed over the microphones to eliminate the noise of the air impinging on the microphone.

NOTES:

1. OPERATING SPEED 2980 RPM (N_o)
2. $\sigma = 17.35 \frac{P_T}{T_i}$

where P_T = INLET TOTAL PRESSURE - IN. HgA

$T_i = {}^oF + 460$

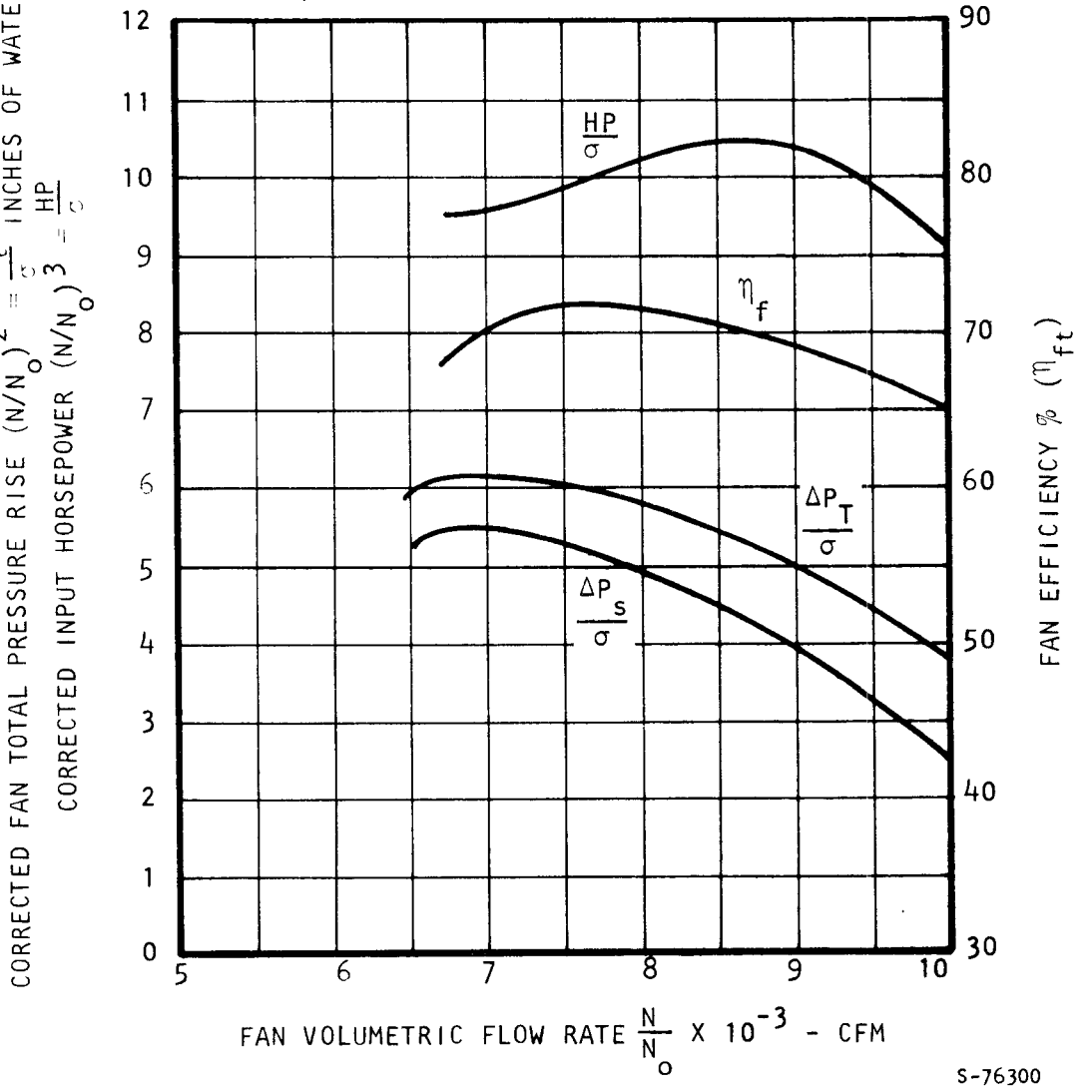

Figure 6-14. Performance of the Aerojet Hydraulic-Motor-Driven Fan, AiResearch PN 605972-1-1

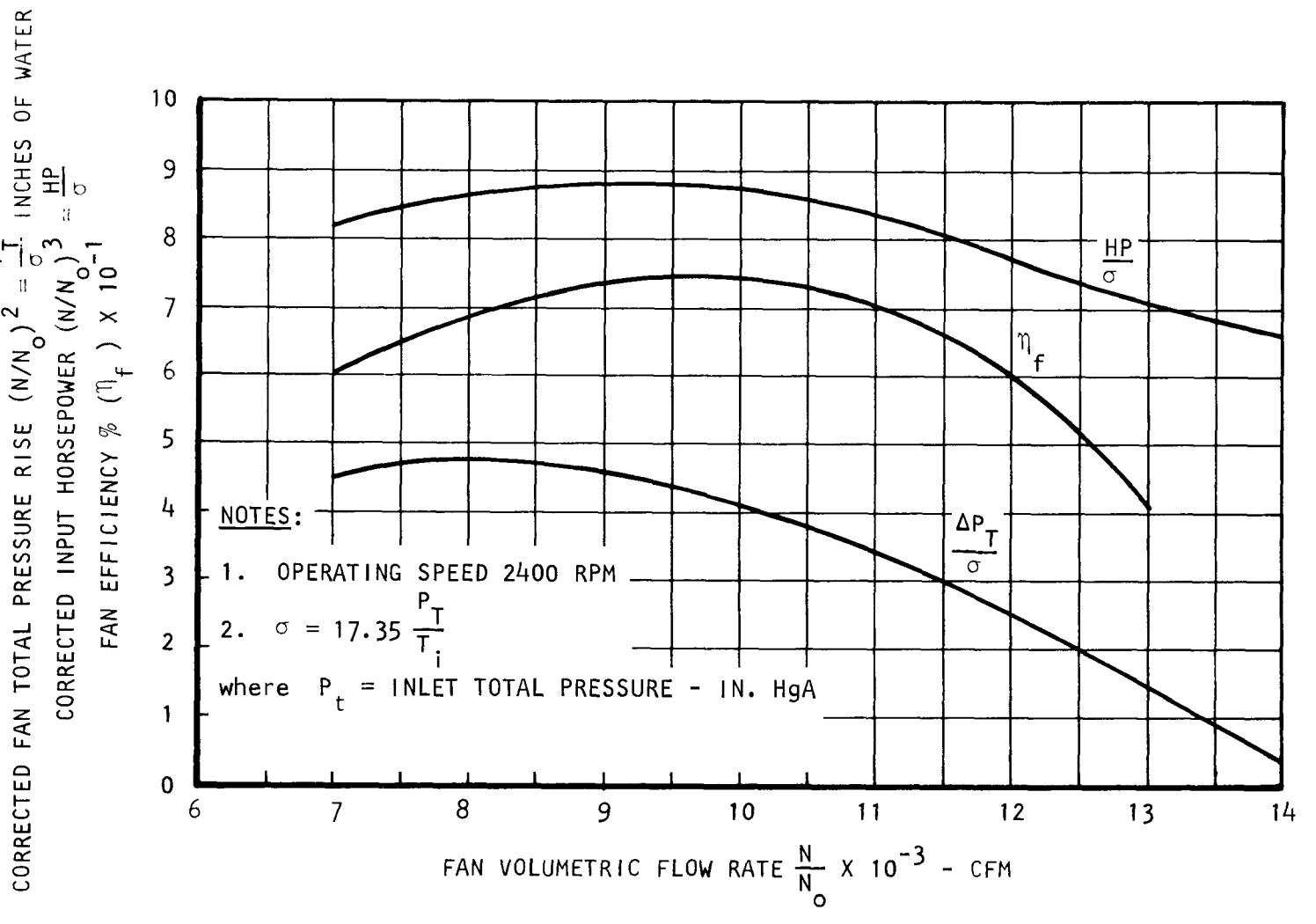

Figure 6-15. Performance of the TECO Shaft-Driven Fan, AiResearch PN 605977-1-1

NOTES:

1. OPERATING SPEED 2360 RPM
2. $\sigma = 17.35 \frac{P_T}{T_i}$

where P_T = INLET TOTAL PRESSURE - IN. HgA

$T_i = {}^{o}F + 460$

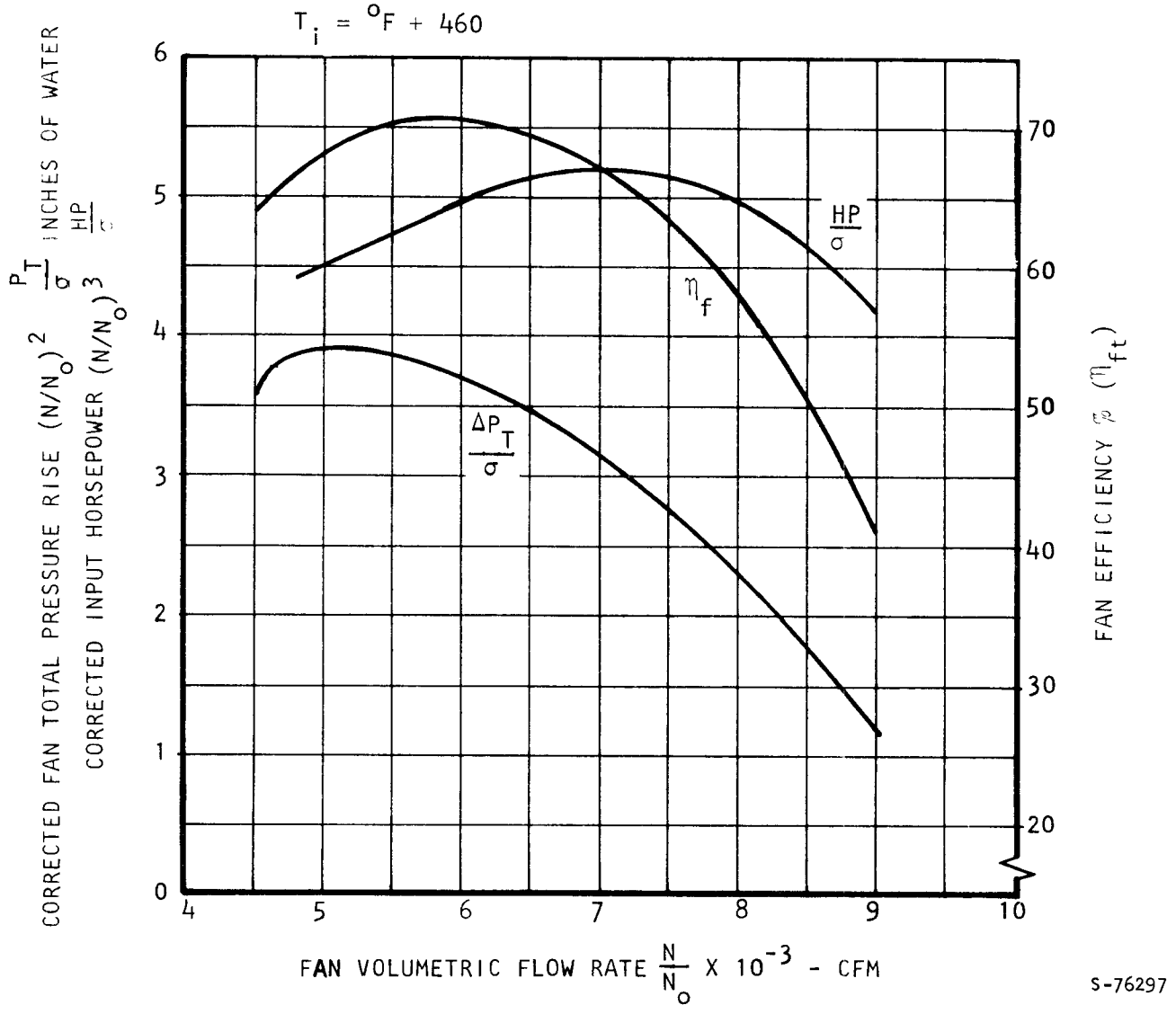

Figure 6-16. Performance of the SES Belt-Driven Fan, AiResearch PN 605982-1-1

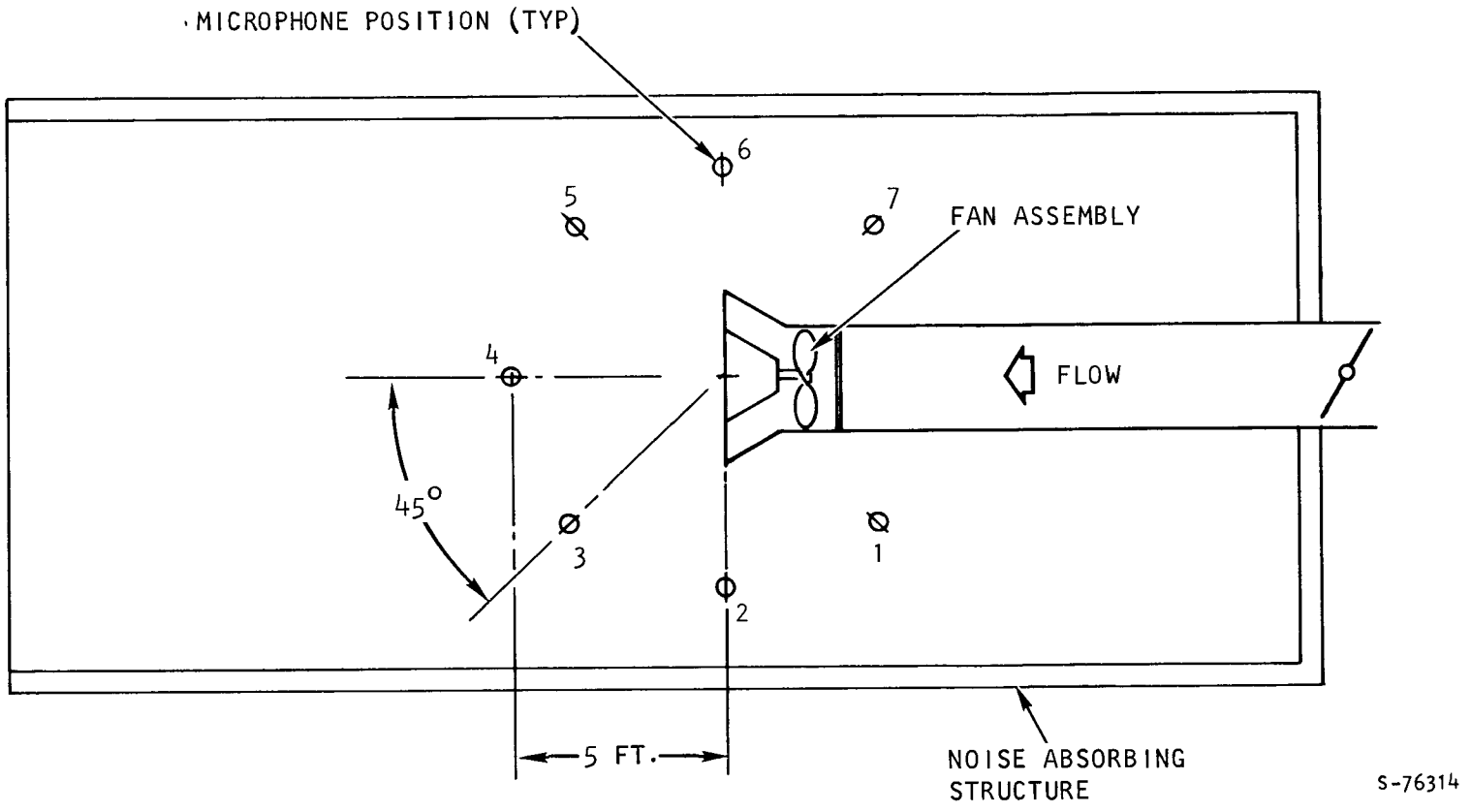

Figure 6-17. Fan Noise Test Setup

1. Aerojet

Figure 6-18 presents the automatic recordings of the sound pressure level obtained for the Aerojet fan. Figure 6-19 shows the measurement of the background noise in the chamber indicated by sound pressure levels below 200 Hz. The average overall sound pressure five ft from the fan was 88.5 db(A). This value includes the noise generated by the HPI hydraulic motor.

The HPI M20-90155-01 hydraulic motor for the Aerojet fan was removed from the fan and connected to a dummy load as shown in Figure 6-20. Microphones were placed five ft from the hydraulic motor as shown in Figure 6-20. The motor was operated at 2820 rpm and 1930 psi ΔP (9.75 hp) which is the approximate fan shaft horsepower at rated load conditions. A background noise level test was also run with the motor stopped. Test results are presented in Figure 6-21. The background noise and the inconsistency between the 1/3 octave and full octave analyzer indicates that the noise below 100 or possibly 200 Hz, was background noise and not caused by the motor. A comparison between the fan noise and motor noise shows that the dominant fan noise was in the 100 Hz octave band, at which the motor noise was quite low, indicating the motor was not a significant contributor to the fan noise. In all octave bands, the motor noise was at least five db lower than fan noise, indicating that the motor did not contribute more than approximately 1-1/2 db to fan noise in any octave band. The principal noise source was aerodynamic noise as generated by the fan.

2. Thermo Electron

The installation of the TECO fan was as shown on Figure 6-17. Figure 6-22 is a picture of the installation; the microphone positions are indicated by X's on the floor. A laboratory Vickers hydraulic motor was used to drive the fan. The motor was connected to the fan via a drive shaft containing two universal joints.

Test results for seven microphone positions are shown on Figure 6-23. The automatic sound recorder was inoperative and the data were recorded by hand. In this case the noise of the hydraulic motor, which was previously calibrated as described for the Aerojet fan, was analytically subtracted from the measured overall values. The average sound pressure level for the fan alone was 88.6 db(A) at five ft away, operating at design point conditions.

3. Steam Engine Systems

The three EPA fans utilize the same basic impeller and differ only in the fan tip diameter. Thus, the fans could be expected to exhibit similar noise characteristics. Theoretically, the Aerojet fan should be 1.1 db noisier than the TECO fan based on the following relationship.

$$\Delta db = \log_{10} \frac{(CFM)_A}{(CFM)_T} + 20 \log_{10} \frac{\Delta P_A}{\Delta P_T}$$

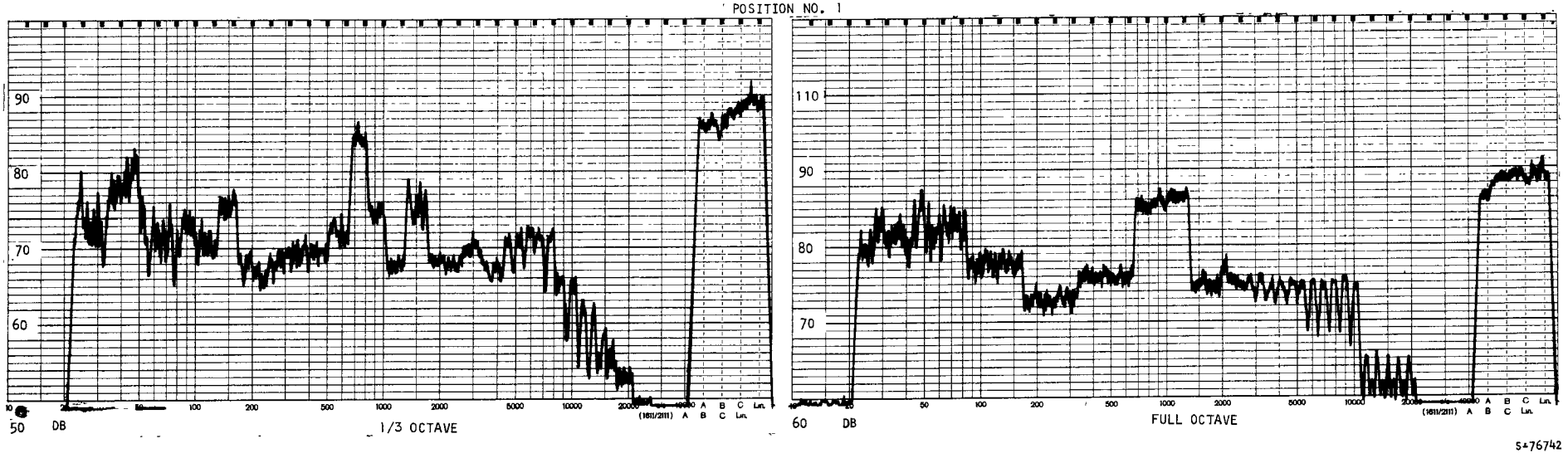

Figure 6-18. Sound Pressure Levels for Aerojet Fan Assembly P/N 605972-1

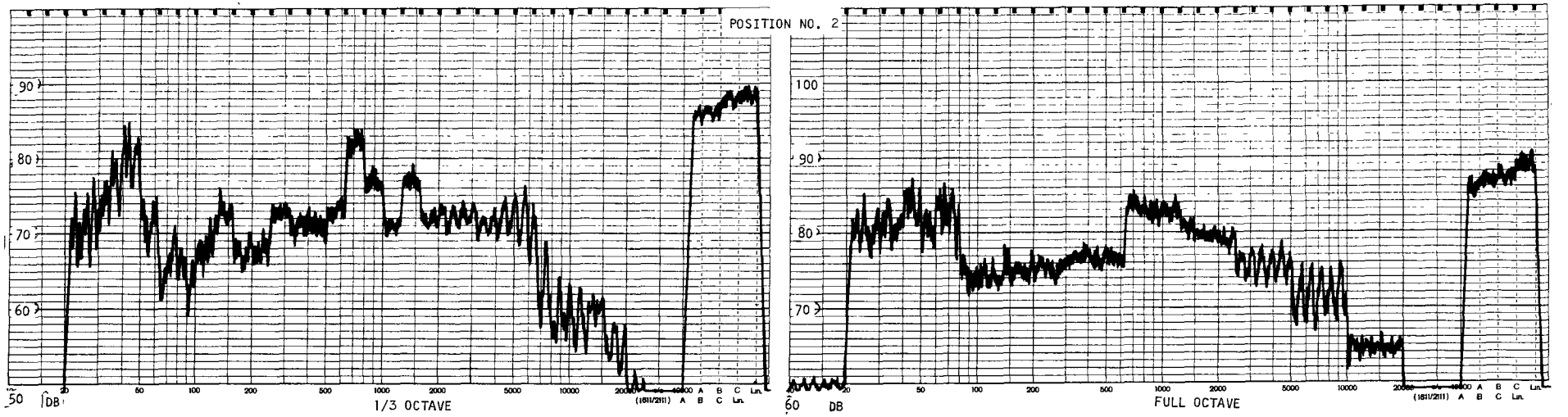

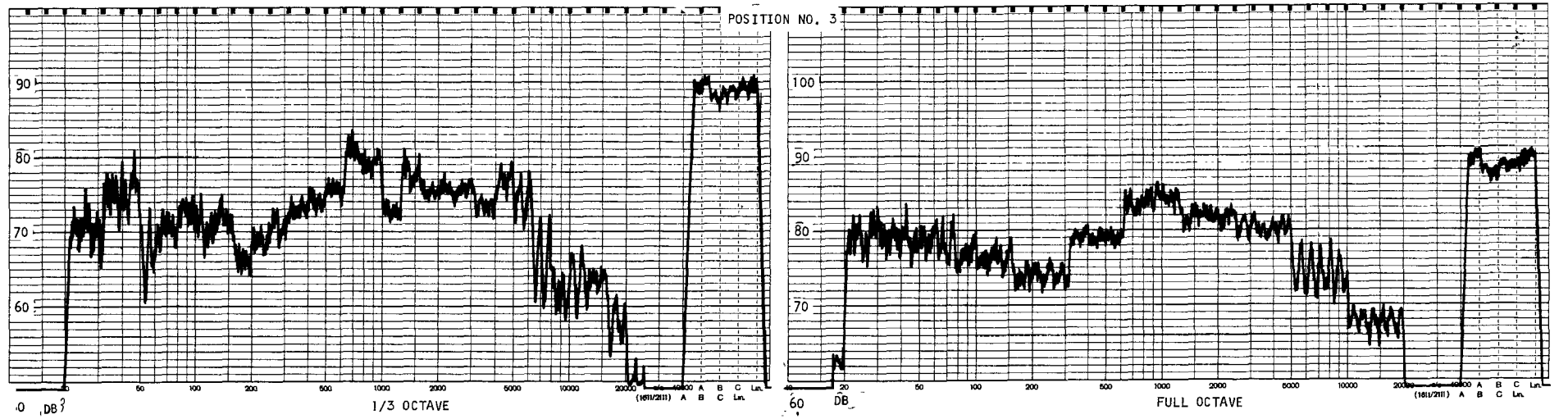

S-76740

Figure 6-18 (Continued)

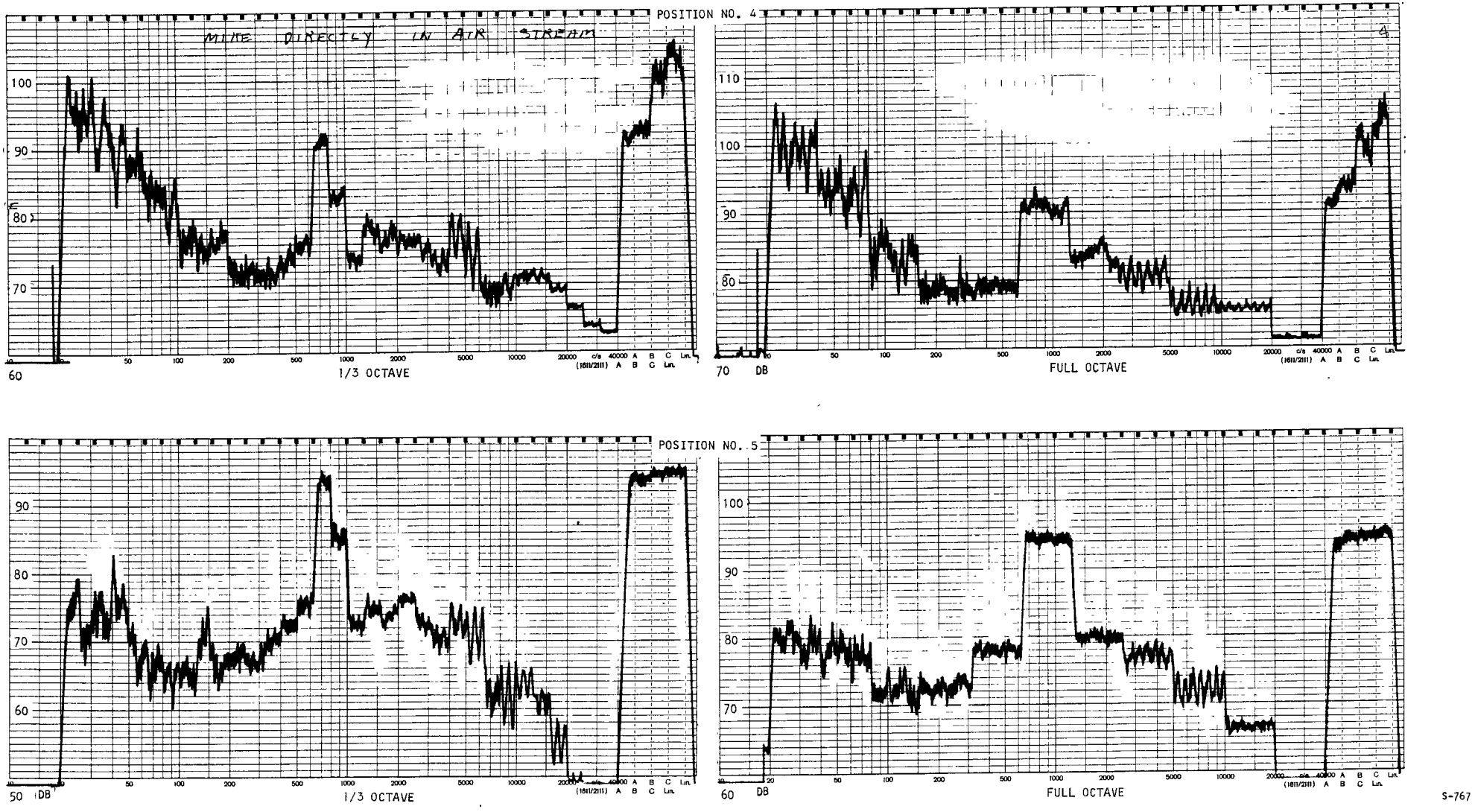

Figure 6-18 (Continued)

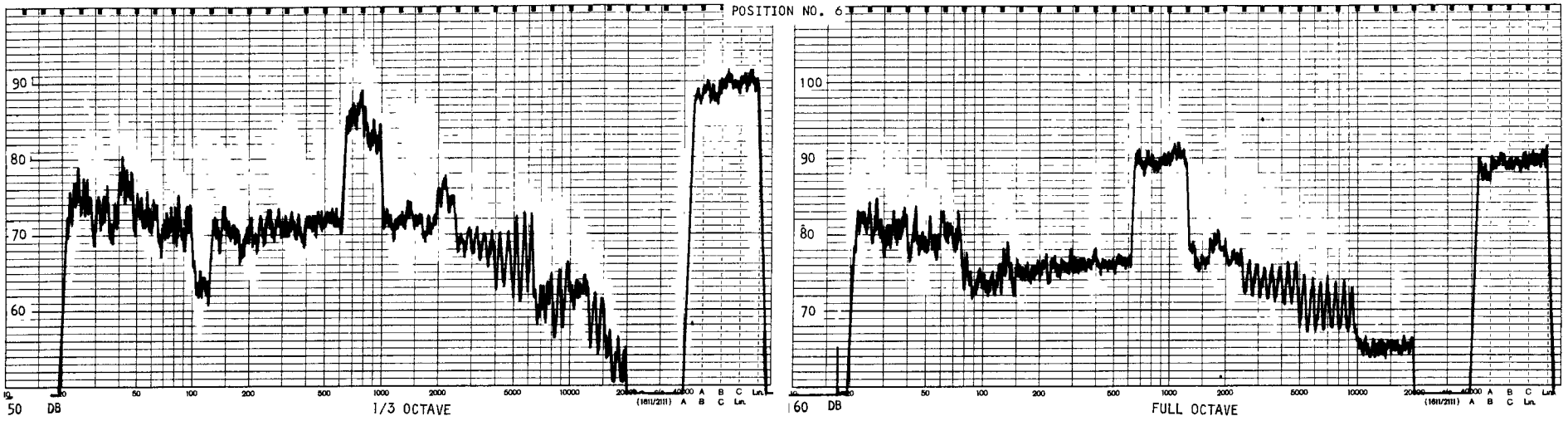

S-76741

Figure 6-18 (Continued)

EPA FAN ASSEMBLY P/N 605972-1

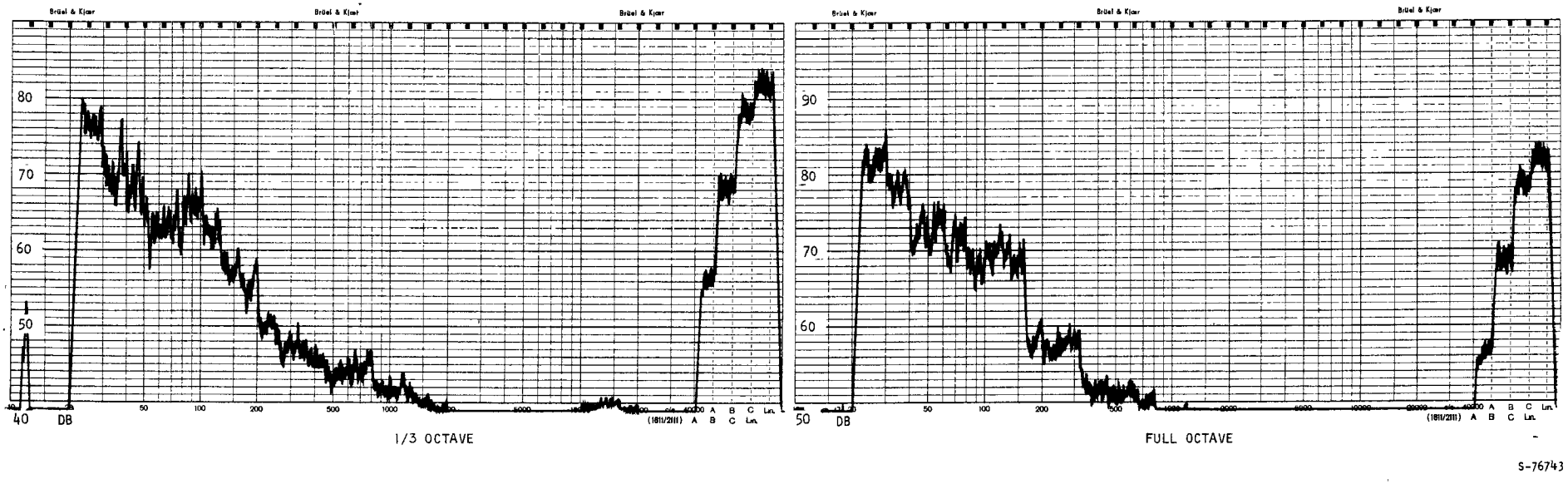

Figure 6-19. Reference Background Sound Pressure Level for Aerojet Fan Assembly P/N 605972-1

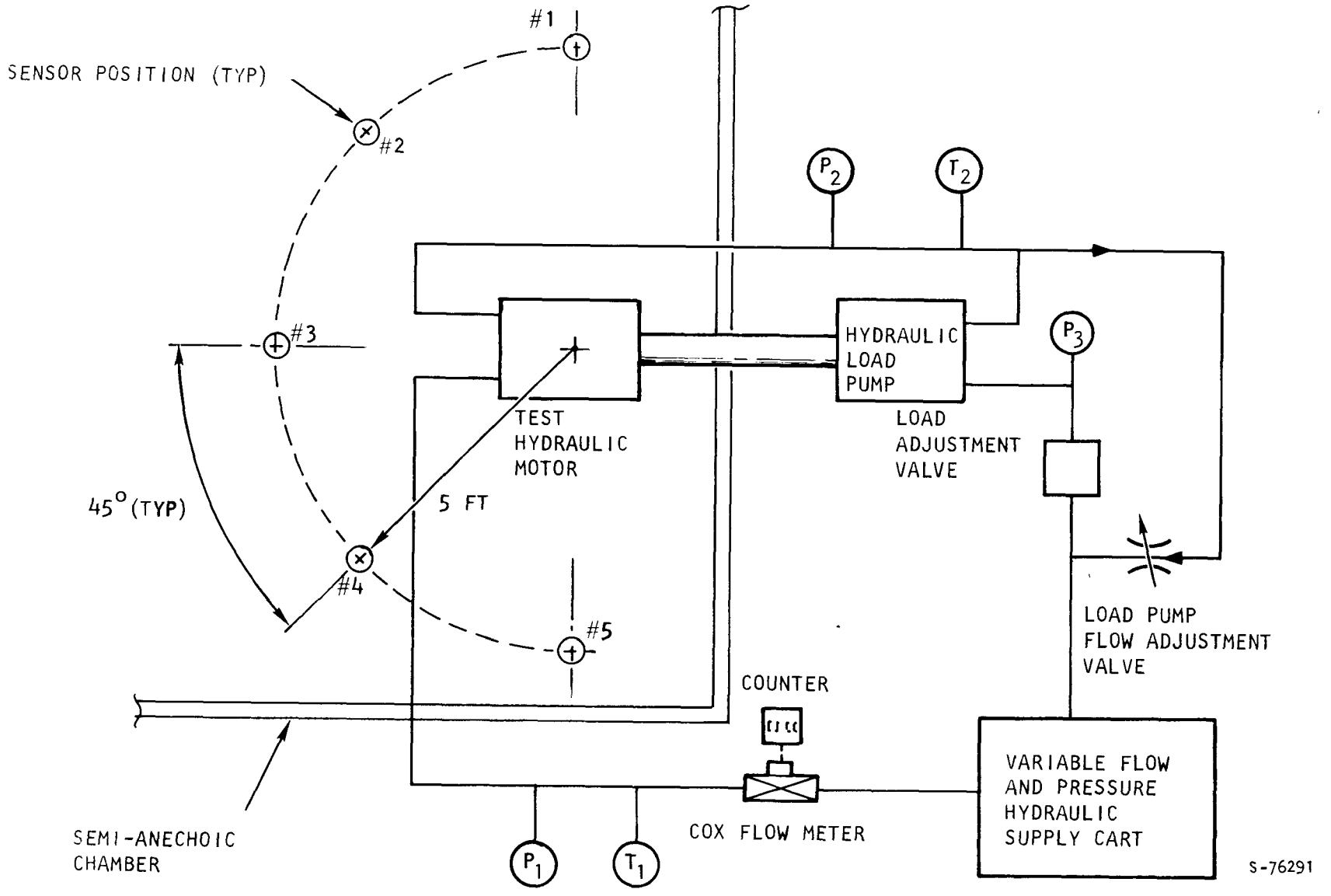

Figure 6-20. Hydraulic Motor Sound Pressure Level Test Setup

Where the subscripts A and T refer to Aerojet and TECO, respectively. Actual measurements were

$$\text{Aerojet} = 88.5 \text{ db(A)}$$

$$\text{TECO} = 88.6 \text{ db(A)}$$

$$\Delta \text{db(A)} = -0.1$$

This difference is well within the experimental error of ± 1 db on each measurement and thus, it was concluded that the two fans obey the theory.

In view of the low sound pressure levels achieved and the conformance of the fans to the fan lows it was decided not to test the SES fan, but to calculate its sound pressure level based on the Aerojet test results. Based on the above expression for change in noise level, the calculated noise of the SES fan is 83.2 db.

4. Summary

Test results are summarized on Table 6-4. Assuming a spherical radiation pattern, the sound pressure levels at 50 ft would be 20 db lower than at five ft. To determine the noise level for two fans as is the case for the actual installation, 3 db should be added to the noise values shown on Table 6-4.

Fan specifications do not include a specific noise limitation. However, a noise standard is imposed on the complete automobile and a maximum level of 77 db(A) at 50 ft is cited. Since the fans are expected to be the major noise source on the vehicle, it would appear that the vehicle noise standards can be met.

TABLE 6-4

NOISE TEST RESULTS

System Contractor	Rotational Speed	Sound Pressure Level Overall Average at 5 ft, dbA	Sound Pressure Level Overall Average at 50 ft, dbA
Aerojet	2980	88.5 *	68.5 **
TECO	2400	88.6 *	68.6 **
SES	2360	83.2 **	63.2 **

*Measured
**Calculated

NOTES: (1) All data are for a single fan
(2) Calculated values at 50 ft assume a spherical radiation pattern

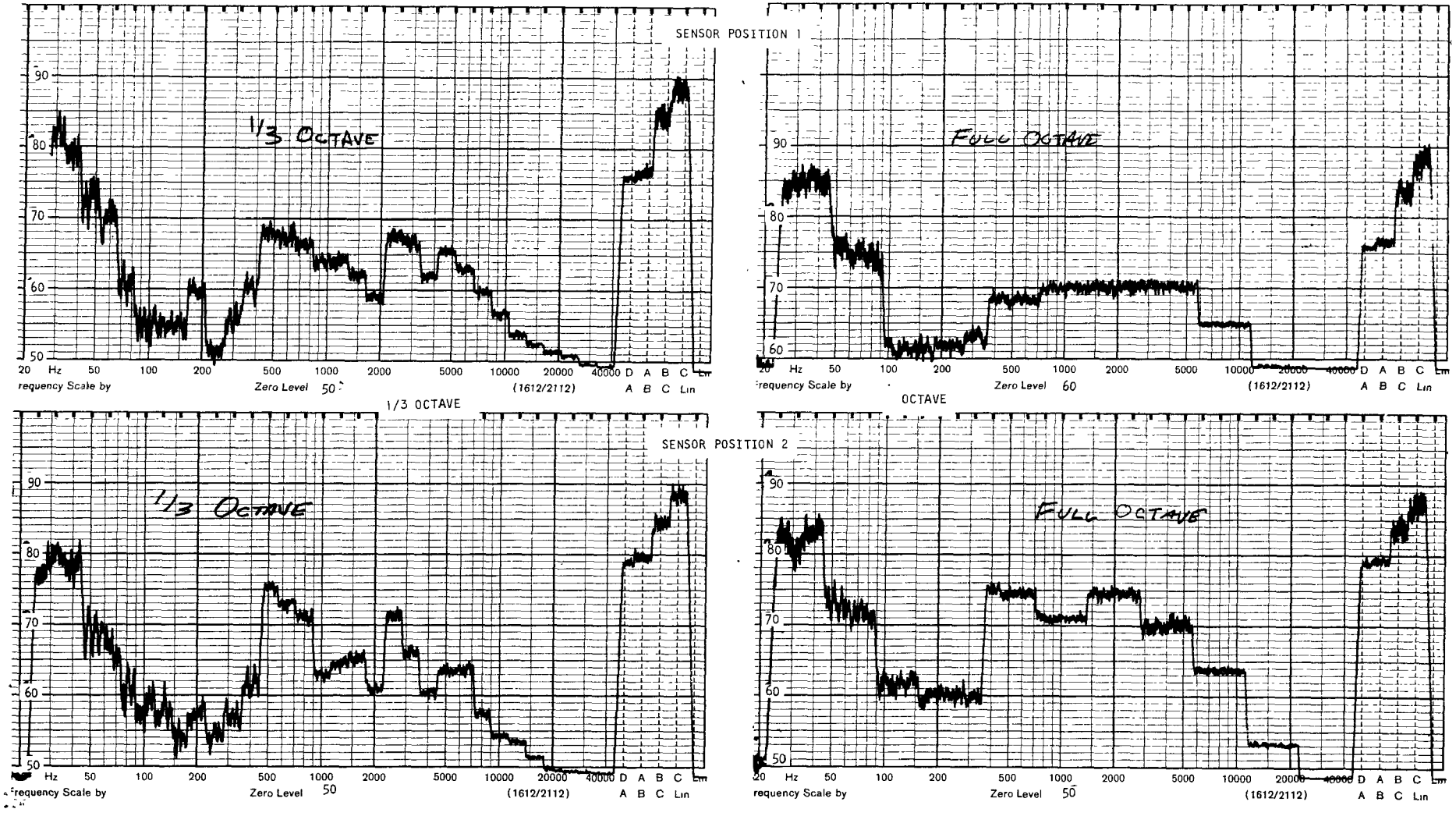

S-76744

Figure 6-21. Sound Pressure Level for HPI Hydraulic Motor M20-90155-01, S/N G20047

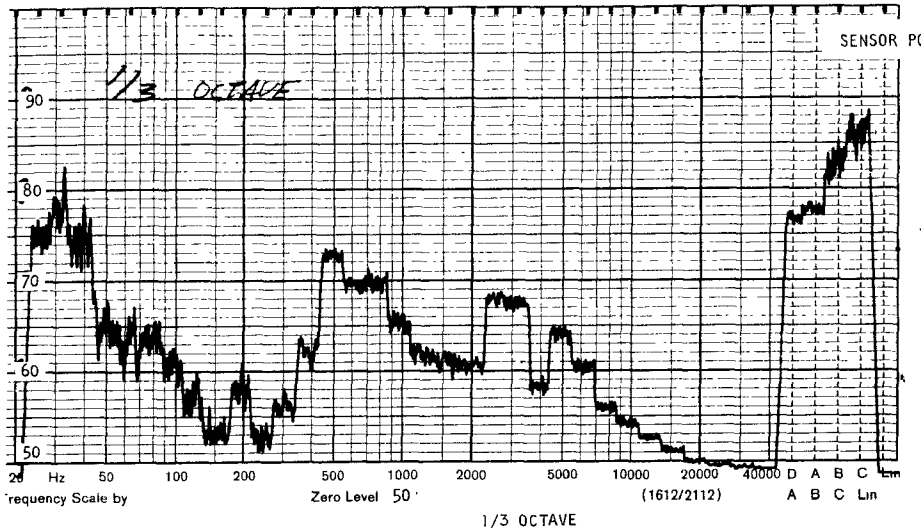

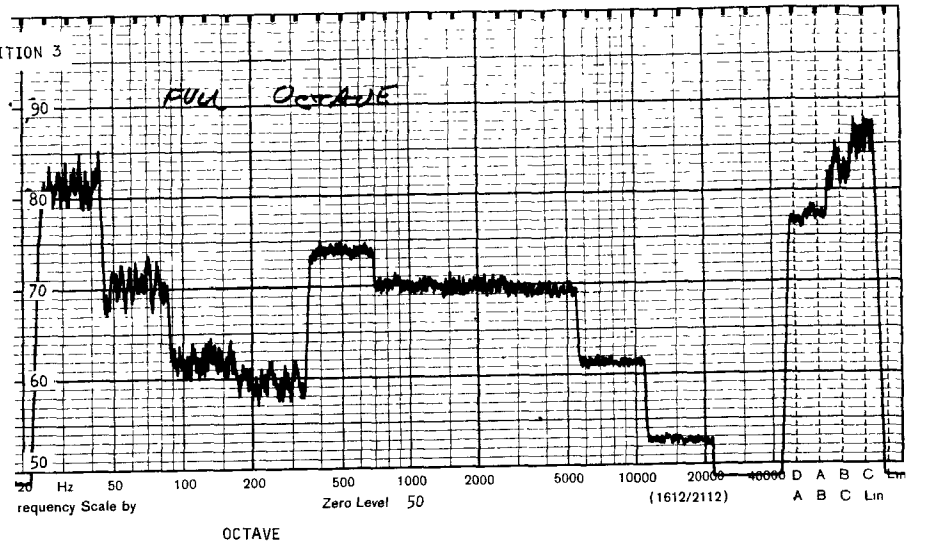

1/3 OCTAVE

OCTAVE

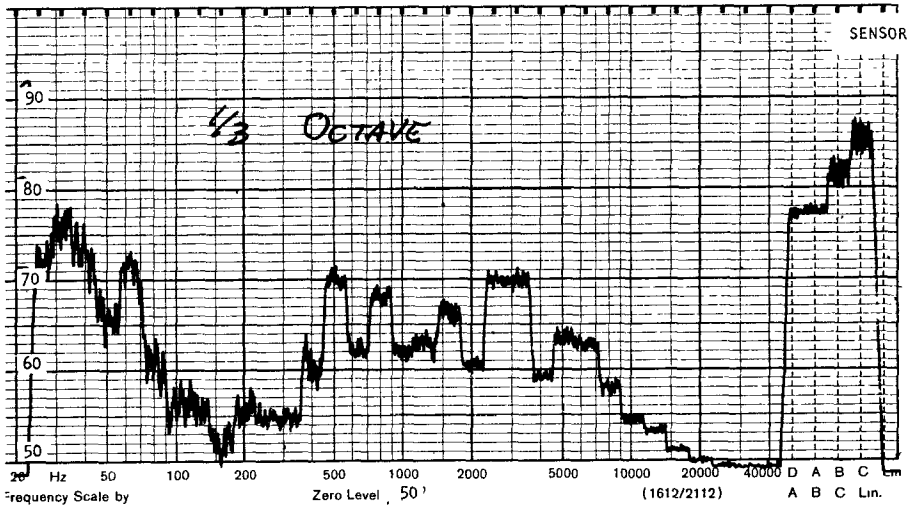

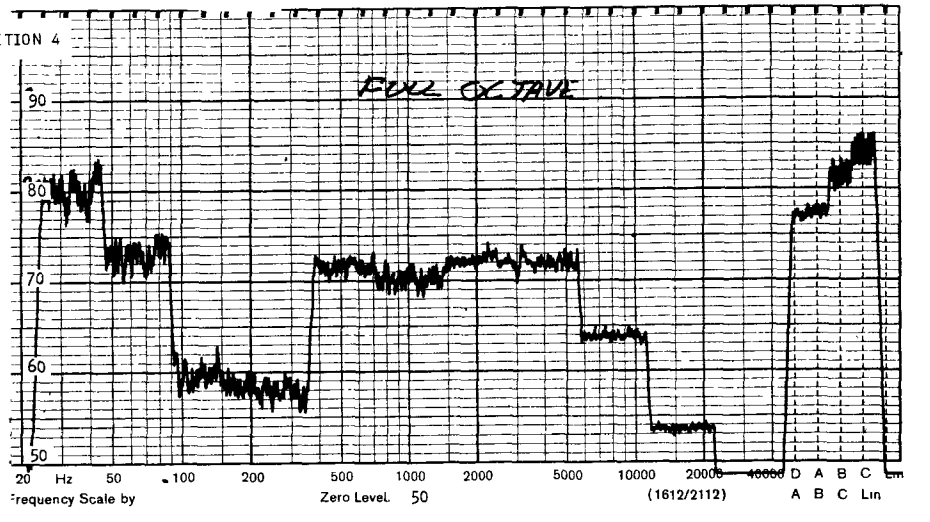

Figure 6-21 (Continued)

SENSOR POSITION 5

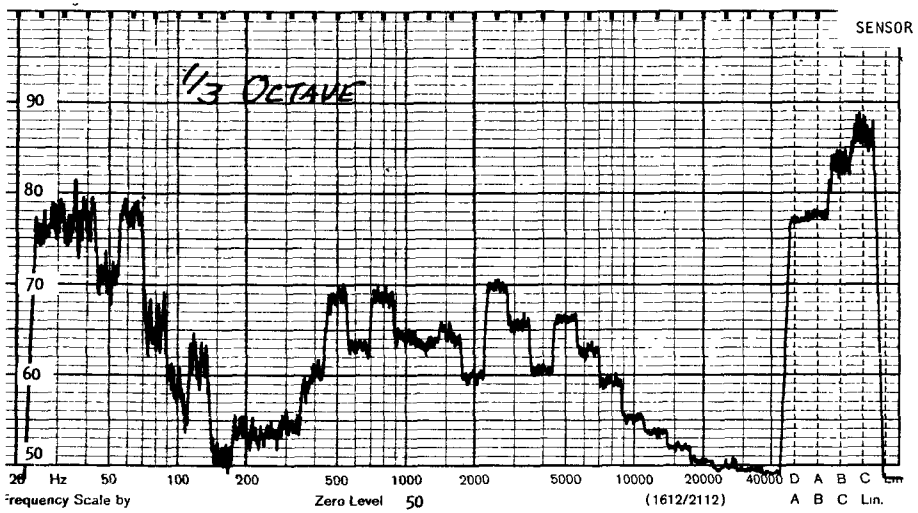

1/3 OCTAVE

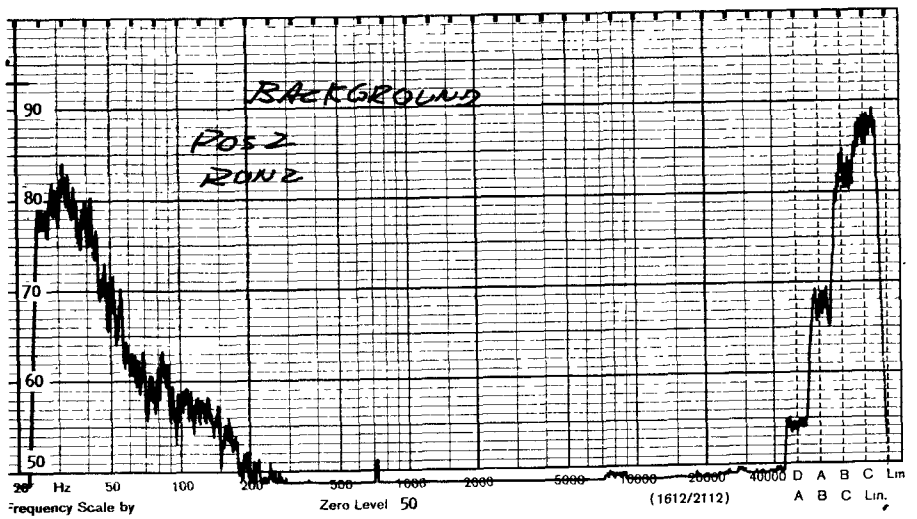

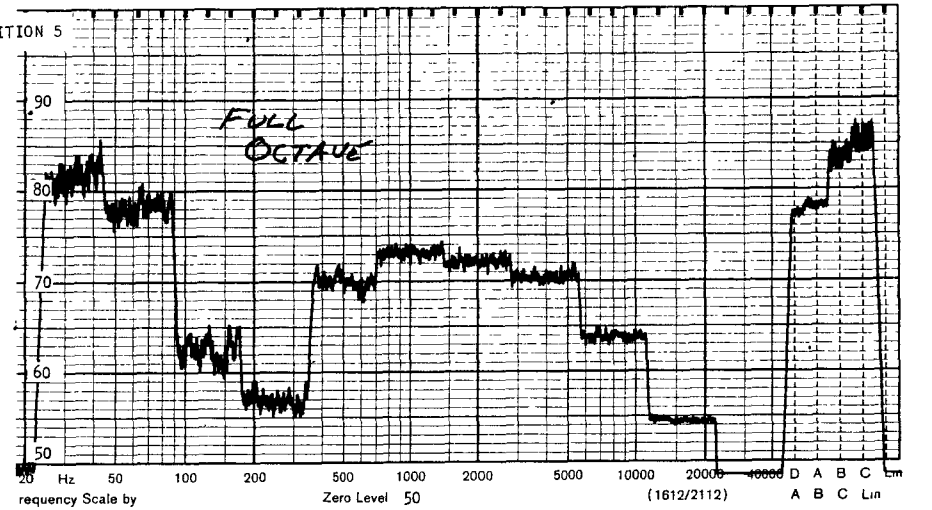

OCTAVE

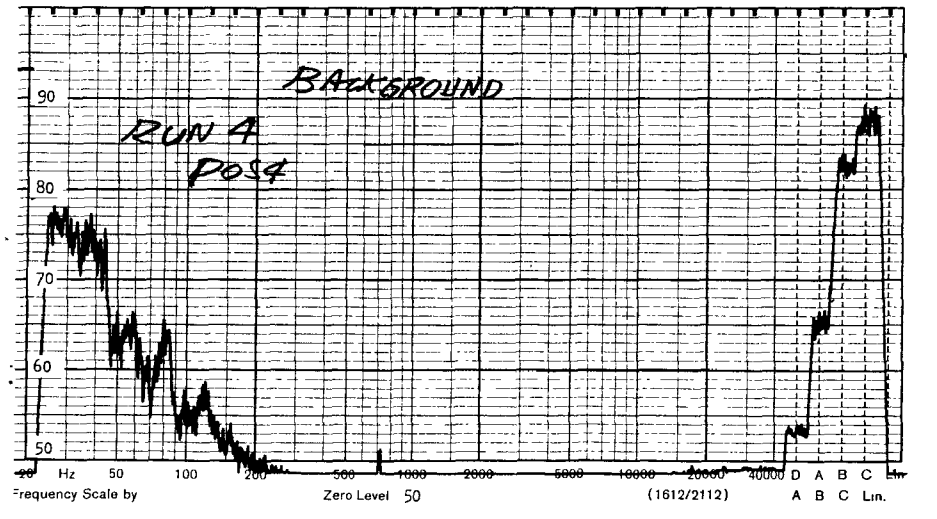

S-76737

Figure 6-21 (Continued)

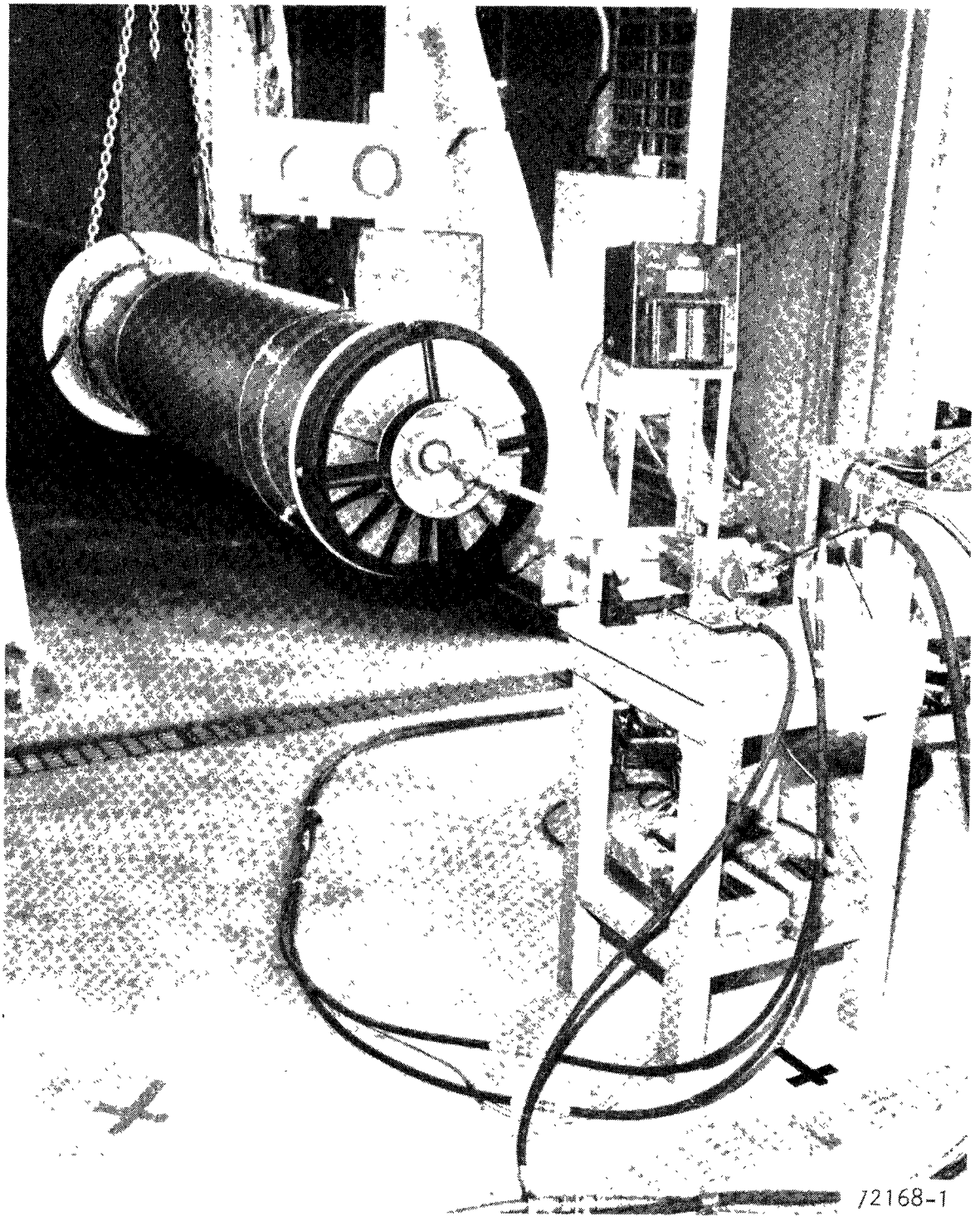

Figure 6-22. TECO Fan Assembly Installed in Noise Test Setup

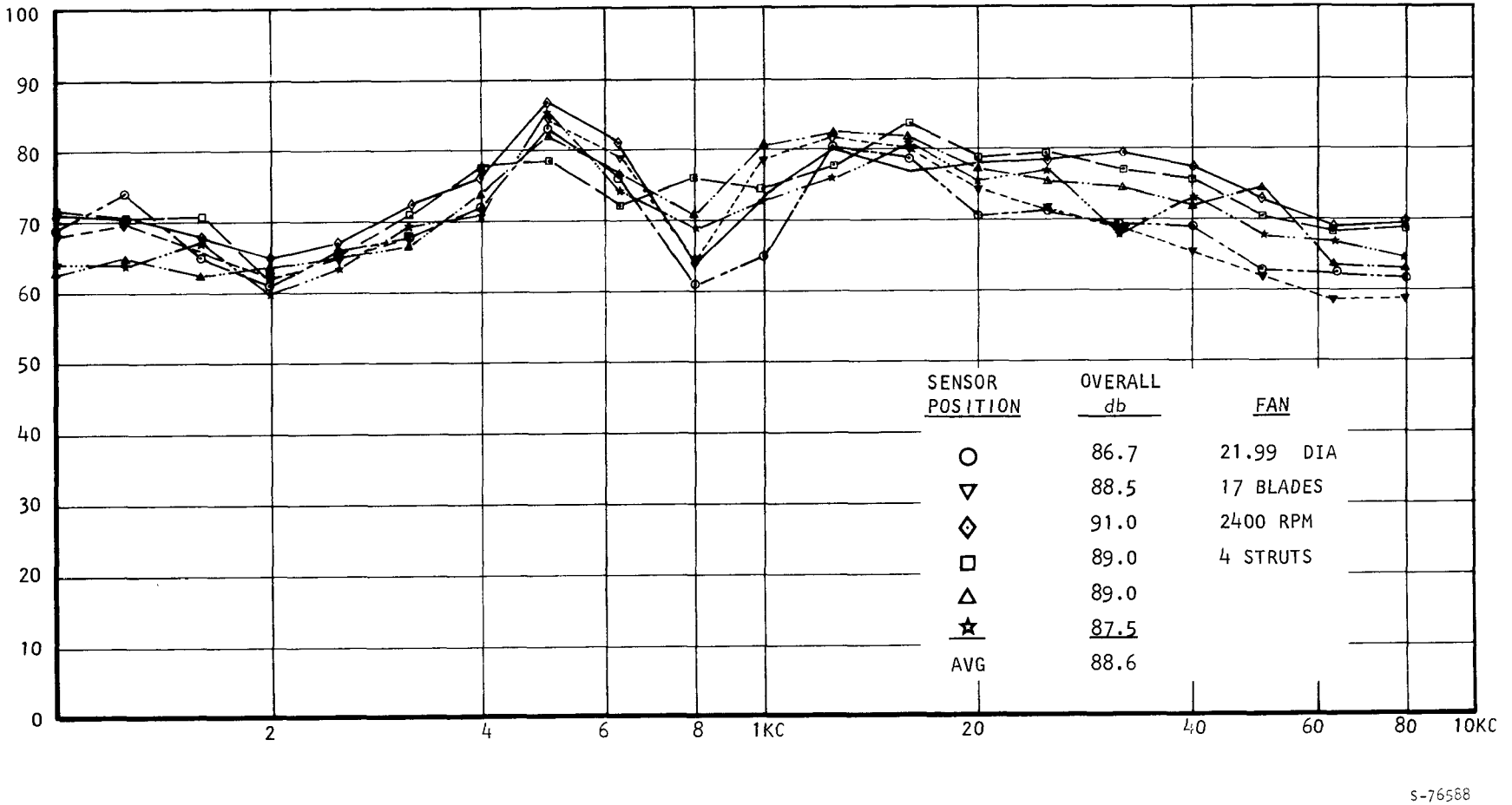

Figure 6-23. Sound Pressure Level for Thermo Electron Fan Assembly P/N 605977-1

SECTION 7

CONDENSER AND FAN AIRFLOW TEST

SECTION 7

CONDENSER AND FAN AIRFLOW TEST

Testing was conducted to determine isothermal airflow rate as a function of fan speed for both the TECO and SES condenser and fan assemblies. The purpose of these tests was to obtain an estimate of actual airflow to the condenser when the condenser and fan are joined as a single assembly. Thus, the results include the effect on performance of any flow maldistribution, both in the condenser core and at the fan inlet face, due to the close-coupling of these two components.

Figure 7-1 is a schematic of the test setup showing the airflow system and the location of the condenser and fans. Figures 7-2 and 7-3 show the completed setup with the TECO and SES assemblies installed. To ensure uniform air flow velocity across the condenser inlet face, two perforated screens (50 percent open area) were installed in the rectangular air inlet duct and a bellmouth contour was located just upstream of the condenser inlet face. The bellmouth contour was adjusted as required to conform to the front face dimensions of TECO and SES condensers. Views of the bellmouth contour (SES configuration) and one of the perforated screens are shown on Figures 7-4 and 705. The two thermocouples which were used to record the inlet air temperature are also shown in Figures 7-4 and 7-5.

A single hydraulic motor was used to drive both fans as shown on Figures 7-6 and 7-7. A spur gear was incorporated on each fan shaft to generate pulses for the electronic speed pickup. During testing the speed difference between the two fans was limited to less than 1.0 percent at the maximum power input conditions.

The tests were run by varying the rotational speed of the fans and adjusting the air flow at the air system inlet to obtain the desired static pressure upstream of the condenser. In most cases, the upstream pressure was maintained at zero gage pressure. It was necessary to maintain at least zero gage pressure at the condenser inlet to prevent the fan from operating in a surge condition. With the SES unit, runs were also made at 1.0 and 2.0 in. H_2O positive pressure at the condenser inlet face.

Inlet air pressure was measured with eight static wall taps located as shown in Figure 7-8, and airflow was measured with a standard orifice section at the air inlet. The air was dumped directly to ambient at the fan outlet face. During testing, the maximum deviation in any one inlet air static pressure reading from the average of the eight measured values was less than 0.1 in. H_2O.

Figures 7-9 and 7-10 summarize the test results for the two fan/condenser assemblies. In both cases, airflow is a linear function of fan rotational speed. The points run with a positive inlet pressure to the SES condenser show virtually the same results as those plotted in Figure 7-9.

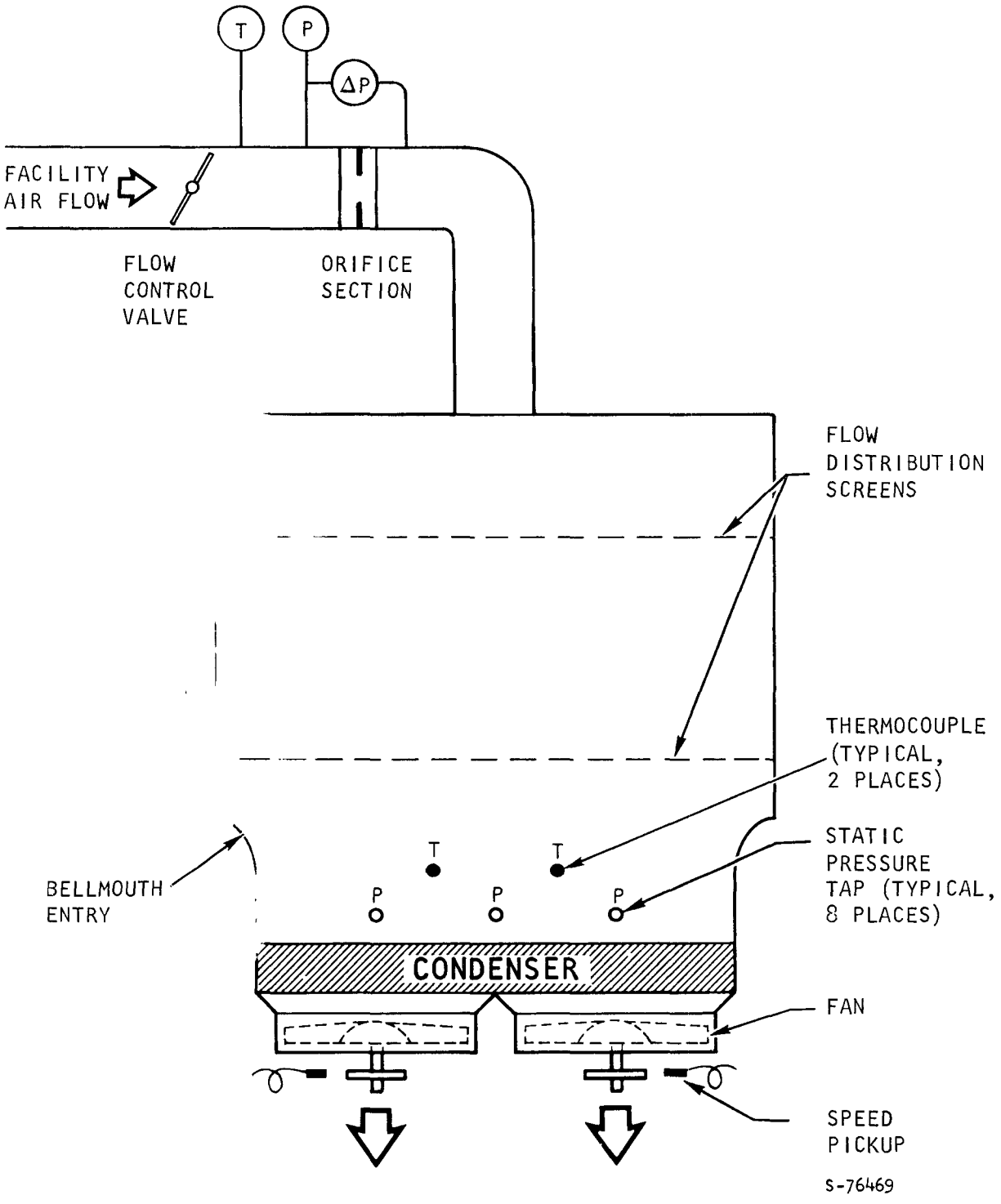

Figure 7-1. Condenser and Fan Airflow Test Setup

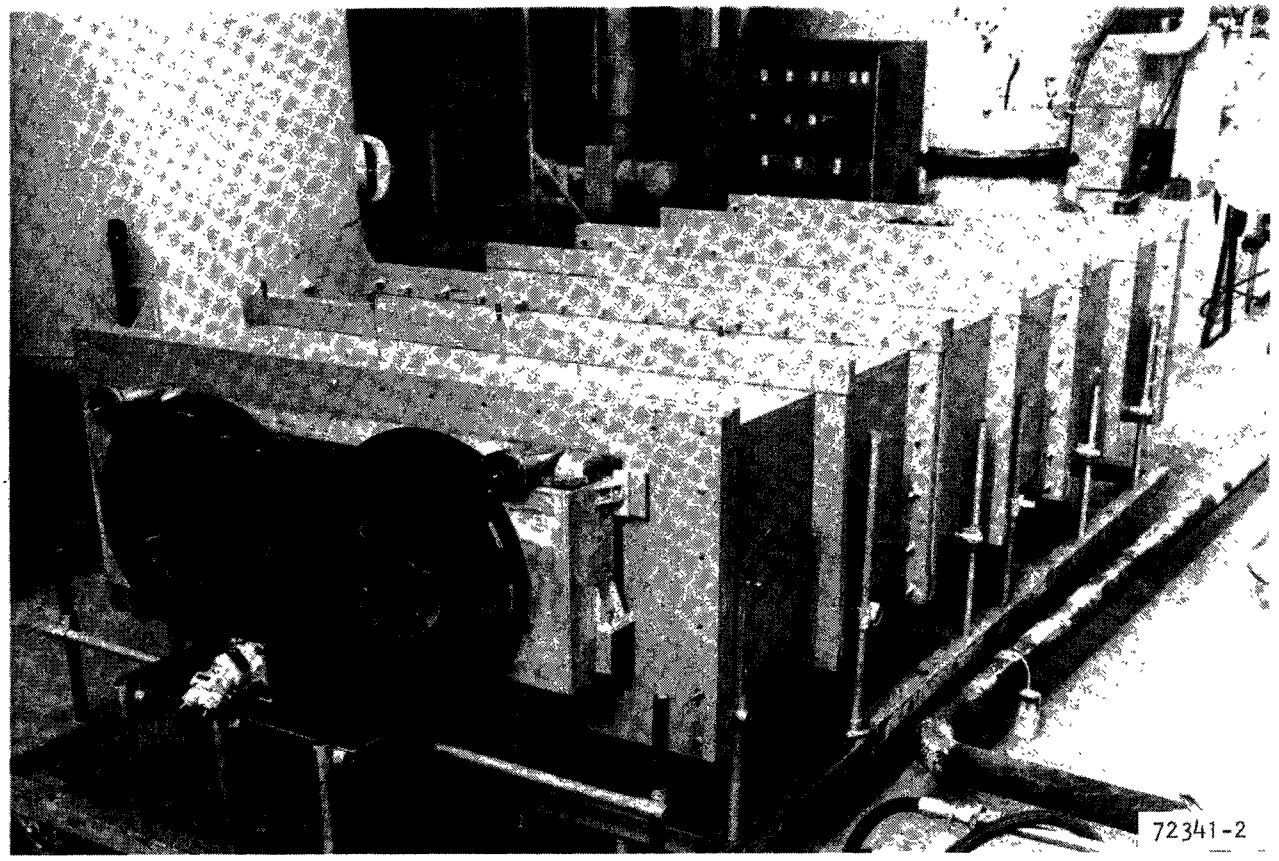

Figure 7-2. TECO Assembly Installed in Test Rig

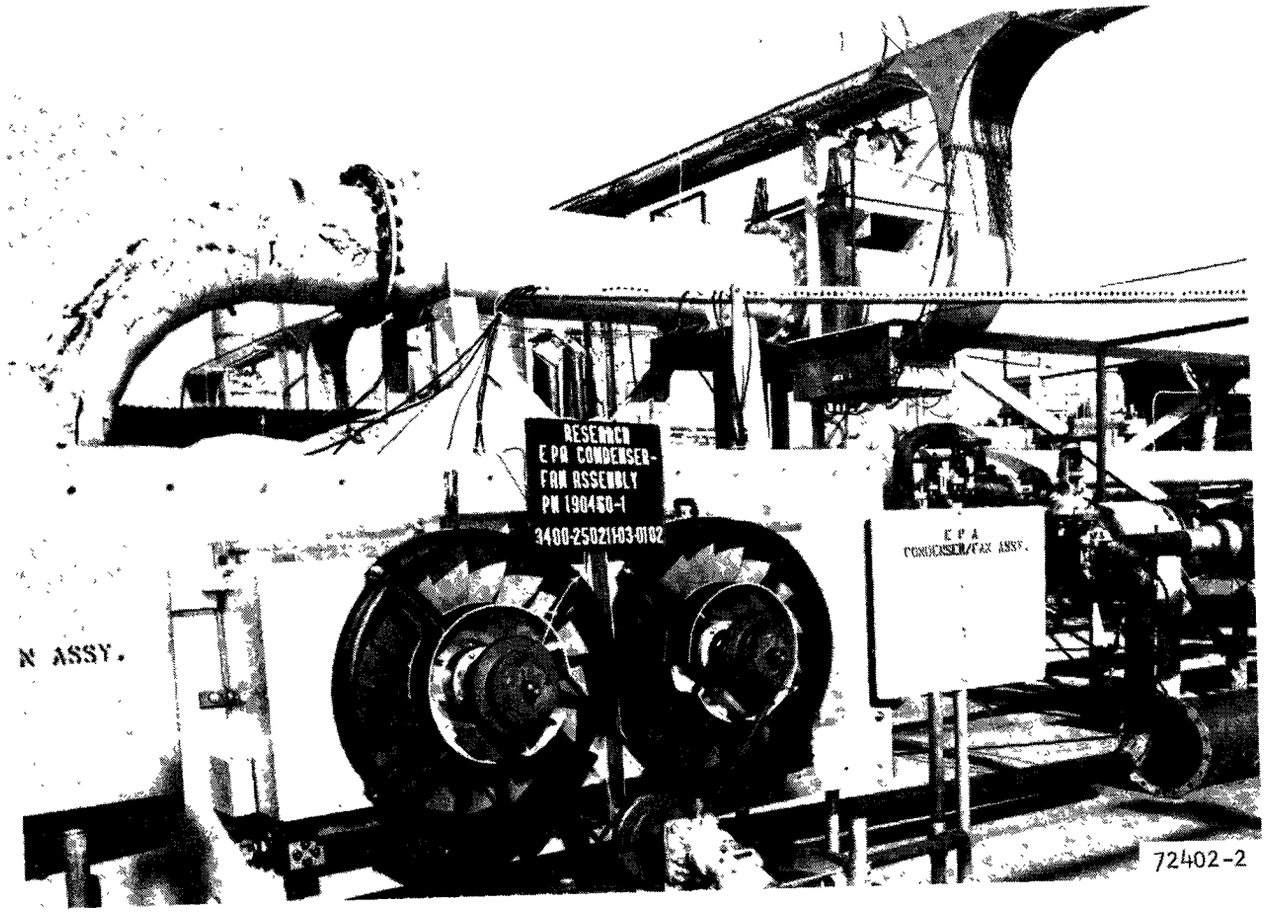

Figure 7-3. SES Assembly Installed in Test Rig

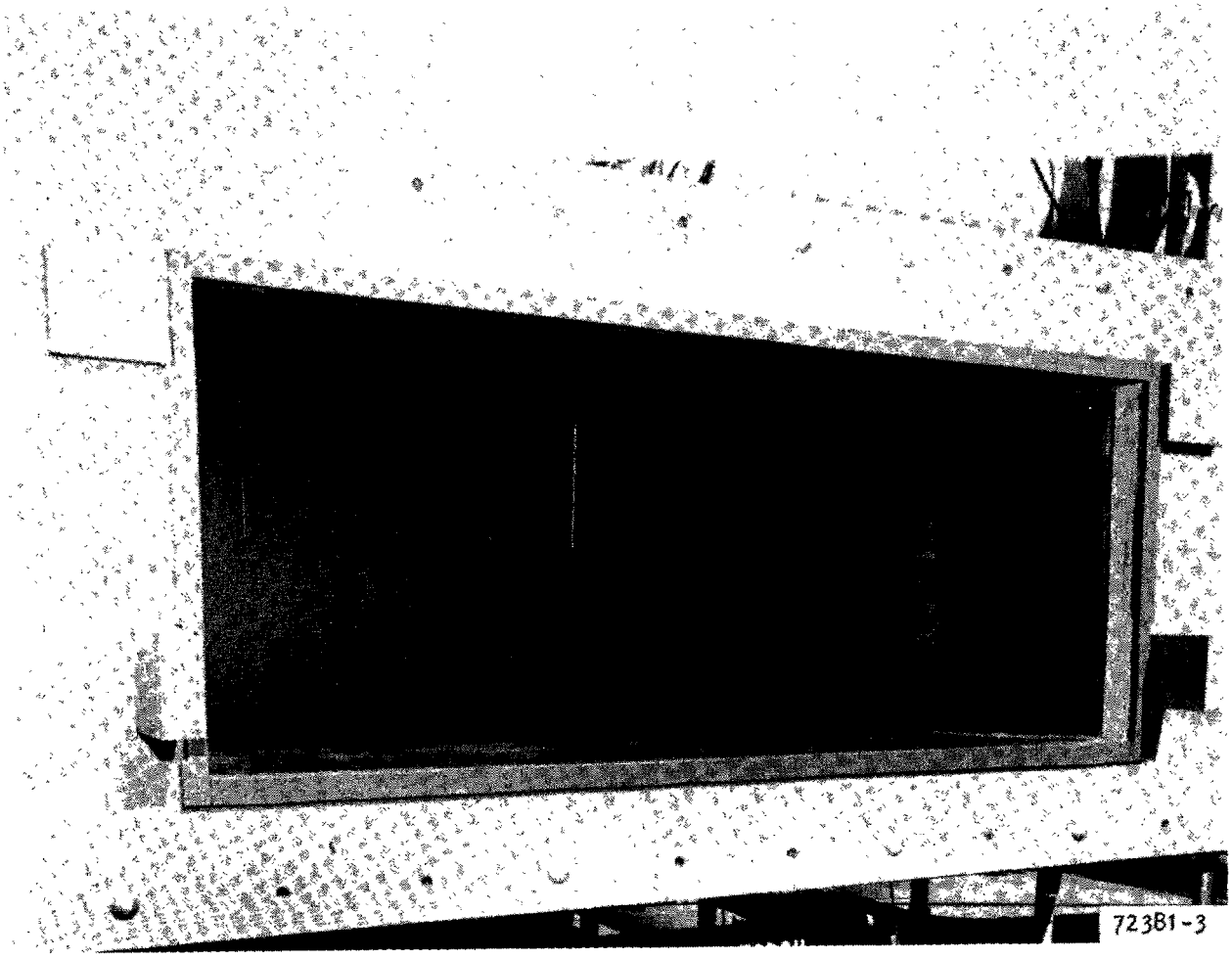

Figure 7-4. Duct Configuration at Condenser Inlet

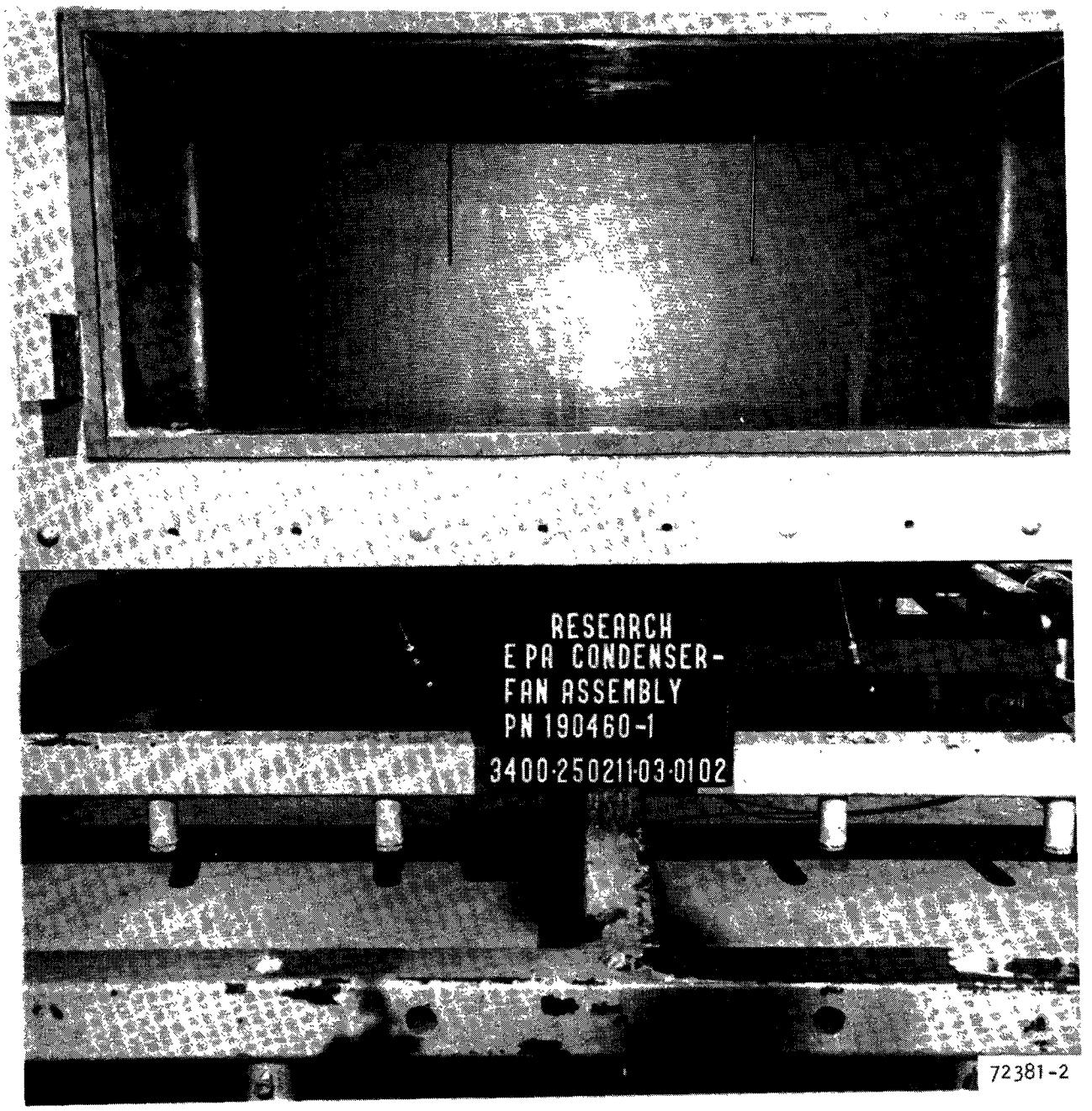

Figure 7-5. Duct Configuration at Condenser Inlet

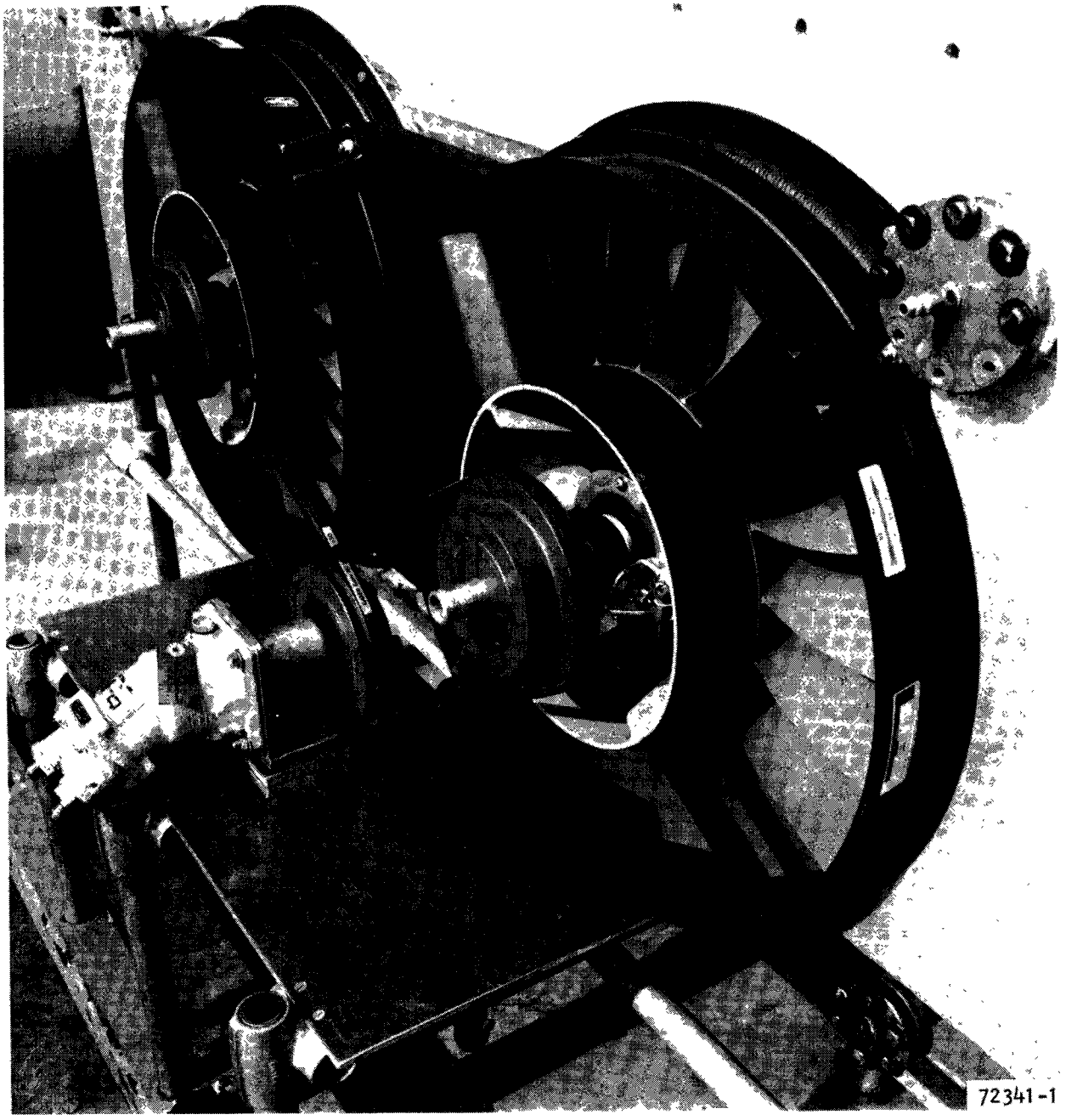

Figure 7-6. Hydraulic Motor Fan Drive

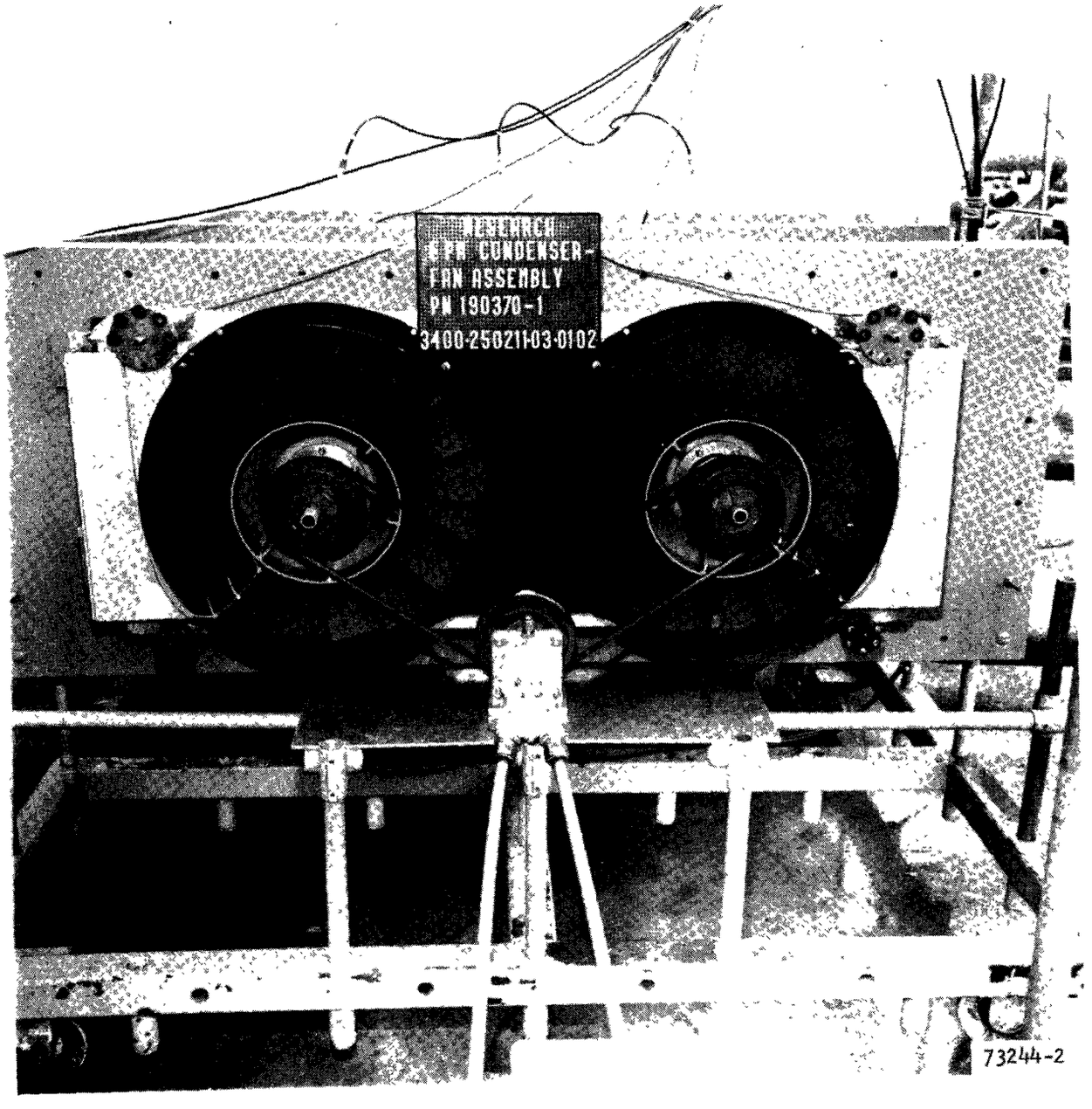

Figure 7-7. Hydraulic Motor Fan Drive

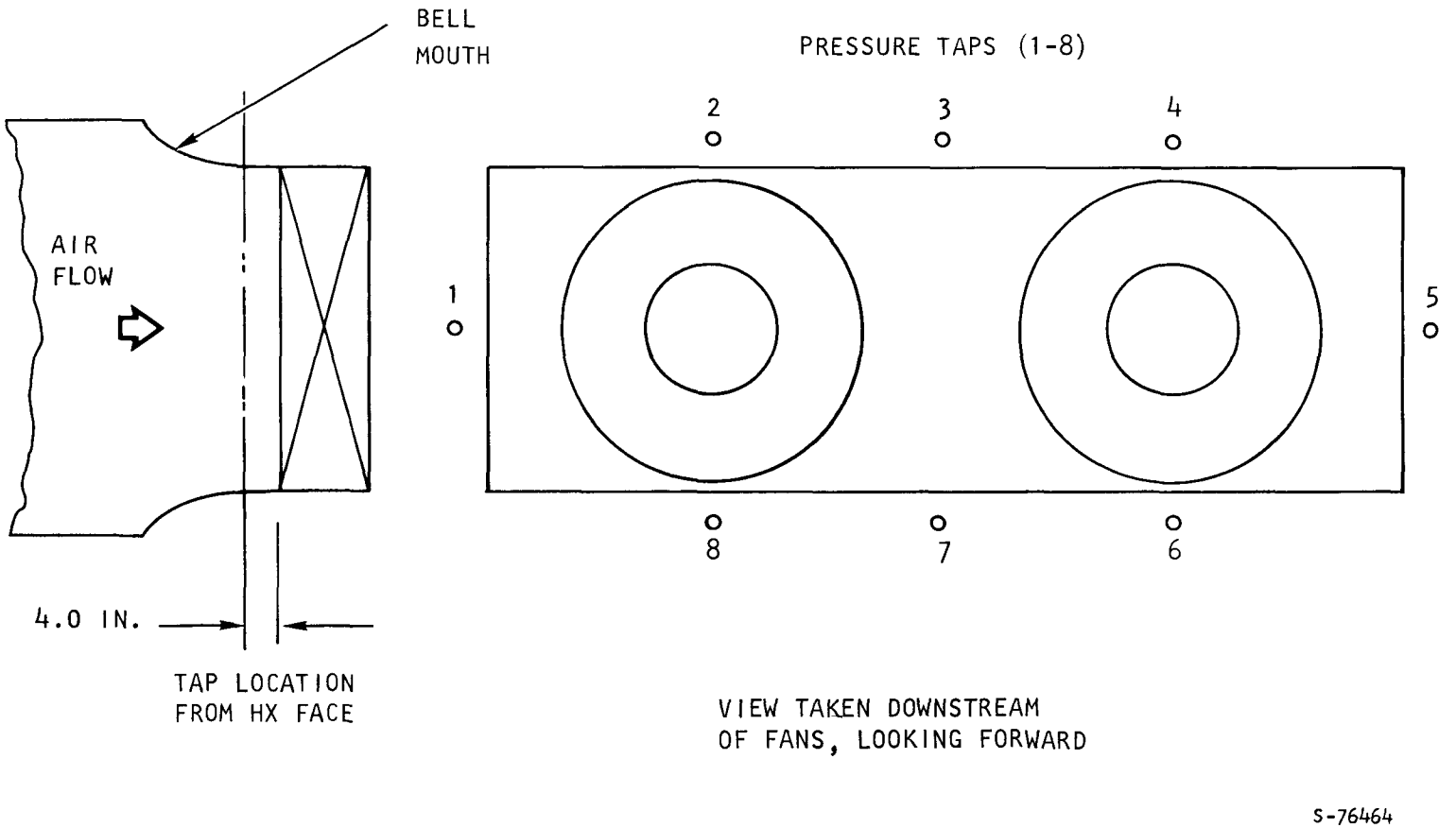

Figure 7-8. Pressure Tap Locations

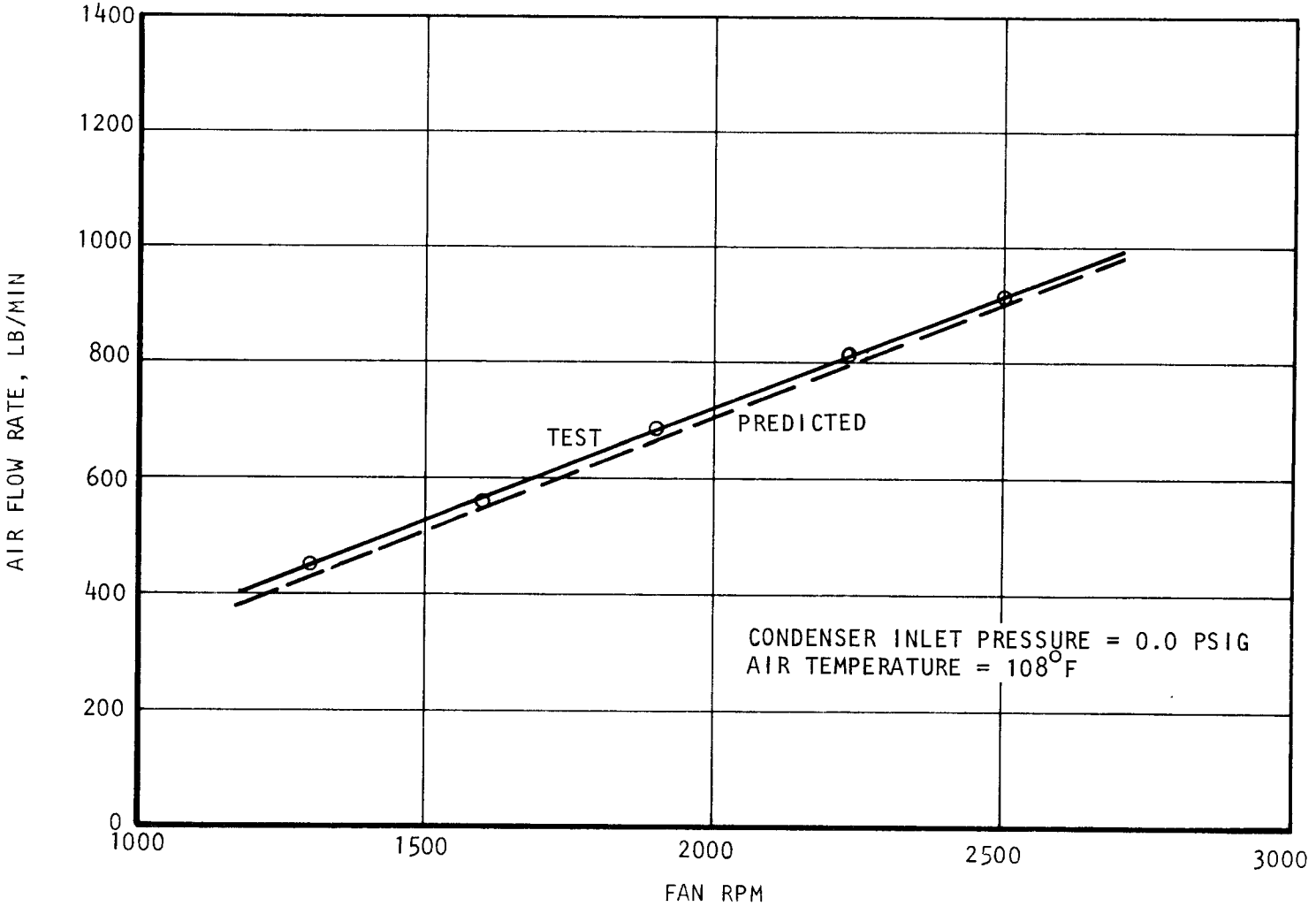

Figure 7-9. SES Condenser and Fan Airflow Test Results

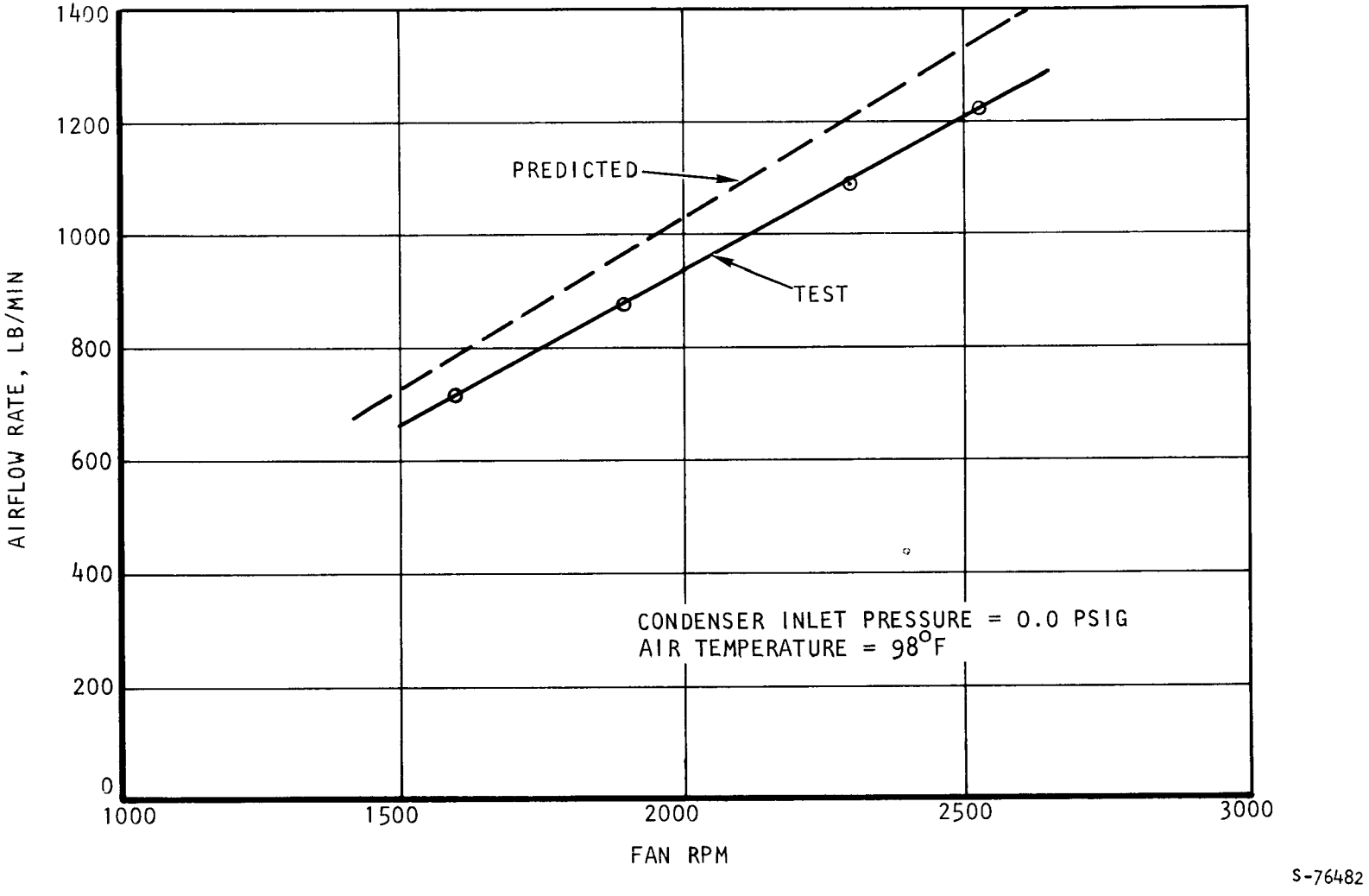

Figure 7-10. TECO Condenser and Fan Airflow Test Results

The predicted system performance, as represented by a dashed line on Figures 7-9 and 7-10, was determined as follows: The fans were assumed to perform in accordance with their respective calibration curves (see Figures 6-15 and 6-16). This is not entirely correct since any flow maldistribution at the fan inlet would affect performance. The fan laws were then used to determine the fan flow and pressure rise at speeds differing from that of the calibration curve. It was assured that one velocity head was lost at the fan exit. The pressure drop across the condenser was based on the predicted condenser air side pressure drop as presented in Section 5. Finally, for a given fan speed, the airflow at which the fan static pressure rise was equal to the pressure drop across the condenser was determined.

The airflow in the SES unit is seen to be slightly higher than predicted, whereas the TECO airflow is nine percent less than predicted over the rpm test range. The discrepancy between predicted and test performance for the TECO unit is believed to be primarily due to flow distribution effects caused by the transition between core outlet face and fan inlets. The power performance of the TECO unit relative to the SES unit is probably due to (1) a closer spacing between condenser and fan (1.94 in. for TECO versus 2.51 in. for SES) which restricts the redistribution of flow in the transition plenum, and (2) the slight oversizing of the TECO fans relative to the condenser face (i.e., the fan diameter of 22 in. is about one inch greater than the core height) which tends to restrict flow to the tops of the TECO fans where they overhang the core.

Based on Figure 7-10, it established that for the TECO unit the required fan horsepower is increased by 27 percent over the previous prediction at design point airflow conditions. The estimated power requirement for the SES fans is unchanged based on the close correlation between test flow and prediction shown by Figure 7-9.

SECTION 8

INSTALLATION AND AIRFLOW TEST

SECTION 8

INSTALLATION AIRFLOW TEST

Cooling air flow through a Rankine cycle engine condenser is about 3 to 5 times greater than that through a conventional IC automobile engine radiator. It would be expected then, that the air flow pressure losses across the bumper and grille and through the engine compartment, referred to as the installation loss, could easily become excessive in the case of a Rankine cycle engine (RCE).

Installation pressure losses are of considerable interest because they directly affect the fan design. The system contractors were contacted to determine how they evaluated the engine installation air flow losses. Thermo Electron determined the losses by assigning an assumed loss coefficient to each element in the system. Steam Engine Systems assumed the losses were equal to three condenser exit velocity heads. Aerojet assumed that the total losses were equivalent to 25 percent of the ram air velocity head. The assumed installation losses ranged from 0.3 to 2.0 in. H_2O. It was apparent that there was no reliable test data available from which to compute the installation loss.

An electric analog study was performed to obtain an estimate of the losses in the TECO installation. This study indicated that, due to the limited flow area in the engine compartment, a high compartment pressure loss could be expected.

Test data for the pressure losses through the grille, air conditioning condenser, radiator, fan shroud, and engine compartment of a 1971 Galaxie as a function of air throughflow was obtained from Ford (Reference 6-1). The data was obtained in a wind tunnel, and as indicated by Ford, does not correlate accurately with driving conditions. However, it should give an idea of the magnitude of the actual losses. Using loss coefficients calculated from the Ford data, the pressure drops through the Galaxie grille, air conditioning condenser, and the Galaxie engine compartment were calculated at the TECO design air flow rate to be 3.6, 1.3, and 8.8 in. H_2O respectively. The total loss assigned to the installation by TECO was about 2.8 in. H_2O. Thus, it would appear that installation of the TECO engine in an unmodified engine compartment would result in excessive fan power consumption.

Because of the potential for a significant impact on the fan design, a test program was undertaken to determine the actual loss. It was expected that their data would help to guide the system contractors in modification of their respective systems to provide greater cooling air flow area which would in turn, result in a reasonable limit on fan power consumption.

The basic test plan was to use an actual engine compartment (obtained from a junked automobile) and install wood and Styrofoam mockups of the RCE in the compartment. A known amount of air would be flowed through the grille and across the bumper into the compartment. The resultant pressure drops would be recorded. Results of these installation air flow tests are described below.

Thermo Electron/Ford Installation

The front end of a 1971 Ford Galaxie was obtained and a mockup of the Thermo Electron Engine was installed. Photographs of the completed installation are shown in Figures 8-1, 8-2, and 8-3.

Figure 8-1 shows the condenser mockup which for purposes of this test, was constructed of 2 in. diameter tubes which acted as flow straighteners. The 58 in. wide rectangular condensers stretched across the entire width of the engine compartment. Condenser flow resistance was designed to be simulated by layers of tight mesh screen. The two annular openings just downstream of the condenser represent the fan blade sweep area. The frame rails were modified to go along the side of the condenser which required locating the bumper supports outboard of the condenser.

Figure 8-2 presents a clear view of the rectangular vapor generator which is located immediately behind the fans. Figure 8-3 shows the close spacing (about 3 in.) between the fans and the vapor generator.

An adaptor plate as shown on Figure 8-4 was made to connect the vehicle inlet to the laboratory air duct. The adaptor also included a simulated bumper. The real bumper was not used because the supports were relocated as noted above. As shown on Figure 8-5, the adapter plate was fitted to cover the entire area between the lower lip of the head and the bottom of the simulated bumper between the fender projections. The vehicle springs were collapsed until the vehicle was at a height equivalent to that of a normally loaded automobile. A rectangular plywood duct was fitted to the adapter plate to supply air flow to the condenser. The airflow was supplied by two engine-driven blowers, and flow measurement was accomplished by calibrated bellmouth inlets fitted to the blowers. The completed test setup is shown on Figure 8-6.

Test results obtained for the TECO installation are presented on Figure 8-7. The overall loss at the design point conditioner is about 3.0 in. H_2O. This installation loss includes losses across the bumper and through the engine compartment, but does not include that of the grille because it was removed for their test. The loss across the condenser mockups was assumed to be zero (no flow resistance screens were used during this test).

Attempts were made to measure engine compartment and simulated bumper losses separately. It was found, however, that there was no representative location at which a static pressure could be measured between the bumper and the compartment. Thus, an average volumetric flow must be used to estimate the overall installation pressure drop.

According to the Thermo Electron fan problem statement summarized in Table 6-1, 2.8 in. H_2O pressure loss is allowed for the installation. The measured loss with no grille is about 3.0 in. H_2O. It would appear that the specified installation loss could be met with some vehicle modifications and a non-restrictive grille. This test was run, however, at a condition of zero vehicle speed. It would be expected that with vehicle motion, the airflow exit from the engine compartment would be restricted because of the airflow underneath the vehicle. This effect would tend to increase the compartment pressure drop.

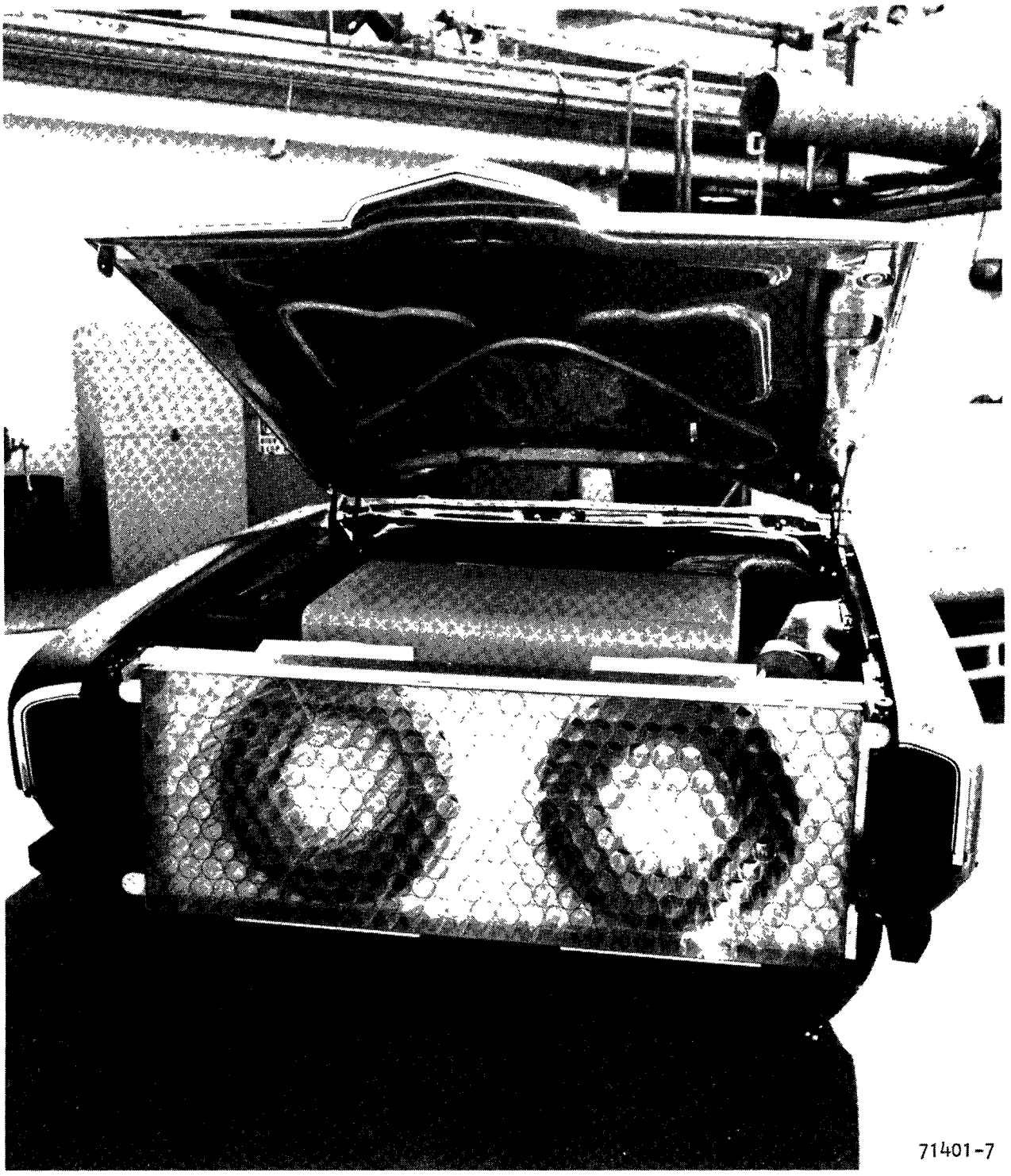

Figure 8-1. Thermo Electron Engine Mockup

Figure 8-2. Thermo Electron Engine Mockup

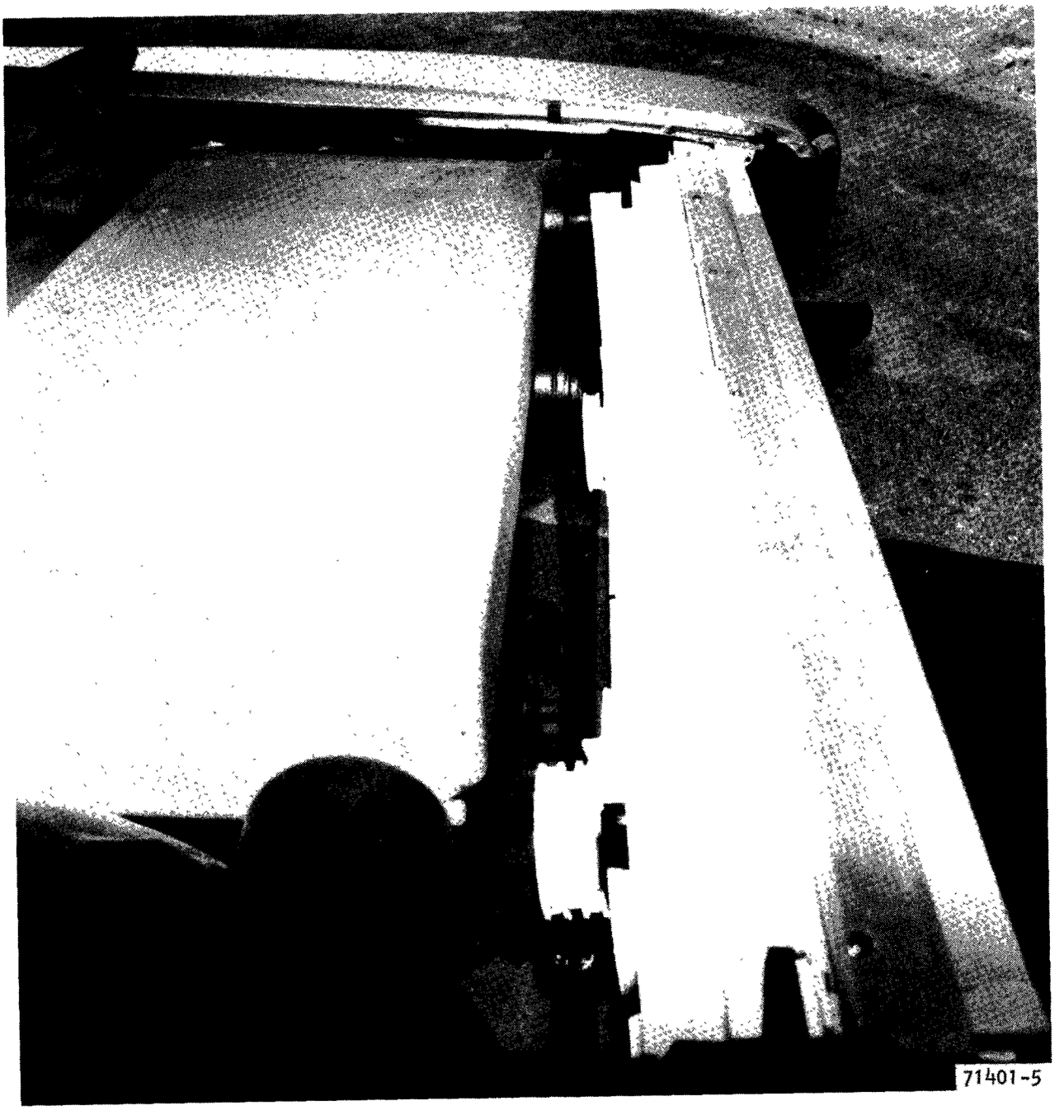

Figure 8-3. Thermo Electron Engine Mockup

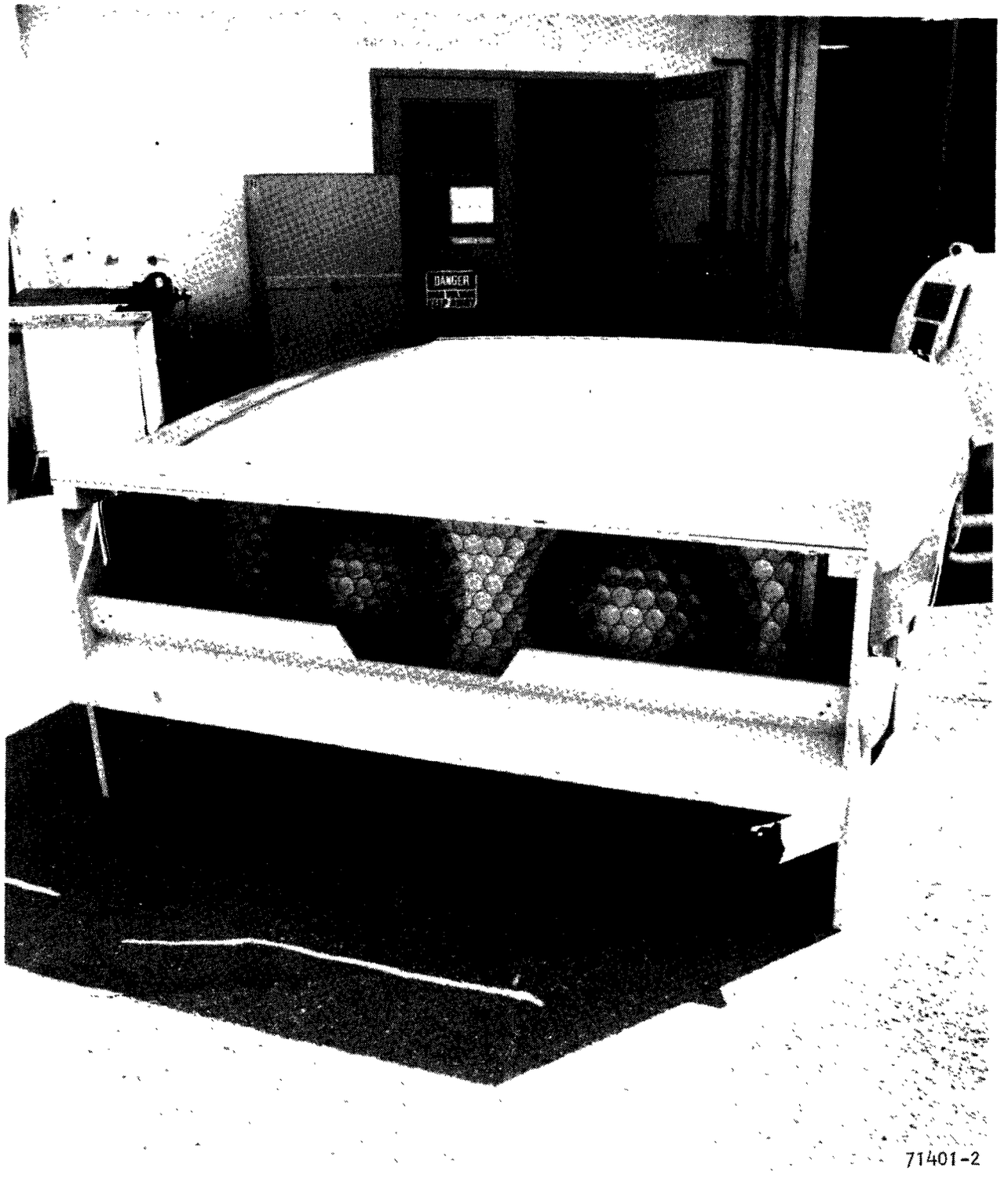

Figure 8-4. Adaptor Plate with Simulated Bumper

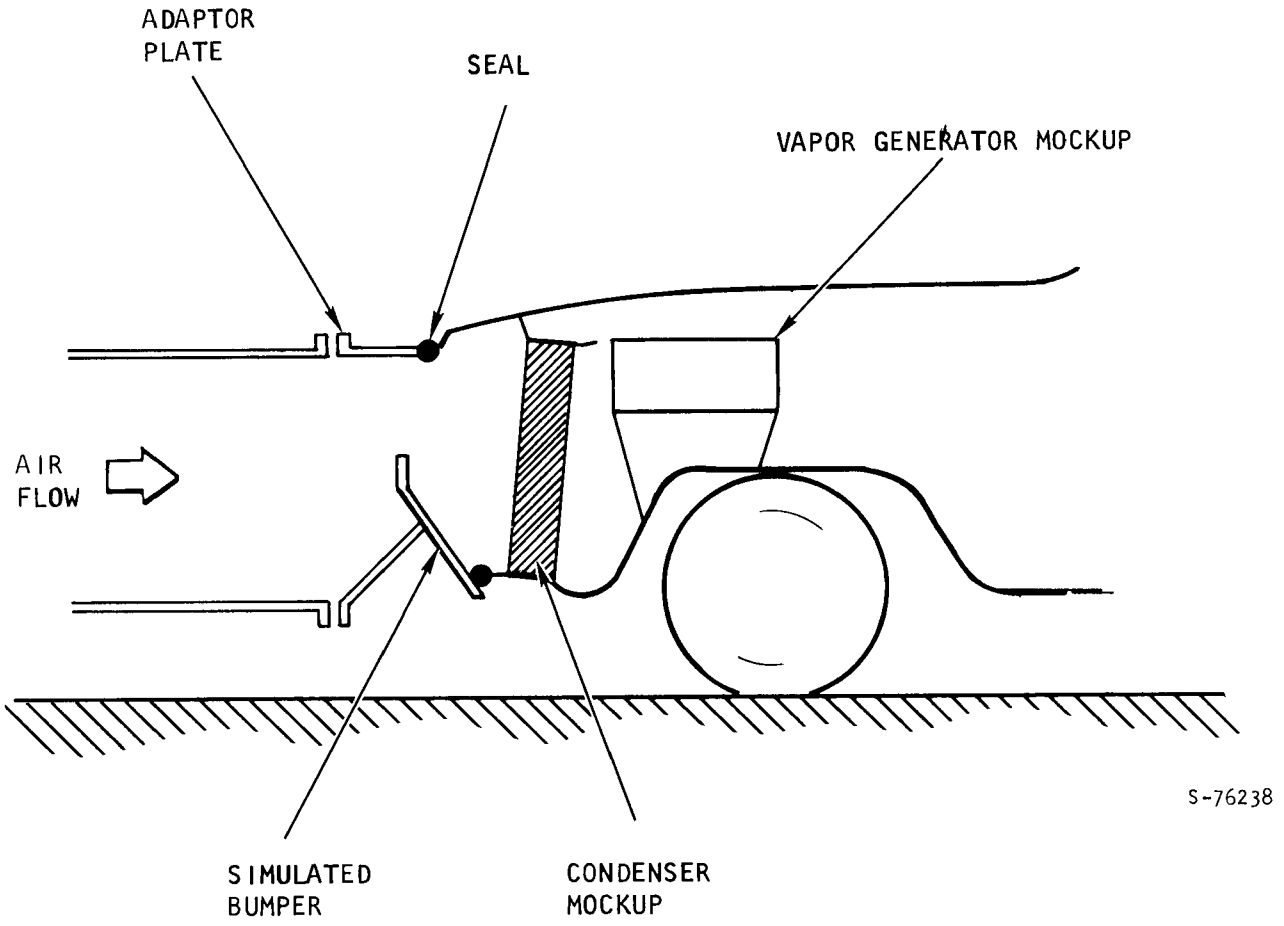

Figure 8-5. Air Flow Ducting

Figure 8-6. Thermo Electron Installation Air Flow Test Setup

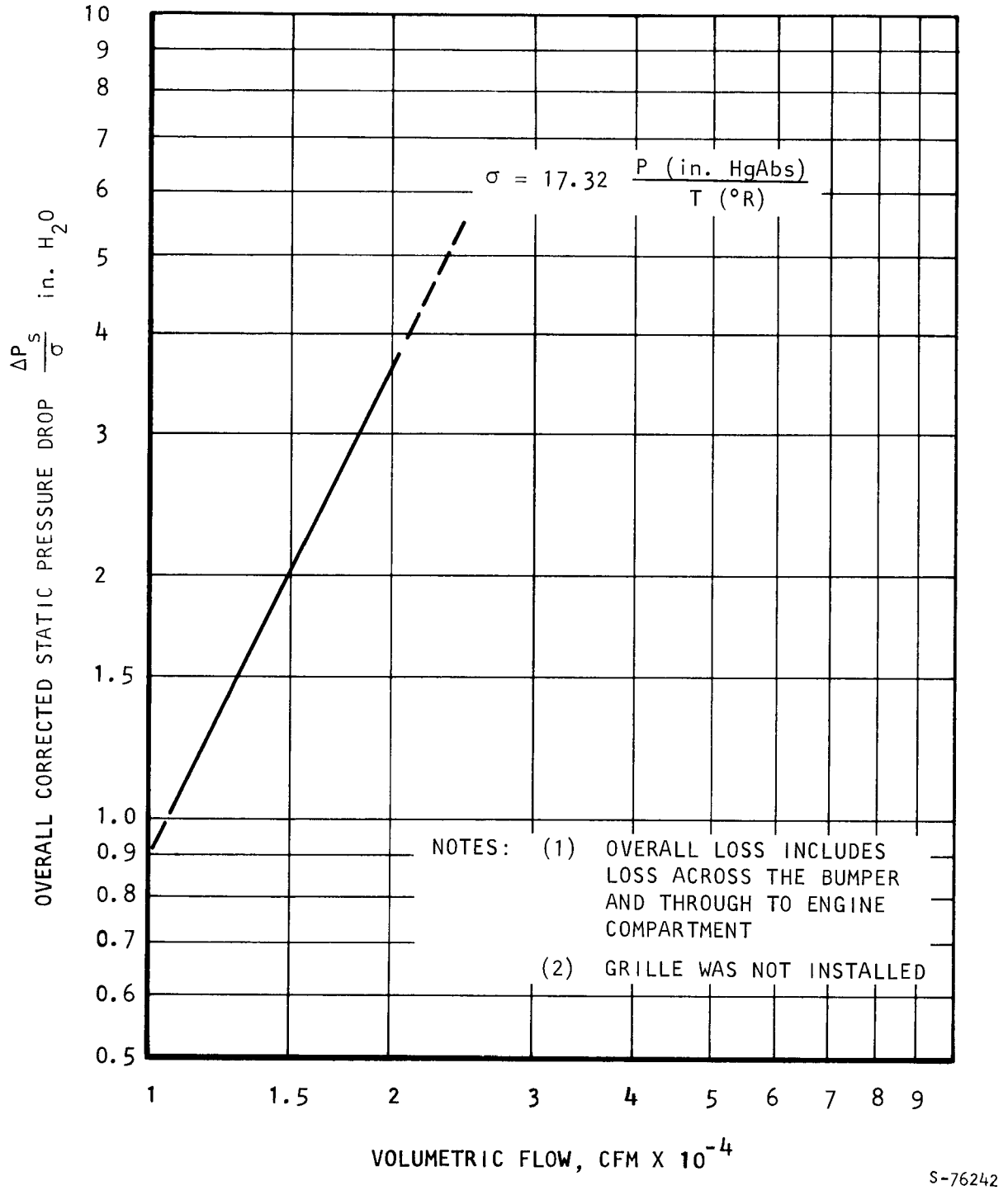

Figure 8-7. Thermo Electron Installation Air Flow Test Results

Subsequent to this test, Thermo Electron completely redesigned the vapor generator. The resulting cylindrical configuration provides additional flow area at the fan exit. It would be expected that the engine compartment pressure drop would be less with the new vapor generator configuration.

Aerojet/Chevrolet Installation

The compartment mockup was loaned to AiResearch by the Aerojet Liquid Rocket Comapny for purposes of this test. The equipment consisted of the engine compartment, bumper, grille, hood, and front running gear of a 1971 Chevrolet Impala fitted with Styrofoam mockups of the major components of the Aerojet engine. Two different vapor generator configurations were supplied. The first mockup was 26 in. in diameter and represented the current configuration, while the second mockup was basically 23 in. in diameter and was configured to show an advanced vapor generator design.

The mockup was modified by AiResearch to position two fan housings ahead of the engine. This necessitated the complete removal of the front main support panel and radiator brackets. The two front shock absorbers were replaced with tie down rods to compress the coil spring suspension and position the car at the proper height above ground level. Plywood panels were added to ensure that all condenser air entering the grille passed through the fan housing mockup. A condenser mockup was not used in the installation because its pressure drop was known and the lack of a condenser would not affect the determination of the installation pressure drop.

A rectangular duct the height of the bottom of the car bumper and extending approximately 2 ft either side of the car was terminated 3 ft in front of the car tires as shown on Figure 8-8. The purpose of this duct was to supply air to the under-side of the car to simulate vehicle motion. The duct was fitted with flow straighteners and a flow splitter to promote uniform air velocity across the discharge of the duct.

The duct was supplied with low pressure air. The discharge air velocity was controlled so that the discharge air velocity across the duct was maintained within 3 mph of the desired value.

A second rectangular duct was fitted on top of the lower duct to supply the fan airflow. This duct was fitted to cover the entire area between the lower lip of the hood and the bottom of the bumper between the fender projections, as shown in Figure 8-8. The airflow for this duct was supplied by two engine-driven blowers, and flow measurement was accomplished by calibrated bellmouth inlets fitted to the blowers.

Instrumentation consisted of (1) four total-static pressure probes located approximately 3 ft from the vehicle inlet in the upper duct, (2) two static pressure taps, two total-static pressure probes, and a thermocouple located 6 in. from the vehicle inlet in the upper duct, and (3) a total-static traverse probe located at the discharge of the lower duct. Figure 8-9 is a photograph of the partially completed installation.

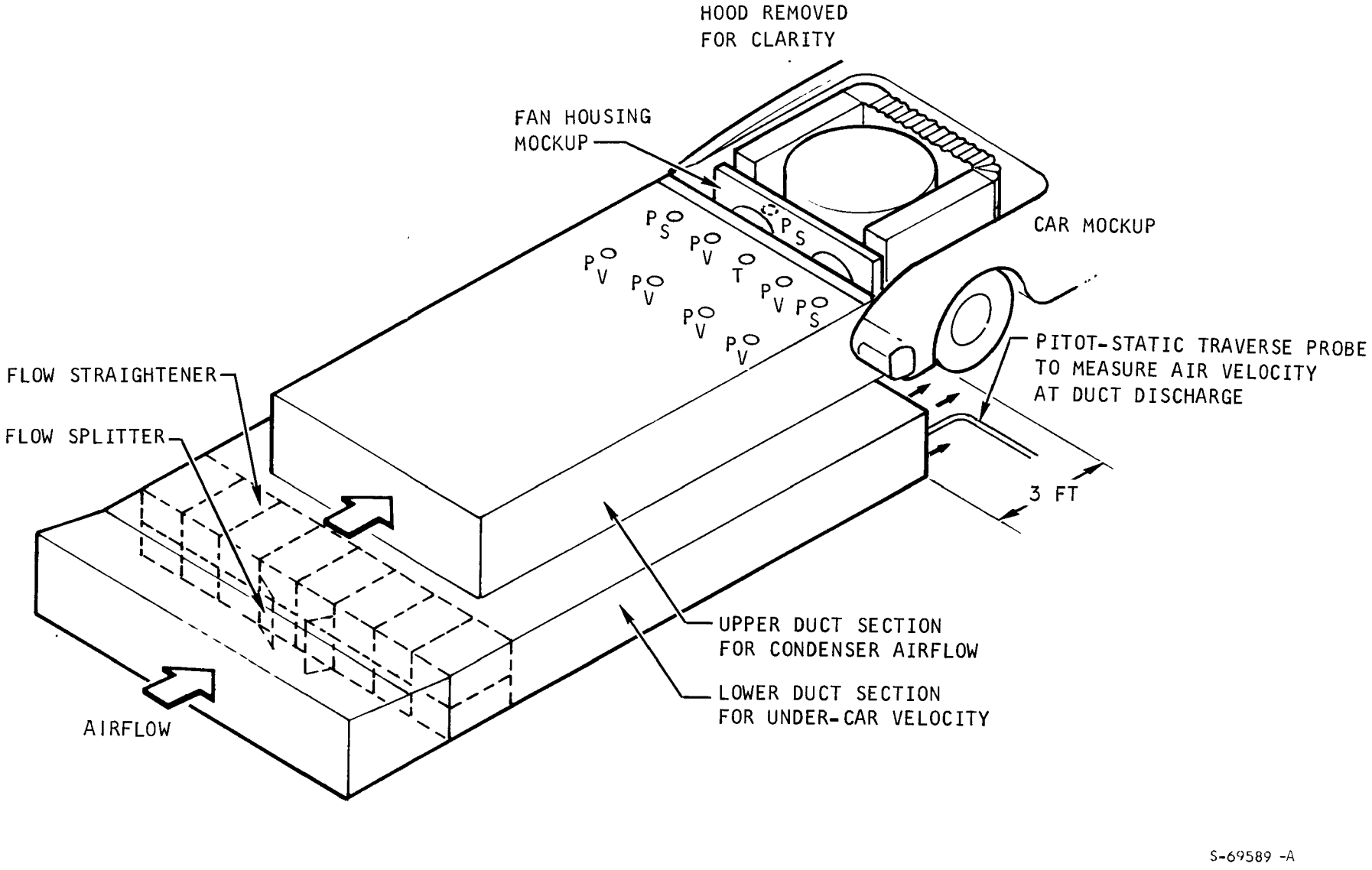

Figure 8-8. Aerojet Installation Airflow Test Setup

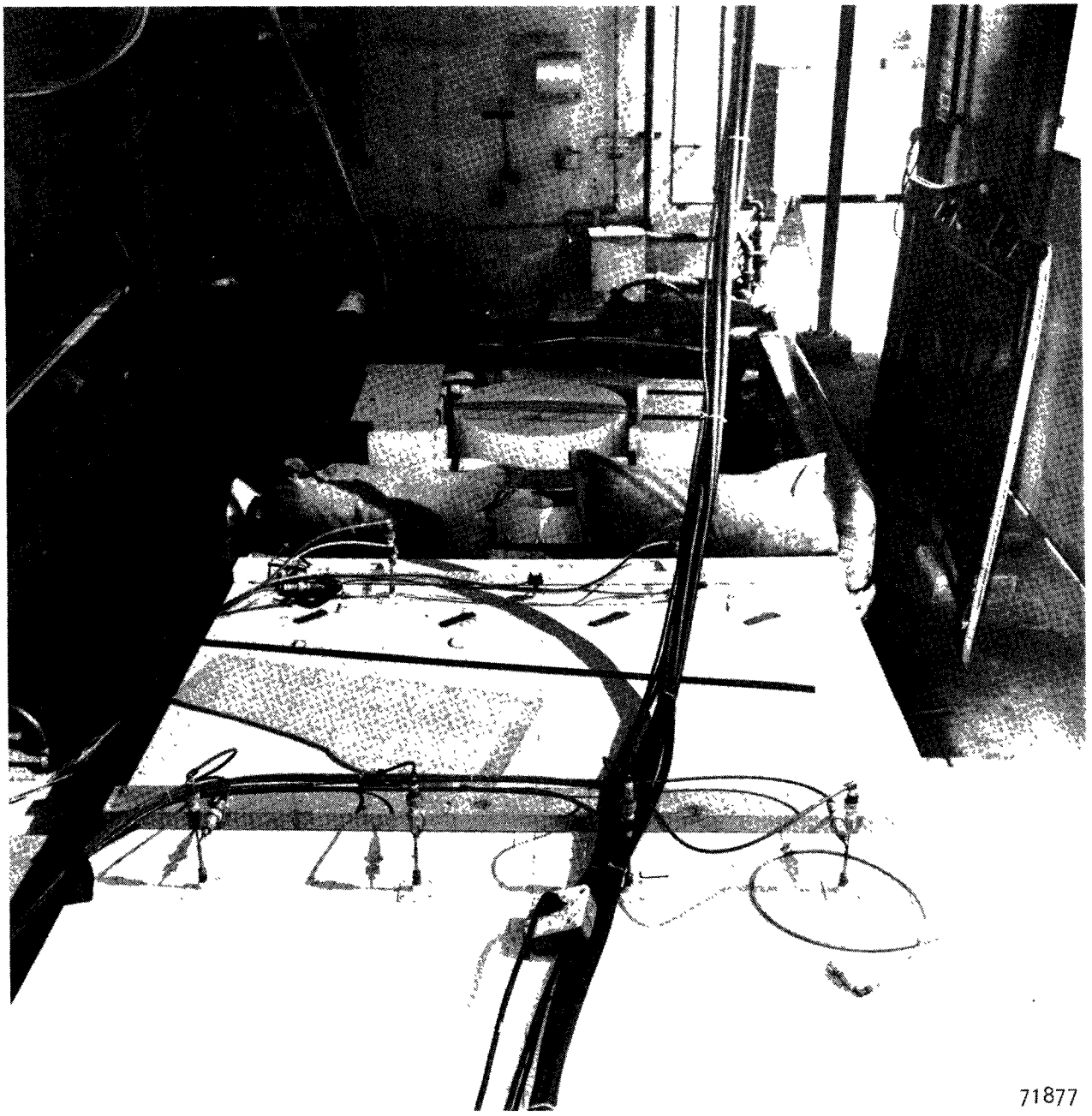

Figure 8-9. Aerojet Installation Air Flow Test Setup

Attempts were made to measure the pressure drop across the grille and bumper directly, but no representative location could be found for the condenser-side pressure pickup to ensure accurate readings. Accordingly, the simulated engine components were removed from the engine compartment, and the engine compartment to atmosphere pressure drop and the pressure drop from just upstream of the bumper and grille to atmosphere were measured at simulated condenser flows of 10,880, 14,500, and 20,600 cfm. In all cases, the engine compartment pressure drop was less than 0.3 in. WC at maximum flow, no matter where measured.

Therefore, to simplify testing, the pressure drop of the empty engine compartment was assumed to be zero and the entire pressure drop from in front of the bumper and grille to atmosphere was assigned to the bumper and grille.

The grille and bumper pressure drop was run with no lower duct flow to simulate vehicle motion. The simulated engine components were reinstalled in the engine compartment and the pressure drop from just upstream of the grille to atmosphere was again measured at simulated condenser flow rates of 10,880, 14,500, and 20,600 cfm with lower duct discharge velocities of 0. 20, 40, and 60 mph. The bumper and grille pressure drop was assumed to be independent of lower duct velocity, so the bumper and grille pressure drop found earlier was subtracted from the pressure drop with under-car airflow and the difference was taken as the engine compartment pressure drop.

Since the pressure drop was quite high during the original bumper and grille pressure drop tests, the two inboard headlights were removed, resulting in a substantial reduction in the bumper and grille pressure loss. The engine compartment loss was determined for both the 23-in. and 26-in. dia vapor generator configurations.

The test data are summarized in Figure 8-10. General conclusions based on these test results are as follows:

(a) The grille on the test car had a high pressure drop, and relatively minor increases in open area (removal of 2 headlights) produced a very significant reduction in pressure drop.

(b) The change from a 23-in. dia vapor generator to a 26-in. dia vapor generator produced significant changes in engine compartment pressure drop. This suggests that the engine compartment is quite sensitive to relatively minor changes in size of components and quite possible to their placement as well.

(c) The effect of under-car velocity on the engine compartment pressure drop was relatively minor. The compartment pressure drop increased by only 15 percent when the under-car velocity was increased from zero to 60 mph.

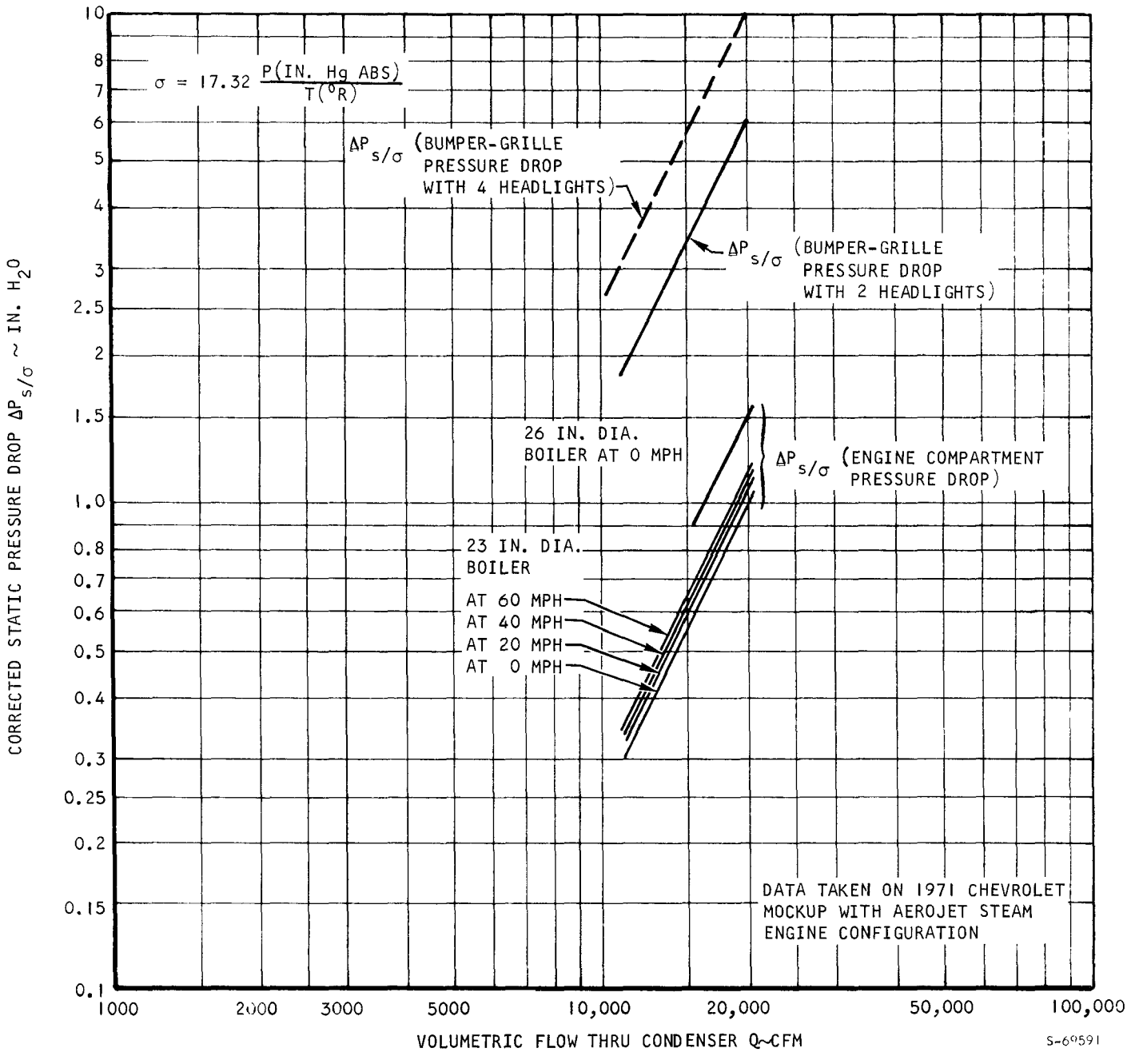

Figure 8-10. Aerojet Installation Airflow Test Results

A comparison between the Aerojet fan specification requirements as outlined on Table 6-1 and the requirements calculated on the basis of the present test results is shown in Table 8-1. The comparison is made for a 23-in. dia vapor generator engine configuration with two headlights removed to provide additional airflow area. The test results indicate that with this configuration, about a 23 percent increase in fan input power would be required to overcome the increase in the specified installation loss. The increase in fan input power can be minimized, however, by further modifications to the vehicle grille and bumper to provide additional inlet airflow area.

TABLE 8-1

AEROJET INSTALLATION DESIGN POINT COMPARISON

	Specification	Performance Based on Test Results
Condenser airflow, lb per hr	52,000	52,000
Condenser inlet temperature, ^{o}F	85	85
Condenser inlet pressure, psia	14.7	14.7
Condenser inlet volume flow, cfm	11,900	11,900
Bumper and grille static pressure loss,* in. H_2O	-	2.04
Fan outlet temperature, ^{o}F	206	206
Fan outlet volume flow, cfm	14,540	14,540
Vehicle speed, mph	50	50
Engine compartment static pressure loss, 26-in. dia vapor generator, in. H_2O	-	0.89
Engine compartment static pressure loss, 23-in. dia vapor generator, in. H_2O	-	0.46
Fan exit velocity head, in. H_2O	-	0.56
Installation total pressure loss,** in. H_2O	1.67	3.06
Condenser pressure loss, in. H_2O	3.91	3.91
Ram pressure rise, in. H_2O	0.91	0.91
Fan total pressure rise, in. H_2O	4.67	6.06

*2 headlights removed

**Total loss = bumper and grille plus engine compartment (23-in. dia vapor generator) plus fan velocity head.

SECTION 9

REFERENCES

SECTION 9

REFERENCES

1. Wong, S. et al, Final Report, Compact Condenser for Rankine Cycle Engine, AiResearch Report 71-7464, August 1971.

2. Soliman, M., Schuster, J., and P. Berenson, "A General Heat Transfer Correlation for Annular Flow Condensation", Journal of Heat Transfer, Transactions of the ASME, May 1968.

3. Personal Communication from Bill Macauly, Ford Motor Company, Dec 1971.

APPENDIX

CONDENSER AND FAN ASSEMBLY SPECIFICATIONS

APPENDIX

SPECIFICATION

CONDENSER AND FAN ASSEMBLY
PART NUMBER 190390

AEROJET LIQUID ROCKET COMPANY
AUTOMOTIVE PROPULSION SYSTEM

Prepared for the

Environmental Protection Agency

Division of Advanced Automotive Power Systems Development

Ann Arbor, Michigan 48105

Contract 68-01-0407

1. GENERAL

This specification defines the requirements for a condenser and fan assembly to be utilized on a low emission, Rankine cycle automotive propulsion system. The assembly is designed to operate on a pre-prototype engine which will be tested for 150 hours on a dynamometer test setup. The condenser and fans have been designed to fit within the engine compartment, although the assembly is not considered to be a fully roadable design.

2. CONDENSER PERFORMANCE

Design point performance goals are as follows:

Vapor Side

Working fluid	AEF-78
Total heat rejection, Btu/hr	1.50×10^6
Flow, lb/hr	20,000
Inlet temperature, ^{0}F	241
Inlet pressure, psia	32.7
Condensing temperature (avg), ^{0}F	235
Condensing pressure (avg), psia	31.3
Outlet temperature, ^{0}F	192.5
Subcooling, ^{0}F	38.5
Core pressure drop, psi	2.8
Overall pressure drop, psi	3.1

Air Side

Flow, lb/hr	52,000
Inlet temperature, ^{0}F	85
Inlet pressure, psia	14.7
Outlet temperature, ^{0}F	205
Temperature effectiveness	0.80 Condenser 0.62 Subcooler
Overall core pressure drop, in. H_2O	4.0

2.1 Condenser Design

The condenser shall be a plate-fin crossflow design utilizing bar and plate, brazed and welded construction. The material of construction shall be aluminum alloy. The unit shall be fluxless brazed to avoid contamination in the vapor passages.

3. FAN PERFORMANCE

Design point performance goals are as follows:

Total air flow, lb/hr	52,000
Total no. of fans	2
Inlet temperature, ^{0}F	205
Inlet pressure, psia	14.7
Airflow per fan, cfm	7250
Total pressure rise, in. H_2O	4.7
Efficiency, percent	70
Shaft power input, hp	7.5

3.1 Fan Design

The fan shall be a tube-axial type of the following configuration:

Tip diameter, in.	19.2
Number of blades	17
Fan rotation as viewed from driver's seat	ccw
Maximum operation speed, rpm	3600
Material	Aluminum alloy

3.2 Fan Drive

The fan shall be designed to be directly driven by a hydraulic motor. Interface requirements as they pertain to the hydraulic motor shall be as specified in AiResearch Source Control Drawing 499-001. The motor shall be supplied by others.

3.3 Noise Standards

No specific limit on the noise generated by the condenser and fan assembly is specified. The fans shall be designed, however, to produce a minimum amount of noise.

4. INSTALLATION

Overall dimensions, mounting arrangements, provisions for differential thermal expansion, inlet and outlet port configuration, and weight shall be as shown on Outline Drawing 190390.

4.1 Air Flow Characteristics

Condenser and fan design point airflow rating of 52,000 lb/hr shall be based on the following installation characteristics specified by the system contractor:

Vehicle speed, mph	50
Inlet flow dynamic pressure, in. H_2O	1.17
Inlet recovery factor, percent	78
Net ram pressure rise, in. H_2O	0.91
Installation pressure loss*, in. H_2O	1.67

5. STRUCTURAL DESIGN

The condenser shall be designed to withstand a maximum operating pressure of 50 psig at a metal temperature of 300°F. The corresponding proof pressure shall be 85 psig at room temperature. The condenser, fans and the support structure shall be designed to withstand the stresses associated with a bench test of the pre-prototype engine.

6. FINISH

All external surfaces of the condenser and fan assembly, with the exception of the air-side fins and the fan impellers, shall be painted in accordance with AiResearch Process Specification FP-73F04 (epoxy paint, flat black color).

*Installation loss includes the pressure losses as a result of airflow across the vehicle bumper and grille, and the losses associated with the fan discharge airflow through the engine compartment.

7. ACCEPTANCE TEST

7.1 Proof Pressure

The condenser shall be pressurized to 85 psig at room temperature. After pressure has been released, there shall be no evidence of permanent deformation.

7.2 Leakage

After completing the proof pressure test, the condenser assembly shall be leak checked. Leakage shall be less than 1×10^{-6} scc/sec of helium with the interior of the condenser evacuated and the exterior surfaces surrounded by helium at one atmosphere pressure.

7.3 Fan Calibration

The fan shall be tested as a component to establish its performance. The fan shall be run at the design point speed, and the fan pressure rise shall be determined over a range of airflows.

7.4 Condenser and Fan Performance

The condenser and fans shall be tested as an assembly to establish the airflow characteristics of the system. The assembly shall be tested without any inlet or outlet flow obstructions, and the airflow through the system shall be determined over a range of fan operating speeds including the design point speed.

SPECIFICATION

CONDENSER AND FAN ASSEMBLY
PART NUMBER 190370

THERMO ELECTRON CORPORATION
AUTOMOTIVE PROPULSION SYSTEM

Prepared for the

Environmental Protection Agency

Division of Advanced Automotive Power Systems Development

Ann Arbor, Michigan 48105

Contract 68-01-0407

1. GENERAL

This specification defines the requirements for a condenser and fan assembly to be utilized on a low emission, Rankine cycle automotive propulsion system. The assembly is designed to operate on a pre-prototype engine which will be tested for 150 hours on a dynamometer test set-up. The condenser and fans have been designed to fit within the engine compartment, although the assembly is not considered to be a fully roadable design.

2. CONDENSER PERFORMANCE

Design point performance goals are as follows:

Vapor Side

Working fluid	Fluorinal-85
Total heat rejection, Btu per hr	1.88×10^6
Flow, lb per hr	9860
Inlet temperature, ^0F	238
Inlet pressure, psia	40.0
Condensing temperature (avg), ^0F	212
Condensing pressure (avg), psia	36.4
Outlet temperature, ^0F	193
Subcooling, ^0F	17
Core pressure drop, psi	2.6
Overall pressure drop, psi	5.0

Air Side

Flow, lb per hr	75,300
Inlet temperature, ^{0}F	85
Inlet pressure, psia	14.7
Outlet temperature, ^{0}F	189
Temperature effectiveness	0.80
Overall core pressure drop, in. H_2O	4.1

2.1 Condenser Design

The condenser shall be a plate-fin crossflow design utilizing bar and plate, brazed and welded construction. The material of construction shall be aluminum alloy. The unit shall be fluxless brazed to avoid contamination in the vapor passages.

3. FAN PERFORMANCE

Design point performance goals are as follows:

Total airflow, lb	75,300
Total no. of fans	2
Inlet temperature, ^{0}F	189
Inlet pressure, psia	14.7
Airflow per fan, cfm	10,300
Total pressure rise, in. H_2O	3.1
Speed, rpm	2640
Efficiency, percent	70
Shaft power input, hp	7.2

3.1 Fan Design

The fan shall be a tube-axial type of the following configuration:

Tip diameter, in.	22.0
Number of blades	17
Fan rotation as viewed from driver's seat	ccw
Maximum operation speed, rpm	3600
Material	Aluminum alloy

3.2 Fan Drive

The fan shall be designed to be belt driven. Interface requirements shall be as specified on Outline Drawing 190370. Maximum load imposed on the fan bearing assembly by the belt drive during any operating condition shall be limited to 600 lb.

3.3 Noise Standards

No specific limit on the noise generated by the condenser and fan assembly is specified. The fans shall be designed, however, to produce a minimum amount of noise.

4. INSTALLATION

Overall dimensions, mounting arrangements, provisions for differential thermal expansion, inlet and outlet port configuration, and weight shall be as shown on Outline Drawing 190370.

4.1 Airflow Characteristics

Condenser and fan design point airflow rating of 75,300 lb per hr shall be based on the following installation characteristics as specified by the system contractor:

Vehicle speed, mph	90
Inlet flow dynamic pressure, in. H_2O	3.8
Inlet recovery factor, percent	100
Net ram pressure rise, in. H_2O	3.8
Installation pressure loss*, in. H_2O	2.8

5. STRUCTURAL DESIGN

The condenser shall be designed to withstand a maximum operating pressure of 100 psig at a metal temperature of 300°F. The corresponding proof pressure shall be 183 psig at room temperature. The support structure shall be designed to withstand the stresses associated with a bench test of the pre-prototype engine.

6. FINISH

All external surfaces of the condenser and fan assembly, with the exception of the air-side fins and the fan impellers, shall be painted in accordance with AiResearch Process Specification FP-73F04 (epoxy paint, flat black color).

*Installation loss includes the pressure losses as a result of airflow across the vehicle bumper and grille, and the losses associated with the fan discharge airflow through the engine compartment.

7. ACCEPTANCE TEST

7.1 Proof Pressure

The condenser shall be pressurized to 183 psig at room temperature. After pressure has been released, there shall be no evidence of permanent deformation.

7.2 Leakage

After completing the proof pressure test, the condenser assembly shall be leak checked. Leakage shall be less than 1×10^{-6} scc/sec of helium with the interior of the condenser evacuated and the exterior surfaces surrounded by helium gas at one atmosphere pressure.

7.3 Fan Calibration

The fan shall be tested as a component to establish its performance. The fan shall be run at the design point speed, and the fan pressure rise shall be determined over a range of airflows.

7.4 Condenser and Fan Performance

The condenser and fans shall be tested as an assembly to establish the airflow characteristics of the system. The assembly shall be tested without any inlet or outlet flow obstructions, and the airflow through the system shall be determined over a range of fan operating speeds including the design point speed.

SPECIFICATION

CONDENSER AND FAN ASSEMBLY
PART NUMBER 190640

STEAM ENGINE SYSTEMS
AUTOMOTIVE PROPULSION SYSTEM

Prepared for the

Environmental Protection Agency

Division of Advanced Automotive Power Systems Development

Ann Arbor, Michigan 48105

Contract 68-01-0407

1. GENERAL

This specification defines the requirements for a condenser and fan assembly to be utilized on a low emission, Rankine cycle automotive propulsion system. The assembly is designed to operate on a pre-prototype engine which will be tested for 150 hours on a dynamometer test set-up. The condenser and fans have been designed to fit within the engine compartment, although the assembly is not considered to be a fully roadable design.

2. CONDENSER PERFORMANCE

Design point performance goals are as follows:

Vapor Side

Working fluid	Water
Total heat rejection, Btu per hr	1.21×10^6
Flow, lb per hr	1285
Inlet temperature, ^{0}F	258
Inlet pressure, psia	34.0
Condensing temperature (avg), ^{0}F	256
Condensing pressure (avg), psia	33.3
Outlet temperature, ^{0}F	256
Subcooling, ^{0}F	0.0
Core pressure drop, psi	0.6
Overall pressure drop, psi	1.0

Air Side

Flow, lb per hr	38,200
Inlet temperature, ^{0}F	85
Inlet pressure, psia	14.7
Outlet temperature, ^{0}F	217
Temperature effectiveness	0.763
Overall core pressure drop, in. H_2O	2.1

2.1 Condenser Design

The condenser shall be a plate-fin crossflow design utilizing bar and plate, brazed and welded construction. The material of construction shall be aluminum alloy. The unit shall be fluxless brazed to avoid contamination in the vapor passages.

3. FAN PERFORMANCE

Design point performance goals are as follows:

Total airflow, lb per hr	38,200
Total no. of fans	2
Inlet temperature, ^{0}F	217
Inlet pressure, psia	14.7
Airflow per fan, cfm	5440
Total pressure rise, in. H_2O	2.9
Speed, rpm	2360
Efficiency, percent	70
Shaft power input, hp	3.6

3.1 Fan Design

The fan shall be a tube-axial type of the following configuration:

Tip diameter, in.	18.85
Number of blades	17
Fan rotation as viewed from driver's seat	ccw
Maximum operation speed, rpm	3600
Material	Aluminum alloy

3.2 Fan Drive

The fan shall be designed to be belt driven. Interface requirements shall be as specified on Outline Drawing 190640. Maximum load imposed on the fan bearing assembly by the belt drive during any operating condition shall be limited to 600 lb.

3.3 Noise Standards

No specific limit on the noise generated by the condenser and fan assembly is specified. The fans shall be designed, however, to produce a minimum amount of noise.

4. INSTALLATION

Overall dimensions, mounting arrangements, provisions for differential thermal expansion, inlet and outlet port configuration, and weight shall be as shown on Outline Drawing 190640.

4.1 Airflow Characteristics

Condenser and fan design point airflow rating of 38,200 lb per hr shall be based on the following installation characteristics as specified by the system contractor:

Vehicle speed, mph	32
Inlet flow dynamic pressure, in. H_2O	0.44
Inlet recovery factor, percent	100
Net ram pressure rise, in. H_2O	0.44
Installation pressure loss*, in. H_2O	1.22

5. STRUCTURAL DESIGN

The condenser shall be designed to withstand a maximum operating pressure of 35 psig at a metal temperature of 280°F. The corresponding proof pressure shall be 86 psig at room temperature. The support structure shall be designed to withstand the stresses associated with a bench test of the preprototype engine.

6. FINISH

All external surfaces of the condenser and fan assembly, with the exception of the air-side fins and the fan impellers, shall be painted in accordance with AiResearch Process Specification FP-73F04 (epoxy paint, flat black color).

*Installation loss includes the pressure losses as a result of airflow across the vehicle bumper and grille, and the losses associated with the fan discharge airflow through the engine compartment.

7. ACCEPTANCE TEST

7.1 Proof Pressure

The condenser shall be pressurized to 86 psig at room temperature. After pressure has been released, there shall be no evidence of permanent deformation.

7.2 Leakage

When pressurized to 86 psig, the proof pressure, there shall be no visible leakage.

7.3 Fan Calibration

The fan shall be tested as a component to establish its performance. The fan shall be run at the design point speed, and the fan pressure rise shall be determined over a range of airflows.

7.4 Condenser and Fan Performance

The condenser and fans shall be tested as an assembly to establish the airflow characteristics of the system. The assembly shall be tested without any inlet or outlet flow obstructions, and the airflow through the system shall be determined over a range of fan operating speeds including the design point speed.